Phenotypic Modelling of the Polyfunctional T Cell Response

By

NICOLA CHARLOTTE TRENDEL



Magdalen College

Sir William Dunn School of Pathology

UNIVERSITY OF OXFORD

A thesis submitted for the degree of DOCTOR OF PHILOSOPHY

TRINITY TERM, OCTOBER 2018

Abstract

T cells are important mediators of adaptive immunity and promising agents in immunotherapies. When T cell receptors (TCRs) on the surface of $CD8^+$ T cells detect pathogenic peptides presented by major histocompatibility complexes class I (pMHC) on antigen-presenting cells (APCs), a complicated intracellular signalling process is initiated that results, among other functional responses, in the secretion of cytokines to fight the pathogenic threat. An overwhelming number of molecular components that are involved in the translation of the pMHC stimulus into an appropriate cytokine response have been identified, but a mechanistic understanding of how the quality of the pMHC stimulus, i.e. pMHC dose and affinity, determines the response phenotype is lacking. Here, reductionist T cell stimulation experiments were combined with a coarse-grained phenotypic modelling approach to identify prevailing modules that shape the phenotype of cytokine secretion in response to stimulation with pMHC. $CD8^+$ primary human T cells transiently produced the four cytokines TNFα, MIP-1β, IFNγ and IL-2 and adaptation was paralleled by rapid and sustained TCR downregulation. Direct fitting of a phenotypic model constructed from known features of T cell signalling to the experimental data showed that TCR downregulation was sufficient to explain adaptation as well as other striking features of the cytokine response, including high-dose suppression (bell-shaped dose-response curve). Interestingly, secretion of TNFα, MIP-1β, IFNγ and IL-2 ceased at similar time scales and appeared equally sensitive to pMHC dose and affinity, contrary to previous reports. These findings thus suggest that T cells possess an intrinsic adaptation mechanism and reveal a surprisingly uniform early activation phenotype for multiple cytokines.

Acknowledgements

The past four years have been intensely inspiring, challenging and somewhat unreal. So many people have helped in so many ways to make it special.

First and foremost, I would like to thank my supervisor Omer Dushek for his support and guidance over the past three years. I could at no point (including his two paternity leaves) have wished for better supervision as he was always willing to generously give his time and discuss this work. I moreover appreciate the conversations we had beyond science and greatly value his continuous encouragement as a mentor who also took the leap from physics to immunology.

I would like to extend thanks to all past and present members of the van der Merwe and Dushek groups as well as Marion H. Brown and Johannes Breuning for so willingly sharing their expertise and for really fun lunch breaks – I will keep such fond memories of my time at the Dunn School. I would like to offer special thanks to Hong-Sheng Lim, Enas Abu Shah, Philipp Kruger and John Nguyen for introducing me to wet lab science so patiently and forgivingly.

Profound gratitude also goes to Forrest Bradbury and Andrew Mugler for priming my interest in systems biology during my time at the Amsterdam University College. I would not have made it through the Liberal Arts jungle without their dedicated guidance and mentoring. Thank you for encouraging me to embark on the systems biology path, which I enjoy so much.

Last but certainly not least, I would like to thank my family. I will be forever grateful to my parents for their love and support since 1991 and for the encouraging facetime sessions during my time in Oxford. My sister always knew how to cheer me up when things were difficult. And finally, I could not have completed this project without my

partner Desi, who was endlessly understanding and who found the right words every time it mattered. Thank you!

This research was funded by the Engineering and Physical Sciences Research Council and the Konrad Adenauer Foundation. I would like to thank everyone who helped me secure funds to realise this project, including the porters at the Magdalen College Lodge for making long shifts as pleasant as possible and everyone who supported my scholarship applications, including Carmen Argmann, Forrest Bradbury, Alex Diwa, Omer Dushek, David Gavaghan, Jim Johnson, Samantha Miles, Andrew Mugler, Bart van Heerikhuizen and Christopher Yau.

Contributions

These experiments were conducted by other members in the laboratory:

Fig. 3.11: Intracellular cytokine staining confirms that T cells stop producing cytokines
The experiment was conducted by Stephanie Gaglione under supervision of Philipp Kruger, John Nguyen and Nicola Trendel.

Fig. 4.1: TCR downregulation is reduced by inhibition of Lck at low but not high doses of stimulating pMHC
The experiment was conducted by Philipp Kruger.

Fig. C.1: Overview of SPR measurements to determine binding parameters between the 4A5A and 4A5P8K low-affinity pMHC variants and the 1G4Hi TCR
SPR measurements were performed by Mikhail Kutuzov.

Table of Contents

Page

List of Tables xi

List of Figures xiii

List of Abbreviations xix

1 General introduction 1

1.1 Antigen discrimination by T cells 3

1.1.1 Central tolerance 4

1.1.2 Peripheral tolerance 5

1.1.3 Mechanistic models of antigen discrimination 5

1.1.4 T cell specialisation and licensing 6

1.2 Signal 1: TCR-mediated intracellular signalling 7

1.2.1 The TCR/CD3 complex recognises pMHC ligands 8

1.2.2 TCR signalling is proximally transduced by Lck and ZAP-70 . . . 11

1.2.3 Signal diversification from the LAT-GADS-SLP-76 signalosome . 13

1.2.3.1 ADAP-mediated changes in cell adhesion 14

1.2.3.2 Cdc42-mediated changes in the actin cytoskeleton . . . 14

1.2.3.3 PI3K/Akt-mediated changes in metabolism 16

1.2.3.4 PLCγ-mediated changes in gene transcription 16

1.2.3.5 Redundancy, crosstalk and feedback loops are characteristic of T cell signalling 18

1.2.4 Post-transcriptional regulation 18

1.2.5 Effector functions 20
1.2.5.1 The immunological synapse coordinates the targeted release of effector molecules 20
1.2.5.2 TNFα, MIP-1β, IFNγ and IL-2 are important effector molecules secreted by $CD8^+$ T cells 21
1.3 Signal 2: Co-modulation of T cell signalling 23
1.3.1 Mechanisms of co-modulation 24
1.3.2 Co-modulatory receptors and T cell unresponsiveness 24
1.4 Signal 3: Modulation of T cell signalling by cytokines 25
1.5 Manipulating T cell signalling for immunotherapies 26
1.6 Phenotypic modelling of T cell signalling 27
1.7 Fitting phenotypic models to experimental data by ABC-SMC 28
1.8 Summary of thesis 30

2 Materials and methods 33

2.1 The 1G4 high-affinity TCR 33
2.1.1 Production of soluble TCR for affinity measurements 34
2.1.2 Production of lentiviral particles for transduction 35
2.2 NY-ESO-$1_{157\text{-}165}$ pMHC variants 36
2.2.1 Production of biotinylated pMHC ligand 36
2.2.2 Production of PE-conjugated pMHC tetramers 37
2.3 Affinity measurements by SPR 37
2.4 T cells 38
2.4.1 Jurkat T cells 38
2.4.2 Primary human T cells 38
2.5 Characterisation of T cell differentiation states 40
2.6 Functional T cell stimulation experiments 41
2.6.1 Preparation of stimulation plates 41
2.6.2 Immobilisation control 41
2.6.3 T cell stimulation protocols 42

2.6.3.1 TCR and cytokine production time course 43
2.6.3.2 TCR recovery 43
2.6.3.3 Inhibition of TCR signalling by Src-family kinase inhibitors 43
2.6.3.4 Stimulation experiments with a panel of pMHC variants 44
2.6.4 Enzyme-Linked Immunosorbent Assay (ELISA) 44
2.6.5 Flow cytometry 44
2.6.5.1 Staining of cell surface markers 45
2.6.5.2 Intracellular cytokine staining 45
2.7 Mathematical modelling 46
2.7.1 Averaging of experimental data 46
2.7.2 Extraction of E_{max} and EC_{50} from the experimental data 47
2.7.3 Fitting of experimental data by ABC-SMC 48

3 T cells limit their cytokine response to pMHC 51

3.1 Introduction 52
3.1.1 T cell differentiation 52
3.1.2 The strength of the stimulus is dictated by the dose of pMHC and its affinity to the TCR 53
3.1.3 The T cell response is polyfunctional and dynamic 54
3.1.4 The 1G4 high-affinity TCR and NY-ESO-$1_{157\text{-}165}$ pMHC 55
3.1.5 Biological adaptation 58
3.1.6 Chapter overview 58
3.2 Results 59
3.2.1 Protocol for generating pMHC-specific $CD8^+$ T cells results in an effector phenotype 60
3.2.2 T cells adapt their cytokine response to pMHC dose and affinity 66
3.2.3 Adaptive cytokine dynamics challenge assumptions underlying the KPL-IFF model 72
3.2.4 TCR is rapidly removed from the T cell surface for several days . 75

3.2.5 T cells adapted to a low-affinity pMHC can be reactivated with a higher-affinity pMHC . . . 77
3.3 Discussion . . . 79
3.3.1 The adaptation phenotype is consistent across different donors despite heterogeneous differentiation marker expression . . . 79
3.3.2 Relation between adaptation and previously described unresponsive states . . . 81
3.3.3 A TCR-proximal signalling block is associated with unresponsiveness *in vivo* . . . 83
3.3.4 *In vitro* experiments suggest calibration of the T cell response by tuning TCR expression levels . . . 85
3.3.5 Functional significance of prolonged TCR downregulation . . . 86

4 A phenotypic model explains adaptation at all pMHC doses with TCR downregulation 89
4.1 Introduction . . . 90
4.1.1 Receptor downregulation as a mechanism to induce adaptation . 90
4.1.2 Cooperative binding between TCR and pMHC . . . 90
4.1.3 Digital signalling in T cell activation . . . 91
4.1.4 Engaged and non-engaged TCRs are downregulated by two independent mechanisms . . . 92
4.1.5 Summary of the experimental phenotype to be explained by the phenotypic model . . . 93
4.1.6 Chapter overview . . . 95
4.2 Results . . . 96
4.2.1 A phenotypic model explains the full target phenotype . . . 96
4.2.2 Cooperative binding reconciles fast TCR downregulation and slow re-expression . . . 101
4.2.3 Signalling-dependent downregulation of non-engaged TCRs explains signalling requirements for TCR downregulation . . . 105

4.2.4 Switch-like activation of downstream signalling explains functional adaptation . . . 106
4.2.5 Temporal integration of short-lived TCR signals determines adaptation timescale . . . 109
4.2.6 The model predicts reactivation of T cells adapted to a low-affinity pMHC by a high-affinity pMHC . . . 109
4.3 Discussion . . . 111
4.3.1 Discussion of fit parameters . . . 113
4.3.2 Model improvements . . . 114
4.3.3 Alternative model architectures . . . 115
4.3.4 Comparison to previously published models . . . 116

5 Different cytokines are secreted by CD8$^+$ T cells with a similar threshold but at a different rate 119

5.1 Introduction . . . 120
5.1.1 Dose thresholds in CD8$^+$ T cells . . . 120
5.1.2 Affinity thresholds in CD8$^+$ T cells . . . 121
5.1.3 Formalised analysis of dose- and affinity-thresholds . . . 121
5.1.4 Chapter overview . . . 122
5.2 Results . . . 123
5.2.1 EC_{50} and E_{max} of the TNFα, MIP-1β, IFNγ and IL-2 response correlate with pMHC affinity . . . 125
5.2.2 The overall TNFα, MIP-1β, IFNγ and IL-2 signalling phenotypes are similar . . . 127
5.2.3 The dose thresholds for secretion of TNFα, MIP-1β, IFNγ and IL-2 are similar . . . 129
5.2.4 The absolute amounts and hierarchy of TNFα, MIP-1β, IFNγ and IL-2 secretion are heterogeneous and donor-specific . . . 131
5.2.5 The quality of the T cell response is similar for a wide range of pMHC doses and affinities . . . 132

5.2.6 A single-switch model with differential temporal integration is consistent with the experimental data . . . 137
5.3 Discussion . . . 139
5.3.1 Comparison to previous studies . . . 139
5.3.2 Support for cytokine-specific temporal integration . . . 142
5.3.3 Concluding remarks . . . 143

6 General discussion **145**
6.1 Mechanistic evidence that TCR downregulation can induce adaptation . 146
6.2 Functional significance of TCR downregulation in peripheral tolerance . 147
6.3 Relevance for CAR immunotherapies . . . 148
6.4 The single-switch model of T cell activation . . . 148
6.5 Future directions . . . 150

A Supplementary information to Chapter 3 **153**
A.1 Supplementary figures . . . 154

B Supplementary information to Chapter 4 **159**
B.1 ODEs . . . 160
B.1.1 Complete model . . . 160
B.1.2 Simple binding and cooperative binding models . . . 161
B.2 MATLAB implementation of ABC-SMC . . . 162
B.3 Supplementary figures . . . 167

C Supplementary information to Chapter 5 **171**
C.1 Supplementary figures . . . 172

Bibliography **177**

List of Tables

Table **Page**

2.1 Buffer recipes 34

2.2 List of antibodies 35

4.1 Definition of the target phenotype, key model features and figure references 95

4.2 Full list of model parameters 97

5.1 Updated list of NY-ESO-$1_{157\text{-}165}$ pMHC variants that bind the 1G4Hi TCR with milli- to picomolar affinities 124

List of Figures

Figure **Page**

1.1 Overview of T cell signalling modules 8

1.2 Binding between the TCR/CD3 complex to pMHC is stabilised by CD8 . . . 9

1.3 Lck and ZAP-70 transmit TCR signalling 13

1.4 LAT-GADS-SLP-76 orchestrates changes in adhesion, actin cytoskeleton, metabolism and gene transcription 15

1.5 Post-transcriptional modifications stabilise mRNA 19

1.6 Schematic illustration of parameter fitting by ABC-SMC 29

2.1 Example of immobilisation control 42

3.1 pMHC dose and affinity determine the strength of the pMHC input and elicit a dynamic and polyfunctional T cell output 54

3.2 The 1G4 high-affinity TCR binds NY-ESO-$1_{157\text{-}165}$/HLA-A2*02:01 pMHC variants with altered affinities 57

3.3 Schematic illustration of adaptation 59

3.4 A standard protocol for TCR transduction and expansion of $CD8^+$ primary T cells in cell culture yields heterogenous, yet antigen-experienced T cell populations 61

3.5 Comparison of T cell differentiation dynamics in culture between bulk and subset-enriched T cell populations 64

3.6 Timeline quantification of T cell differentiation, antigen experience and 1G4Hi TCR expression in culture 65

3.7 T cells derived from mixed, naïve or memory T cell populations respond to pMHC with similar activation thresholds 67
3.8 Experimental setup to determine the dynamics of multiple effector functions in response to a titration of pMHC ligand 68
3.9 T cells adapt their cytokine response to stimulation with a high-affinity pMHC 70
3.10 T cells adapt their cytokine response when stimulated with a low-affinity pMHC 73
3.11 Intracellular cytokine staining confirms that T cells stop producing cytokines 74
3.12 T cell receptor (TCR) is downregulated to a dose-dependent steady level within 1–2 hours of stimulation 76
3.13 Re-expression of TCR on the cell surface is slow compared to the experimental timescale 78
3.14 Adapted T cells can be reactivated by a higher-affinity pMHC 80

4.1 TCR downregulation is impaired by inhibition of Lck at low but not high doses of stimulating pMHC 94
4.2 A phenotypic model explains the full target phenotype 96
4.3 The phenotypic model is capable of explaining the full target phenotype . . 99
4.4 ABC-SMC illustrates correlations between model parameters 100
4.5 A simple binding model cannot simultaneously explain fast TCR downregulation and slow re-expression 102
4.6 Cooperative binding reconciles fast TCR downregulation and slow re-expression 104
4.7 Signalling-dependent downregulation of non-engaged TCRs explains controversial findings about signalling requirements for TCR downregulation . . . 107
4.8 Switch-like activation of downstream signalling explains adaptation as a result of TCR downregulation 108
4.9 Temporal integration of short-lived TCR signals determines adaptation timescale 110
4.10 The phenotypic model predicts that T cells adapted to the low-affinity pMHC can be reactivated by stimulation with the high-affinity pMHC 112
4.11 Examples of signalling modules for cooperative binding, switch-like T cell activation, TCR downregulation and temporal integration 118

5.1 Use of EC_{50} and E_{max} to quantify how dose- and affinity-thresholds affect the quality of the T cell response . . . 120
5.2 Schematic illustration of the experimental setup . . . 124
5.3 The TNFα, MIP-1β, IFNγ and IL-2 signalling phenotypes are similar across donors and pMHC variants . . . 126
5.4 EC_{50} and E_{max} of the TNFα, MIP-1β, IFNγ and IL-2 response correlate with pMHC affinity . . . 128
5.5 Overlay of the normalised TNFα, MIP-1β, IFNγ and IL-2 response highlights similar signalling phenotypes and activation thresholds . . . 130
5.6 The EC_{50}s of the TNFα, MIP-1β, IFNγ and IL-2 responses are similar . . . 131
5.7 Overlay of the TNFα, MIP-1β, IFNγ and IL-2 response (absolute amounts) highlights donor-specific differences in the amount and hierarchy of cytokines produced . . . 133
5.8 E_{max} ranking of the TNFα, MIP-1β, IFNγ and IL-2 response suggests a dominant IL-2^{low} IFNγ^{high} secretion profile . . . 134
5.9 Hierarchies are variable between donors, but consistent over a large range of pMHC affinity within each donor . . . 136
5.10 The quality of the cytokine response is similar over a wide range of affinities 137
5.11 A single-switch model is consistent with the experimental data . . . 140

A.1 Overlay of single-cell activation marker expression in populations derived from bulk, naïve-enriched or memory-enriched T cells confirms similar activation thresholds . . . 154
A.2 The absolute amount and hierarchy of cytokines produced varies between donors . . . 155
A.3 The timescale of adaptation is delayed in Jurkat cells . . . 156
A.4 TCR downregulation could not be determined reliably at earlier time points 157
A.5 pMHC tetramers staining of the 1G4Hi on $CD4^+$ primary human T cells . . 158

B.1 The sensitivity of the effective on-rate to TCR downregulation increases with the degree of cooperativity . . . 167

B.2 Systematic variation of TCR re-expression and downregulation rates in the simple binding model 168
B.3 Systematic variation of TCR re-expression and downregulation rates in the cooperative binding model 169

C.1 Overview of SPR measurements to determine binding parameters between the 4A5A and 4A5P8K low-affinity pMHC variants and the 1G4Hi TCR . . 172
C.2 Determination of EC_{50} from an interpolating function 173
C.3 Cytokine secretion does not scale linearly with the TCR transduction level . 173
C.4 The E_{max} of different cytokine responses changes similarly with pMHC affinity 174
C.5 Relative changes in $E_{max}^{(i)\prime}$ between cytokine readouts as a function of pMHC affinity for all donors 175

List of Abbreviations

×g Gravitational force

β_{2M} β-2 microglobulin

µM Micromolar

µg Microgram

µl Microlitre

% Percent

°C Degrees celsius

1G4Hi c58c61 high-affinity TCR, recognises NY-ESO-$1_{157\text{-}165}$

ABC-SMC Approximate Bayesian Computation Sequential Monte Carlo

ADAP Adhesion- and degranulation-promoting adapter protein

AF488 Alexa Fluor 488®

AF647 Alexa Fluor 647®

AICD Activation-induced cell death

ANOVA Analysis of variance

AP-1 Activator protein 1

APC Antigen-presenting cell

ARE AU-rich element

Arp2/3 Actin-related proteins 2/3

B_{max} Maximum RU at saturating doses

BV421 Brilliant Violet 421®

CAR Chimeric antigen receptor

CCR7 C-C chemokine receptor type 7

CD Cluster of differentiation

CD45RA Cluster of differentiation 45, RA isoform

CD45RO Cluster of differentiation 45, RO isoform

Cdc42 Cell division control protein 42 homologue

CDR Complementarity-determining region

CM Central memory

CO_2 Carbondioxide

DAG diacylglycerol

DAMP Danger-associated molecular patterns

DMEM Dulbecco's Modified Eagle's Medium

E_{max} Maximal overall response

EC_{50} pMHC dose producing a half-maximal response

EDTA Ethylenediaminetetraacetic acid

ELISA Enzyme-linked immunosorbent Assay

EMRA Terminally differentiated effector memory T cells expressing CD45RA

ERK Extracellular signal-regulated kinases

Fas First apoptosis signal receptor

FBS Fetal bovine serum

FITC Fluorescein isothiocyanate

g Gram

GADS Grb2-related adapter protein 2

GDP Guanosine diphosphate

gMFI Geometric mean fluorescence intensity

Grb2 Growth factor receptor-bound protein 2

GTP Guanosine-5'-triphosphate

HBS HEPES buffered saline

HEK293T Human embryonic kidney cells 293

HEPES 4-(2-Hydroxyethyl)-1-piperazineethanesulfonic acid

HLA Human Leukocyte Antigen

HRP Horseradish peroxidase

HuR Human antigen R

ICAM Intercellular Adhesion Molecule

IFF Incoherent feed-forward loop

IFNγ Interferon γ

IgG Immunoglobulin G

IL-2 Interleukin 2

IL-2R IL-2 receptor

IL-7Rα IL-7 receptor α-chain

IL-8 Interleukin 8

IP_3 Inositol 1,4,5-trisphosphate

ITAM Immunoreceptor tyrosine-based activation motif

K_D Dissociation constant

kDa Kilodalton

KPL-IFF Model consisting of KPR, limited signalling and an IFF [127]

KPR Kinetic Proofreading

l Litre

LAT Linker for activation of T cells

Lck Lymphocyte-specific protein tyrosine kinase

LFA-1 Lymphocyte function-associated antigen 1

LOWESS Locally Weighted Scatterplot Smoothing

M Molar

mg Milligram

MHC Major histocompatibility complex

MIP-1β Macrophage inflammatory protein 1β

miRNA Micro ribonucleic acid

ml Millilitre

mM Millimolar

mRNA Messenger ribonucleic acid

mTORC1 Mammalian target of rapamycin complex 1

NaCl Sodium chloride

Nck Non-catalytic region of tyrosine kinase adaptor protein 1

NFκB Nuclear factor κ-light-chain-enhancer of activated B cells

NF90 Nuclear factor 90

NFAT Nuclear factor of activated T cells

ng Nanogram

nM Nanomolar

NY-ESO-$1_{157\text{-}165}$ Human tumour antigen recognised by 1G4Hi TCR

ODE Ordinary differential equation

PAMP Pathogen-associated molecular patterns

PBS Phosphate buffered saline

PD-1 Programmed cell death protein 1

PDK1 Phosphoinositide-dependent kinase-1

PE Phycoerythrin

PenStrep Penicillin Streptomycin

pg Picogram

PH Pleckstrin homology

PI3K Phosphoinositide 3-kinase

PIP_2 Phosphatidylinositol 4,5-bisphosphate

PIP_3 Phosphatidylinositol (3,4,5)-trisphosphate

PKCθ Protein kinase C θ

PLCγ Phospholipase C γ

pM Picomolar

pMHC peptide presented by major histocompatibility complex

PMSF Phenylmethane sulfonyl fluoride

PRR Pattern-recognition receptor

R^2 Coefficient of determination

Rap1 Ras-related protein 1

RapL Regulator of cell adhesion and polarisation enriched in lymphoid tissues

RIAM Rap1-GTP-interacting adapter molecule

RPMI Roswell Park Memorial Institute

RU Response units

SD Standard deviation

SEM Standard error of the mean

SH Src Homology

SHP-1 Src homology region 2 domain-containing phosphatase-1

SKAP55 Src kinase-associated phosphoprotein 55

SLP-76 SH2-domain containing leukocyte protein of 76 kDa

SMAC Supramolecular Activation Cluster

SOS Son of Sevenless

SPR Surface Plasmon Resonance

SSR Sum of squared residuals

T_{CM} Central memory T cells

T_{EM} Effector memory T cells

T_{reg} Regulatory T cell

T_{SCM} Stem cell-like memory T cells

TCR T cell receptor

TMB 3,3',5,5'-Tetramethylbenzidine

TNFα Tumour necrosis factor α

U Unit

UTR Untranslated region

Vav1 Vav guanine nucleotide exchange factor 1

WASp Wiskott-Aldrich syndrome protein

ZAP-70 ζ-chain-associated protein kinase 70

CHAPTER 1

General introduction

The immune system consists of multiple layers that collectively protect the human body against pathogenic invaders. They can be broadly classified as constitutive and inducible mechanisms [158]. Constitutive mechanisms include anatomical barriers, such as the skin, and coating of exposed interfaces with, for example, antimicrobial peptides. Inducible mechanisms are activated when pathogens overcome these barriers and they rely on recognition of the pathogen by the immune system. Two branches of inducible mechanisms, the innate and adaptive immune system, have evolved different strategies to recognise pathogenic threats. Although originally innate and adaptive immunity have been thought to be triggered sequentially, it is now clear that these two branches are intricately linked throughout the immune response.

The innate immune system comprises several types of white blood cell, including macrophages, dendritic cells and neutrophils. These cells express pattern-recognition receptors (PRRs), of which approximately a few hundred are thought to exist [159]. PRRs are germline-encoded and therefore have a genetically predetermined specificity. Using their PRR, innate immune cells can detect highly conserved molecular structures that are typically important for the survival and immunogenicity of pathogens, and that are produced exclusively by pathogens and not by the host (self-nonself discrimination model [158, 159]). It is now known, however, that *selfness* does not preclude

immunogenicity: Innate immune cells also recognise DAMPs (danger-associated molecular patterns) that are, for instance, released by injured cells (danger model [152]). Finally, some innate immune cells can also detect the absence of self (discontinuity model [191]). Effector functions of innate immune cells include opsonisation and activation of the alternative complement pathway by secreted PRRs and phagocytosis. Because the innate immune response relies on a pre-existing population of immune cells, it provides a rapid (minutes to hours) first line of defence upon pathogen challenge [158]. In addition, innate immune cells can secrete messenger molecules, express co-stimulatory ligands and present antigens in the form of small peptides to activate the adaptive immune system.

The adaptive immune system consists of B cells and T cells. Their antigen receptors are not germline-encoded but generated somatically through random rearrangement of gene segments during development. B and T cell populations can thereby recognise a larger number of antigens (10^{14} and 10^{18}, respectively) than innate immune cells [159]. The frequency of each clone with a given specificity, however, is low in the resting state, so that an effective immune response requires expansion of the useful clone that recognises the pathogenic invader. The onset of the adaptive immune response is therefore delayed (days) compared to the innate immune response [159]. Once activated through their antigen receptors, B cells and T cells employ different mechanisms to eliminate the pathogenic threat. Whereas B cells secrete their antigen receptors as antibodies to opsonise targets and induce the classical complement pathway, the T cell antigen receptor remains surface-bound and, when engaged, initiates cell-cell contact interfaces that can result in direct killing of afflicted cells or in the provision of help to other immune cells for effective pathogen clearance.

The focus of this thesis will be on the inducible immune response by T cells in the adaptive immune system. T cells patrol the body searching for signatures of pathogens using T cell receptors (TCR) on their surface to recognise peptide fragments presented by major histocompatibility complexes (pMHC) on antigen-presenting cells (APCs). Detection of pathogenic pMHC can activate T cells to proliferate, secrete effector molecules and change the expression of surface molecules that amplify or regulate their response. Important effector molecules include cytokines that communicate with

other components of the immune system to orchestrate an effective immune response. Dysregulation of the cytokine response can compromise immune protection or cause severe harm to healthy tissues [248].

Because the specificity of immune cells in the adaptive immune system is generated randomly, an inherent risk exists that a T cell clone reacts to endogenous molecular structures. Yet, T cells are capable of distinguishing pathogenic pMHC from innocuous self-pMHC (antigen discrimination) with remarkable sensitivity and specificity that is achieved by developmental checkpoints, on the one hand, and cellular signalling mechanisms, on the other hand (Section 1.1). During pMHC ligand encounter, T cells integrate multiple molecular cues to execute an informed response, including, on the single-cell level, TCR-mediated signalling initiated by binding between TCR and cognate pMHC (Signal 1, Section 1.2) and various co-modulatory signals (Signal 2 in Section 1.3 and Signal 3 in Section 1.4) that are typically provided by innate immune cells after triggering of PRRs. Thereby, the immune system manages to balance an effective T cell response with minimal risk of damage to the organism.

In the present study, we employed a modularised view on TCR-mediated T cell signalling to understand how pMHC stimulation effects an appropriate cytokine response in the absence of co-modulatory signals. Understanding T cell signalling is of importance for the design of immunotherapies (Section 1.5), but the overwhelming molecular complexity of the T cell signalling network impedes mechanistic understanding of the whole pathway connecting the TCR with the cytokine response. A phenotypic modelling approach was applied to gain quantitative insights into T cell signalling (Section 1.6), and model predictions were directly compared to experimental data by an ABC-SMC algorithm (Section 1.7).

1.1 Antigen discrimination by T cells

Antigen discrimination describes the ability of T cells to respond to minute amounts of foreign pMHC while remaining tolerant to the large number of self-pMHCs they are constantly presented with. Because failure to distinguish innocuous self-pMHC

from pathogenic pMHC can result in lethal autoimmune disease or pathogen escape, antigen discrimination is a crucial requirement for successful immune protection and it is conferred by a multitude of regulatory layers. Highly self-reactive T cells are deleted during development in the thymus (central tolerance, Section 1.1.1). Central tolerance is however leaky, and additional mechanisms apply in peripheral tissues to regulate T cell reactivity (Section 1.1.2). Despite these central and peripheral tolerance mechanisms, sensitive and specific ligand recognition by T cells remains difficult for us to understand and has motivated the formulation of mechanistic mathematical models to explain antigen discrimination on a single-cell level (Section 1.1.3). Finally, T cells are reliant on signals from other (immune) cells that license them to respond to a particular pMHC and thereby improve discrimination between self and pathogenic pMHC (Section 1.1.4).

1.1.1 Central tolerance

Circulating T cells express a broad repertoire of clonotypic TCRs that generally have a weaker affinity for self-pMHC than for agonist pMHC that activates T cells. This repertoire is established during T cell maturation in the thymus. Here, progenitor T cells express random TCRs that are generated by the combinatorial assembly of variable (V), diversity (D) and joining (J) gene segments encoding different components of the TCR. These TCRs are tested for reactivity to self-pMHC: T cells bearing a TCR that binds self-pMHC with high affinity die by apoptosis (negative selection) whereas those bearing a TCR with low affinity to self-pMHC receive a survival signal and enter the periphery (positive selection) [115, 168]. Unresponsive T cells die by neglect, presumably to separate out T cells that express non-functional TCRs [115]. As a result, TCRs expressed by positively selected mature T cells that exit the thymus into the periphery bind self-pMHC with low affinity, and this weak interaction is known to be critical for T cell survival [84]. However, central tolerance is leaky and self-reactive T cells are thought to occasionally enter the periphery [244], so that additional tolerance mechanisms are required.

1.1.2 Peripheral tolerance

Self-reactive T cells occasionally escape central tolerance in the thymus [244]. Additional mechanisms therefore regulate T cell activity in peripheral tissues. Mechanisms of peripheral tolerance include suppression of T cells by regulatory T cells (T_{regs}) [26, 206], activation-induced cell death (AICD) [71] and functional unresponsiveness [216]. At least three distinct states of functional unresponsiveness, anergy, adaptive tolerance and exhaustion, have been identified. Whereas anergic T cells fail to execute certain effector functions such as IL-2 secretion and clonal expansion, adaptive tolerance and exhaustion are characterised by a global impairment of effector functions. Further differences in induction, maintenance and reversal of unresponsive states exist, but the molecular mechanisms governing different types of unresponsiveness remain incompletely understood [31, 216, 220].

1.1.3 Mechanistic models of antigen discrimination

T cells display remarkable sensitivity and specificity in antigen discrimination. As a result of thymic selection, TCRs on circulating T cells interact weakly with self-pMHC, and it is unclear how T cells distinguish this high level of noise from the low level of pathogenic signal [258]. T cells are continuously presented with abundant (10^5–10^6-fold excess) low-affinity self-pMHC, yet they are capable of detecting even a single interspersed high-affinity pathogen-derived pMHC [8, 89]. A simple occupancy model, in which TCR signalling is directly proportional to the number of engaged TCRs, is inconsistent with these experimental observations as it predicts that high doses of a low-affinity or low-doses of a high-affinity pMHC can achieve identical levels of TCR occupancy.

Specificity of the T cell response is further illustrated by the finding that small differences in the lifetime of the TCR-pMHC complex can disproportionately affect TCR signalling. A threefold decrease in pMHC affinity as a result of a single amino acid substitution sufficed in a study by Altan-Bonnet and Germain [8] to convert an agonist pMHC into a non-agonist pMHC [8]. The kinetic proofreading model (KPR) offers the explanation that pMHC ligands must bind the TCR for a sufficiently long period of

time before a productive signal is generated [157]. In this model, the TCR traverses through a series of modifications before it reaches a signalling-competent state, and the modifications are rapidly reversed when the TCR unbinds the pMHC ligand. As a result of the time delay between binding and signalling, pMHCs with fast dissociation rates are less likely to produce the fully-activated receptor state even at high pMHC doses, so that pMHC abundance cannot compensate for low pMHC affinity [55]. By scaling the length of the KPR chain, small differences in the binding affinity between pMHC and TCR can be amplified with increasing resolution.

The KPR model of antigen discrimination has been modified extensively to correct for attendant decreases in the speed and sensitivity of ligand detection. Activation of downstream signalling occurs on the order of few seconds [28] and this time scale limits the precision of affinity discrimination that can be achieved by KPR [258]. KPR has therefore been complemented with a negative feedback loop that is triggered by early KPR steps and opposes KPR progression to suppress noise from low-affinity pMHC [64]. An additional positive feedback loop has been implemented to amplify the response and explain digital activation of downstream signalling [8, 234]. Other models show that rapid rebinding of pMHC to the TCR has the potential to enhance sensitivity to few pMHC ligands [56]. A combination of multiple signalling motifs is thus required to reconcile specificity in affinity discrimination with the observed speed and sensitivity of the T cell response.

1.1.4 T cell specialisation and licensing

T cells specialise on detecting certain types of pathogens by expressing one of the two co-receptors CD4 or CD8. CD4 and CD8 interact with MHC class II (MHCII) or MHCI, respectively, and thereby direct T cell attention to different types of cells and pathogens [168]. Whereas MHCI is expressed on all cells and presents peptides derived from intracellular pathogens (e.g. viruses), MHCII is expressed on immune cells that sample peptides from their environment, which can be indicative of extracellular pathogens (e.g. helminths). These types of pathogens require distinct elimination strategies: Infected

cells presenting viral peptides on MHCI are directly killed by cytotoxic $CD8^+$ T cells to prevent further replication of the virus, but $CD4^+$ T cells assist other immune cells specialised on eliminating large extracellular pathogens instead. As a result, CD4/MHCII and CD8/MHCI interactions condition the T cell response to peptide presentation by other (immune) cells, and thereby enable T cells to discriminate between different types of pathogens and to tailor the T cell response accordingly.

In addition to pMHC stimulation, naïve T cells that have not previously encountered their cognate pMHC rely on co-stimulatory signals provided by other immune cells to become licensed effector T cells (two-signal model) and more rapidly respond to pMHC during future pMHC encounters. The co-stimulatory signal 2 is, however, only generated during active infections: When dendritic cells detect Pathogen-Associated Molecular Patterns (PAMPs), for example, they upregulate expression of the co-stimulatory ligands CD80 and CD86 [227]. A self-reactive T cell cannot become activated in the absence of these pathogenic markers and their effects on other immune cells, and co-stimulation thereby improves antigen discrimination.

In summary, T cell reactivity in the periphery is regulated by embedding T cells in a network of immune cells that collectively inform whether an immune response is initiated. To study the effect of pMHC dose and affinity on the T cell response in an isolated system, the present study focused on the activation of mature antigen-experienced $CD8^+$ T cells which have previously been licensed to perform effector functions and thus do not rely on co-stimulation to respond to MHCI-presented cognate peptide.

1.2 Signal 1: TCR-mediated intracellular signalling

On a molecular level, a large number of components are involved in translating pMHC ligand detection into a functional response, such as cytokine release. In Fig. 1.1, the T cell signalling machinery has schematically been divided into five modules that are discussed sequentially. An intricate molecular network converts binding between pMHC and TCR

(Section 1.2.1) into an intracellular signal (Section 1.2.2) that then stimulates four main signalling pathways with important functional effects (Section 1.2.3). Cytokine production requires enhanced gene transcription, as well as post-transcriptional modifications to mRNA that regulate protein production (Section 1.2.4). After polarisation of the T cell towards the target cell, cytokines and other effector molecules are secreted (Section 1.2.5). Although not exhaustive, the following discussion illustrates the dimensions and complexity of the network.

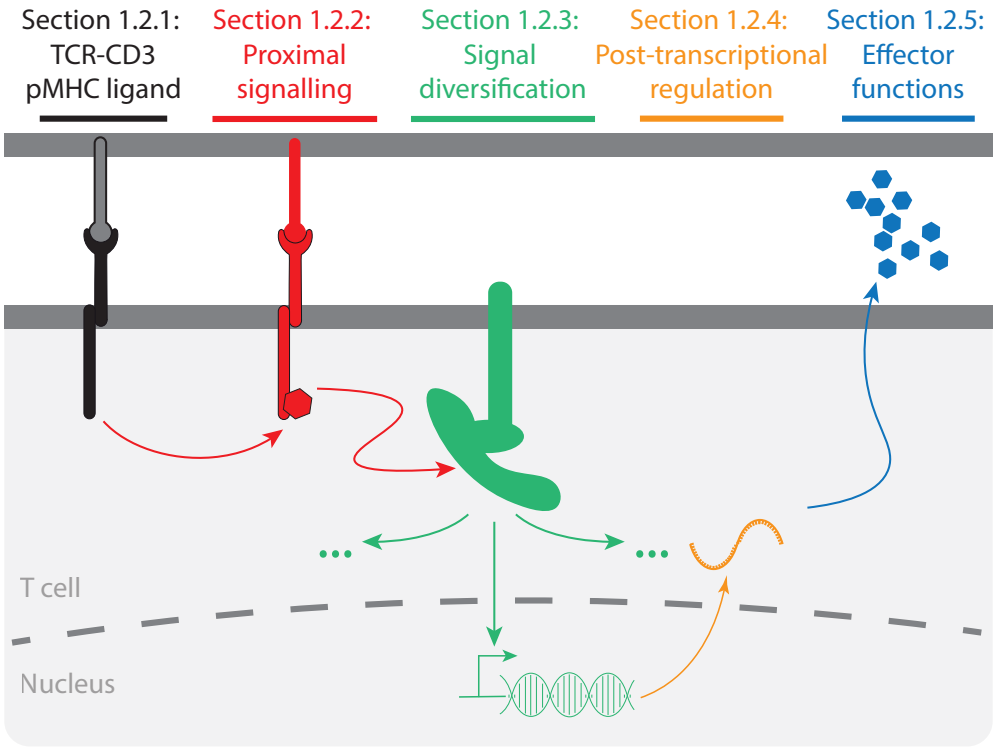


Figure 1.1: Overview of T cell signalling modules. The translation of a recognition event between pMHC and TCR into a functional cytokine response involves TCR-proximal signalling molecules, signal diversification and post-transcriptional regulation. These modules are summarised sequentially in Sections 1.2.1–1.2.4. The controlled execution of effector functions with a focus on cytokine secretion is discussed in Section 1.2.5.

1.2.1 The TCR/CD3 complex recognises pMHC ligands

T cells continuously scan other cells for their cognate **pMHC ligand** (Fig. 1.2). The ligand recognised by $CD8^+$ T cells is a peptide derived from pathogenic material that

has entered the target cell's cytosol, for example, during a viral infection. Pathogenic proteins as well as other, non-pathogenic cytosolic proteins are processed into smaller peptide fragments in the proteasome. Peptide fragments of 8–10 amino acid length are then imported into the endoplasmic reticulum (ER) and loaded onto MHC class I molecules [91]. MHC consisting of the heavy α-chain and β_2-microgobulin (β_{2M}) is stabilised by binding of the peptide and only then is the complex transported to and presented on the membrane [91]. The sum of pMHC ligand complexes the T cell is typically presented with is a mixture of abundant self-peptides and few pathogenic peptides.

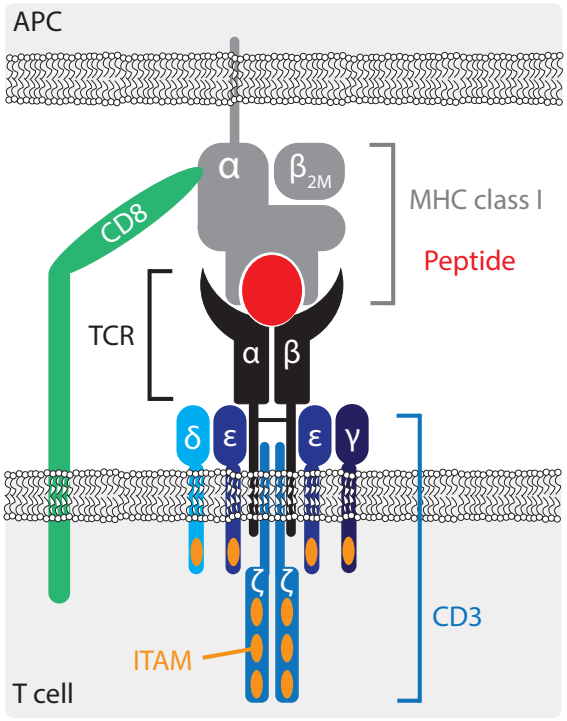


Figure 1.2: Binding between the TCR/CD3 complex to pMHC is stabilised by CD8. The $\alpha\beta$TCR associated with the CD3 complex ($\delta\epsilon$, $\zeta\zeta$, $\epsilon\gamma$) binds pMHC ligands on the APC. ITAM signalling domains are located on the CD3 cytoplasmic tails. The interaction between TCR and pMHC is stabilised by the CD8 co-receptor.

T cell receptors (TCRs) on the T cell surface detect pMHC ligands on target cells (Fig. 1.2). The TCR is a $\alpha\beta$-heterodimer that is structurally related to the Fab (Fragment antigen-binding) of an antibody [66]. A disulfide link connects the constant regions (Cα, Cβ) and the variable regions (Vα, Vβ) containing four complementarity-determining regions (CDRs) each. Crystal structures of a large number of TCRs in complex with

pMHC have revealed that the TCR binds pMHC at an angle of roughly 30°, so that the number of possible binding orientations between pMHC and TCR is thought to be constrained [66]. In contrast to antibodies, TCRs do not undergo affinity-maturation. Theoretical considerations of the size of the peptide repertoire compared to the number of clonotypic TCRs showed that TCRs must be able to detect more than one pMHC to provide sufficient immune protection [221].

The TCR has a short cytoplasmic tail that is incapable of signalling on its own. Instead, the TCR associates with the **CD3 complex** that has a longer signalling tail and consists of the $\epsilon\delta$ and $\gamma\epsilon$ heterodimers as well as a $\zeta\zeta$ homodimer (Fig. 1.2) [271]. CD3ζ differs from other CD3 components [5, 271]. First, it is produced in limiting amounts and critically determines TCR expression on the T cell surface because the full TCR-CD3 complex is needed for stable expression [164, 271]. Second, it cycles separately from the remaining TCR-CD3 complex between cell surface and endosomes [5]. Third, it has 3 Immunoreceptor Tyrosine-based Activation Motifs (ITAMs) in its tail, while the other CD3 components have 1 ITAM each. Tyrosine phosphorylation of ITAMs is central to TCR-CD3 signalling [237], and ITAM multiplicity scales the magnitude and potency of the functional response [167].

In contrast to pMHC ligands that remain on the surface of APCs for several days [91], surface expression of the TCR-CD3 complex is highly dynamic. In the resting state, TCR and CD3 reside on microvilli that are dynamically extended and retracted to probe target cells for pMHC ligands [102]. TCR and CD3 rapidly cycle between the cell surface and endosomes [117, 133, 161, 163]. Among other motifs [240], exposure of a di-leucine motif on CD3γ serves as an active sorting signal to recruit adapter proteins 1 and 2 that mediate endocytosis of the complex in a clathrin-dependent manner [48, 49, 163]. Mutation of the di-leucine motif consequently led to increased TCR baseline expression [16, 49]. Complete assembly of the TCR with all CD3 subunits, in particular CD3ζ, masks the internalisation motif, so that rapid cycling of the TCR-CD3 complex could be an important quality control mechanism [5, 48, 122]. In addition, constitutive recycling also sustains an intracellular pool of TCRs that can rapidly be transported to the target cell contact site upon pMHC ligand detection [180].

Binding between TCR and pMHC is stabilised by the **CD8 co-receptor** that recognises invariant sites on MHC class I (Fig. 1.2) [278]. CD8 exists as a transmembrane $\alpha\alpha$-homodimer or an $\alpha\beta$-heterodimer. TCR and CD8 can interact with the same pMHC ligand, and the additional contact established by CD8 has been shown to decrease the dissociation rate of pMHC from the TCR [278]. As a result, the recognition of low doses of pMHC becomes several orders of magnitude more sensitive as lower-affinity pMHCs can engage the TCR for sufficient time to elicit a response [277, 278]. By this mechanism, CD8 enables clonotypic TCRs to recognise multiple pMHC ligands (crossreactivity) and to provide sufficient immune cover [277]. Conversely, CD8 downregulation on peripheral T cells has been implicated in making T cells less responsive [121].

1.2.2 TCR signalling is proximally transduced by Lck and ZAP-70

It is currently unclear how binding of cognate pMHC to the TCR is translated into an intracellular signalling event, and the complexity of TCR-proximal signalling could be symptomatic of the unique demands made on T cells to recognise pathogenic pMHC ligands with high sensitivity and specificity. Several models of TCR triggering have been proposed and the emerging picture is a complex spatiotemporal interplay of ligand-induced conformational changes, aggregation of TCRs with CD8 and spatial segregation of activating from inhibitory molecules [258]. TCR triggering is manifested in the tyrosine phosphorylation of ITAMs (Immunoreceptor Tyrosine-based Activation Motifs) on CD3 subunits predominantly by the Src-family kinase Lck (Lymphocyte-specific protein tyrosine kinase, Fig. 1.3) [99, 237]. Phosphorylated ITAMs then provide docking sites for the tyrosine kinase ZAP-70 (ζ-chain-associated protein kinase 70) [99]. Two key targets of ZAP-70 are the adapter proteins LAT (Linker for Activation of T cells) and SLP-76 (SH2 domain-containing leukocyte protein of 76 kDa) that form a hub for signal diversification. Both Lck and ZAP-70 adopt different conformational states that tune their enzymatic activity. The relative spatiotemporal dynamics of ITAMs, Lck and ZAP-70 as well as their regulators are furthermore important determinants of productive

signalling [134, 217]. Protein tyrosine phosphatases such as SHP-1 (Src Pomology region 2 domain-containing Phosphatase-1) have been implicated in regulating TCR-proximal signalling by counteracting tyrosine phosphorylation by Lck and ZAP-70.

The enzymatic activity of **Lck** is under tight control by Csk (C-terminal Src kinase) and CD45 [217]. An inactive, closed conformation is induced by Csk, which phosphorylates Lck at the tyrosine residue Y505 in the C-terminus region that subsequently interacts intramolecularly with the SH2 domain and shields the catalytic site [15]. Autophosphorylation of Lck at Y394, on the contrary, stabilises an open, enzymatically active conformation [281]. CD45 dephosphorylates Lck at both Y394 and Y505 and thereby biases Lck towards an open, primed conformational state. Interestingly, a large proportion of Lck (~40%) has been shown to be in the Y394-phosphorylated active conformation in the resting state, and TCR ligation only marginally increased conformational activation of Lck [176]. Besides conformational regulation of Lck activity, the precise spatial redistribution of active Lck relative to ITAMs on CD3 determines the signalling outcome. Dissociation of CD3 cytoplasmic tails from the plasma membrane upon TCR engagement, for example, increases accessibility of ITAMs and interactions between CD8 and MHC could recruit CD8-associated Lck to the bound TCR [111]. An imaging study by Casas et al. [28], however, showed that an early phase of TCR signalling that is not mediated by CD8-associated Lck precedes the recruitment of CD8 coreceptor. Questions about the exact spatiotemporal dynamics of Lck and how it mediates TCR signalling therefore remain.

ZAP-70 is recruited to phosphorylated ITAMs via its tandem SH2 domain. Inactive ZAP-70 has been shown to be constitutively bound to partially phosphorylated ITAMs in freshly isolated T cells, presumably as a result of mild stimulation through the interaction with self-pMHC [2, 28, 217]. Activation of ZAP-70 to phosphorylate its downstream targets LAT (Linker for Activation of T cells) and SLP-76 (SH2-domain containing leukocyte protein of 76 kDa), requires co-localisation of ZAP-70 with Lck. Lck phosphorylates ZAP-70 at Y319 to expose a kinase domain [99, 282]. Intriguingly, Lck can bind phosphorylated ZAP-70 itself via its SH2-domain and LAT via its SH3-domain, and it has been suggested that it scaffolds a complex between ZAP-70 and its substrate

LAT [134]. Through the phosphorylation of LAT and SLP-76, ZAP-70 initiates the nucleation of an important signalling hub that coordinates a diverse array of signalling effects.

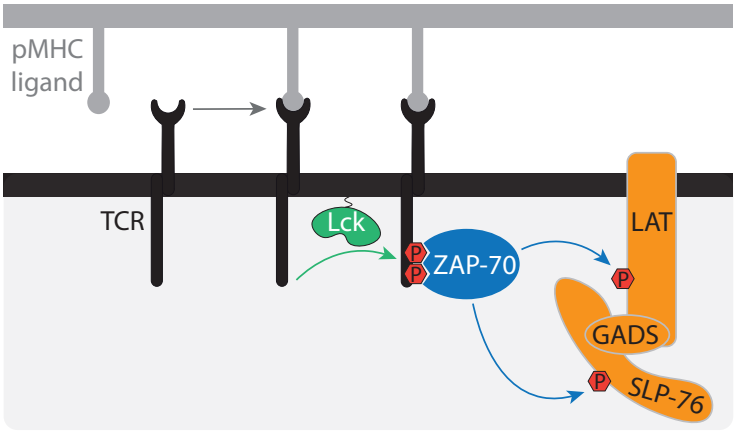


Figure 1.3: Lck and ZAP-70 transmit TCR signalling. The exact mechanism of TCR triggering is incompletely understood, but the Src-family kinase Lck and ZAP-70 critically relay TCR signals. ITAMs on CD3ζ are phosphorylated by Lck and subsequently recruit ZAP-70 via its tandem SH2-domain. ZAP-70 then phosphorylates tyrosine residues on LAT and SLP-76 and thereby activates the LAT-GADS-SLP-76 signalling hub.

The protein tyrosine phosphatase **SHP-1** negatively regulates TCR-proximal tyrosine phosphorylation. SHP-1 is recruited to ITIMs (Immunoreceptor Tyrosine-based Inhibition Motifs) on CD5 and PD-1, as well as LAT via Grb2 (Growth factor receptor-bound protein 2), but the precise spatiotemporal movements of SHP-1 are unclear [183]. The substrates for SHP-1 have not been conclusively identified, but SHP-1 knockout and overexpression studies suggest that it regulates TCR-proximal signalling [183], possibly by interacting directly with Lck and ZAP-70 [189, 234].

1.2.3 Signal diversification from the LAT-GADS-SLP-76 signalosome

LAT and SLP-76 are phosphorylated by ZAP-70 and together provide a large number of docking sites for kinases and adapters that mediate various downstream signalling pathways (Fig. 1.4). Binding partners for a total of 9 phosphotyrosines on LAT include

Vav1 (Vav guanine nucleotide exchange factor 1) and GADS (Grb2-related Adapter protein Downstream of Shc), an adapter-like protein that binds both LAT and SLP-76. The LAT-GADS-SLP-76-Vav1 complex then recruits ADAP (Adhesion- and Degranulation-promoting Adapter Protein), Cdc42 (Cell division control protein 42 homologue), PI3K (Phosphoinositide 3-Kinase) and PLCγ1 (Phospholipase C γ1) that initiate an increase in T cell adhesion to the target cell (Section 1.2.3.1), actin cytoskeletal rearrangement (Section 1.2.3.2), glucose metabolism (Section 1.2.3.3) and gene transcription programmes (Section 1.2.3.4). Although these pathways are here presented in a linear fashion, it is important to note that there is significant crosstalk, feedback and redundancy between them (Section 1.2.3.5).

1.2.3.1 ADAP-mediated changes in cell adhesion

Adhesion to APCs is important for the targeted delivery of T cell effector molecules and it is established by integrin receptors such as LFA-1 (Lymphocyte Function-associated Antigen-1). LFA-1 on T cells binds ICAM (Intercellular Adhesion Molecule) to both increase pMHC ligand-induced adhesion to target cells (inside-out signalling) and to transmit co-stimulatory signals (outside-in signalling) [166]. Inside-out LFA-1 signalling (Fig. 1.4) is initiated by ADAP coupled to SKAP55 (Src Kinase-Associated Phosphoprotein of 55 kDa). SKAP55 recruits RapL (Regulator of cell adhesion and polarisation enriched in Lymphoid tissues), which in turn interacts with the activated Ras superfamily GTPase Rap1 (Ras-related Protein 1) [108, 109]. The SKAP55-RapL-Rap1 complex then binds the α-chain of LFA-1 [108]. Active Rap1 is furthermore able to interact with RIAM (Rap1-GTP-Interacting Adapter Molecule) that forms a complex with the cytoskeletal protein talin and the β-chain of LFA-1. These multimolecular structures induce an affinity-enhancing conformational change in the LFA-1 ectodomain as well as clustering of LFA-1 [166, 200].

1.2.3.2 Cdc42-mediated changes in the actin cytoskeleton

Rearrangement of the actin cytoskeleton is required to form a stable interface with the APC once cognate pMHC has been detected. TCR triggering leads to the recruitment and

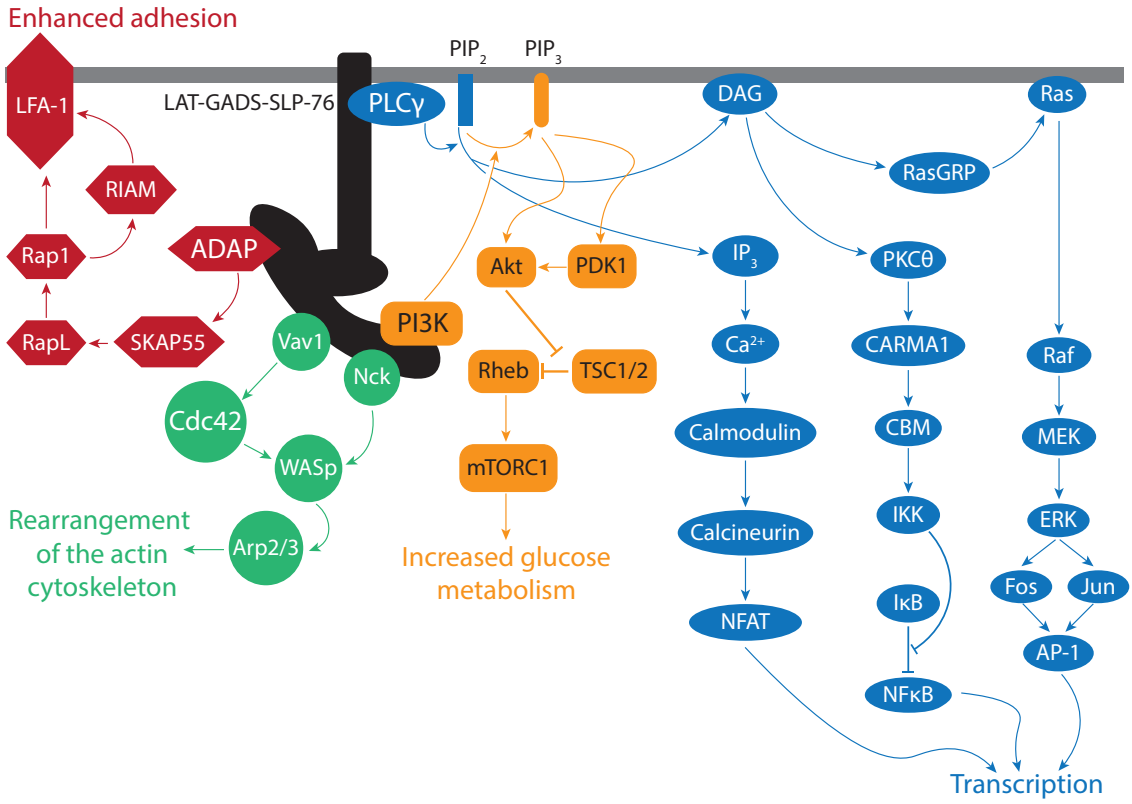


Figure 1.4: LAT-GADS-SLP-76 orchestrates changes in adhesion, actin cytoskeleton, metabolism and gene transcription. A large number of signalling molecules are recruited to the LAT-GADS-SLP-76 signalling hub that stimulates four major signalling branches (from left to right): ADAP mediates increased adhesion to target cells by inducing LFA-1 to adopt a high-affinity conformation (red), Cdc42 initiates rearrangement of the actin cytoskeleton by activating Arp2/3 (green), PI3K enhances glucose metabolism via mTORC1 (orange) and PLCγ signalling increases activity of the master transcription factors NFAT, NFκB and AP-1 (blue). Signalling branches are presented linearly for clarity, but significant redundancy, crosstalk and feedback loops exist between them (Section 1.2.3.5).

activation of the Rho-family GTPase Cdc42 by the SLP76-associated guanine nucleotide exchange factor Vav1 (Fig. 1.4) [13]. Nck (Non-Catalytic region of tyrosine Kinase adapter protein 1), also associated with SLP-67, recruits the actin nucleation-promoting factor WASp (Wiskott-Aldrich-syndrome protein). Once Cdc42 and WASp are brought into close proximity, Cdc42 induces a conformational change in WASp [119, 288] that allows it to interact with the nucleation factor Arp2/3. Arp2/3 then initiates actin polymerisation and cytoskeletal rearrangements.

1.2.3.3 PI3K/Akt-mediated changes in metabolism

To meet the energy demands of the T cell response, T cells switch from catabolic oxidative phosphorylation to anabolic metabolism and utilise aerobic glycolysis to obtain substrates required for the synthesis of mRNA and proteins [101, 181]. Glycolysis is enhanced by an increase in the expression of the glucose transporter Glut1 on the plasma membrane as well as several rate-limiting glycolytic enzymes [63, 73, 181]. PI3K is an important regulator in this pathway (Fig. 1.4). Once recruited to the LAT-GADS-SLP76 complex, it converts PIP_2 in the plasma membrane to PIP_3 [38]. PIP_3 subsequently recruits PDK1 (Phosphoinositide-Dependent protein Kinase 1) and its substrate the serine/threonine kinase Akt to the membrane via their PH-domains [38]. Active Akt then phosphorylates TSC1/2 (Tuberous sclerosis complex 1 and 2) and thereby hinders it from inhibiting the GTPase Rheb (Ras homologue in brain). Rheb, in turn, activates mTORC1 (mammalian Target Of Rapamycin Complex 1) [18, 96, 101]. The net result of mTORC1 activation is an increase in glucose uptake, expression of glycolytic enzymes and translational activity, but the exact mechanisms are incompletely understood [63, 212].

1.2.3.4 PLCγ-mediated changes in gene transcription

PLCγ plays a central role in activating the three master transcription factors of T cell activation (Fig. 1.4): NFAT (Nuclear Factor of Activated T cells), AP-1 (Activator protein 1) and NFκB (Nuclear Factor κ-light-chain-enhancer of activated B cells). PH-, SH2- and SH3-domains recruit PLCγ to the plasma membrane and the LAT-GADS-SLP76 complex and thus bring it into proximity of its substrate PIP_2 [13, 22, 280]. Hydrolysation of PIP_2 by PLCγ yields the diffusible messenger IP_3 (Inositol 1,4,5-triphosphate) and membrane-associated DAG (Diacylglycerol). IP_3 activates NFAT, whereas DAG activates NFκB via PKCθ (Protein Kinase C θ) and AP-1 via the Ras-ERK (Extracellular signal-Regulated Kinase) pathway. Together, these three master transcription factors regulate the transcription of important effector molecules, including IFNγ and IL-2.

IP_3 enables the nuclear translocation of cytosolic **NFAT** through an increase of intracellular calcium (Ca^{2+}) levels (Fig. 1.4). When IP_3 binds to receptors on the ER

(Endoplasmic Reticulum), it triggers the release of Ca^{2+} stores into the cytosol. Depletion of ER Ca^{2+} stores then causes the additional influx of Ca^{2+} from the extracellular space through the physical interaction of STIM1 (Stromal interaction molecule 1) oligomers on the ER with CRAC (Calcium Release-Activated Calcium channels) channels in the plasma membrane [262]. Cytosolic Ca^{2+} activates calmodulin (calcium-modulated protein), which in turn activates the serine/threonine phosphatase calcineurin to dephosphorylate NFAT thus unmasking a nuclear translocation motif that is in the resting state concealed [179]. In the nucleus, NFAT can pursue its role in transcription [140].

PKCθ recruited to the plasma membrane by DAG actuates **NFκB** (Fig. 1.4). In the resting state, NFκB associates with IκB (Inhibitor of κ B) that prevents nuclear translocalisation. PKCθ initiates degradation of IκB by phosphporylating the membrane scaffold CARMA1 (Caspase Recruitment Domain (CARD)-containing MAGUK protein 1) [151]. Phosphorylated CARMA1 nucleates the CBM complex with BCL10 (B-Cell Lymphoma 10) and MALT1 (Mucosa-Associated Lymphoid Tissue lymphoma translocation protein 1) [268], which then recruits and activates IKK (IκB Kinase) [267, 268]. As a result, IκB is phosphorylated by IKK, ubiquitinated and targeted for degradation. Active NFκB can then translocate into the nucleus and initiate transcription.

Finally, DAG stimulates synthesis and assembly of **AP-1** via the Ras-MAPK (Mitogen-Activated Protein Kinase) pathway (Fig. 1.4). The guanine nucleotide exchange factor RasGRP (Ras Guanyl-Releasing Protein) binds DAG and converts membrane-associated GDP-bound Ras into active RasGTP [67]. Active Ras then triggers the Raf-MEK-ERK three-kinase signalling cascade. ERK activates the AP-1 heterodimer subunit Jun and induces expression of the second AP-1 subunit Fos because, in contrast to NFAT and NFκB, activation of AP-1 requires the *de novo* synthesis of one of its constituents [222]. The completely assembled AP-1 heterodimer then initiates gene transcription in the nucleus.

1.2.3.5 Redundancy, crosstalk and feedback loops are characteristic of T cell signalling

A high level of redundancy, crosstalk and feedback exists within and between these signalling arms. PDK1, for example, enhances glucose metabolism in a PI3K-Akt-dependent (Section 1.2.3.3) and -independent manner, because the knockout of PI3K and Akt did not completely abrogate the TCR-mediated increase in glucose metabolism [63, 181]. In addition, PDK1 has been shown to be capable of activating PKCθ, thus establishing crosstalk with the PLCγ-mediated increase in NFκB transcriptional activity [181, 185]. Finally, LAT activates both positive and negative feedback loops: SOS (Son Of Sevenless) binds LAT via the adapter Grb2. It catalyses activation of Ras and its catalytic rate is increased by binding of active Ras to an allosteric pocket (positive feedback loop) [41]. LAT-Grb2 also recruits a complex consisting of DOK1/2 (Downstream of Kinase 1 and 2) and SHIP-1 (SH-2 containing inositol 5' polyphosphatase 1) that negatively regulate TCR-proximal (ZAP-70) and downstream (Akt) signalling (negative feedback) [52]. These examples illustrate the complexity of the T cell signalling network.

1.2.4 Post-transcriptional regulation

Gene transcription is required but not sufficient for the secretion of some cytokines such as IFNγ and IL-2 as cytokine secretion is furthermore regulated by post-transcriptional modifications that control the amount of protein produced (Fig. 1.5). Ligand-induced mTORC1 signalling enhances mRNA translation into protein by phosphorylation of S6K (ribosomal protein S6 kinase) and 4E-BP (Eukaryotic translation initiation factor 4E-binding protein) [63, 212]. In addition, TCR triggering has been shown to stabilise mRNA via multiple mechanisms. First, mRNAs in activated T cells contain shorter 3'-UTRs (Untranslated Regions), thus providing fewer binding sites for suppressive miRNA molecules that otherwise accelerate mRNA degradation [215]. Secondly, activated $CD8^+$ T cells have been found to express higher amounts of long non-coding RNA (lncRNA) that regulate mRNA stability by sequestering miRNA [80, 182]. Finally, TCR signalling leads to nuclear export of NF90 (Nuclear Factor 90) and HuR (Human antigen R)

that decorate AREs (AU-Rich Elements) in 3'-UTRs of, for example, IL-2, TNFα or IFNγ mRNA [223, 269]. It is not clear how binding of NF90 and HuR enhances mRNA stability, but it has been proposed that they compete with decay-inducing proteins or miRNA [209]. Despite increasing evidence for an important role of post-transcriptional modifications in the regulation of the T cell response, the precise underlying mechanisms remain incompletely understood.

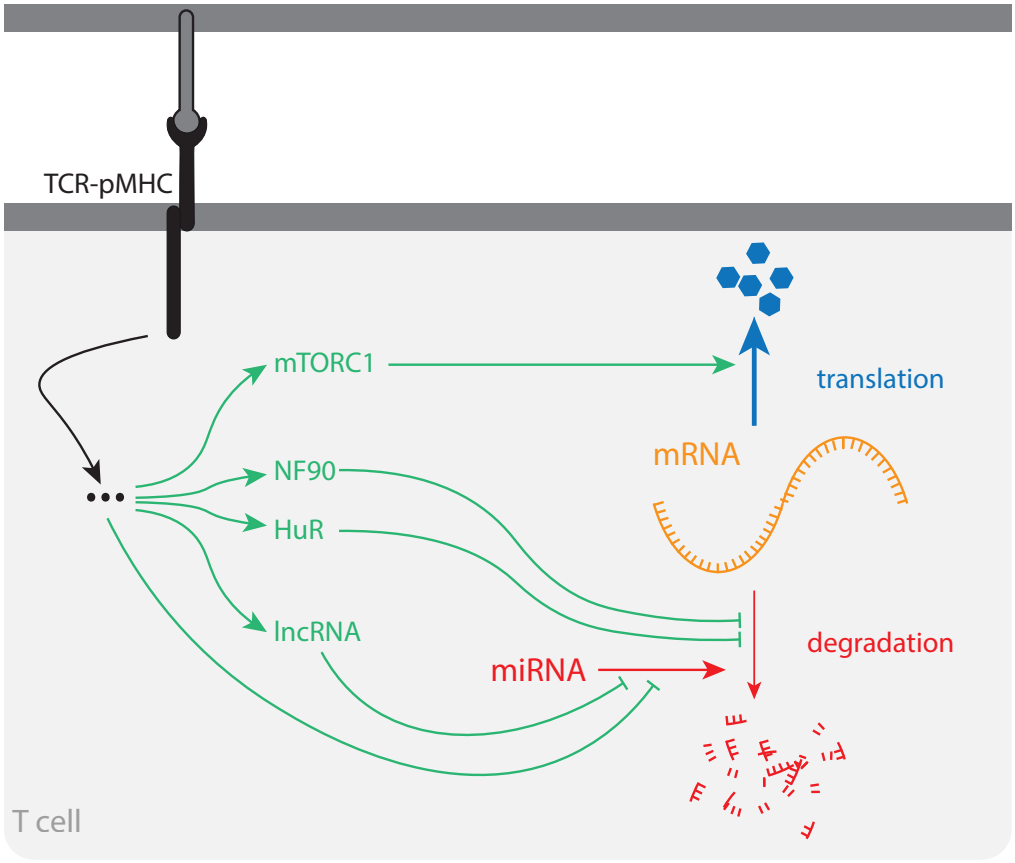


Figure 1.5: Post-transcriptional modification stabilise mRNA. TCR-mediated production of effector molecules (blue) is achieved by an increased translation rate via mTORC1 and by a decrease in the mRNA degradation rate: TCR signalling decreases the amount of suppressive miRNA that otherwise enhances mRNA degradation and leads to the expression of lncRNA to sequester miRNA. In addition, NF90 and HuR shield mRNA from binding to decay-inducing factors.

1.2.5 Effector functions

The successful execution of T cell effector functions and cytokine secretion in particular requires the coordinated integration of all signalling pathways to establish a stable contact with the target cell and to produce and deliver effector molecules.

1.2.5.1 The immunological synapse coordinates the targeted release of effector molecules

T cells are motile during their search for antigen, but halt and form a stable interface, the immunological synapse or SMAC (Supramolecular Activation Cluster), with a target cell within minutes after foreign pMHC has been detected. Formation of the SMAC requires, among others, the coordinated action of ADAP-SKAP55-mediated adhesion and Cdc42-WASp-Arp2/3-mediated remodelling of the actin cytoskeleton [104, 123]. The topology of the immunological synapse is variable [245], but a distinctive pattern of three concentric rings has frequently been observed: The distal dSMAC contains molecules with large ectodomains (e.g. CD45), the peripheral pSMAC contains adhesion molecules (e.g. LFA-1) and the central cSMAC contains activating molecules (e.g. TCR, Lck and PKCθ) [119]. TCR microclusters formed in the periphery of the immunological synapse move laterally into the cSMAC. Their movement is controlled by retrograde actin flow as well as the motor proteins actomyosin IIa and dynein [279, 283]. Interestingly, co-localisation of the TCR with the signalling molecules ZAP-70 and LAT occurs in the pSMAC [284] and movement into the cSMAC terminates the signal by the internalisation and subsequent degradation of the TCR [149, 260].

Concomitant reorientation of the Golgi apparatus and MTOC (Microtubule-Organising Centre) from the cell's uropod to the contact site polarises vesicular transport and secretion of effector molecules towards the target cell [198]. Important signalling molecules that lead to T cell activation (e.g. TCR [42, 61], Lck and LAT [197]) are delivered to the immunological synapse from distal and intracellular pools to enhance signalling. Spent TCRs in the cSMAC can be internalised and degraded, possibly together with pMHC from the target cell (trogocytosis) [149], or shed [33]. Components of the intraflagellar transport

system, Rabs (Ras-related proteins) and SNAREs (Soluble N-ethylmaleimide-sensitive factor Attachment Protein Receptors), direct molecular transport and allow for directional secretion of cytolytic granules [62, 180, 235], some cytokines [93, 94, 120] and vesicles containing suppressive factors such as miRNA or Fas ligand [62]. The immunological synapse is therefore a site of active vesicular traffic and intercellular communication.

1.2.5.2 TNFα, MIP-1β, IFNγ and IL-2 are important effector molecules secreted by CD8$^+$ T cells

The differential regulation of TNFα, MIP-1β, IFNγ and IL-2 in response to pMHC stimulation remains elusive. Expression of the cytokines TNFα and IFNγ, the interleukin IL-2 and the chemokine MIP-1β involves a complex interplay of transcription factors, including NFAT, AP-1 and NFκB that can bind some promoters cooperatively [139, 224, 230]. Cytokine/chemokine expression therefore marks a point at which multiple signalling arms converge. Post-transcriptional modifications and susceptibility to co-stimulation add complexity to the dynamics of cytokine and chemokine production. Once the cytokines and chemokines have been produced, they can be secreted. Secretion of the cytokines differs as IL-2 and IFNγ appear to be secreted in a directional, and TNFα in a non-directional manner [93, 94]. The overall mechanisms that control the timed production and secretion of these effector molecules are unclear.

It is reasonable to hypothesise differential regulation of TNFα, MIP-1β, IFNγ and IL-2 secretion because they have functionally distinct roles. **TNFα (Tumour Necrosis Factor α)** is important for the containment and clearance of, for example, viral infections. Secretion of TNFα is rapid as it relies on the translation of preformed mRNA [208]. It enhances the expression of adhesion molecules by endothelial cells to allow for the extravasation of immune cells from the blood and simultaneously induces them to initiate blood clotting to prevent spreading of the pathogen through the blood [168]. Binding of TNFα to TNFRI (TNF Receptor I) or TNFRII determines the effect of TNFα on other cells: TNFRI is ubiquitously expressed on all cell types and contains a death domain that induces apoptosis through the activation of caspases, whereas TNFRII is expressed on endothelial and immune cells, enhances gene transcription and has been associated

with anti-apoptotic signals [4]. Understanding the regulation of TNFα secretion is of therapeutic interest because systemic TNFα release can lead to shock, organ failure and eventually death, and pharmacological inhibition of TNFα with specific antibodies is used as a treatment against the autoimmune disease rheumatoid arthritis [4].

MIP-1β (Macrophage Inflammatory Protein-1β) is a chemoattractant secreted by $CD8^+$ T cells to amplify the immune response through the recruitment and activation of other immune cells. Secreted MIP-1β emanates from the translation of both preformed and newly synthesised mRNA [186]. It binds the receptor CCR5 (CC Chemokine Receptor 5) that is predominantly expressed on various immune cells and is often attributed a potentiating role in the T cell response because it, for example, stimulates cytokine production in macrophages. In a transgenic mouse model, however, MIP-1β was also critical for the recruitment of T_{regs}, and MIP-1β depletion resulted in autoimmune disease [24]. Finally, MIP-1β prevents HIV (Human Immunodeficiency Virus) entry into $CD4^+$ T cells by blocking chemokine receptors [195]. Its potentiating and regulatory role as well as its capacity to prevent HIV spreading make MIP-1β an interesting subject of study.

IFNγ (Interferon-γ) plays an especially important role during the clearance of viral infections. It is produced from both preformed and newly synthesised mRNA [174, 186, 208] and binds the IFN receptor that is expressed on several immune cells, including macrophages, T cells and B cells. IFNγ improves the quantity, quality and repertoire of peptides loaded onto MHC molecules by modifying MHC expression and the composition of the APC's proteasome [219]. It furthermore activates macrophages to increase their rates of phagocytosis and pinocytosis, and equips them with increased levels of lysosomal enzymes. Finally, IFNγ mediates the transition from an innate to the adaptive immune response by polarising $CD4^+$ T cell differentiation towards the type I helper T cell subset and by inducing class switching in B cells [219]. IFNγ-deficient transgenic mice are less resistant to bacterial, viral and parasitic pathogens, and knockout of the IFNγ receptor or neutralising antibodies against IFNγ impaired tumour control in a transgenic mouse model [193, 194].

IL-2 (Interleukin-2) is a growth factor and affects the differentiation of $CD8^+$

T cells into effector or memory T cells. IL-2 secretion requires *de novo* mRNA production and translation. The IL-2 receptor (IL-2R) is expressed predominantly on NK (Natural Killer) and T cells and has three known subunits (α, β, γ_c) that in different combinations alter the affinity of the receptor to IL-2. Activated T cells upregulate expression of the α subunit that enhances formation of the high-affinity $\alpha\beta\gamma_c$ receptor [230]. T_{regs}, on the contrary, constitutively express the high-affinity IL-2R. Studying the effect of IL-2 signalling-deficiency has been challenging because IL-2 affects functionally opposing cell types (effector T cells and T_{regs}) and because a knockout of the receptor inevitably has side-effects as the γ_c subunit is a shared component of multiple cytokine receptors. IL-2 signalling defects have thus been linked to both immunodeficiency and autoimmune disease [230].

In summary, the effector cytokines TNFα, MIP-1β, IFNγ and IL2 have diverse functions that collectively assist T cells to initiate and regulate adaptive immune responses.

1.3 Signal 2: Co-modulation of T cell signalling

Priming of naïve T cells to become effector T cells requires binding of cognate pMHC to the TCR (Signal 1) as well as additional co-stimulatory receptor-ligand interactions (Signal 2). This observation motivated the two-signal model of T cell activation, but it is now known that the engagement of a large number of receptors can enhance (e.g. CD28, 4-1BB) or limit (e.g. CTLA-4 (Cytotoxic T-Lymphocyte-Associated protein 4), PD-1 (Programmed Death protein 1)) the T cell response. The term *co-modulation* is thus used here to describe the sum of additional stimulatory and inhibitory receptor-ligand interactions that directly modulate the T cell response. Co-modulatory ligands are expressed on the surface of different cell types, but professional APCs are particularly important in delivering co-modulatory signals. Signalling through co-modulatory receptors is dynamically regulated as the density of co-modulatory receptors and their ligands on T cells and APCs, respectively, changes during the course of an immune response. 4-1BB and PD-1, for example, are expressed on effector T cells several hours after stimulation with pMHC [43]. The two-signal model does not capture the dynamics of co-modulation.

Zhu et al. [292] therefore proposed an alternative tidal model of co-modulation in which an early activating wave elicits a T cell response that is paralleled by the replacement of co-stimulatory receptors with co-inhibitory receptors and thus leads to signal termination. The exact sequence of events however is likely more complicated as the expression of both co-stimulatory (e.g. 4-1BB) and co-inhibitory (e.g. PD-1) receptors is upregulated during T cell activation. The timed combination of different co-modulatory receptor-ligand interactions determines the net effect of co-modulation [29]. Whereas the mechanisms underlying co-modulation have been studied for some co-modulatory receptors and their ligands individually, it is currently unclear how multiple receptor-ligand pairs integrate.

1.3.1 Mechanisms of co-modulation

The mechanisms of co-modulation are highly diverse and operate at different levels of TCR-mediated signalling. Signalling through the co-stimulatory receptor CD28, for example, integrates with TCR proximal signalling by providing docking sites for Lck [85], but also with downstream signalling, including the PI3K-Akt, Ras-ERK and PKCθ pathways [29, 199]. The co-inhibitory receptor PD-1 provides docking sites for phosphatases (e.g. SHP-1/2 [29, 285]) that impact TCR proximal signalling, enhances TCR downregulation by increasing expression of the E3 ubiquitin ligase Cbl-b [106] and it inhibits downstream signalling of the Ras-ERK pathway [184]. Interestingly, PD-1 has been reported to primarily inhibit CD28 signalling through tyrosine dephosphorylation [90], suggesting crosstalk between these two pathways. Other co-modulatory mechanisms include competition for ligands and receptors as a result of structural similarities between molecules that serve opposite functional outcomes. The co-inhibitory receptor CTLA-4, for example, binds the same B7 ligands as the co-stimulatory receptor CD28 [29]. Multiple modes of action therefore exist by which co-modulatory signals influence TCR-mediated signals.

1.3.2 Co-modulatory receptors and T cell unresponsiveness

Three distinct states of T cell unresponsiveness, anergy, adaptive tolerance and exhaustion, have been discussed in the context of peripheral tolerance (Section 1.1.2). Signalling

through co-modulatory receptors has been associated with induction and maintenance of at least two of these unresponsive T cell states, namely anergy and exhaustion. Sub-optimal stimulation of naïve T cells in the absence of co-stimulation through CD28 induces an anergic state that is characterised by inhibition of IL-2 secretion and proliferation [220]. T cell exhaustion correlates with increased expression of the co-inhibitory receptors PD-1 [14]. Blockade of PD-1 binding to its ligand reinvigorated T cells to resume effector functions [216, 272]. These examples illustrate that signalling through co-modulatory receptors can be both required or limiting for the execution of effector functions.

1.4 Signal 3: Modulation of T cell signalling by cytokines

The list of signals required for successful priming of T cells has furthermore been extended by cytokine receptor-mediated signalling (Signal 3). For $CD8^+$ T cells, the interleukin IL-12 and the type I interferons IFNα and IFNβ, in particular, provide important additional signals that enhance T cell survival and responsiveness, increase the efficiency of the T cell response and allow for the generation of a T cell memory pool [40]. Signal 3 cytokines are predominantly secreted by cells of the innate immune system, including dendritic cells, macrophages and neutrophils. Binding of these cytokines to their receptors on the surface of T cells causes epigenetic changes that induce chromatin remodelling. Greater accessibility to DNA results in the increased expression of genes encoding important effector molecules, such as granzymes and IFNγ, and transcription factors associated with T cell differentiation. Chromatin remodelling furthermore enables the T cell to respond more rapidly to stimulation during a secondary encounter with antigen (memory) [40]. Compared to T cells that only received Signals 1 and 2, T cells that also received Signal 3 during priming displayed altered expression of roughly 700 genes [40]. About 50% of the differentially regulated genes were not specific to the type of Signal 3 cytokine, consistent with the observation that IL-12 and IFNα/β had overlapping functional effects on T cell survival and memory generation *in vivo* when adoptively transferred transgenic

T cells were primed *in vitro* in the presence of either Signal 3 cytokine. The other half of differentially regulated genes were specific to the Signal 3 cytokine, suggesting that, despite a high level of redundancy, the precise cytokine milieu during priming of $CD8^+$ T cells can fine-tune the state of the T cell. The absence of Signal 3 cytokines during priming *in vitro* led to a more transient expression of certain effector molecules, reduced T cell responsiveness and deletion through T cell death after adoptive transfer into antigen-bearing transgenic mice [40].

1.5 Manipulating T cell signalling for immunotherapies

Several approaches have been devised to fight immune-related diseases by suppressing (in the case of e.g. autoimmune diseases) or enhancing (in the case of e.g. cancer) T cell responses. A major challenge is that most treatments perturb the balance between effective immunity and tolerance of self, and to avoid severe side effects as a result of non-specific interventions that globally suppress or activate the immune system, an active area of research focuses on the manipulation of specific pMHC recognition by T cells. One strategy to eradicate cancer involves equipping autologous T cells with engineered TCRs that recognise tumour-specific pMHC ligands. The MHCI-restricted 1G4 high-affinity (1G4Hi) TCR was developed in the clinic to recognise NY-ESO-$1_{157\text{-}165}$ cancer/testis peptide with picomolar therapeutic affinity (compared to the micromolar physiological regime). Transduced $CD8^+$ T cells lost peptide specificity because they cross-reacted with MHCI, but $CD4^+$ T cells transduced with the 1G4Hi TCR were capable of specifically eliminating tumour cells [289]. Alternatively, high-affinity TCRs fused to immunostimulatory CD3-specific single-chain antibody fragments can be used in soluble form to direct and activate T cells to tumour antigen-bearing cells [130]. Excessive immune responses and associated toxicities, however, remain a risk in immunotherapies, and a better understanding of T cell regulation is desirable for the improvement of current strategies.

1.6 Phenotypic modelling of T cell signalling

To understand how a pMHC input is translated into a functional response such as cytokine secretion, it is not feasible to model the whole signalling pathway in molecular detail. Mass spectrometry analyses of the phosphoproteome identified more than 10,000 unique phospho-sites in activated T cells [207, 242] and provide a scale of the T cell signalling network, of which not all components and interactions that connect the ligated TCR and the downstream response have been identified. While the identification of additional signalling intermediates enables the construction of increasingly detailed schematic models, the construction of predictive models is further complicated by the high uncertainty associated with the kinetic parameters that describe molecular interactions as they can rarely be determined accurately in a physiological setting. The effect of a given pMHC stimulus on the magnitude and quality of the T cell response can therefore not be deduced intuitively from current molecular models.

In the present study, a phenotypic modelling approach was used to better understand the functional T cell response to pMHC stimulation. The objective of phenotypic modelling is to identify a minimal model architecture that is capable of explaining the relation between a stimulus and an experimental phenotype without accommodating all known molecular detail. The T cell's signalling machinery is viewed as a black-box that converts a pMHC input into an appropriate functional output. The complexity of the phenotypic model that connects the pMHC input to the functional output adapts to the experimental data available, so that a phenotypic model consists of few coarse-grained signalling motifs that minimise the number of *a priori* assumptions about model topology and rate parameters. Although simplicity was unlikely the guiding principle in the evolution of the T cell (and other cellular) signalling networks, the overall signalling phenotype can be a useful description of the pathway and this approach has been applied successfully in other scientific disciplines [75, 173]. Fluid mechanics, for example, provides a valuable theoretical framework to describe and predict the flow of water without making any reference to its precise molecular makeup [173]. Similarly, phenotypic models can be used to gain mechanistic understanding of cellular signalling processes even if the molecular

mechanisms underlying these processes are incompletely understood and to formulate testable experimental predictions.

1.7 Fitting phenotypic models to experimental data by ABC-SMC

Outputs from mathematical models are often compared to experimental data by directly fitting the model to the data. But the determination of the model parameters that optimise agreement between model and data can be challenging. Prior knowledge of the model parameters is often limited. This is particularly true for phenotypic models because molecular processes are summarised into a coarse-grained representation of the underlying signalling machinery. Phenotypic model parameters are therefore conglomerates of multiple unspecified molecular steps that together perform a function in the T cell. Moreover, the larger a mathematical model, the more unlikely it is that parameter values can be determined independently, and the minimal structure of phenotypic models does not grant the independence of model parameters.

Here, an Approximate Bayesian Computation with Sequential Monte Carlo (ABC-SMC) approach was used to assess the agreement between the phenotypic model and an experimentally determined target phenotype. ABC-SMC is a computational method to estimate parameters in large dynamical models by approximating the posterior distribution on model parameters in a simulation-based procedure [250]. The algorithm does not locally optimise parameter values but instead allows for the global exploration of a predefined parameter space. ABC-SMC furthermore informs in an intuitive way on parameter sensitivity as well as correlations between model parameters that cannot be determined independently.

The ABC-SMC method is schematically illustrated in Fig. 1.6. Briefly, a large number of particles defined as a specific combination of parameter values are initialised uniformly in parameter space. The population of particles is then propagated through a series of iterations (t = 1,...,T), such that the parameter space with particles that produce the best

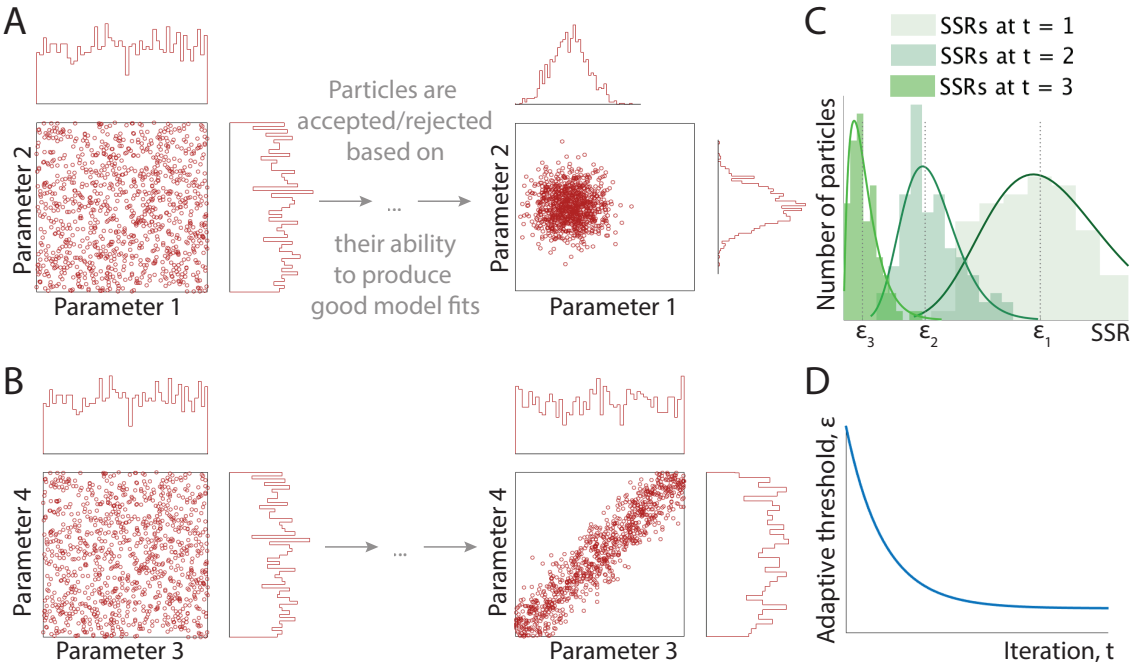


Figure 1.6: Schematic illustration of parameter fitting by ABC-SMC. **(A)** Particles, defined as combinations of specific parameter values, are initialised uniformly in parameter space. The population of particles is then propagated through a series of iterations such that the parameter space with particles that produce the best fits is preferentially explored. At each iteration, t, the goodness of the fit produced by a particle is quantified by the sum of squared residuals (SSR) between experimental data and the particle-specific model fit. **(B)** Schematic example of two correlated fit parameters. The visualisation of particle populations in parameter space provides an intuitive way to identify model parameters that cannot be determined independently (compare to well-defined parameters in (A)). **(C)** The population's median SSR at each iteration determines the adaptive threshold, ϵ_t. Particles with associated SSR above ϵ_t are rejected and particles with SSR below ϵ_t are propagated to the new iteration, t+1. As a result, the distribution over SSR tightens and **(D)** the adaptive threshold ϵ_t decreases with each iteration. The algorithm is described in detail in Methods Section 2.7.3 and a MATLAB (MathWorks, Inc.) implementation is included in Appendix B.2.

fits is preferentially explored (Fig. 1.6A). An increasingly stringent adaptive threshold, ϵ_t, is applied at each iteration so that only those particles which come closest to predicting the experimental data are propagated into the next iteration. The adaptive threshold was here defined as the population's median sum of squared residuals (SSR, Fig. 1.6C) and it tightens to improve the model fits as particle populations are passed through several iterations (Fig. 1.6D). Visualising particle populations in parameter space provides an intuitive way to identify model parameters that cannot be determined independently. Fig. 1.6C, for example, shows that Parameter 3 and Parameter 4 correlate heavily in this schematic example, while Parameter 1 and Parameter 2 (Fig. 1.6A) are well-defined. The algorithm is described in detail in Methods Section 2.7.3 and the MATLAB (MathWorks, Inc.) implementation is included in the Appendix Section B.2.

1.8 Summary of thesis

The aim of this thesis was to experimentally characterise and phenotypically model the translation of pMHC quality into a dynamic polyfunctional T cell response. For this purpose, a large dataset was generated by systematically stimulating T cells with dose titrations of pMHC variants that bind the TCR with different affinities. A coarse-graining phenotypic modelling approach was then employed to investigate how different signalling modules can mediate translation of pMHC stimulation into a cytokine response of the observed experimental phenotype. Interestingly, the cytokines TNFα, MIP-1β, IFNγ and IL-2 were produced only transiently and no grossly different model architectures had to be assumed to explain the signalling phenotype of all four cytokines.

Chapter 2: Materials and Methods. All reagents and protocols to experimentally study the T cell response to pMHC, as well as strategies for data averaging, analysis and fitting are summarised in this chapter.

Chapter 3: T cells limit their cytokine response to pMHC stimulation. The data in this chapter defines the signalling phenotype to be explained by the mathematical

model. $CD8^+$ primary human T cells were isolated from healthy donors, transduced with the 1G4 high-affinity TCR and expanded in culture. They were subsequently characterised according to standard differentiation markers. In functional experiments devoid of co-modulatory signals, these T cells displayed reduced TCR surface expression and only transiently secreted the four cytokines/chemokines TNFα, MIP-1β, IFNγ and IL-2 after 1–8 hours of stimulation. Interestingly, adapted T cells could be reinvigorated to respond with cytokine secretion if they were presented a pMHC of higher affinity.

Chapter 4: A phenotypic model explains adaptation at all pMHC doses with TCR downregulation. In this chapter, a phenotypic model is constructed based on known features of T cell signalling and fitted directly to the experimental data by ABC-SMC to confirm that the TCR downregulation model is sufficient to explain the experimental phenotype described in Chapter 3.

Chapter 5: Different cytokines are secreted by $CD8^+$ T cells with a similar threshold but a different rate. Cytokines have been suggested to obey readout-specific dose- and affinity thresholds that can grossly affect the quality of the T cell response depending on the pMHC stimulus. Interestingly, the dose-thresholds of TNFα, MIP-1β, IFNγ and IL-2 secretion were identical in our minimal experimental system and changes in pMHC affinity affected all cytokines equally. Large variations were, however, observed in the absolute amounts of cytokine secreted.

Chapter 6: General discussion. The experimental and modelling results were integrated with other studies investigating the molecular mechanisms of adaptation *in vitro* and *in vivo*. The relevance of TCR downregulation for CAR immunotherapies is discussed and a conceptual model that reconciles the presented data on surprisingly similar signalling phenotypes for four key cytokines with the versatility of the T cell response observed in more physiological contexts is proposed.

CHAPTER 2

Materials and methods

The 1G4 high-affinity TCR (Section 2.1) that recognises NY-ESO-$1_{157\text{-}165}$ peptide (Section 2.2) was used to systematically investigate the effects of pMHC dose and affinity on the magnitude and quality of the T cell response. Affinity measurements between TCR and pMHC were obtained by Surface Plasmon Resonance (SPR, Section 2.3). The TCR was transduced into T cells (Section 2.4) that were characterised according to standard differentiation markers (Section 2.5) and stimulated for functional experiments (Section 2.6). Recipes for buffers that were used for the experiments presented here are provided in Table 2.1 and all relevant antibodies are listed in Table 2.2. Data averaging and mathematical modelling are described in Section 2.7.

2.1 The 1G4 high-affinity TCR

The c58c61 1G4 high-affinity (1G4Hi) TCR was provided by Adaptimmune Therapeutics plc. It was developed for therapeutic use and recognises the cancer testis peptide NY-ESO-$1_{157\text{-}165}$ (SLLMWITQV) presented by HLA-A*02:01 with high picomolar affinity [129]. The TCR was used in soluble form for affinity measurements by surface plasmon resonance (SPR, Section 2.1.1). For functional experiments, $CD8^+$ primary T cells were lentivirally transduced with the receptor (Section 2.1.2).

Buffer	Recipe
HBS-EP	10 mM HEPES (pH 7.4), 150 mM NaCl, 3 mM EDTA, 0.005% P20 surfactant
TCR refolding buffer	150 mM Tris (pH 8.0), 200 mM L-arginine, 3 M Urea, 1.5 mM Glutathione (reduced), 0.15 mM Glutathione (oxidised), 0.5 mM PMSF
TCR dialysis buffer	10 mM Tris (pH 8.5), deionised H_2O
Low-salt buffer	10 mM NaCl, 10 mM Tris
High-salt buffer	1 M NaCl, 10 mM Tris
pMHC refolding buffer	100 mM Tris (pH 8.0), 400 mM L-arginine hydrochloride, 2 mM EDTA, 5 mM Glutathione (reduced), 0.5 mM Glutathione (oxidised), 0.1 mM PMSF, deionised H_2O
HEK293T cell culture medium	DMEM, 10% FBS, 1% PenStrep
Serum-free HEK293T cell medium	DMEM, 1% PenStrep
RPMI culture medium	RPMI, 10% FBS, 1% PenStrep, 50 U/ml IL-2
DMEM culture medium	DMEM, 10% FBS, 1% PenStrep, 50 U/ml IL-2
Staining buffer	PBS, 2% FBS, 2mM EDTA
Washing buffer (plates)	PBS, 0.05% TWEEN-20®

Table 2.1: Buffer recipes. HEPES: 4-(2-hydroxyethyl)-1-piperazineethanesulfonic acid; NaCl: Sodium chloride; EDTA: Ethylenediaminetetraacetic acid; P20: Polysorbate 20; Tris: tris(hydroxymethyl)aminomethane; PMSF: phenylmethylsulfonyl fluoride; PenStrep: Penicillin Streptomycin mixture; DMEM: Dulbecco's Modified Eagle Medium; RPMI: Roswell Park Memorial Institute; FBS: Fetal bovine serum; PBS: Phosphate-buffered saline

2.1.1 Production of soluble TCR for affinity measurements

Soluble 1G4Hi TCR was produced as described previously [6, 19, 127]. The α- and β-subunits were expressed independently in *Escherichia coli* (*E. coli*) and refolded *in vitro* at a 1:1 ratio in refolding buffer at 4°C . After 1 hour of stirring, the refold mixture was purified by dialysis for a total of 84 hours. Protein precipitates were removed by filtration and the TCR refold was concentrated by anion exchange chromatography through a HiTrap® Q HP column (GE Healthcare). A high-salt buffer eluted the TCR from the column, and fractions with successfully refolded TCR were pooled and concentrated

Target	Fluorophore	Clone	Manufacturer	Cat. #
HLA-A2	FITC	BB7.2	Santa Cruz Biotechnology	sc-32236-FITC
HLA-A,B,C	-	W6/32	BioLegend	311402
LI-COR IRDye goat anti-mouse IgG	680RD		LI-COR Biosciences	926-68070
Fas (CD95)	AF647	DX2	BioLegend	305618
CD45RA	APC	HI100	BioLegend	304150
CD69	PerCP	FN50	BioLegend	310928
IL-7Rα (CD127)	AF488	A019D5	BioLegend	351314
4-1BB (CD137)	AF647	4B4-1	BioLegend	309824
CCR7 (CD197)	BV421	G043H7	BioLegend	353208
TNFα	PE	MAb11	BioLegend	502909
IFNγ	AF647	4S.B3	BioLegend	502516

Table 2.2: List of antibodies. APC: Allophycocyanin; BV: Brilliant Violet™; FITC: Fluorescein; PE: R-phycoerythrin; PerCP: Peridinin chlorophyll; AF: Alexa Fluor®

further using a 30,000 kDa Centricon® centrifugal filter. Finally, the TCR refold was purified by size-exclusion chromatography through a Superdex™ 75 10/300 GL column (GE Healthcare).

2.1.2 Production of lentiviral particles for transduction

For transduction of roughly 1×10^6 T cells, 6×10^5 HEK293T cells were seeded on a cell-culture plate in 3 ml of culture medium and left in the incubator at 37°C and 10% CO_2 overnight resulting in 60–80% confluency the following day. The volume was then carefully reduced to about 2 ml without perturbing the adherent cells. A mixture of lentiviral transfer vectors and packaging plasmids (0.95 µg pRSV-Rev, 0.95 µg pMDLg/pRRE, 0.37 µg pMD2.G and 0.8 µg pLenti containing the TCR construct) was prepared in 200 µl serum-free medium. The third-generation packaging lentivirus and packaging system were obtain from Adaptimmune Therapeutics plc. 9 µl X-tremeGENE™ 9 (Sigma-

Aldrich) transfection reagent were added to the mixture, which was then incubated at room temperature for 15–20 minutes. The transfection mixture was slowly added to HEK293T cells and cells were returned to the incubator. The supernatant containing the viral particles was harvested and filtered (0.45 μm filter) 24 hours after transfection. The virus suspension was then added to the $CD8^+$ primary T cell culture for transduction of the 1G4Hi TCR. Production of lentiviral particles and T cell transduction were routinely performed by John Nguyen.

2.2 NY-ESO-$1_{157\text{-}165}$ pMHC variants

A panel of NY-ESO-$1_{157\text{-}165}$ pMHC variants that bind the 1G4Hi TCR with different affinities were previously designed in our lab by introducing amino acid substitutions that mainly changed the binding off-rate (Table 5.1) [126, 131]. Peptide loading to MHC was not affected by these substitutions. The altered peptide ligands were produced by GenScript (USA) with high purity (> 95%). Peptides were refolded with MHC in our laboratory (Section 2.2.1) for affinity measurements and T cell stimulation experiments. Soluble fluorophore-conjugated pMHC ligands were used to detect the 1G4Hi TCR on T cells (Section 2.2.2).

2.2.1 Production of biotinylated pMHC ligand

Biotinylated pMHC ligands were produced as described elsewhere [6, 126, 127]. HLA-A*02:01 heavy chain (residues 1–278) with a BirA tag on the C-terminus for biotinylation and β_2-microglobulin (β_{2M}) were expressed independently in *E. coli* and subsequently refolded with peptide *in vitro*. For this purpose, 20 mg of peptide dissolved in DMSO to a concentration of 10 $\frac{mg}{ml}$ was added dropwise to filtered refolding buffer at 4°C to a final concentration of 10 μM. Next, the serine protease inhibitor phenylmethane sulfonyl fluoride (PMSF) was added at a 1 in 1000 dilution (final concentration: 0.1 mM) before adding 52 mg β_{2M} (final concentration: 2 μM) and 64 mg MHC heavy-chain (final concentration: 1 μM). The refold was left at 4°C for 40 hours and stirred continuously. The refold solution was filtered (0.45 μm filter) and concentrated through a Centricon® Plus-

70 (Merck Millipore). The concentrated pMHC solution was topped up to 700 µl with 10mM Tris buffer (pH 8.0) before biotinylation. 100 µl of the biotin-protein ligase buffers Biomix A and B as well as biotin (Avidity) were added (1 ml final volume). The mixture was complemented with the protease inhibitors pepstatin, leupeptin and PMSF at a 1 in 1000 dilution. After addition of 3 µl BirA enzyme (Avidity), the refold was left overnight at room temperature. Biotinylated pMHC was then filtered through a Spin-X® (Sigma) centrifuge tube and purified by size-exclusion chromatograph with a Superdex™ 75 10/300 GL (GE Healthcare). Aliquots of pMHC refolds were stored at -80°C and not kept for longer than 6 months. pMHC production was initially performed by Philipp Kruger, John Nguyen and Nicola Trendel, but is now routinely done by Mikhail Kutuzov.

2.2.2 Production of PE-conjugated pMHC tetramers

PE-conjugated pMHC tetramers were produced by adding 10 µl PE-conjugated streptavidin (AbD Serotec) in 10 min intervals (100 µl in total) to 66.6 µg of biotinylated 9V-HLA-A2 monomers. The mixture was kept on a shaker at room temperature for the duration of the process. pMHC tetramers were stored in the dark at 4°C .

2.3 Affinity measurements by SPR

Affinities between the 1G4Hi TCR and various NY-ESO-$1_{157\text{-}165}$ pMHC mutants were determined by Surface Plasmon Resonance (SPR) on the Biacore 3000 (GE Healthcare) as described elsewhere [6, 126, 131]. Experiments were performed at 37°C and with HBS-EP as the running buffer. pMHC ligands were immobilised on CM5 sensor chips (GE Healthcare) using an amine coupling kit (GE Healthcare) following the manufacturer's instructions. Briefly, the carboxymethylated dextran matrix was activated with a mixture of 1-Ethyl-3-(3-dimethylaminopropyl) carbodiimide hydrochloride (EDC) and N-Hydroxysuccinimide (NHS) to generate reactive succinimide esters. Streptavidin was then injected and covalently coupled to the dextran matrix by reaction with esters on the chip. Biotinylated pMHC (1–5 $\frac{\mu g}{ml}$) were immobilised on the chip to about 250 RU

and uncoupled streptavidin binding sites were blocked by injection of biotin. Dilutions of soluble 1G4Hi TCR were sequentially flowed over immobilised pMHC at a rate of 10–30 $\frac{\mu l}{min}$ and at a starting concentration of ideally 1–10× the pMHC dissociation constant, $K_D = \frac{k_{off}}{k_{on}}$. The K_D was extract by fitting a saturating binding curve to the equilibrium binding RU as function of TCR dose in Prism 7 (GraphPad Software, Inc.):

$$Y = \frac{B_{max}X}{K_D + X}$$

where X is the dose of TCR, Y is the binding measurement in RU and B_{max} is the saturated binding RU.

2.4 T cells

2.4.1 Jurkat T cells

The E6.1 Jurkat T cell line was previously generated as described [127] and expressed the 1G4Hi TCR, CD8α and a NFAT/AP-1-luciferase reporter. Jurkat T cells were cultured at 37°C and 10% CO_2 in Dulbecco's Modified Eagle Medium (DMEM) supplemented with 10% FBS and 1% PenStrep at a density of 10^6 $\frac{cells}{ml}$. Stimulation of Jurkat T cells was performed analogously to stimulation of primary human T cells except that the duration of the experiment was extended from 8 to 10 hours.

2.4.2 Primary human T cells

$CD8^+$ primary human T cells were isolated from NC24 leukocyte cones (~3×10^5 $\frac{T\ cells}{ml}$) provided by the Blood service at the John Radcliffe Hospital or from fresh whole blood (~1×10^5 $\frac{T\ cells}{ml}$) donated by healthy individuals. All studies involving human T cells were performed with ethical compliance and approval from the Central University's Research Ethics Committee (CUREC reference number: R51997/RE001, University of Oxford, Oxford, UK). The following standard protocol was used to prepare T cell populations for phenotyping and functional stimulation experiments.

Day 0 HLA-typing, $CD8^+$ T cell isolation and αCD3/αCD28 prestimulation

Day 1 Lentiviral transduction of T cells with the 1G4Hi TCR

Day 6 Removal of αCD3/αCD28 stimulation beads

Day 10+ $CD8^+$ T cells can be used for experiments

HLA-typing

Because the 1G4Hi TCR crossreacts with HLA-A2 [243], only HLA-$A2^-$ donors were suitable for the experiments. For determination of the HLA type, a small sample of whole blood or leukocyte cone blood was incubated with 1 ml Red Blood Cell Lysing Buffer Hybri-Max™ (Sigma) for 5 min at room temperature. The sample was spun down (5 min at 350×g) and the supernatant was discarded. Cells were then resuspended in staining buffer containing a FITC-conjugated antibody against HLA-A2. HLA-A2 expression was measured by flow cytometry.

Isolation of $CD8^+$ T cells

RosetteSep™ Human $CD8^+$ T Cell Enrichment Cocktail (STEMCELL Technologies Inc.) was used to isolate $CD8^+$ T cells according to the manufacturer's instructions. Briefly, 6 $\frac{\mu l}{ml}$ or 150 $\frac{\mu l}{ml}$ of the provided enrichment cocktail were added to 50 ml whole blood or 1–2 ml of the leukocyte cone, respectively, before diluting the sample 1:1 with Phosphate Buffered Saline (PBS) and separating $CD8^+$ T cells from all unwanted and antibody-crosslinked cells by density gradient centrifugation. For this purpose, the sample was placed on top of the density gradient medium Ficoll® Paque and spun at 400×g for 30 min without deceleration. Enriched $CD8^+$ T cells were recovered from the buffy coat and washed twice with PBS.

Expansion, transduction and culture

T cells were resuspended in pre-warmed RPMI (Roswell Park Memorial Institute) culture medium at a density of 10^6 $\frac{cells}{ml}$. Magnetic αCD3/αCD28-coated beads (Gibco® Dynabeads® Human T-Activator CD3/CD28, Thermo Fisher Scientific) were used to

activate and expand the T cell populations following the manufacturer's protocol. 20 µl of 40 $\times 10^6$ $\frac{\text{beads}}{\text{ml}}$ bead suspension were added to 10^6 T cells to achieve a ratio of roughly 0.8 beads per T cell. Activated T cells were lentivirally transduced by adding 1 ml of virus suspension (Section 2.1.2) on day 1 after isolation. Stimulation beads were removed on day 6 after isolation by placing the sample on a magnet for 1–2 min and collecting the cell suspension containing only $CD8^+$ T cells. T cells were counted every 2 days and maintained at a density of 10^6 $\frac{\text{T cells}}{\text{ml}}$ in RPMI culture media at 37°C and 5% CO_2.

2.5 Characterisation of T cell differentiation states

To compare the *ex vivo* differentiation of T cells that were naïve or antigen-experienced on the day of isolation, $CD8^+$ T cells were split into three parts prior to stimulation with αCD3/αCD28-coated beads. One part was enriched for naïve T cells and one for memory T cells using the EasySep™ Human Naïve $CD8^+$ T Cell Enrichment Kit and EasySep™ Human Memory $CD8^+$ T Cell Enrichment Kit (STEMCELL Technologies), respectively, following the manufacturer's instructions. Briefly, 50 µl of Enrichment Cocktail and 50 µl of CD45RO depletion Cocktail (only for enrichment of naïve T cells) were added to 1 ml of complete $CD8^+$ T cells to crosslink unwanted cells. After 30 min incubation at room temperature, magnetic particles that bind unwanted cells were added and incubated with the sample for 10 min. The sample was then diluted with PBS containing 2% FBS and 1 mM EDTA and the enriched cell suspension was collected by magnetic separation (2 × 5 min in EasySep™ Magnet). The differentiation state of the T cells was determined on the day of isolation, various time points during expansion and transduction and when T cells were ready to use for functional experiments. For this purpose, 100,000 T cells were taken directly from T cell culture and labelled with staining buffer containing fluorophore-conjugated antibodies against the differentiation markers CCR7, CD45RA and Fas for flow cytometric analysis (see Section 2.6.5).

2.6 Functional T cell stimulation experiments

2.6.1 Preparation of stimulation plates

Pierce™ Streptavidin-coated High Capacity 96-well-plates (Thermo Fisher Scientific) were washed once with 200 $\frac{\mu l}{well}$ PBS while pMHC was thawed at room temperature. 50 µl of in PBS serially diluted pMHC (top concentration 40 $\frac{\mu g}{ml}$) were added to the respective wells and incubated overnight at 4°C. Plates with the immobilised pMHC were washed twice with 200 $\frac{\mu l}{well}$ and blotted on absorbent paper after each washing step prior to the addition of T cells.

2.6.2 Immobilisation control

To correct for differences in the concentration of correctly refolded pMHC in different batches of pMHC refolds, plates were prepared in duplicates whenever an experiment involved more than one pMHC. A conformation-sensitive mouse anti-human HLA primary antibody (clone W6/32, BioLegend) was added to each well (50 µl at a 1 in 500 dilution) and incubated at room temperature for 30 min. The plate was then washed three times with 300 $\frac{\mu l}{well}$ PBS washing buffer. Next, 100 $\frac{\mu l}{well}$ of the IRDye® goat anti-mouse secondary antibody (LI-COR Biosciences) were added to each well at a 1 in 5000 dilution and incubated for 45–60 min in the dark at room temperature. The plate was washed three times with 300 $\frac{\mu l}{well}$ PBS washing buffer and analysed on an Odyssey® Infrared Imaging system (LI-COR Biosciences).

The fluorescence for each well as a function of the target pMHC dose was fitted with a Hill function of slope 1 (Equation 2.1) to obtain the EC_{50} for each immobilised pMHC. The x-axis (pMHC dose) was then corrected for each pMHC relative to an index pMHC immobilisation according to the difference between their binding potency (Equation 2.2):

$$Y = Y_0 + \frac{(Y_{max} - Y_0)}{1 + 10^{\log(EC_{50}) - X}} \tag{2.1}$$

$$\log([pMHC]_j)^i_{corrected} = \log([pMHC]_j)^i + \left(\log(EC_{50})^{index} - \log(EC_{50})^i\right) \tag{2.2}$$

where i denotes the pMHC whose x-axis is being corrected and j indexes the pMHC dose. $\log(EC_{50})^{index}$ is the EC_{50} of the index pMHC that is used for normalisation. See Figure 2.1 for an example.

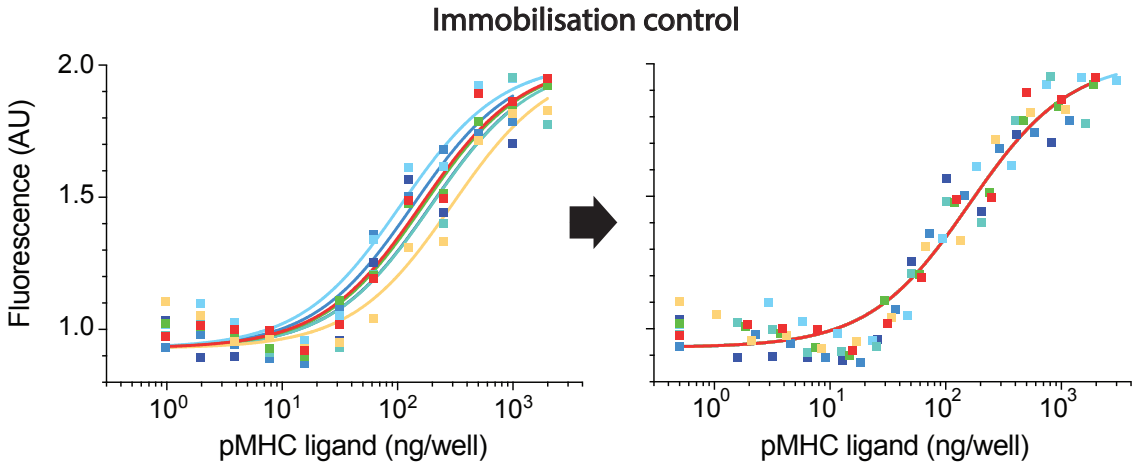


Figure 2.1: Example of immobilisation control. When a panel of pMHC mutants was used to stimulate T cells and responses elicited by different pMHCs were directly compared, variations in the immobilisation of pMHC mutants were corrected for by including an immobilisation control on a duplicate stimulation plate. The amount of correctly refolded pMHC immobilised on the plate was detected by labelling HLA-A2 with a conformation-sensitive primary antibody and a fluorophore-conjugated secondary antibody. Colours in this example correspond to different pMHC ligands. Variations in the amount of pMHC were corrected for by adjusting the x-axis relative to an index pMHC (Equation 2.2).

2.6.3 T cell stimulation protocols

T cells were diluted to a density of 10^6 $\frac{cells}{ml}$ on the day before the experiment. For all stimulation experiments, ~50,000 T cells were added to each well (irrespective of 1G4Hi transduction efficiency) in a volume of 200 µl of fresh pre-warmed RPMI (primary T cells) or DMEM (Jurkat T cells) supplemented with 10% FBS and 1% PenStrep. Stimulation plates were gently spun down at room temperature to initiate conjugation between T cells and plate-immobilised pMHC. The stimulation plates were then left in the incubator at 37°C and 5% CO_2 until measurements were performed.

2.6.3.1 TCR and cytokine production time course

T cells were stimulated with a titration of either a high- (9V) or a low-affinity (4A8K) pMHC (8 replicates) as described for 1–8 hours. Time courses measurements of supernatant or intracellular cytokine were performed as separate experiments. At each time point, the plate was briefly removed from the incubator to transfer one replicate of stimulated T cells and supernatant from the stimulation plate to a V-bottom plate for further analysis. For intracellular cytokine staining, Brefeldin A (BioLegend) was added to the media 1 hour before the response was measured to prevent cytokine secretion. T cells were spun down at 4°C to separate them from the supernatant. Pellets containing the T cells were prepared for analysis by flow cytometry whereas supernatants were used for ELISA.

2.6.3.2 TCR recovery

T cells were stimulated with a titration of the 8K pMHC (6 replicates) in the presence or absence of 50 $\frac{\text{U}}{\text{ml}}$ of recombinant IL-2. After 4 hours of stimulation, T cells stimulated in the presence and T cells stimulated in the absence of IL-2 (one replicate each) were separated from the supernatant by centrifugation at 4°C and analysed for TCR expression by fluorescent staining and flow cytometry. Meanwhile, the remaining replicates were transferred to a tissue culture plate without pMHC stimulus and returned to the incubator. After an additional 4 and 20 hours, T cells were harvested and analysed for TCR re-expression by fluorescent labelling and flow cytometry.

2.6.3.3 Inhibition of TCR signalling by Src-family kinase inhibitors

A titration of the 4A8K pMHC ligand was prepared and immobilised on the stimulation plate in duplicates. T cells were resuspended in media either with or without 300–500 nM of the A-770041 Lck inhibitor [232] and added to the pMHC stimulation plate. T cells were separated from the supernatant by centrifugation at 4°C after 4 hours of stimulation and analysed for TCR expression by fluorescent staining and flow cytometry.

2.6.3.4 Stimulation experiments with a panel of pMHC variants

T cells were stimulated with a titration of different pMHC ligands (7–8 variants) immobilised on the stimulation plate as described. After 8 hours of stimulation at 37°C and 5% CO_2, the supernatant was separated from T cells by centrifugation at 4°C and the concentration of cytokines and chemokines in the supernatant was determined by ELISA.

2.6.4 Enzyme-Linked Immunosorbent Assay (ELISA)

The cytokines TNFα, MIP-1β, IFNγ, IL-2 and IL-8 were measured in the supernatant using ELISA Ready-SET-Go!™ Kits (invitrogen, Thermo Fisher Scientific) following the manufacturer's instructions. Briefly, Nunc MaxiSorp® flat-bottom ELISA plates were coated with a capture antibody overnight at 4°C. ELISA plates were washed thoroughly and blocked with ELISA diluent for 1 hour at room temperature to prevent unspecific binding. Supernatant samples were added to the ELISA plate at a 1 in 10 dilution unless otherwise stated to bind the cytokine of interest. In addition, a known concentration of the cytokine was serially diluted to obtain 8 standard concentrations for reference on each ELISA plate. The plate was sealed and incubated at 4°C overnight, washed and then coated with detection antibody to label plate-bound cytokines. After 1 hour incubation at room temperature, ELISA plates were washed thoroughly and incubated with Avidin-conjugated HRP (Horseradish peroxidase) at room temperature for 30 minutes. Plates were then soaked and flushed to remove any unbound Avidin-HRP. The HRP-substrate TMB (3,3',5,5'-Tetramethylbenzidine) was added to the wells until the colouring of the well contents appeared blue. 2 N sulfuric acid was used to stop the enzymatic reaction. ELISA plates were analysed on the SpectraMax® M5 reader (Molecular Devices), and cytokine concentration was calculated using the fitted standard curve as a reference.

2.6.5 Flow cytometry

All flow cytometry experiments were performed on the DxP Athena™ 8 (Cytek), BD FACSCalibur™ (BD Biosciences), MACSQuant® Analyzer 10 (Miltenyi Biotec) or BD LSRFortessa™ X-20 (BD Biosciences). The running buffer was PBS and all data was analysed

in the FlowJo™ 10 analysis software. Possible spillover between fluorophores into other detection channels was corrected for when T cells were stained with more than one colour at the same time. For this purpose, single-stained T cell samples or compensation beads (MACS® anti-mouse IgGκ Compensation Bead Kit, Miltenyi Biotec) were analysed to quantify spillover. Data collected on the BD LSRFortessa™ X-20 (BD Biosciences) was compensated automatically after the single-stained compensation bead samples were collected. Otherwise, the compensation matrix was created with the compensation tool in the FlowJo™ 10 analysis software (FlowJo, LLC) and applied after data collection.

2.6.5.1 Staining of cell surface markers

Fluorescently-labelled antibodies (see Table 2.2) or PE-conjugated pMHC tetramers (Section 2.2.2) were diluted 1 in 200 in ice-cold staining buffer to label T cell surface markers and the 1G4Hi TCR. Antibody and pMHC tetramer concentrations were not measured directly. Instead, optimal antibody and pMHC tetramer dilutions were determined by testing serial dilutions of antibodies/tetramers in solution and selecting the dilution with the best signal-to-noise ratio. T cell pellets were then resuspended in 50 µl of the staining dilution and incubated at 4°C in the dark for 30–60 minutes. Samples were washed twice with ice-cold PBS and resuspended in 50 µl PBS for flow cytometry.

2.6.5.2 Intracellular cytokine staining

For intracellular cytokine staining, T cells were fixed and permeabilised using the BD Cytofix/Cytoperm™ Fixation/Permeabilization Kit (BD Biosciences). Briefly, T cells were resuspended in the Fixation/Permeabilisation solution at 4°C for 20 minutes and washed twice in BD Perm/Wash™ (BD Biosciences) buffer. T cells were then resuspended in the staining solution containing fluorescently-labelled antibodies for 30 minutes at 4°C and washed twice in PBS. The stained sample was resuspended in PBS for flow cytometric analysis.

2.7 Mathematical modelling

Mathematical models were described as systems of coupled Ordinary Differential Equations (ODEs) and evaluated in MATLAB (MathWorks, Inc.) using the in-built *ode15s* ODE solver. Model predictions were directly compared to averaged experimental data and model parameters were estimated by the MATLAB (MathWorks, Inc.) function *lsqcurvefit* (only the basal upregulation rate, k_{syn}) or Approximate Bayesian Computation with Sequential Monte Carlo (ABC-SMC).

2.7.1 Averaging of experimental data

Time course experiments. The amplitudes of the functional cytokine data and TCR downregulation were normalised and subsequently averaged over multiple independent experimental repeats. Cytokine data were normalised to the maximum level of cytokine after 8 hours of stimulation with different doses of the 9V (N = 3) or 4A8K pMHC (N = 3). The geometric mean fluorescence intensity (gMFI) of TCR expression after stimulation with the 9V (N = 2) or 4A8K (N = 5) pMHC were normalised to the gMFI of unstimulated T cells after background fluorescence was subtracted to account for variations in flow cytometer settings and differences in the TCR transduction levels between experiments.

Transfer experiments. Cytokine levels in transfer experiments were normalised to the maximum cytokine level after stimulation with different doses of 9V pMHC for 5 hours. Data were then averaged directly over 3 independent experimental repeats. TCR levels were normalised to the unstimulated control after subtraction of background fluorescence as described in the previous paragraph.

TCR re-expression experiments. Data were averaged by normalising both the amplitude and EC_{50} of the TCR dose-response curves. For each experimental repeat, a Hill function was fitted to TCR dose-response curves in Prism 7 (GraphPad). Within each experimental repeat, TCR re-expression was normalised relative to the fitted upper and lower plateau of the dose-response curve resulting from pre-stimulation of T cells for 4 hours. Across experimental repeats, the EC_{50}s of the pre-stimulation dose-response

curves were aligned by normalising the x-axis to a representative repeat according to Equation 2.2. The correction accounts for repeat-specific differences in the pMHC immobilisation as well as possible donor-specific signalling changes that affect the potency of TCR downregulation. To obtain an accurate representation of all experimental repeats, aligned data from all experimental repeats (without IL-2: N = 6; with IL-2: N = 4) were pooled directly.

Lck inhibitor experiments. TCR downregulation in the presence and absence of the A-770041 Lck inhibitor [232] was averaged similarly to the TCR re-expression experiments. Each experimental repeat (N = 3) was normalised to the fitted upper and lower plateau of the TCR dose-response curve after 4 hours of stimulation with pMHC without the inhibitor. The same dose-response curve was also used to normalise the x-axis between experimental repeats (Equation 2.2) as described in the previous paragraph.

The model was fitted to 4 types of averaged experimental data. First, dose-response curves of pooled TCR re-expression data were fitted using MATLAB's (MathWork) *lsqcurvefit* function to determine the basal TCR up- and downregulation rates. The remaining 3 experiments were fitted simultaneously by ABC-SMC: Dose-response curves of (1) cumulative TNFα and (2) TCR downregulation after 1–8 hours of stimulation with a low- or a high-affinity pMHC were fitted directly. (3) The relation between TCR downregulation and signalling was included by fitting dose-response curves after 4 hours of stimulation in the presence and absence of the Lck inhibitor A-770041. The pooled average of TCR downregulation with and without A-770041 naturally contained a larger number of data points. Instead of simulating each datapoint, the model was evaluated at a reduced number of evenly-spaced pMHC doses and compared to the Hill function that best described the pooled data.

2.7.2 Extraction of E_{max} and EC_{50} from the experimental data

For the systematic analysis of the large dataset in Chapter 5, the dose yielding a half-maximal response (EC_{50}) and the maximal response across all doses of a particular pMHC

mutant (E_{max}) were extracted from the experimental data using MATLAB (Mathworks, Inc.). The EC_{50} was determined by fitting an interpolating function (the difference of two sigmoids to match the bell-shape) with 10,000 data points spaced evenly on a log-scale to the experimental data. The EC_{50} could only be estimated if the cytokine response at the lowest dose of pMHC was less than $\frac{1}{2}E_{max}$, if it saturated at the highest doses of pMHC and if it did not display a phenotype other than a bell-shaped or sigmoidal dose-response curve (see Appendix Fig. C.2). To maximally exploit all data collected, the E_{max} was determined directly from the raw data.

2.7.3 Fitting of experimental data by ABC-SMC

The algorithm used for fitting experimental data was a modified version of the Approximate Bayesian Computation with Sequential Monte Carlo (ABC-SMC) protocol by Toni et al. [250]. ABC-SMC returns an estimate of the 13-dimensional posterior distribution of the parameter vector, θ. Candidate parameter combinations $\theta^{\star}$ are sampled from 13-dimensional parameter space and will be referred to as *particles*. A population of N = 10,000 particles was propagated through a total of T = 15 iterations. The distribution of particles in parameter space converges to the posterior distribution on the model parameters if the adaptive threshold ϵ becomes sufficiently small [250]. The MATLAB (MathWorks, Inc.) implementation of the protocol below is included in the Appendix (Section B.2) and it was run on Oxford's Advanced Research Computing facility.

ABC-SMC protocol

1. Set the population indicator $t = 0$.
2. To sample a population of $N = 10{,}000$ particles,
   a) Set the particle indicator $i = 1$.
   b) If $t = 0$, sample $\theta^{\star\star}$ independently from the uniform prior distribution $\pi(\theta)$. Else, sample $\theta^{\star}$ from the previous population $\{\theta_{t-1}^{(i)}\}$ with weights w_{t-1} and perturb the particle to obtain $\theta^{\star\star} \sim K_t(\theta|\theta^{\star})$, where K_t is a multivariate normal perturbation kernel that takes into account cross-correlations between parameters.
   c) Simulate a candidate dataset $x^{\star} \sim f(x|\theta^{\star\star})$. Compare the distance function $d = SSR$ to the adaptive threshold $\epsilon_t = median(SSR)$ of $\{\theta_{t-1}^{(i)}\}$. If $d(x^{\star}, x_0) \geq \epsilon_t$, re-sample (return to 2b).
   d) Set $\theta_t^{(i)} = \theta^{\star\star}$ and calculate the weight for particle $\theta_t^{(i)}$ according to

$$w_t^{(i)} = \begin{cases} 1 & \text{if } t = 0, \\ \dfrac{\pi(\theta_t^{(i)})}{\sum_{j=1}^{N} w_{t-1}^{(j)} K_t(\theta_{t-1}^{(j)}, \theta_t^{(i)})} & \text{if } t > 0. \end{cases}$$

   e) If $i < N$, set $i = i + 1$ and sample the next particle (return to 2b).
3. Normalise the weights.
4. If $t < (T = 15)$, set $t = t + 1$ and re-sample particles (return to 2a).

CHAPTER 3

T cells limit their cytokine response to pMHC

Antigenic pMHC ligands on APCs bind to the TCR on the surface of the T cell and initiate a complicated intracellular signalling cascade that instructs the T cell to perform effector functions. The outcome of stimulation depends both on the state of the T cell as well as the strength of the pMHC stimulus. In this chapter, an experimental assay was developed to systematically interrogate the human T cell signalling machinery by varying the pMHC input in a controlled way and measuring multiple cytokine outputs. Cytotoxic $CD8^+$ T cells were found to adapt their cytokine response to the pMHC stimulus and adaptation was paralleled by a reduction of TCR density on the T cell surface. These data were used in subsequent chapters to inform a minimal mathematical model and to quantitatively assess a possible role of TCR downregulation in T cell adaptation.

3.1 Introduction

3.1.1 T cell differentiation

The cellular differentiation state influences the quality and magnitude of the T cell response. Naïve T cells, which have not yet encountered their cognate antigen, require prolonged stimulation with pMHC as well as co-stimulatory ligands to become activated [160, 168]. This priming process takes several days [160] and involves expansion into a pMHC-specific effector T cell population that subsequently travels to the site of infection [141]. Effector T cells are less dependent on co-stimulation and are capable of responding immediately to stimulation with their cognate pMHC [95, 112]. T cells can also differentiate into memory T cells that confer immunological memory after the acute threat has been eliminated. They too respond to pMHC more readily than naïve T cells [211, 261]. The differentiation state of the T cell thus affects both the strength and the dynamics of the response.

Because signalling changes occur as T cells progress through various staged of differentiation, T cell populations used for functional experiments were first characterised according to standard differentiation markers. The expression of the RA isoform of the phosphatase CD45 (CD45RA) and expression of the C-C chemokine receptor 7 (CCR7) allow the classification of T cells into four T cell subsets: Central memory (T_{CM}), naïve, effector/CD45RA$^+$ effector memory (EMRA) and effector memory (T_{EM}) (Fig. 3.4A). The expression of CD45RA is lost when T cells differentiate into memory T cells [162]. T_{CM} express CCR7, which binds chemokines that direct them to secondary lymphoid tissues, while T_{EM} and effector T cells are typically found in the periphery and therefore do not express CCR7 [142, 211]. In addition to changes in CD45RA and CCR7, Fas is known to be upregulated on antigen-experienced T cells. With these three markers, it was possible to distinguish naïve from pre-activated T cells and to rule out significant differences in the cellular activation thresholds within the T cell populations that were used for functional experiments.

3.1.2 The strength of the stimulus is dictated by the dose of pMHC and its affinity to the TCR

The strength of the pMHC stimulus is critically determined by two input dimensions. First, the dose of pMHC affects the magnitude of the T cell response. The dose-response relation has routinely been measured in various receptor-ligand systems to gain information about ligand-induced cellular activation [36]. When T cells were stimulated with a titration of pMHC ligand and a marker of activation was quantified for each dose, it was shown that the T cell response to some pMHC ligands was reduced when stimulating T cells with high pMHC doses resulting in a bell-shaped dose-response curve (also called: high-dose suppression) [64, 127]. Secondly, the affinity between pMHC and TCR has been shown in a large number of studies to be an important determinant of the quality and magnitude of the T cell response. The potency of a pMHC ligand generally correlates with its affinity and more specifically with the pMHC off-rate as predicted by the KPR model [9, 55, 86, 97, 150]. Multiple studies [97, 105, 127] furthermore suggested the existence of an optimal off-rate that elicits the strongest response because higher affinities incur a penalty for being unable to ligate multiple TCRs sequentially. The dose and affinity of the pMHC stimulus are thus two important factors that nonlinearly determine the quality and magnitude of the T cell response.

The two input dimensions are to some degree interdependent and it is therefore important to consider variations in pMHC dose and affinity simultaneously to obtain a more comprehensive signalling phenotype. The bell-shaped dose-response curve, for example, is typically seen when stimulating T cells with high-affinity pMHC ligands while low-affinity ligands elicit saturating dose-response curves [127]. Furthermore, Gonzalez et al. reported that an optimal affinity was not observed when T cells were stimulated with high doses of pMHC. The T cell signalling phenotype as a function of the strength of the pMHC stimulus therefore changes according to the pMHC dose- and affinity-regime under consideration, so that the two parameters cannot be studied independently. A large dataset that considers both pMHC dose and affinity over a wide range cannot, however, be collated from previous studies. Data is not easily concatenated because variations in the experimental setups do

not allow a direct quantitative comparison of the data. Some studies, for example, use APCs to stimulate T cells [37, 86, 97, 105, 247], making it difficult to precisely control pMHC dose and to rule out effects of accessory receptor-ligand interactions [147, 247]. Moreover, the affinity between pMHC and TCR has often been varied by introducing mutations in the TCR, which complicates the interpretation of results because TCR transduction levels are unlikely to match exactly [30, 37, 69, 86, 97, 105, 290]. The complex dependencies of the T cell response on pMHC dose and affinity highlight the need to study the T cell response over a wide range in both input dimensions in a single experimental system that allows the precise control over both parameters.

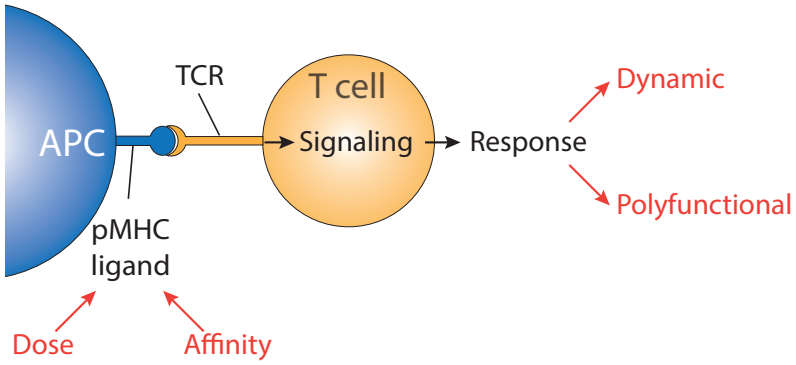


Figure 3.1: pMHC dose and affinity determine the strength of the pMHC input and elicit a dynamic and polyfunctional T cell output. Experiments that did not consider both input parameters have in the past led to controversial findings about the dose- and affinity-dependence of the T cell response. Moreover, the protective capacity of T cell populations correlates with the multitude of dynamic, time-integrated effector functions. The comprehensive study of T cell signalling therefore necessitates the systematic variation of the input parameters (pMHC affinity and dose) and time-dependent measurements of multiple T cell effector functions (highlighted in red). In this thesis, a receptor-ligand system consisting of the 1G4 high-affinity TCR that recognises variants of the NY-ESO-$1_{157\text{-}165}$/HLA-A2 pMHC was utilised to independently control pMHC dose and affinity and to measure multiple effector functions at different time points after stimulation.

3.1.3 The T cell response is polyfunctional and dynamic

T cells perform a large number of effector functions when they are activated by stimulation with pMHC. $CD8^+$ T cells secrete the cytokines TNFα, MIP-1β, IFNγ and IL-2 with important effects on both target cells and other immune cells. Of interest for

immunotherapies, gene knockouts of these effector molecules has revealed that each one of them contributes individually to the control of tumour growth in an *in vivo* mouse model. In fact, the deficiency of TNFα or IFNγ production was shown to more dramatically impair tumour growth control than perforin-deficiency that compromises direct cytolysis of target cells [193, 194]. In addition, the ability of T cells to produce more than one of the signature effector molecules TNFα, MIP-1β, IFNγ and IL-2 at the same time (polyfunctionality) has been shown to positively correlate with the efficacy of the immune response in *in vitro* infection models [21]. It is therefore important to measure multiple effector molecules when characterising the immune response by $CD8^+$ T cells.

The temporal integration of different effector molecules is critical for efficient pathogen clearance. Han et al. [78] measured cytokines secreted into the supernatant by single T cells embedded in nanowells. Their data suggested that T cells secrete cytokines sequentially and that polyfunctionality is transient on a single-cell level. Prolonged protection through a population of T cells could thus be achieved by the summation of individual responses that begin secretion of various effector molecules in a time-shifted manner. The secretion of granzymes/perforin and TNFα, for example, can both directly lead to target cell killing, but they operate on different time scales. In an *in vivo* mouse model, perforin-deficiency introduced a delay in the killing of tumour cells that was sufficient to allow the tumour to escape immune protection by antigen loss [193, 194]. These data highlight that different killing mechanisms are not redundant because they effect immediate and prolonged T cell responses that collectively provide sufficient immune protection. The present study therefore considered both the dynamics and multiplicity of T cell effector molecules.

3.1.4 The 1G4 high-affinity TCR and NY-ESO-$1_{157\text{-}165}$ pMHC

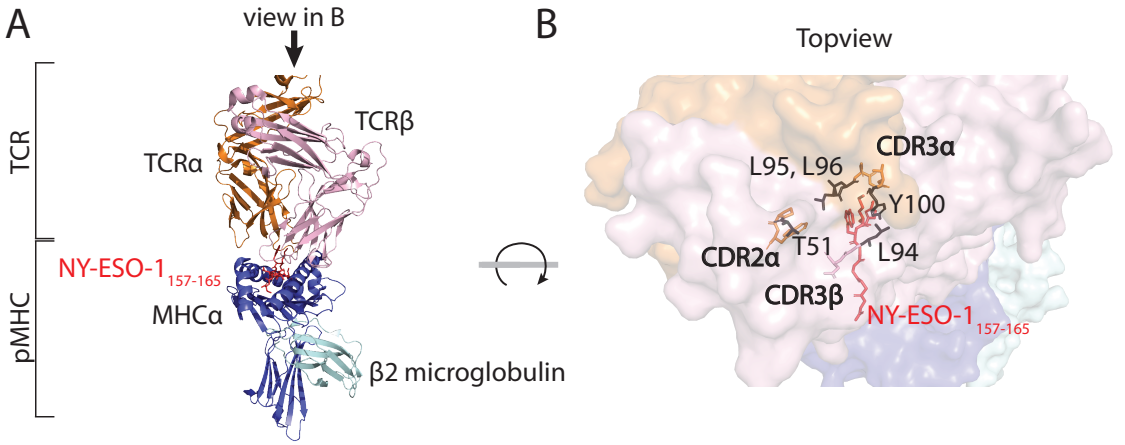
The therapeutic use of engineered TCRs was facilitated by two critical advancements in molecular immunology. First, Boulter et al. [19] pioneered the production of soluble

TCR by introducing a non-native disulphide link between the TCRα- and β-chains that enhanced the stability of the otherwise membrane-anchored protein. Second, phage display technology enabled the screening of large libraries of TCR mutants as described in [129]. Briefly, TCRs were presented on the surface of M13 bacteriophage by fusing them to the viral coat protein pIII. The TCR protein could therefore be presented to plate-bound pMHC while the genetic information encoding the TCR was stored within the bacteriophage. If a TCR presented on the bacteriophage recognised pMHC on the plate with high affinity, it was used to infect *E. coli* that produced the TCR protein in large quantities for further analyses. Affinity-enhanced TCRs are now utilised in immunotherapies in soluble form [20, 178] or expressed on transduced and adoptively transferred T cells [202].

The c58c61 1G4 high-affinity (1G4Hi) TCR that was derived from the 1G4 TCR by phage display [129] and its cognate NY-ESO-$1_{157\text{-}165}$ pMHC ligand were here employed to interrogate the T cell signalling network in a clinically relevant framework. The crystal structure of the 1G4Hi TCR in complex with its cognate peptide NY-ESO-$1_{157\text{-}165}$ presented by HLA-A*02:01 was resolved by Sami et al. [213] and it is shown in Fig. 3.2A. It revealed that the 1G4Hi TCR binds diagonally to the axis of the peptide so that the binding mode is comparable to the binding mode of the 1G4 wild-type TCR to the same pMHC. The affinity is therefore enhanced while maintaining a native binding configuration. The increase in the binding affinity is a result of mutations in the complementarity regions (CDR) 2 and 3 [213] (Fig. 3.2). The Tyrosine 100 residue (Y100) on the TCR α-chain and Leucine 94 (L94) on the TCR β-chain, both in CDR3, surround the protruding Methionine 4 and Tryptophan 5 (M4W5) central region of the NY-ESO-$1_{157\text{-}165}$ peptide. The Leucine 95 and 96 residues on CDR3α furthermore interact with Threonine 51 in CDR2α. The sum of these interactions increases the surface of the contact area between the TCR and decreases the rate of unbinding [129, 213]. Fig. 3.2 lists the binding parameters for a high- and a low-affinity pMHC variant that were used in this chapter for the stimulation of primary $CD8^+$ human T cells.

The 1G4Hi TCR and its NY-ESO-$1_{157\text{-}165}$ pMHC ligand are particularly suitable for a systematic study of the dose- and affinity-dependence of the T cell response to pMHC

stimulation because both input dimensions, pMHC dose and affinity, can be varied in a controlled way. pMHC ligands could be immobilised on a 96-well plate at different doses by biotin/streptavidin-coupling, which is more precise than pulsing APCs and precludes confounding signals from other receptor-ligand interactions. Affinity alterations were achieved by mutations on the peptide and not the TCR, so that the affinity-dependence of the T cell response could be examined without correcting for mismatches in TCR expression levels.



C

Name	Sequence	Dissociation constant (μM)	on-rate ($\mu M^{-1}\ s^{-1}$)	off-rate (s^{-1})	Affinity regime
9V	SLLMWITQV :	$K_D = 7.07 \times 10^{-5}$	$k_{on} = 1.17 \times 10^{0}$	$k_{off} = 8.26 \times 10^{-5}$	Therapeutic
4A8K	SLLAWITKV :	$K_D = 1.78 \times 10^{0}$	$k_{on} = 1.10 \times 10^{0}$	$k_{off} = 1.95 \times 10^{0}$	Physiological

Figure 3.2: The 1G4 high-affinity TCR binds NY-ESO-$1_{157\text{-}165}$/HLA-A2*02:01 pMHC variants with altered affinities. (A) Crystal structure of the affinity-enhanced c58c61 1G4 high-affinity TCR bound to NY-ESO-$1_{157\text{-}165}$ presented by HLA-A2*02:01 (pMHC) reveals a binding mode diagonal to the axis of the peptide and comparable to the wild type 1G4 TCR (not shown). Refer to [213] for a direct overlay of the two structures. **(B)** Top view of the TCR/pMHC binding site reveals that mutations in CDR2 and CDR3 increase the contact area between the peptide and TCR and thereby reduce the dissociation rate. Participating residues are highlighted in black. Y100 in CDR3α and L94 in CDR3β form a lock around the protruding central M4W5 region on the peptide. L95 and L96 in CDR3α interact with T51 in CDR2α. **(C)** Binding parameters for a high-affinity (9V) and a low-affinity (4A8K) pMHC variant that were used for stimulation of primary $CD8^+$ human T cells in this chapter.

3.1.5 Biological adaptation

Biological adaptation describes the phenomenon that some biological sensory systems can reset themselves after experiencing a stimulus [3, 39, 138, 228]. The phenomenon is illustrated in Fig. 3.3: A persistent input (Fig. 3.3A) results in a rapid output that subsequently returns to a lower level despite the continued presence of the stimulus (Fig. 3.3B). Adaptation is *perfect* when the adapted output level (O_{adap} in Fig. 3.3B) is equal to the basal output level at $t < 0$. Adaptation desensitises cells to constant stimulation, but, importantly, preserves their ability to detect fold-changes in the stimulus [3, 138]. Adaptation can furthermore increase the dynamic range of inputs that a sensory system can detect [3, 138].

In immunology, the *tunable activation thresholds* model [72] and the more recent *discontinuity theory of immunity* [191] postulate that adaptation ensures tolerance of immune cells to self while they remain capable of responding to changes in the environment that could be associated with danger. Multiple mechanisms can cause adaptation, including the internalisation of cell surface receptors [3, 39, 70, 137, 191, 228, 231]. Even though it has been known for a long time that the TCR is downregulated upon stimulation of T cells with pMHC [25, 163, 218, 255, 286], the functional significance of TCR downregulation remains controversial: Adaptation was associated with clear changes in TCR expression in some [60, 218, 233, 241] but not all studies [79, 81, 125, 205, 225].

3.1.6 Chapter overview

$CD8^+$ primary T cells were expanded in culture by αCD3/αCD28-stimulation and transduced with the 1G4 high-affinity TCR according to a standard transduction protocol that is used to prepare T cells for adoptive transfer in immunotherapy. Because the requirements for full T cell activation change during the lifecycle of a T cell, the differentiation state of T cells used for stimulation experiments was first characterised (Section 3.2.1). Despite heterogeneity in the differentiation markers CCR7 and CD45RA, all T cells were antigen-experienced after expansion in culture and no differences were found in the activation thresholds in populations of T cells derived from distinct T cell

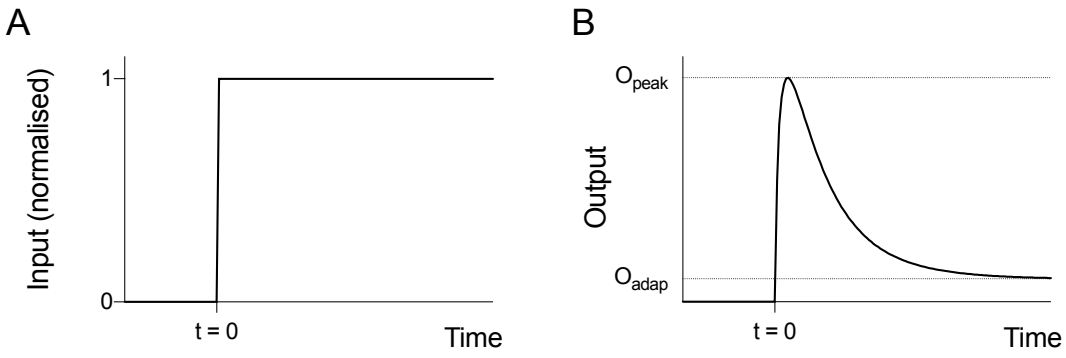


Figure 3.3: Schematic illustration of adaptation. (A) In this schematic example, a constant and persistent input is provided from t = 0. **(B)** The output produced by an adaptive system is a transient response with peak level O_{peak} and a lower steady-state O_{adap} at late time points, despite the continued presence of the input.

subsets. Next, a large dataset was generated by systematically measuring the dynamic polyfunctional T cell response to a dose titration of a low- and a high-affinity pMHC. T cells were found to adapt their response to the pMHC stimulus at all doses and affinities with similar kinetics for the secretion of TNFα, MIP-1β, IFNγ and IL-2 (Section 3.2.2). TCR expression on the T cell surface was concomitantly reduced rapidly and expression recovered only on the order of several days (Section 3.2.4). Upon sequential stimulation with first a low- and then a high-affinity pMHC, however, T cells were able to produce cytokine during the secondary stimulation (Section 3.2.5). The data presented in this chapter suggest a TCR proximal self-regulatory mechanism that enables T cells to limit their response even in a reduced experimental setting without confounding factors such as inhibitory ligands or regulatory cell types.

3.2 Results

Functional experiments throughout this thesis were conducted with primary $CD8^+$ human T cell populations from healthy donors that were transduced with the 1G4Hi TCR and expanded in cell culture as described in Methods Section 2.4. Functional experiments are described in detail in Methods Section 2.6.

3.2.1 Protocol for generating pMHC-specific CD8$^+$ T cells results in an effector phenotype

Engineered high-affinity TCRs are used in immunotherapy in different forms to redirect T cells to tumours. One strategy is to expand T cells from the patient in cell culture and to equip them with an engineered TCR. We followed a standard protocol that is used in these immunotherapies for the *ex vivo* expansion of autologous T cells [128, 153, 190, 203]. Peripheral CD8$^+$ primary T cells were isolated from healthy donors and lentivirally transduced with the 1G4Hi TCR. To improve the transduction efficiency and to expand the population, T cells were stimulated with αCD3/αCD28-coated beads. The stimulation beads were removed after 7 days and T cells were then rested for another 5–7 days in cell culture. By this time, the number of T cells had typically increased 20–100fold and 30–90% of cells expressed the 1G4Hi TCR. Because signalling changes occur as T cells progress through various differentiation stages, it was important to characterise the T cell populations used subsequently for functional experiments. Expression of CD45RA, CCR7 and Fas were measured to identify T_{CM}, naïve, effector/EMRA and T_{EM} cells (Fig. 3.4A). Fas expression was measured to further distinguish between naïve and pre-activated T cells.

Donor-specific variability between isolated CD8$^+$ primary T cell populations before and after expansion in culture

The relative frequencies of T_{CM}, naïve, effector and T_{EM} T cells were donor-dependent on the day of isolation (Fig. 3.4B, top). Simultaneous fluorescent staining for CCR7 and CD45RA showed that nearly 50% of CD8$^+$ T cells from Donor 1 were initially in the naïve state, while the same was true only for about 18% of CD8$^+$ T cells from Donor 2. These differences were not unexpected because the composition of peripheral T cell populations is a function of multiple parameters including the age and the donor's (recent) infectious history [116].

Donor variability persisted after transduction and expansion in culture. T cells from Donor 1 exhibited a higher degree of heterogeneity after *ex vivo* expansion than cells

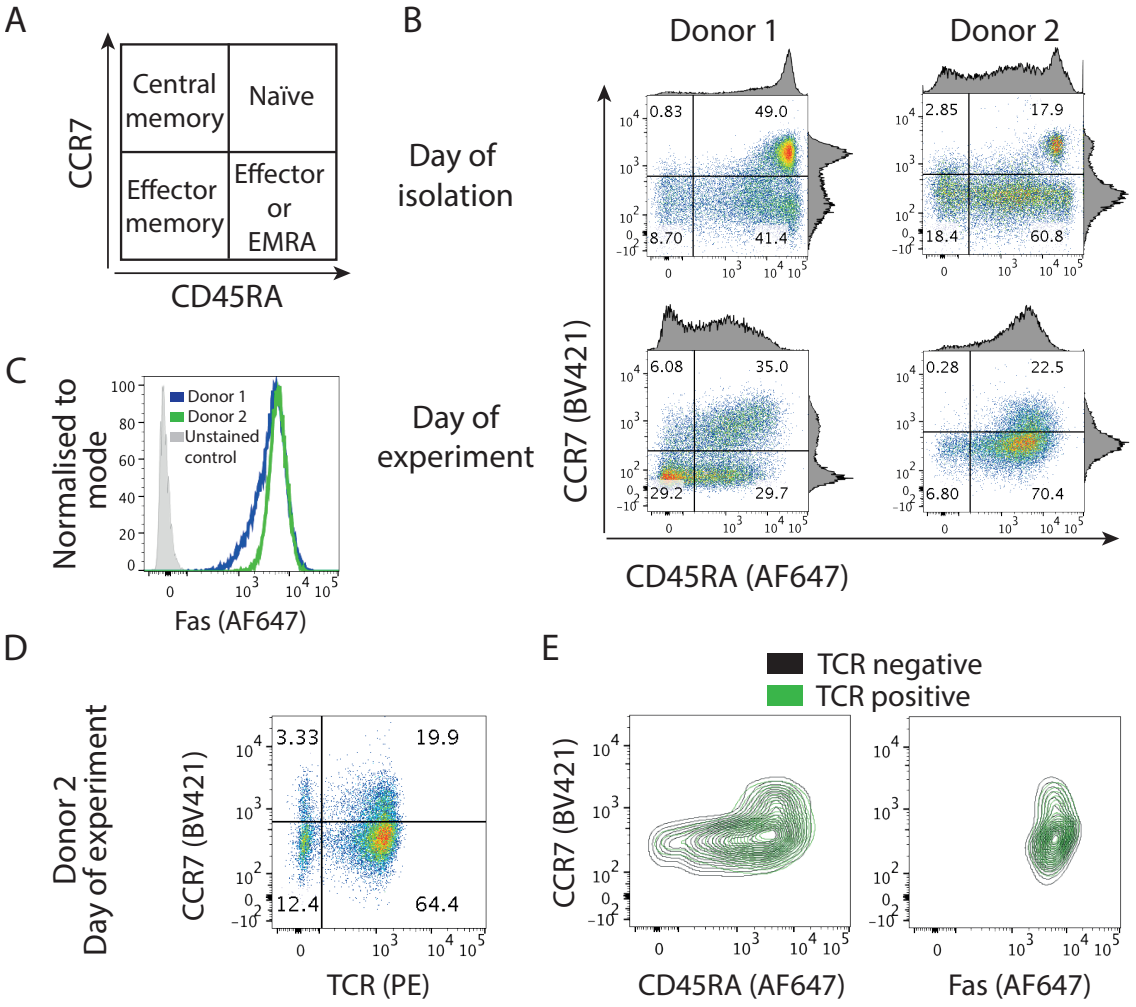


Figure 3.4: A standard protocol for TCR transduction and expansion of CD8$^+$ primary T cells in cell culture yields heterogenous, yet antigen-experienced T cell populations. (A) Classification of T cells as central memory, naïve, effector/EMRA or effector memory according to expression of the RA isoform of CD45 and the homing receptor CCR7. **(B)** Inter-subject variability in the composition of T cell populations was observed both on the day of isolation (top) and after expansion in culture (bottom). **(C)** Uniform expression of Fas indicated that all T cells were antigen-experienced after expansion. **(D)** Transduction of T cells with the 1G4Hi TCR typically yielded populations with 30–80% of T cells expressing the TCR (representative data). **(E)** TCR$^-$ (black) and TCR$^+$ (green) T cell populations exhibited identical subset compositions suggesting that different T cell subsets were transduced with equal efficiency. Therefore, the same level of heterogeneity existed for the whole T cell population and the subset of TCR-transduced T cells. Co-staining for TCR and differentiation markers was only performed on T cells from Donor 2. Expression of CD45RA, CCR7 and Fas were measured by immunofluorescent labelling and TCR expression was quantified by pMHC tetramer staining followed by flow cytometry.

isolated from Donor 2. Most notably, T cells isolated from Donor 1 formed a visible double-negative T_{EM} population after expansion while the fraction of T_{EM} decreased in T cells isolated from Donor 2 (Fig. 3.4B). Prestimulation, transduction and expansion in culture did thus not result in assimilation of the two T cell populations. Generally, however, the CCR7-negative effector and T_{EM} differentiation states were dominant in the final T cell populations as expected (Donor 1: ~59%; Donor 2: ~77%).

All T cells are antigen-experienced after transduction and expansion in culture

A relatively large proportion of T cells both in Donor 1 and 2 displayed a naïve-like $CCR7^+CD45RA^+$ phenotype after expansion in culture that involved stimulation with αCD3/αCD28-coated beads. Yet, 100% T cells in Donor 1 and Donor 2 were antigen-experienced as determined by measuring the expression of Fas. Fas is known to be upregulated on antigen-experienced T cells and ligation of the receptor on less differentiated T cells by Fas ligand (FasL) expressed on memory T cells can produce an apoptotic or a non-apoptotic signal that instead synchronises the behaviour of T cells by accelerating metabolic, functional and transcriptional changes [114]. Single-cell flow cytometric profiles of Fas expression were unimodal distributions with mean expression levels that were comparable between both donors (Fig. 3.4C). Stimulation with αCD3/αCD28-coated beads thus successfully activated the whole T cell population despite the fact that a quarter to a third of T cells in Donor 1 and 2 expressed differentiation markers that are typically associated with naïve T cells.

The level of heterogeneity in whole and 1G4Hi$^+$ T cell populations is identical

Only 1G4Hi$^+$ T cells respond to stimulation with NY-ESO-$1_{157\text{-}165}$ pMHC variants in functional experiments. If one subset of $CD8^+$ T cells was preferentially transduced with the 1G4Hi TCR, the 1G4Hi$^+$ T cell population could be more homogeneous than the entity of all $CD8^+$ T cells. We co-stained for CD45RA, CCR7, Fas and the TCR to test whether T cell subset heterogeneity is the same on the level of the whole T cell

population and among 1G4Hi$^+$ T cells only. CD8$^+$ T cells were lentivirally transduced with the 1G4Hi TCR one day after isolation from blood. By day six, 30–90% of T cells typically expressed the TCR (Fig. 3.4D, 3.5). Multicolour flow cytometry suggested that the subset composition of T cell populations is in fact identical among 1G4Hi$^+$ and 1G4Hi$^-$ T cells (Fig. 3.4E). The heterogeneity of the 1G4Hi TCR expressing T cell population thus mirrored the heterogeneity of bystander T cells.

T cells derived from naïve or memory subsets respond similarly to pMHC stimulation after expansion in culture

Naïve and effector T cells are known to have different activation thresholds [141, 160, 168]. The analysis thus far focused on bulk T cell populations (Fig. 3.4). Given that on the day of the experiment, a substantial fraction of the bulk T cell population expressed naïve-like differentiation markers, we wondered if individual subsets in the starting populations (1) developed differently in cell culture and (2) had distinct activation thresholds after having undergone the same expansion protocol. In order to compare individual subsets, they were first isolated from human blood as described in Methods Section 2.5, expanded separately in cell culture and subsequently analysed in functional experiments.

Three samples of CD8$^+$ T cells from the same donor were either unseparated or enriched for naïve (70%) or T_{EM} (43%) cells, respectively, on the day of isolation (Fig. 3.5). For T_{EM} enrichment, CCR7$^+$ cells were successfully depleted with 96% purity, but 53% of T cells still expressed CD45RA (see Fig. 3.5B, top row). According to the manufacturer, a higher fraction of CD8$^+$ than CD4$^+$ T cells are T_{EMRA}. CD45RA$^+$ cells were therefore, with the CD8$^+$ T cell enrichments kits that were sold at the time, not efficiently depleted (email correspondence with Sophie New, STEMCELL Technologies, 18 January 2017). Yet, quantification of how CD45RA/CCR7 expression profiles changed in time showed that T cells generally adopted an increasingly effector-like CCR7/CD45RA expression phenotype irrespective of the starting population (Fig. 3.5B, Fig. 3.6A). Importantly, all T cells were antigen-experienced by Day 4 when 100% of T cells expressed Fas (Fig. 3.5C).

The three T cell populations that were derived from bulk, naïve-enriched or memory-

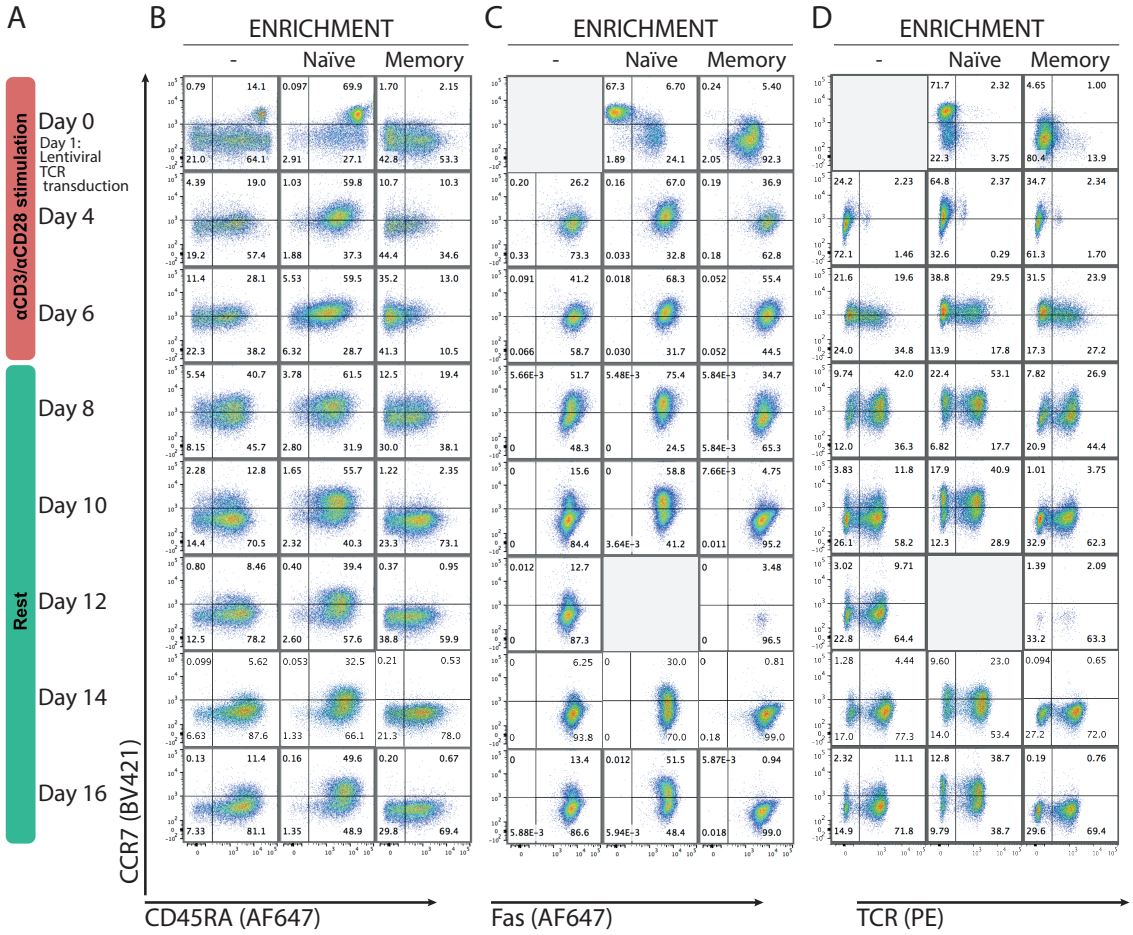


Figure 3.5: Comparison of T cell differentiation dynamics in culture between bulk and subset-enriched T cell populations. (A) $CD8^+$ T cells were isolated from peripheral blood and lentivirally transduced with the 1G4Hi TCR on the following day. To produce a large population of T cells in culture, they were also stimulated with αCD3/αCD28-coated beads for a week and subsequently rested. **(B)** T cells derived from bulk, naïve- or memory- enriched starting populations maintained dissimilar CD45RA and CCR7 expression profiles in culture, but a tendency towards CCR7-negative effector and T_{EM} populations was indicated. **(C)** Antigen-experience determined by Fas expression and **(D)** 1G4Hi TCR expression levels were comparable between bulk and enriched T cell populations. See Fig. 3.6 for a quantification of differentiation states, antigen-experience and 1G4Hi TCR expression as a function of time. All T cell populations stem from the same donor and isolation. This exploratory experiment was conducted once.

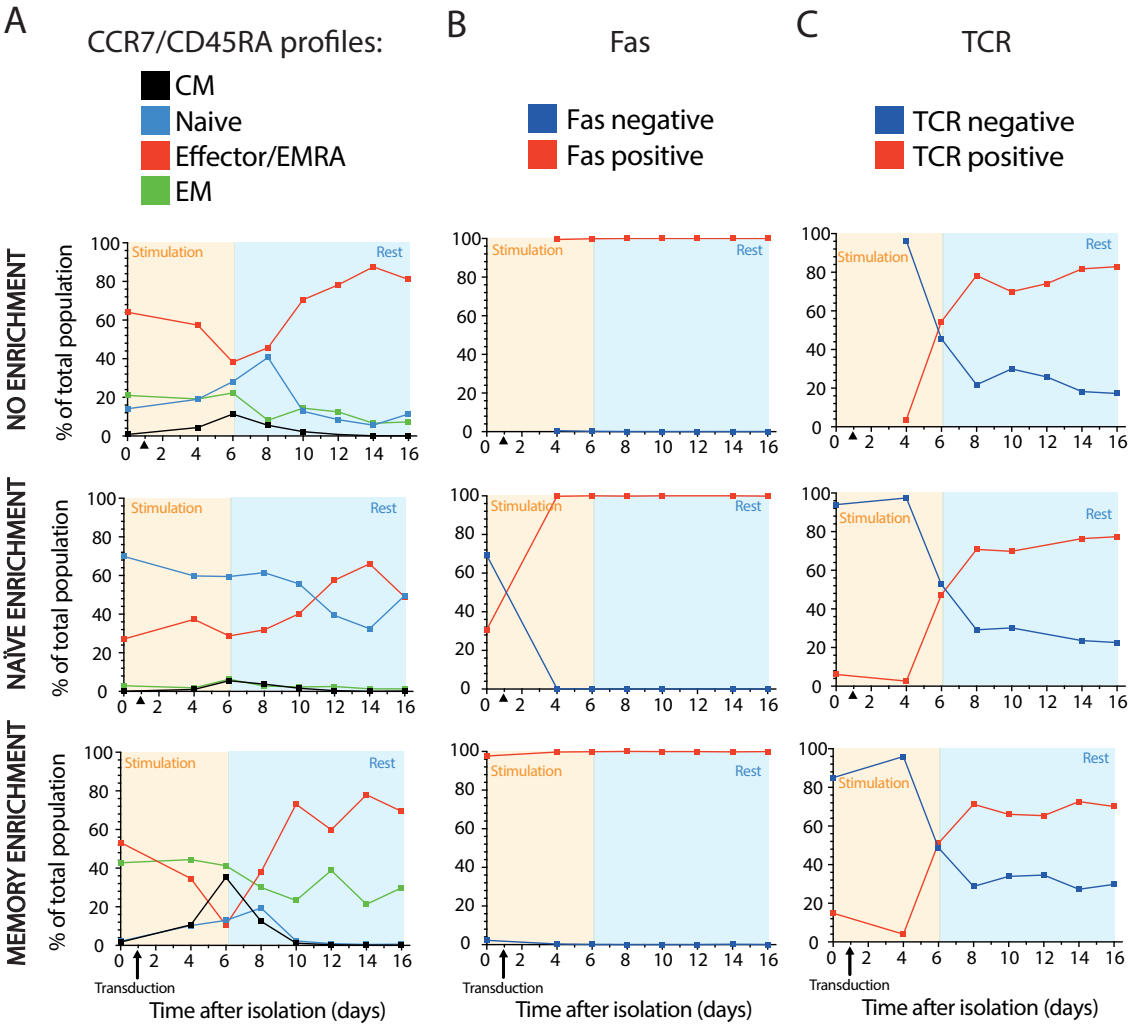


Figure 3.6: Timeline quantification of T cell differentiation, antigen experience and 1G4Hi TCR expression in culture. Quantification of data in Fig. 3.5. **(A)** Percentages of T cells in each one of the four quadrants in Fig. 3.5B. Throughout expansion in culture, T cells tended to lose the CD45RA/CCR7 expression profile associated with the naïve compartment (blue) and progress towards an effector/EMRA phenotype (red) independent of the starting population on the day of isolation. **(B)** Summed up percentages of Fas^- (left two quadrants) and Fas^+ (right two quadrants) in Fig. 3.5C. Fas expression peaked early during expansion, implying that all T cells are antigen-experienced by Day 4. **(C)** Summed up percentages of $1G4Hi^-$(left two quadrants) and $1G4Hi^+$(right two quadrants) in Fig. 3.5D. The percentage of 1G4Hi-expressing T cells reached a steady-level seven days after addition of the TCR lentivirus. The transduction efficiency was comparable between the initially whole and enriched T cell populations.

enriched starting populations were then directly compared in their ability to respond to pMHC stimulation after expansion in culture to investigate whether they required different doses of pMHC to be activated. A functional experiment confirmed that all T cells were able to respond similarly to pMHC after expansion in culture even though they expressed diverse combinations of CD45RA and CCR7. T cells derived from bulk, naïve or memory T cell pools were stimulated with a titration of 4A8K pMHC (physiological affinity) and fluorescently stained for expression of the activation markers 4-1BB, CD69 and the α-chain of the IL-7 receptor (IL-7Rα) (Fig. 3.7). The same percentage of cells upregulated 4-1BB and CD69. Interestingly, fewer T cells derived from memory T cells, which are associated with increased IL-7 sensitivity [103], expressed IL-7Rα in the resting state. It suggests that these T cells had lost their memory phenotype throughout expansion in culture consistent with previous reports [34]. Nonetheless, the pMHC dose threshold required to trigger a T cell response was the same for all three populations of T cells and all activation markers. The flow cytometric single-cell data in Supplementary Fig. A.1 furthermore shows that activated T cells expressed similar levels of CD69 and 4-1BB in all three T cell populations. For simplicity, non-separated, bulk $CD8^+$ T cell populations were used for transduction, expansion and functional experiments throughout the remainder of this thesis.

3.2.2 T cells adapt their cytokine response to pMHC dose and affinity

The T cell response was studied in a reductionist experimental setup and multiple cytokines served as a proxy for T cell activation. $CD8^+$ primary T cells were stimulated with a titration of pMHC for 1–8 hours (Fig. 3.8). The cytokines TNFα and IFNγ, the chemokine MIP-1β and the interleukin IL-2 were measured in the supernatant by enzyme-linked immunosorbent assays (ELISA). Stimulated T cells were furthermore labelled with fluorescent PE-conjugated pMHC tetramers to determine the expression of the 1G4Hi TCR on the cell surface. This minimal experimental system allowed the systematic study of the effects that pMHC dose and affinity have on several T cell effector

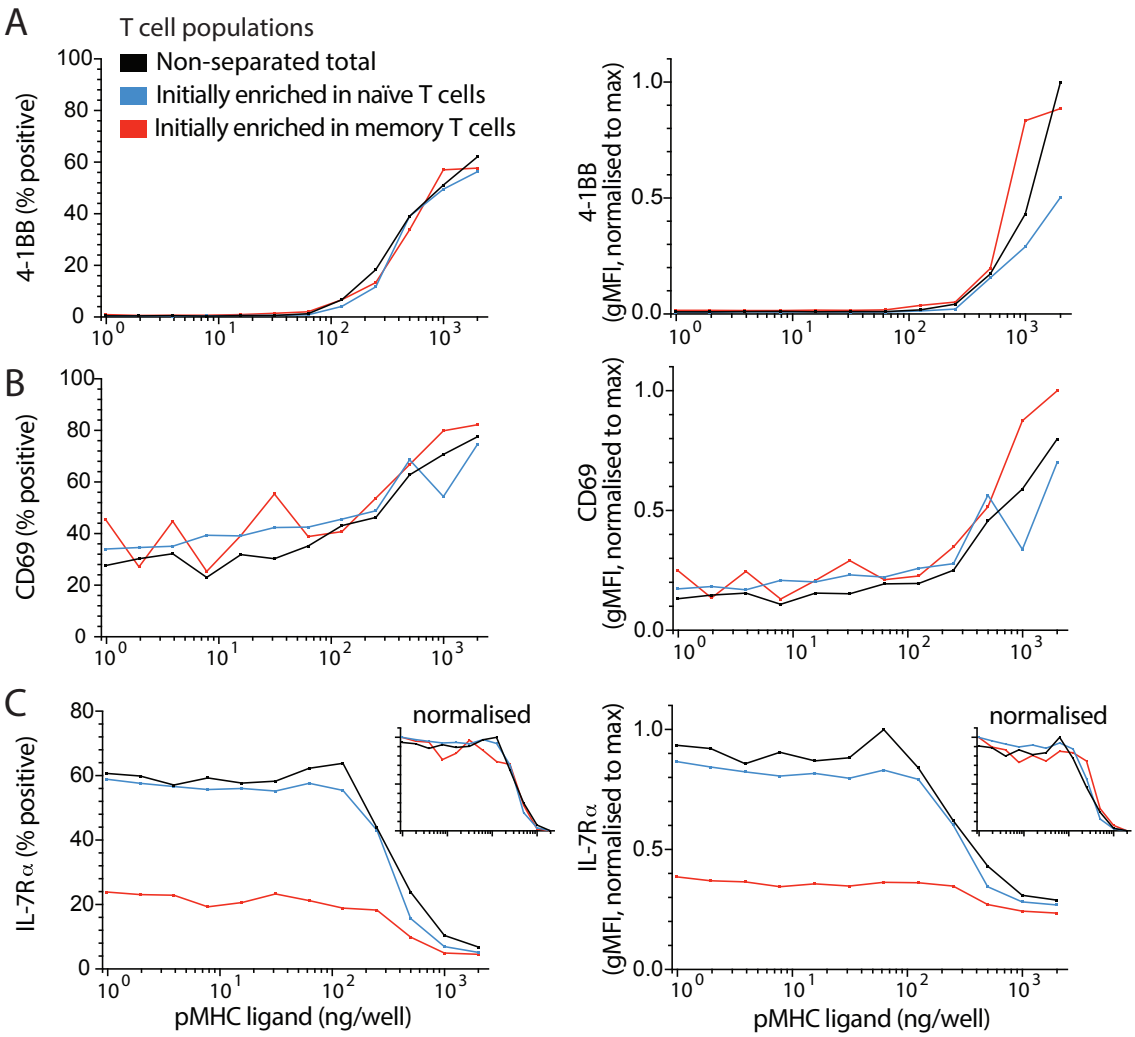


Figure 3.7: T cells derived from mixed, naïve or memory T cell populations respond to pMHC with similar activation thresholds. The percentage of T cells (left) that expressed the activation markers **(A)** 4-1BB and **(B)** CD69 in response to stimulation with the 4A8K pMHC for 8 hours was independent of the T cell subset on the day of isolation at all doses. Differences in the mean fluorescence intensity (right) were within experimental error and did not reflect subset-specific expression levels on activated T cells (see Fig. A.1). **(C)** The frequency of IL-7Rα-expressing T cells was lower in populations derived from the memory pool, but the pMHC dose threshold for downregulation was identical for all populations (insets). TCR transduction levels were comparable between the populations (Total: 76%; Naïve: 72%; Memory: 69%). This exploratory experiment was conducted once.

functions without contributions from co-modulatory receptor-ligand interactions such as PD-1 or CD28.

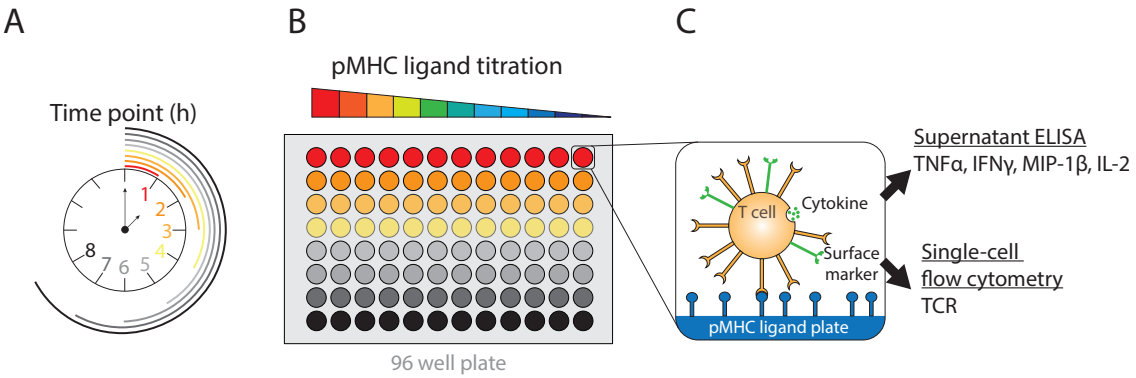
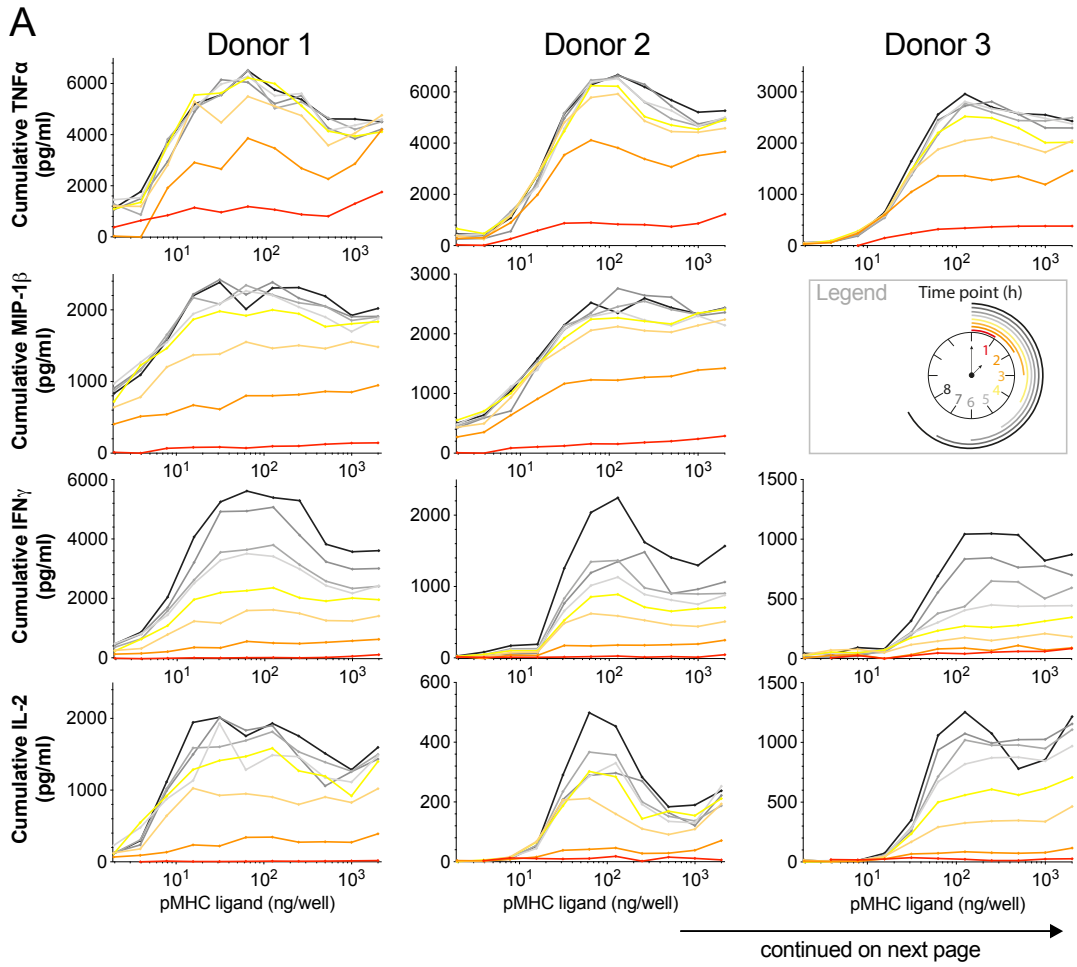


Figure 3.8: Experimental setup to determine the dynamics of multiple effector functions in response to a titration of pMHC ligand. (A) The cumulative cytokine response was measured at 1–8 hours after stimulation with pMHC. **(B)** A titration of biotinylated NY-ESO-$1_{157\text{-}165}$ pMHC was immobilised on a streptavidin-coated 96-well plate. $CD8^+$ primary T cells transduced with the 1G4Hi TCR were added to the plate and well contents were harvested for analysis at the respective time points. **(C)** TNFα, MIP-1β, IFNγ and IL-2 were secreted into the supernatant when T cells contacted the immobilised pMHC, so that their concentrations were measured in the supernatant by ELISA. The level of TCR on the cell surface was determined by PE-conjugated pMHC-tetramer staining followed by flow cytometry.

TNFα, MIP-1β, IFNγ and IL-2 concentrations were measured in the supernatant after 1–8 hours of stimulation with pMHC. T cell populations derived from three donors were stimulated in independent experiments and experimental repeats were averaged by normalising each dose-response curve to the maximum amount of cytokine produced after 8 hours of stimulation. Relative differences in the amount of TNFα, MIP-1β, IFNγ and IL-2 were not taken into account here, but will be discussed in more detail in Chapter 5. Briefly, the amount of each cytokine produced was donor-specific and did not scale linearly between experimental repeats (Appendix Fig. A.2).

Cytokine that was secreted into the supernatant in response to a titration of pMHC with therapeutic affinity (9V, K_D = 7.07 $\times 10^{-5}\mu$M) reached a steady level after 4–6 hours of stimulation (Fig. 3.9). TNFα was the most readily detectable cytokine after 1 hour of stimulation, consistent with the production of TNFα predominantly from pre-formed mRNA [174, 186, 208]. The onset of IFNγ and IL-2 was delayed by roughly 1 hour relative



to TNFα, and secretion of both of these cytokines is known to rely on *de novo* synthesis of mRNA [174, 186, 208]. The kinetics at which secretion of all four cytokines stopped were similar. TNFα, MIP-1β and IL-2 secretion ceased at about 4–6 hours (Fig. 3.9C). The kinetics of IFNγ appeared the most strikingly different, but close inspection of the experimental data revealed biphasic secretion kinetics: Dose-response curves for individual donors in Fig. 3.9A–B showed signatures of an early stop of IFNγ secretion around 5–6 hours and a second surge of secretion between 7–8 hours. The adaptation kinetics are thus similar for four key cytokines, and they are furthermore consistent with a recent study that simultaneously measured TNFα, IFNγ and IL-2 mRNA and protein production after stimulation with PMA/ionomycin for 6 hours [174]. Of note, biphasic IFNγ secretion has also been reported elsewhere and it has been linked to pMHC-induced upregulation of CD25 (IL-2Rα) after 6–10 hours of stimulation (data not shown and [78, 246]), which allows for IL-2/IL-2R feedback to enhance further secretion of IFNγ at these late time

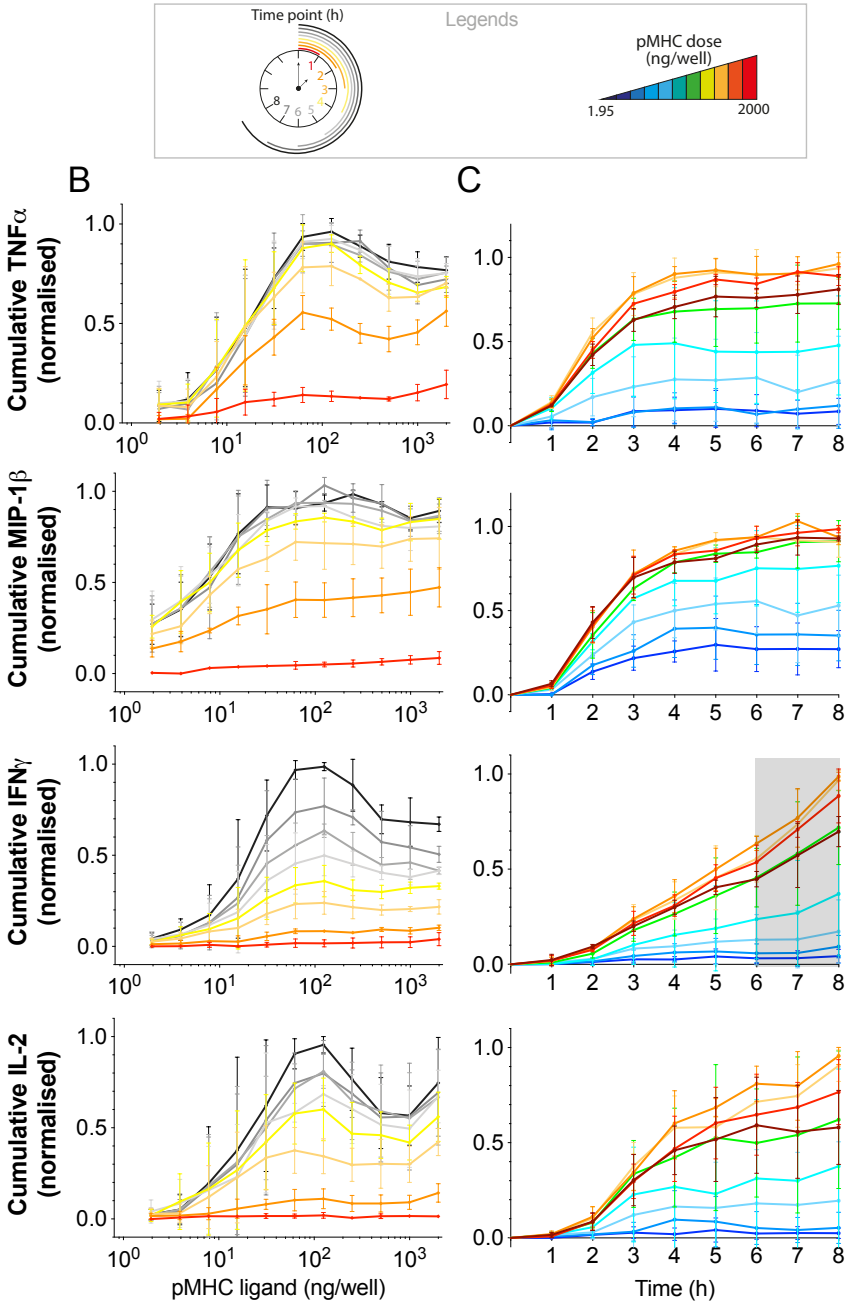


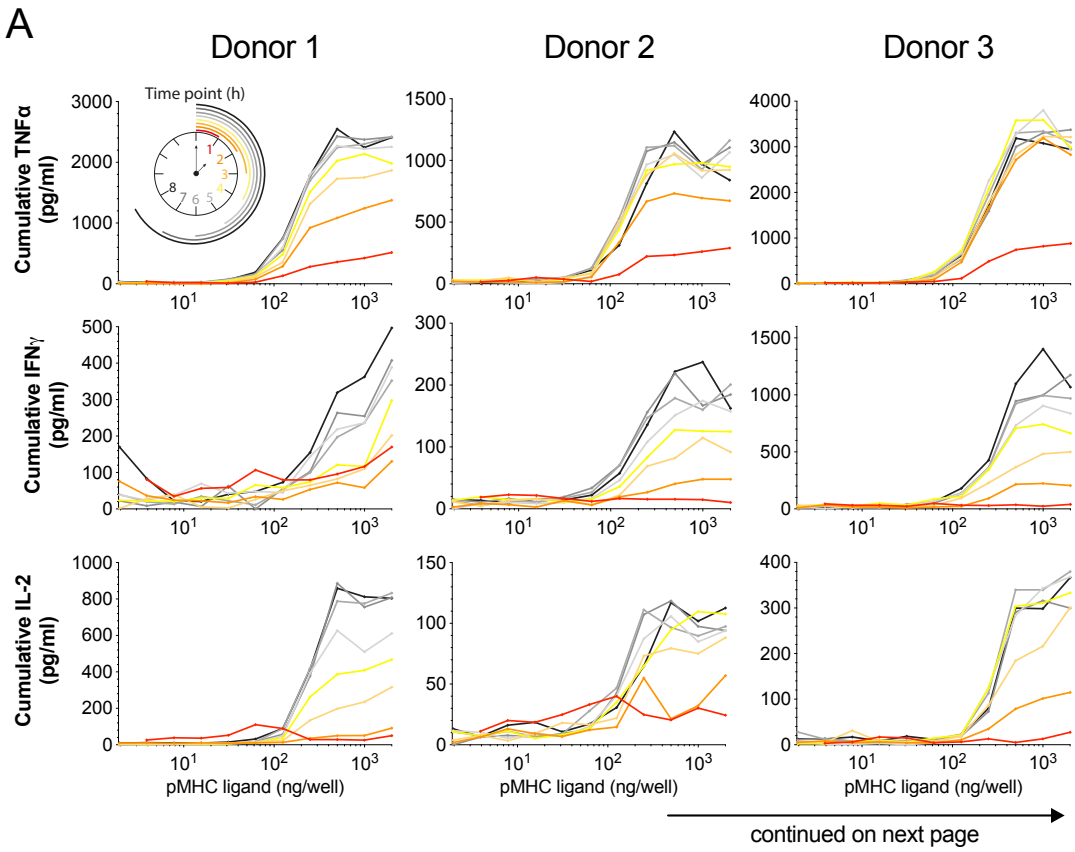
Figure 3.9: T cells adapt their cytokine response to stimulation with a high-affinity pMHC. CD8$^+$ primary T cells were stimulated with a titration of the 9V pMHC that binds the 1G4Hi TCR with therapeutic affinity. **(A)** Concentrations of TNFα, MIP-1β, IFNγ and IL-2 were measured in the supernatant as a function of pMHC dose after 1–8 hours of stimulation. The experiment was conducted independently with T cells from three donors. IFNγ secretion kinetics appeared biphasic with an early secretion stop at 5–6 hours, consistent with [78, 246]. **(B)** Average and error (SD) of the dose-response curves shown in (A). For averaging, each dataset was normalised to the maximum cytokine/chemokine level after 8 hours of stimulation. **(C)** Cumulative cytokine response as a function of time for different doses of pMHC. Secretion of all four cytokines consistently ceased at high doses first, so that a bell-shaped dose-response curve emerged at late, but not at early time points. Biphasic IFNγ secretion dynamics were barely conserved after averaging 6–8 hours (shaded area).

points [107, 156, 246].

The striking bell-shaped dose-response curves and the adaptation phenotype were not a result of activation-induced cell death (AICD). Common to all four functional readouts, the rate of cytokine release decreased more rapidly when T cells were stimulated with high doses of pMHC. This caused the dose-response curves to appear bell-shaped at late time points. We have previously shown that AICD is minimal ($< 5\%$) in these experiments and AICD as a function of pMHC dose mirrors the bell-shaped activation dose-response curve [127], so that maximal cell death would be expected after stimulation with intermediate doses. In addition, T cells were able to produce IFNγ beyond 6 hours of stimulation, suggesting that T cells were still alive. Adaptation as well as the preferential decrease in the cytokine response after T cells were stimulated with high doses of pMHC were therefore not a result of T cell death.

Given that a stop in cytokine secretion was observed when stimulating T cells with a pMHC ligand that binds the 1G4Hi TCR with supraphysiological affinity, it was important to determine whether this phenotype can also be observed in response to physiological ligands. Fig. 3.10 demonstrates that T cells were found to adapt their cytokine response to a pMHC with physiological affinity (4A8K, $K_D = 1.78 \times 10^0 \mu M$). IFN$\gamma$ again displayed signatures of biphasic secretion dynamics (Fig. 3.10A) and the timescale on which cytokine secretion ceased was similar. The dose required to initiate a T cell response was however substantially higher, consistent with previous reports [55, 110]. MIP-1β secretion was not measured after stimulating T cells with the physiological ligand because the ELISA kits were temporarily not available.

The observation that cytokine levels in the supernatant reached a steady level could be a result of a decrease in the cytokine production rate or an increase in the consumption of cytokines by T cells. To address this question, cytokine secretion by T cells in response to stimulation with the 9V pMHC was blocked with Brefeldin A and TNFα and IFNγ were subsequently detected by intracellular cytokine staining and flow cytometry. The frequency of cytokine-producing T cells decreased in time mirroring the dynamics of cytokine accumulation measured in the supernatant (Fig. 3.11), consistent with previous reports [208]. These data support the notion that T cells adapt their cytokine response



to the stimulus by reducing the cytokine production rate.

3.2.3 Adaptive cytokine dynamics challenge assumptions underlying the KPL-IFF model

We previously published the KPL-IFF model containing a Kinetic Proofreading, Limited signalling and an Incoherent Feed-Forward signalling motif, to explain efficient ligand discrimination, an optimal dissociation time and the bell-shaped dose-response curve, respectively [127]. The detailed time course of the cytokine response to a titration of pMHC in Fig. 3.9–3.10 revealed that the bell-shaped dose-response curve emerges dynamically after 3–4 hours when T cells stimulated with high doses of pMHC preferentially slowed down cytokine secretion. The KPL-IFF model, however, was based on the assumption that cytokine secretion was linear in time, supported by experimental data collected in the immortalised Jurkat T cell line. We conducted a similar time course experiment of IL-8 and MIP-1β secretion by Jurkat T cells in response to a titration of pMHC and

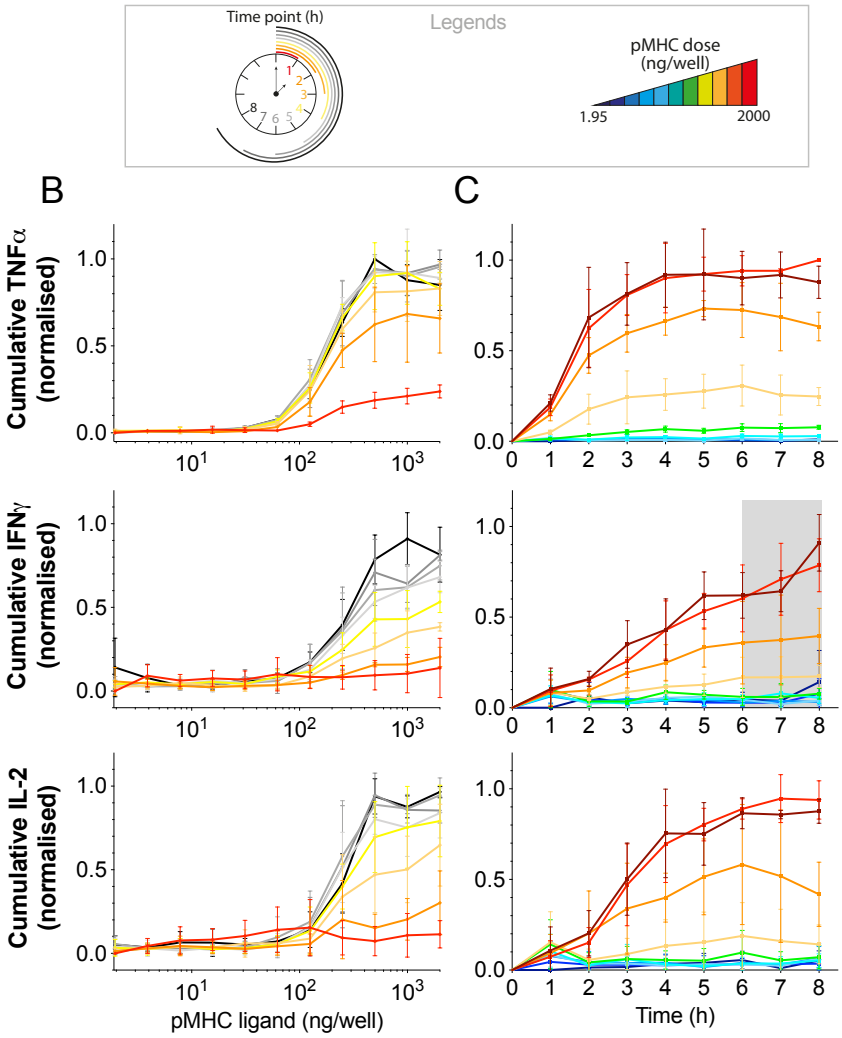


Figure 3.10: T cells adapt their cytokine response when stimulated with a low-affinity pMHC. CD8$^+$ primary T cells were stimulated with a titration of the 4A8K pMHC that binds the 1G4Hi TCR with physiological affinity. **(A)** Concentrations of TNFα, IFNγ and IL-2 were measured in the supernatant as a function of pMHC dose after 1–8 hours of stimulation. MIP-1β secretion was not measured after stimulating T cells with the physiological ligand because the ELISA kits were temporarily not available. The experiment was conducted independently with T cells from three donors. **(B)** Average and error (SD) of the dose-response curves shown in (A). For averaging, each dataset was normalised to the maximum cytokine level after 8 hours of stimulation. **(C)** The adaptation timescales were comparable to adaptation timescales after stimulation with a high-affinity pMHC (compare Fig. 3.9C) and comparable between TNFα, IFNγ and IL-2. Traces of biphasic IFNγ secretion again appeared biphasic with an early adaptation phase at 5–6 hours and a second secretion pulse between 6–8 hours (shaded area). MIP-1β secretion was not measured after stimulating T cells with the physiological ligand because the ELISA kits were temporarily not available to order.

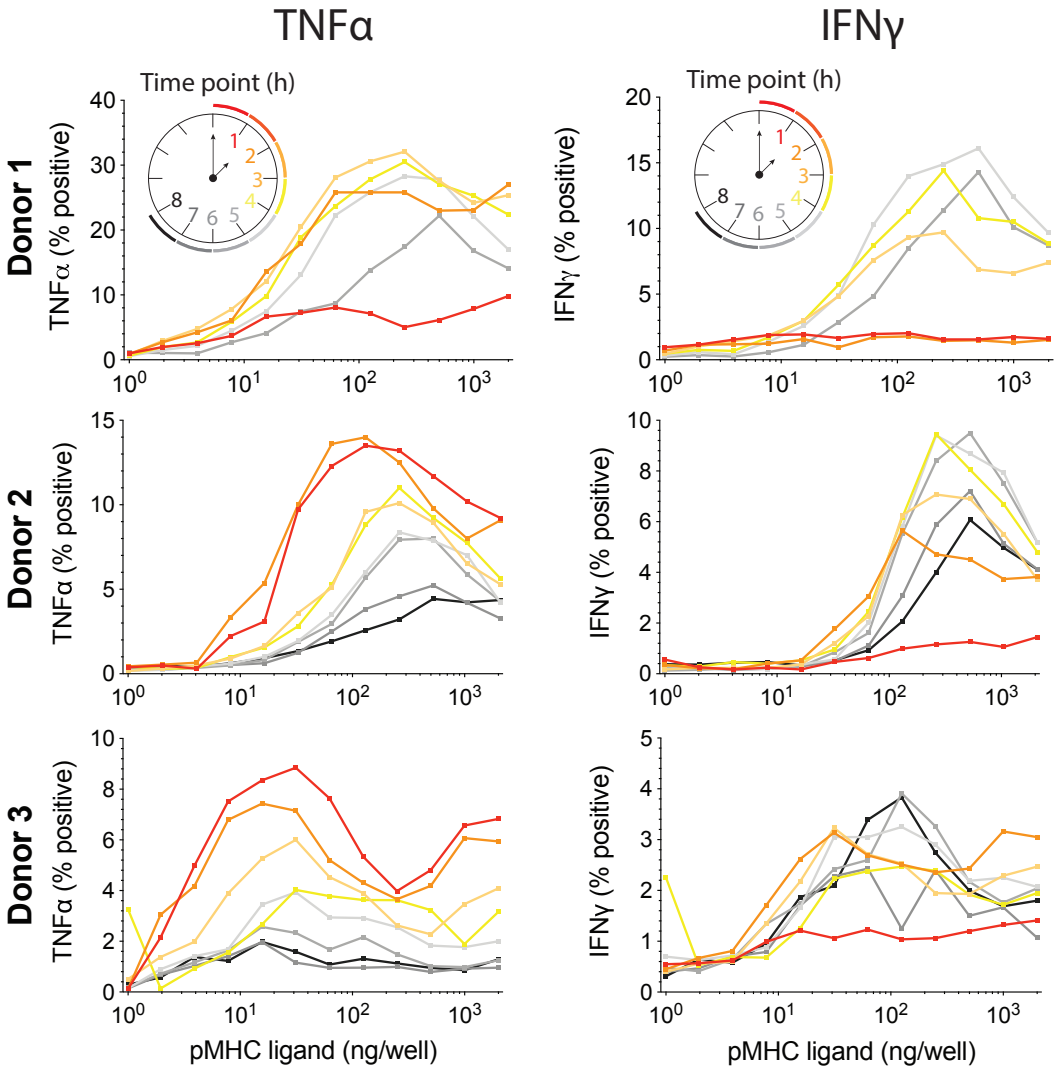


Figure 3.11: Intracellular cytokine staining confirms that T cells stop producing cytokines. T cells from three donors were stimulated with a titration of the high-affinity 9V pMHC for 1–8 hours. Brefeldin A was added to the samples for 1 hour prior to intracellular cytokine staining to block the secretion of cytokines and thus to determine the number of cytokine-producing T cells per hour. The frequency of TNFα- (left) and IFNγ-producing T cells (right) changed with kinetics that are consistent with the kinetics of cytokine accumulation measured in the supernatant by ELISA. These experiments were conducted by Stephanie Gaglione under supervision of Philipp Kruger, John Nguyen and Nicola Trendel.

found that secretion indeed appeared linear over the time period that was considered in our previous work (shaded area in Appendix Fig. A.3), but that it was similarly followed by adaptation. Importantly, because the rate of cytokine production appeared to be at steady-state, TCR downregulation was eliminated at the time as a mechanism producing the bell-shaped dose-response curve [127]. We have now shown that the timespan over which cytokine secretion is linear in primary T cells is much shorter than in Jurkat T cells, and the data presented here challenges the steady-state assumption and predictions of the KPL-IFF model.

3.2.4 TCR is rapidly removed from the T cell surface for several days

The TCR is known to be downregulated when T cells are presented with pMHC ligand [163, 255, 286]. Given that cytokine production requires continuous TCR signalling [92], we measured the level of TCR on T cells stimulated for 1–8 hours by pMHC-tetramer staining to assess whether TCR downregulation can explain the observed adaptation phenotype. TCR expression was quickly downregulated to a steady level after 1–2 hours of stimulation at all doses and affinities tested (Fig. 3.12A–D), consistent with the rapid downregulation observed in previous studies [47, 136, 254–256]. Fig. 3.12E shows that TCR downregulation was not an all-or-none response. Instead, 1G4Hi^{+} T cells reduced the level of TCR on their surface in an analogue manner, consistent with previous reports [83]. Partial TCR downregulation was maintained in response to intermediate pMHC doses even though the stimulus persisted (Fig. 3.12E). TCR expression therefore rapidly adopted a steady level that was dependent on the dose and affinity of the stimulating pMHC ligand.

Earlier dynamics of TCR downregulation could not be resolved reliably in this experimental system. Fewer T cells were retrieved from wells with high densities of immobilised pMHC after stimulation periods of less than 1 hour (Appendix Fig. A.4). It is possible that T cells still expressing the 1G4Hi TCR adhered to the stimulation plate at these early times, because the percentage decrease was comparable to the transduction level.

At later time points, the percentage of T cells expressing early activation markers such as CD69 in response to high doses of pMHC matched the transduction level so that a bias towards untransduced bystander T cells could be excluded.

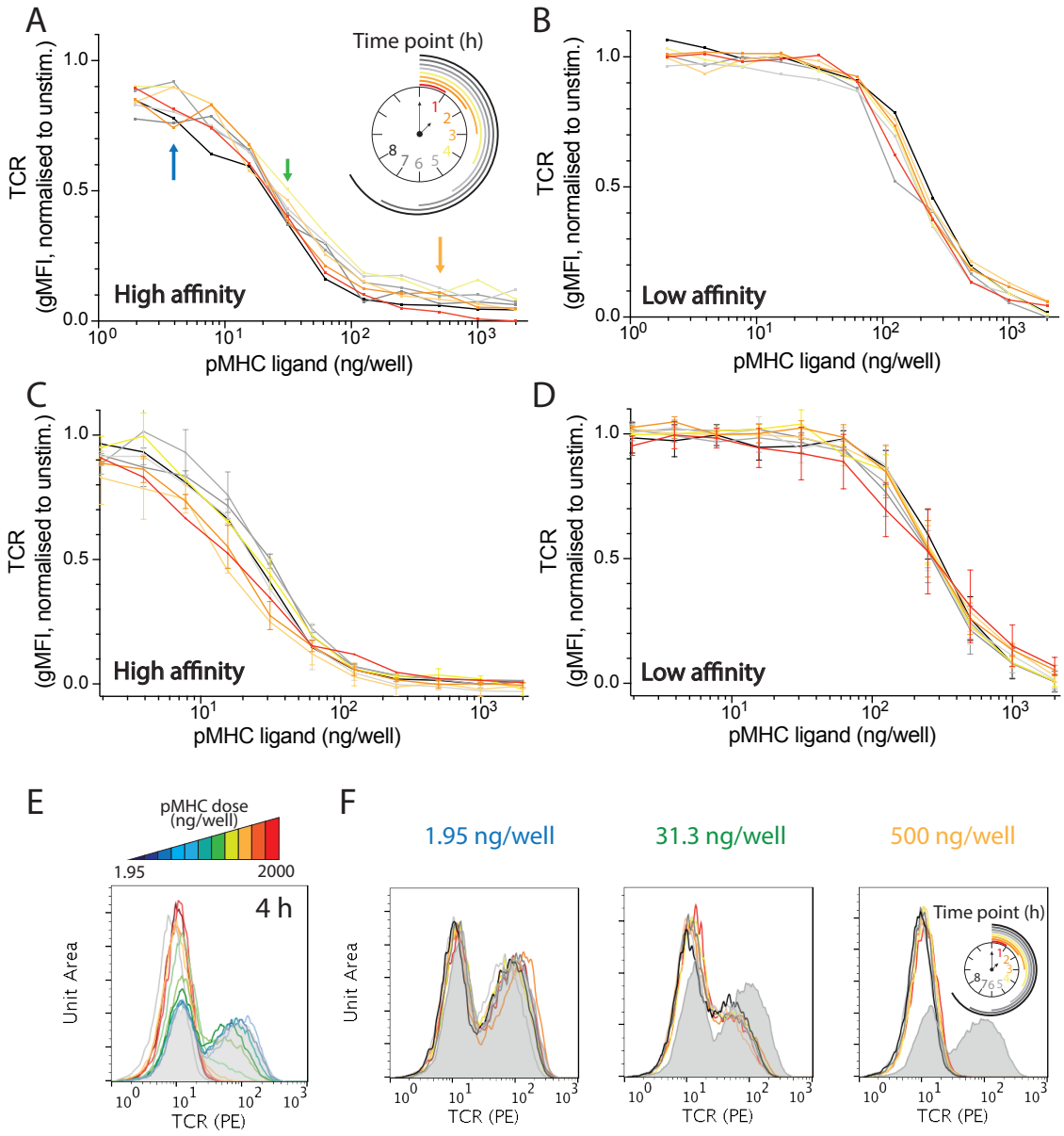


Figure 3.12: TCR is downregulated to a dose-dependent steady level within 1–2 hours of stimulation. Stimulation with the **(A)** 9V high-affinity pMHC or the **(B)** 4A8K low-affinity pMHC resulted in the rapid downregulation of TCR expression to a dose-dependent steady level (representative data). **(C)–(D)** Average of data from three independent experiments confirms the phenotype. **(E)** Different doses of the high-affinity 9V pMHC induced a graded decrease in TCR levels compared to the unstimulated control (gray). **(F)** The overlay of TCR expression at 1–8 hours after stimulation with three doses of pMHC confirms the rapid, analog and limited nature of TCR downregulation.

The steady intermediate level of TCR expression on the T cell surface could be a result of a balance between ligand-induced TCR downregulation and re-expression or a self-limiting process whereby the downregulation of the TCR reduces the rate of further TCR downregulation. To differentiate between these two possibilities, TCR downregulation was induced by stimulating T cells for 4 hours and recovery of the TCR on the T cell surface was monitored after removing the cells from the pMHC stimulus for 4–20 hours. The reduced TCR expression levels were relatively stable on the timescale of the 8-hour stimulation experiments and only recovered on the order of days (Figure 3.13A, C) consistent with previous reports [133, 161, 229, 265]. The TCR re-expression rate was similarly slow in the presence of 50 $\frac{\mathrm{U}}{\mathrm{ml}}$ of exogenous IL-2, suggesting that TCR re-expression was not hindered by cellular stress as a result of IL-2 deprivation (Figure 3.13B, D). TCR re-expression was therefore too slow to account for the observed steady-state suggesting that instead the rate of TCR downregulation ceases.

3.2.5 T cells adapted to a low-affinity pMHC can be reactivated with a higher-affinity pMHC

In an *in vivo* setting, T cells are likely to encounter pMHC ligands of varying strength, and TCRs have been shown to be highly crossreactive [274, 276]. We wondered how adaptation to one pMHC ligand would affect the T cell response in a subsequent encounter with a different pMHC ligand. T cells were pre-stimulated with different doses of either a high-affinity (9V) or a low-affinity pMHC (4A8K) for 5 hours and then transferred to either the same dose of the same pMHC or the same dose of a pMHC ligand with a different affinity (Fig. 3.14A, B). After the first 5 hours of stimulation, T cells had adapted to the pMHC stimulus because transfer to the same pMHC stimulus for another 5 hours resulted in a reduced TNFα or IFNγ response (Fig. 3.14C–D). Pre-stimulation with the high-affinity pMHC also led to unresponsiveness in the second encounter with a lower-affinity pMHC, but T cells that had been pre-stimulated with the low-affinity pMHC were still capable of responding to the higher-affinity pMHC. T cells adapted to a low-affinity pMHC could therefore be reinvigorated by stimulation with a high-affinity

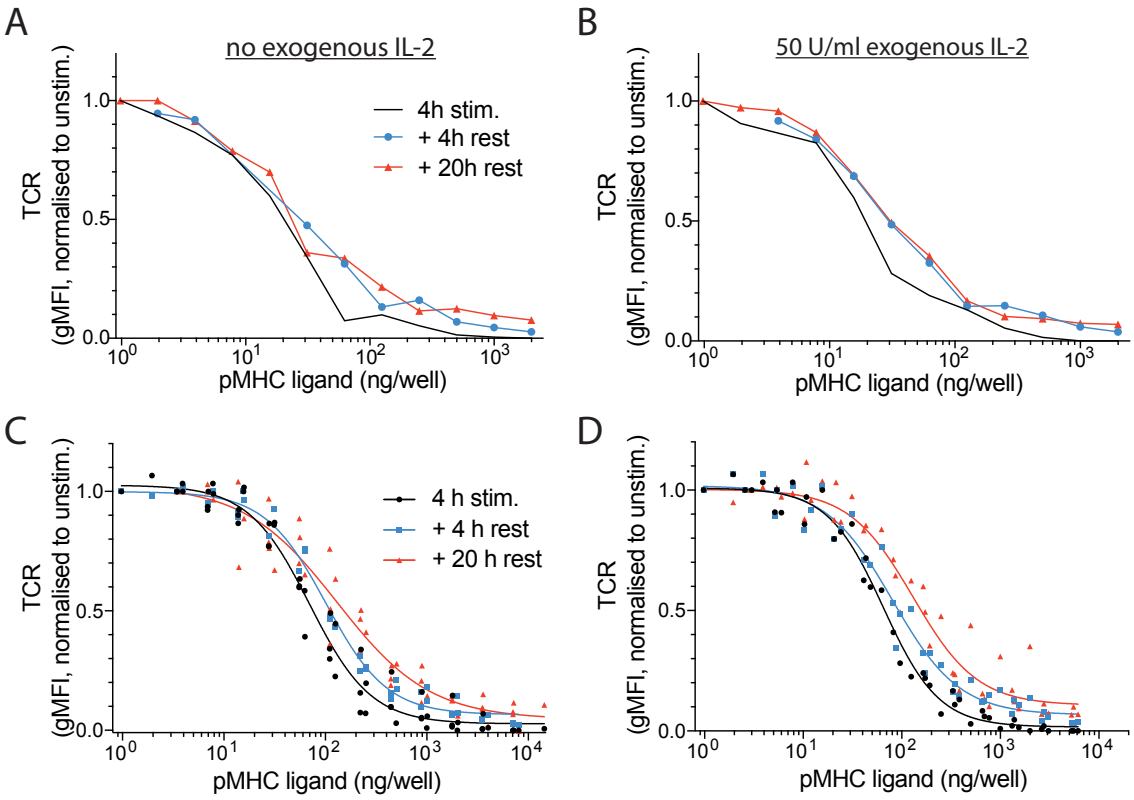


Figure 3.13: Re-expression of TCR on the cell surface is slow compared to the experimental timescale. T cells were stimulated with different doses of the intermediate-affinity 8K pMHC. **(A)** TCR expression was measured on the T cell surface after 4 hours of stimulation and after an additional 4–20 hours of rest in the absence of pMHC. **(B)** The TCR recovery rate was similar when 50 $\frac{U}{ml}$ exogenous IL-2 were added to the T cell suspension. **(C)-(D)** Averaging of six and four independent repeats, respectively, confirms the recovery rates in (A) and (B). To compare experiments with different TCR transduction levels, each dataset was normalised to the minimum and the maximum TCR expression after 4 hours of stimulation. A decreasing Hill function was then fitted to the pooled data (solid lines).

pMHC, indicating that T cells were not inherently unresponsive. Of note, the experiment furthermore showed that adaptation was not mediated by cytokine feedback because replacement of the supernatant between the first and second stimulation did not enable T cells to resume cytokine secretion.

3.3 Discussion

This chapter lays the foundation for the phenotypic mathematical model discussed in the following chapter by experimentally defining the target signalling phenotype to be explained by the model. T cells were found to adapt their cytokine response to a therapeutic high-affinity as well as to a physiological ligand of lower affinity on the order of several hours. Adaptation was observed at all doses of pMHC tested and it was concurrent with rapid TCR downregulation. Consistent with a role of TCR downregulation in adaptation, T cells that had adapted to a low-affinity pMHC remained responsive to stimulation with a high-affinity pMHC, whereas the sequential encounter of first a high- and then a low-affinity pMHC did not result in a cytokine response. Interestingly, an intermediate level of TCR was maintained at some doses of pMHC. These data thus raised the important question whether TCR downregulation can be the mechanism underlying functional adaptation even if some TCR remains on the surface of the cell (see following chapter).

3.3.1 The adaptation phenotype is consistent across different donors despite heterogeneous differentiation marker expression

The experiments were conducted in primary human $CD8^+$ T cells and, remarkably, the adaptation phenotype was robust across three donors although T cell populations expressed heterogeneous differentiation marker profiles. Functional experiments with human cells are typically highly variable, resulting in large error bars on averaged data or limiting analyses to representative repeats. Given the variability in the expression of differentiation markers before and after expansion of T cells in culture, we furthermore anticipated large functional discrepancies. Surprisingly, adaptation and the emergent bell-shaped dose-response curve were robust features of T cell activation that were consistent between donors. Normalising each dataset to the highest level of cytokine after 8 hours of stimulation was sufficient to directly average data across experiments without

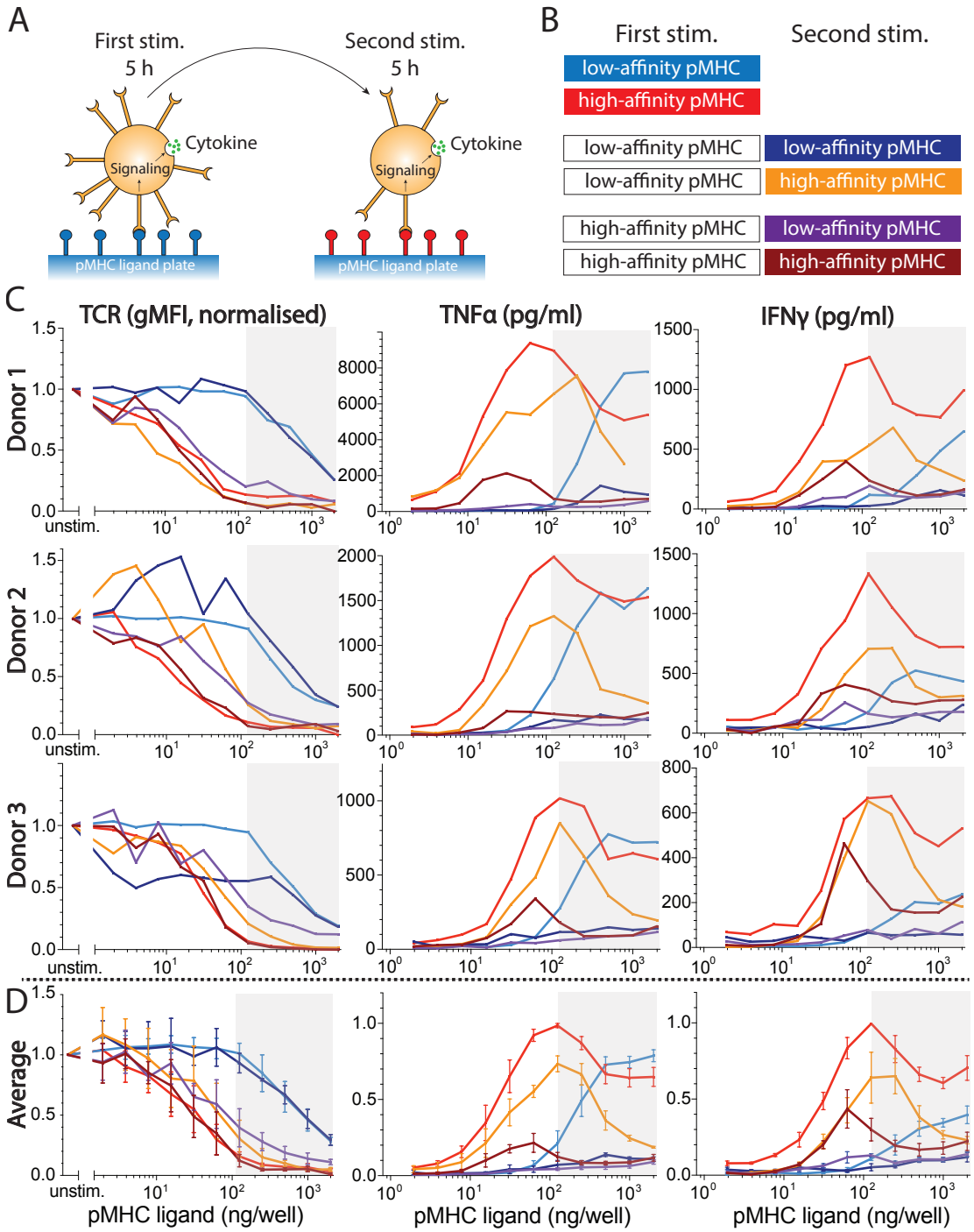


Figure 3.14: Adapted T cells can be reactivated by a higher-affinity pMHC. (A) Schematic of the experimental setup. T cells were pre-stimulated with either the low-affinity 4A8K or the high-affinity 9V pMHC for 5 hours and subsequently transferred to pMHC of the same dose and with either the same or a higher/lower affinity. **(B)** Legend for dose-response plots in (C)-(D). **(C)** TCR expression (left) was measured by pMHC-tetramer staining of stimulated T cells after the first or second stimulation, respectively, and the cytokines TNFα (middle) and IFNγ (right) were measured in the supernatant by ELISA after the first or second stimulation, respectively, in three independent experiments. T cells that had adapted to a low-affinity pMHC (from bright blue to dark blue) were capable of responding to the higher-affinity pMHC (orange). **(D)** Mean and SEM of the three independent experimental repeats shown in (C).

altering the functional adaptation phenotype observed in individual repeats, with the exception of biphasic IFNγ secretion, which was evident in individual repeats but not in the averaged data. Measuring the T cell response over a wide range of pMHC doses likely facilitated reproducibility after averaging as the variability in absolute cytokine levels for a given pMHC dose is much larger. We speculate that the specific differentiation state of antigen-experienced T cells predominantly affects the amplitude (absolute amount) of the cytokine response rather than the activation threshold or response dynamics [78], and that these factors were corrected for by the normalisation.

3.3.2 Relation between adaptation and previously described unresponsive states

The term anergy has historically been used to describe T cell populations that are unable to respond to pMHC re-stimulation but survive over an extended period of time [220]. The terminology describing states of T cell anergy was initially ambiguous and multiple states of unresponsiveness are now distinguished on the basis of mechanisms that induce them, the functional phenotype and the requirements for their maintenance. States of T cell unresponsiveness reported in the literature include clonal anergy, exhaustion and adaptive tolerance.

The unresponsive state described here is distinct from clonal anergy. Clonal anergy is induced in naïve T cells after they received a strong but incomplete signal such as strong pMHC stimulation through the TCR in the absence of co-stimulation or a weak TCR signal in the presence of co-stimulation. We, on the contrary, observed adaptation both to the high- and the low-affinity stimulus and at all doses of pMHC. In addition, clonal anergy describes a state of growth arrest and involves impaired IL-2 production specifically, while other cytokines and inflammatory chemokines are only marginally effected [220]. Here, we found that the four cytokines and chemokines TNFα, MIP-1β, IFNγ and IL-2 all show signatures of adaptation. Clonal anergy is reversed by IL-2 [220], while in our experimental system adaptation is initiated while T cells still secreted IL-2, suggesting that at least autocrine IL-2 signalling could not augment T cell responsiveness. Most

importantly, however, the T cell populations used in our experiments were not naïve T cells, but $CD8^+$ effector or T_{EM}.

Exhaustion is a dysfunctional T cell state that has been observed after prolonged stimulation of naïve T cells with pMHC for several weeks *in vivo* [216, 272]. It is characterised by epigenetic and transcriptional changes that favour the expression of inhibitory receptors such as PD-1 [216]. The number of inhibitory receptors expressed on the T cell surface correlates with the extent to which T cell function is exhausted and exhausted T cells can be reinvigorated by antibody blockade of inhibitory receptors [272], suggesting that their modulatory signals play a crucial role in the maintenance of the unresponsive state. The benefit of studying the T cell response in a minimal experimental system like the one used here is that we can exclude regulatory effects through inhibitory receptors because their ligands were not present. Moreover, adaptation preceded the upregulation of PD-1 in response to stimulation (data not shown). The timescale at which T cells become exhausted, the critical role of signalling through inhibitory receptors and the hierarchy according to which effector functions are lost in T cell exhaustion are therefore inconsistent with the adaptation phenotype described here.

The adaptation phenotype we described is most consistent with a state known as adaptive tolerance or *in vivo* tolerance. Chronic antigen exposure has been shown to render T cells unable to secrete a range of cytokines and chemokines [220], consistent with the phenotype we observed for TNFα, MIP-1β, IFNγ and IL-2. Adaptive tolerance is reversed upon antigen removal within several days. This time scale is on the same order as the expected recovery rate of TCR on the T cell surface [133, 161, 229, 265]. It would be interesting to study whether T cells regain their responsiveness to pMHC in our minimal experimental system if they are left without stimulating pMHC for several days, but these experiments are difficult to realise because human T cells only survive for a limited amount of time in culture.

3.3.3 A TCR-proximal signalling block is associated with unresponsiveness *in vivo*

Whether TCR downregulation plays a role in the induction and maintenance of unresponsive states such as adaptive tolerance remains controversial, but an alternative mechanism has not been identified conclusively. Adaptive tolerance has been studied extensively in *in vivo* transgenic mouse models. The analysis of signalling in tolerised $CD4^+$ T cells revealed that their response was attenuated by an early block in TCR signalling. The activity of ZAP-70 but not Lck was reduced in one study [31], though a decrease in the latter has been observed in other adaptation models. While some studies established a clear correlation between reduced TCR levels and adaptive tolerance [60, 218, 233, 241], overt TCR downregulation was not observed in other studies [79, 81, 125, 225]. Of note, most of these studies focused on $CD4^+$ T cells, but adaptive tolerance has also been observed in transgenic mouse models with $CD8^+$ T cell [32, 74].

In particular, two studies in $CD8^+$ T cells support the hypothesis that adaptive tolerance is mediated by TCR downregulation. First, Guillaume et al. [74] confirmed that early TCR signalling was blocked in adaptive tolerance in a transgenic mouse model. They measured lower levels of CD3ζ in tolerised T cells that did not associate efficiently with CD3ϵ and correlated with reduced TCR levels on the cell surface compared to non-tolerised T cells. Consequently, CD3ζ phosphorylation and Src kinase activity were reduced in unresponsive T cells. These data strongly argue for a receptor-mediated tolerance mechanism. Interestingly, the same biochemical changes were not detected in $CD4^+$ T cells and it is thus unclear whether different mechanisms induce unresponsiveness in $CD4^+$ and $CD8^+$ T cells [32].

Second, Teague et al. [244] were able to localise a mechanism of adaptation to the TCR by using a mouse model with $CD8^+$ T cells that expressed two TCRs: One TCR recognised constitutively-expressed self-antigen while the other TCR was specific for exogenous viral antigen. They showed that T cells can become tolerant to the self-antigen, and yet preserve their ability to respond to the exogenous viral antigen through the second TCR. Importantly, tolerised T cells could be activated by αCD3 but

not by antibodies specific to the α- and β-chains of the tolerised TCR in dual receptor T cells only. Furthermore, tolerised T cells were unable to form a normal synapse and the signalling block was located as far upstream as ZAP-70 recruitment and phosphorylation. Because no overt TCR downregulation was observed, the authors argued that instead the TCR must be in a tolerised conformation.

It is structurally unclear what this tolerised conformation would be. One possibility is that after chronic stimulation, the TCR is separated from the CD8 co-receptor as suggested by Demotte et al. [44]. In an *in vitro* experiment, the authors found a decrease in the cytolytic potential of T cells that were stimulated with peptide-pulsed APCs that coincided with decreased labelling of T cells with pMHC tetramers. They argued that the apparent loss in tetramer staining was not a result of TCR downregulation, but the experiments are not conclusive as TCR expression was only analysed on $CD3^+$ T cells. Because the stability of TCR and CD3 is interdependent, these results do not preclude the coordinated loss of TCR and CD3. A kinetic experiment in the study indeed suggested a transient decrease in TCRα and TCRβ expression but the time resolution is low so that the exact dynamics cannot be deduced. Nonetheless, it is unlikely that dissociation of CD8 from the TCR caused impaired pMHC-tetramer staining in our study, as we have previously used identical pMHC-tetramers to stain for the 1G4Hi TCR transduced in $CD4^+$ T cells (Appendix Fig. A.5). We were able to detect the 1G4Hi TCR in the absence of CD8 with high signal-to-noise ratio, suggesting that binding between pMHC tetramers and the TCR does not require co-receptor expression or co-localisation.

Other negative regulators of TCR proximal signalling have been studied to explain adaptive tolerance, but no single molecular mechanism transpired as responsible for the unresponsive state. Tolerant T cells were shown to express elevated levels of Fyn and CD5. Choi et al. [32] report however that CD5-deficient as well as Fyn-deficient T cells still became tolerant after continuous *in vivo* stimulation. Alternatively, the protein tyrosine phosphatase SHP-1 has been suggested to inhibit TCR-proximal signalling and recent studies claimed that SHP-1 could be responsible for hyporesponsiveness of T cells transduced with therapeutic TCRs (nanomolar affinity) [82, 192]. A caveat in these studies is that the highest-affinity TCRs crossreacted with HLA and expressed lower basal

surface levels of TCR and CD3 as well as some activation markers, including PD-1. It is therefore unclear whether T cells expressing the highest-affinity TCR were less responsive compared to T cells expressing an intermediate-affinity TCR because they expressed lower level of the TCR, or because TCR-proximal signalling was suppressed by SHP-1. In murine $CD4^+$ T cells, Choi et al. report no effect of a SHP-1 knockout on adaptive tolerance induction [32]. Given that adaptive tolerance has mostly been studied in *in vivo* mouse models, it is likely that the adaptation phenotypes described in the literature reflect the sum of a large number of regulatory mechanisms.

3.3.4 *In vitro* experiments suggest calibration of the T cell response by tuning TCR expression levels

The effect of TCR expression levels on different functional readouts in sequential ligand encounters was studied in transfer experiments comparable to those described in Section 3.2.5. Valitutti et al. [256] showed that calcium signalling was terminated in $CD4^+$ T cells as the TCR was downregulated, but, consistent with our findings, adapted T cells were able to respond to APCs presenting higher doses of the stimulating pMHC. Martin et al. [147] found a strong correlation between the cytolytic activity of tolerised T cells during secondary stimulation and their TCR levels. APCs were used to present P14 transgenic $CD8^+$ T cells with pMHC and induced TCR downregulation in an affinity- and dose-dependent manner. Tolerised T cells were then subjected to a second round of stimulation and their ability to kill target cells correlated with the level of TCR that remained on the T cell surface after primary stimulation. Furthermore, adapted T cells regained responsiveness on the same timescale as they re-expressed the TCR [147]. Together, the *in vitro* transfer experiments described here point towards a TCR proximal tuning mechanism in sequential pMHC ligand encounters and they are consistent with a role of TCR expression levels in calibrating the T cell response.

3.3.5 Functional significance of prolonged TCR downregulation

The 1G4Hi TCR was expressed under an exogenous promoter and this raises the question whether the TCR expression kinetics reported here are relevant when the TCR is under endogenous control. The 1G4Hi TCR was lentivirally transduced into T cells and its expression was controlled by the exogenous EF-1α promoter. Because EF-1α is a strong, constitutively active promoter and CD3ζ is the limiting factor of TCR-CD3 assembly and surface expression [5], the timescale of TCR re-expression under the endogenous TCR promoter is likely to be similar. In the future, CRISPR/Cas9 may be used to replace the endogenous TCR by engineered receptors to exploit natural fine-tuning of TCR expression under the native promoter. Eyquem et al. [58] pioneered by placing a CAR under the control of the TCRα promoter. They found that the location of the receptor impacted the dynamics of TCR expression, but the recovery rate was consistently on the order of days. This timescale is contrasted by rapid TCR downregulation within few hours. The TCR expression kinetics under the exogenous promoter in our as well as other experimental systems that reported similar time scales [47, 133, 136, 161, 163, 229, 254–256, 265] are thus likely comparable to TCR expression kinetics under endogenous control.

Fine-tuning of TCR expression levels could prevent T cells from overreacting to a pathogenic threat. Yet $CD8^+$ T cells are known to be able to kill multiple infected cells sequentially *in vivo* [76]. We did not measure target cell killing in our assays, but cytotoxicity has been shown to underly a lower activation threshold than cytokine secretion [256], so that residual TCR signalling may be enough for killing but not for cytokine secretion. More importantly, however, cytokine feedbacks, such as the stimulatory effect of IL-2 on IFNγ secretion reported here and elsewhere [107, 156, 246], as well antigen-dependent co-stimulation seem capable of overcoming desensitisation by TCR downregulation. We have shown in our lab that co-stimulation of adapted T cells with ligands to 4-1BB or CD28 reinvigorates T cells (unpublished data by Philipp Kruger and John Nguyen). In an inflammatory setting, the T cell response appears to compromise about preventing tissue damage and protection against exogenous threats by conditioning

the T cell response calibrated by TCR downregulation on complementary signals.

CHAPTER 4

A phenotypic model explains adaptation at all pMHC doses with TCR downregulation

The experimental interrogation of the T cell signalling machinery revealed several interesting features about the kinetics as well as the dose- and affinity-dependence of TCR downregulation and cytokine secretion. Of particular interest to us was the relation between TCR downregulation and functional adaptation of the T cell response, which has been controversial in the past. A phenotypic model was therefore constructed based on close inspection of the experimental data in Chapter 3 and the literature to explain the signalling phenotype consisting of the observed TCR downregulation and adaptation of cytokine secretion. The model provides a framework to test hypotheses about the relation between TCR downregulation and signalling for which the underlying molecular mechanisms remain incompletely understood.

4.1 Introduction

4.1.1 Receptor downregulation as a mechanism to induce adaptation

The adaptation phenotype described in Chapter 3 was associated with a rapid and long-lasting decrease in TCR surface expression. Downregulation of receptors, including CD16 in NK cells [70], growth hormone receptors [65] and epidermal growth factor receptors [137], has been found to induce adaptation in other receptor-ligand systems. The role of TCR downregulation in adaptation is, however, controversial. Desensitisation to sustained stimulation was often attributed to other, unidentified signalling changes because a small reduction in TCR levels appeared insufficient to account for complete functional adaptation [79, 87, 125, 225]. The mathematical model presented in this chapter addresses the inherently quantitative question whether TCR downregulation can explain the adaptation phenotype described in the previous chapter when some TCR remains on the T cell surface.

4.1.2 Cooperative binding between TCR and pMHC

Early work suggested that interaction dynamics between TCR and pMHC can be described by the law of mass action [239], but an increasing amount of experimental data [56, 148, 188] and theoretical evidence [12, 229, 252] suggest that binding between TCR and pMHC is cooperative. Cooperative binding means that a binding event between a TCR and pMHC increases the rate of subsequent ligation of further TCRs by pMHC. Here, we investigated whether cooperative binding is consistent with the experimental data in Chapter 3. Because the apparent steady-state of TCR levels after pMHC stimulation was not a result of balanced up- and downregulation rates, we hypothesised that the kinetics of ligand-induced TCR downregulation were dictated by cooperative binding between TCR and pMHC.

The mechanisms that underlie cooperative binding are elusive. It has been proposed that ligand-induced aggregation of TCRs in nanoclusters favours rebinding and serial

ligation of many TCRs by the same pMHC ligand [51, 236, 252]. Additionally, it has recently been suggested that ligation of the TCR can cooperatively induce neighbouring TCRs to adopt an active conformation in a signalling-independent manner [148]. The stoichiometry of TCRs in the resting state remains however controversial [23, 148], and in an imaging study, Pielak et al. observed cooperative binding between TCR and pMHC even when TCRs were micrometers apart [188], implying that the direct physical contact as a result of TCR aggregation is not required for cooperative binding. Instead, the authors speculate that a signalling-dependent mechanism such as remodelling of the T cell-APC interface may confer cooperativity. Irrespective of the molecular mechanism, cooperative binding between pMHC and TCR could improve the sensitivity of antigen discrimination to small numbers of cognate pMHC [56].

4.1.3 Digital signalling in T cell activation

The TNFα dose-response curve after stimulation with the low-affinity pMHC ligand 4A8K was in the previous chapter found to be relatively steep (Fig. 3.10B, Hill coefficient of ~3.1 at 8 hours). Steep dose-response curves can be indicative of digital all-or-none T cell responses on a single-cell level. Indeed, digital cytokine secretion has been reported in other experimental systems [8, 41, 89, 113, 234, 249]. Huang et al., for example, captured secreted cytokines on the T cell surface and simultaneously imaged the number of pMHC ligands in the T cell-APC interface [89]. Their study revealed that T cells are capable of responding to small numbers of pMHC ligands and that the amount of cytokine secreted per cell did not increase as additional pMHC ligands were detected in the interface. In addition, activation markers such as CD69 and 4-1BB show signatures of sharp activation thresholds as their expression profiles appear bimodal on a population level and an increase in the pMHC dose results in an increase in the number of responding T cells rather than a change in the expression level per cell (Appendix Fig. A.1) [7, 41]. Upstream of these functional readouts, sharp activation thresholds were found in the NFκB [113, 172] and ERK signalling pathways [41]. The later has been ascribed to a positive feedback mechanism that digitally catalyses the conversion of inactive RasGDP into active RasGTP

by the guanine exchange factor SOS because the activity of SOS is enhanced when it binds to the RasGTP product of the reaction [8, 41, 234]. Since signatures of sharp activation thresholds exist in multiple TCR-triggered pathways, Kingeter et al. [113] speculated that the switch may be relatively upstream.

4.1.4 Engaged and non-engaged TCRs are downregulated by two independent mechanisms

In order to develop a model of TCR downregulation and its influence on the functional T cell response, it was important to know how these two ligand-induced effects were linked. Early work on TCR downregulation supported the hypothesis that TCR downregulation is signalling-dependent because the IFNγ response as a result of TCR signalling was shown to correlate strongly with TCR downregulation [263]. Direct support for a role of TCR signalling in TCR downregulation came from studies that perturbed the activity of Lck, which initiates TCR signalling by phosphorylation of the CD3ζ chain. Inhibition of Lck was by some studies reported to completely block TCR downregulation [17]. TCR downregulation was enhanced in murine transgenic T cells expressing a constitutively active isoform of Lck, and the effect was reversed in the presence of Lck inhibitors [53]. TCR signalling via Lck was therefore attributed a critical role in TCR downregulation. Subsequent studies however suggested that ligand-induced TCR downregulation does not rely on TCR signalling. Inhibition of Lck by various inhibitors prevented a functional T cell response but not TCR downregulation [25, 210], contrary to previous reports [17]. Ligand-induced TCR downregulation could therefore be dissociated from proximal TCR signalling as well as the functional T cell response, indicating that the two processes are mediated by independent mechanisms.

The consensus now is that at least two pathways prompt ligand-induced TCR downregulation. Detailed analyses of TCR downregulation in dual-receptor T cells showed that non-engaged and engaged TCRs were downregulated by a TCR signalling-dependent and -independent pathway, respectively [165, 214]. PKC, a downstream target of TCR signalling, plays a central role in the signalling-dependent pathway of TCR downregu-

lation [266], consistent with early studies showing that direct stimulation of PKC by phorbol esters induces TCR downregulation [27, 49, 163, 251]. Upon activation, PKC phosphorylates a serine residue (S126) on the cytoplasmic tail of CD3γ that forces the exposure of a membrane-proximal di-leucine motif (L131L132) that is also involved in constitutive cycling of the TCR [16, 48, 49, 175]. However, additional mechanisms may lead to the downregulation of non-engaged TCRs because chimeric receptors containing only the CD3ζ-chain coupled to the trans-membrane and ectodomains of an unrelated protein were downregulated when T cells were stimulated through the TCR [214]. Non-engaged receptors were not trans-phosphorylated by signalling TCRs, so that the mechanism must involve unphosphorylated ITAMs or other motifs on CD3ζ. One possibility is the recruitment of β-Arrestin-1 that can interact with unphosphorylated ITAMs on CD3ζ [61].

Signalling-independent TCR downregulation is less well understood. The process involves ubiquitination of engaged TCRs as several E3 ubiquitin ligases, including Casitas B-Lineage Lymphoma-b (Cbl-b) [170], c-Cbl [169–171] and Gene Related to Anergy In Lymphocytes (GRAIL) [177], are implicated in TCR downregulation. Downregulation of engaged TCRs thus at least in part leads to the degradation of TCR and CD3 by direct targeting of these molecules to the lysosome [53, 133, 170, 254].

Interestingly, the relative contribution of the signalling-dependent and -independent pathways to the observed decrease in TCR surface levels varied according to the dose of the stimulating pMHC: TCR downregulation was largely prevented in the presence of an Lck inhibitor when T cells were stimulated with low doses of pMHC, but it was unaffected by the Lck inhibitor when T cells were stimulated with a high dose of pMHC [165, 214]. These findings were reproduced in our experimental system (Fig. 4.1).

4.1.5 Summary of the experimental phenotype to be explained by the phenotypic model

A phenotypic modelling approach was employed to explain several striking features of the T cell response in our minimal experimental system. Ligand-induced cytokine secretion is regulated by a complex signalling cascade linking ligation of the TCR to

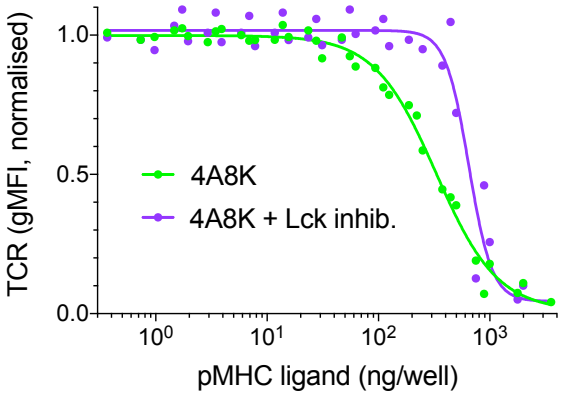


Figure 4.1: TCR downregulation is reduced by inhibition of Lck at low but not high doses of stimulating pMHC. Primary $CD8^+$ T cells transduced with the 1G4Hi TCR were stimulated with the 4A8K pMHC for 4 hours in the presence (purple) or absence (green) of the Lck inhibitor A-770041 [232]. At these doses of the inhibitor, the functional response is completely blocked (data not shown). Surface TCRs were labelled with fluorophore-conjugated pMHC tetramers and TCR expression levels were quantified by flow cytometry. Data from three independent repeats were normalised and pooled as described in Methods Section 2.7.1. The phenotype is similar after 8 hours of stimulation and when 20 μM PP2 were used to inhibit additional Src-family kinases such as Fyn (data not shown). The experiment was conducted by Philipp Kruger.

transcriptional and translational changes via a large number of signalling intermediates. To quantitatively understand whole signalling pathways, it is not feasible to formulate a detailed molecular model of the pathway. Instead, it can be useful to consider the overall, effective mechanisms in the pathway that produce a defined signalling phenotype. Here, the phenotypic modelling approach was used to explain the following target phenotype:

1. TCR is rapidly downregulated to a steady-level despite slow TCR re-expression in the absence of pMHC ligand.
2. Inhibition of TCR signalling impairs TCR downregulation in a pMHC dose-dependent manner.
3. T cells adapt their cytokine response to the pMHC stimulus.

These three features were derived from the systematic experimental interrogation of the T cell signalling machinery in Chapter 3 and the experimental findings on the signalling-requirements for TCR downregulation [165, 214] that we reproduced in our minimal

experimental system (Fig. 4.1). The resulting phenotypic model is of a modular nature and highlights three key signalling modules that together explain the target phenotype. The target phenotype as well as references to relevant experimental data and modelling are summarised in Table 4.1.

4.1.6 Chapter overview

We formulated an effective phenotypic model motivated by features of the experimental data in the previous chapter and by the literature to explain the target phenotype. The model comprises three key modules: (1) Cooperative binding between TCR and pMHC (Section 4.2.2), (2) two pathways for downregulation of engaged and non-engaged TCRs, respectively (Section 4.2.3), and (3) digital activation of downstream signalling (Section 4.2.4). These are discussed individually in the remainder of the chapter. Direct fitting of the phenotypic model to the experimental data by ABC-SMC confirmed good agreement between the model and the target phenotype. The phenotypic model illustrates that adaptation of the T cell response can result from TCR downregulation, even at pMHC doses and affinities that induce only partial TCR downregulation.

Target phenotype	Key model features	Figures	
		Experiments	Model
Rapid TCR downregulation despite slow TCR re-expression	Cooperative binding	Fig. 3.11, Fig. 3.12	Fig. 4.6
pMHC dose-dependent impairment of TCR downregulation in the absence of TCR signalling	Signalling-dependent downregulation of non-engaged TCRs	Fig. 4.1	Fig. 4.7
Adaptation in cytokine production	Switch-like activation of downstream signalling	Fig. 3.8, Fig. 3.9	Fig. 4.8

Table 4.1: Definition of the target phenotype, key model features and figure references.

4.2 Results

Three key assumptions were sufficient to explain the target phenotype in Table 4.1 (Section 4.2.1), and these are discussed sequentially (Sections 4.2.2–4.2.4). An emergent feature from directly fitting the model to the experimental data was temporal integration of short-lived TCR signalling by downstream signalling intermediates (Section 4.2.5). The model furthermore predicted that T cells that have adapted to a low-affinity pMHC are capable of responding to a higher-affinity pMHC (Section 4.2.6), which was confirmed experimentally in the previous chapter.

4.2.1 A phenotypic model explains the full target phenotype

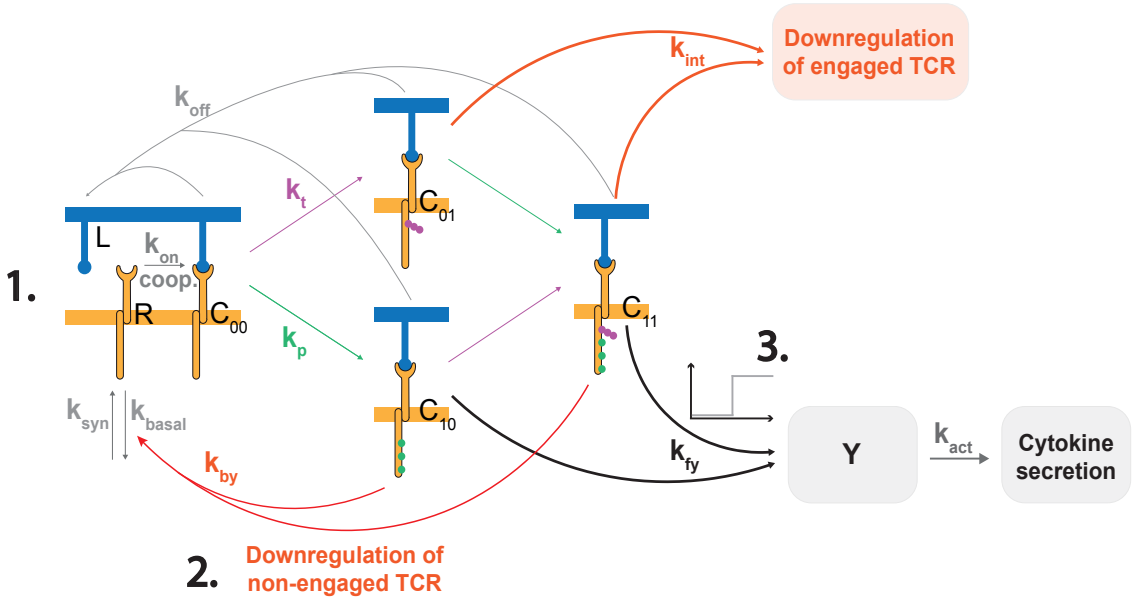


Figure 4.2: A phenotypic model explains the full target phenotype. Schematic of a phenotypic model that explains ligand-induced TCR downregulation and the functional T cell response based on three key signalling modules: (1) Cooperative binding between TCR and pMHC, (2) signalling-dependent downregulation of non-engaged TCRs and (3) digital activation of downstream signalling. A full list of parameters is provided in Table 4.2 and the corresponding ODE model is included in the Appendix Section B.1.

The phenotypic model in Fig. 4.2 consists of a TCR downregulation module that is coupled to TCR signalling and downstream activation. In the model, TCR (R) cooperatively binds pMHC ligand (L) to form a complex (C_{00}) that can be tagged for

downregulation (purple tag, C_{01}), phosphorylated to become signalling-competent (green tag, C_{10}) or both (C_{11}). Bound and unbound TCRs are downregulated at a basal rate (not shown for TCR-pMHC complexes). The rate of downregulation of TCRs is increased when the TCR is engaged and tagged for downregulation. Non-engaged TCR can be downregulated at an increased rate by a signalling-dependent mechanism. The downstream signalling intermediate, Y, is only activated if the sum of signalling-competent TCRs, $C_p = C_{10} + C_{11}$, exceeds a sharp threshold. Finally, the amount of cytokine that accumulates in the supernatant is directly dependent on Y. A full list of model parameters is provided in Table 4.2.

Name	Unit	Description	Name	Unit	Description
k_{prop}	$ng^{-1}\mu m^{-2}$	Conversion from ng/well to μm^{-2}	k_p	s^{-1}	Tagging for signalling / phosphorylation
k_{syn}	$s^{-1}\,\mu m^{-2}$	Basal TCR upregulation rate	k_{int}	s^{-1}	Downregulation rate of ligated TCR
k_{basal}	s^{-1}	Basal TCR downregulation rate	k_{by}	$s^{-1}\,\mu m^2$	Downregulation rate of bystander TCR
k_{on}	$s^{-1}\,\mu m^2$	on-rate	k_{fy}	s^{-1}	Scaling of switch-like activation
n_b	[ ]	Binding cooperativity	k_{ry}	s^{-1}	Degradation of switch
k_{off1}	s^{-1}	off-rate low-affinity ligand	s_y	μm^{-2}	Threshold of switch-like activation
k_{off2}	s^{-1}	off-rate high-affinity ligand	n_y	[ ]	Slope of switch-like activation
k_t	s^{-1}	Tagging for downregulation	k_{act}	s^{-1}	Cytokine production rate

Table 4.2: Full list of model parameters. Overview and description of model parameters as they are annotated in schematics, ODEs and MATLAB (MathWorks, Inc.) code.

To determine whether the phenotypic model was consistent with the target phenotype, we fitted it directly to the corresponding experimental data. The complete dataset is shown in Fig. 4.3 and it consisted of a time course of TCR downregulation and TNFα secretion in response to a low- (A–B) and a high-affinity pMHC (C–D), a TCR re-expression time course (E) and the observed dose-dependent difference between TCR downregulation in the presence and absence of the A-770041 Lck inhibitor (F). The data were averaged across experimental repeats before fitting as described in Methods Section 2.7.1. The model shown schematically in Fig. 4.2 was translated into a coupled system of ordinary differential equations (ODEs, see Appendix B.1) and evaluated in

MATLAB (MathWorks, Inc.).

The model was fitted to the data in a two-step process. In the phenotypic model, TCR re-expression in the absence of pMHC ligand is solely dependent on the constitutive TCR up- and downregulation rates, and so the TCR re-expression time course (Fig. 4.3E) was fitted separately. The basal downregulation rate was fixed to $k_{basal} = \frac{k_{syn}}{R_0}$, with $R_0 = 100\ \frac{molecules}{\mu m^2}$ as an estimate of the density of surface TCR in the resting state [55, 270]. The constitutive upregulation rate was thus the only parameter to be fitted and it was determined to be $k_{syn} \approx 3.1{\times}10^{-4}\ s^{-1}\mu m^{-2}$. As expected, these fitted basal TCR cycling rates were slow compared to the experimental timescale of several hours and they are unlikely to have a noticeable effect on the TCR steady-state that was observed within 1 hour of stimulation. The basal up- and downregulation rates were kept constant in the second step of the fitting procedure to minimise the number of parameters to be determined simultaneously.

An Approximate Bayesian Computation framework with Sequential Monte Carlo (ABC-SMC, Methods Section 2.7.3) was applied to determine the posterior distribution on the remaining 13 model parameters. 10,000 particles (combinations of specific values for the 13 parameters) were initialised uniformly in parameter space. The population of particles was then propagated through 15 iterations such that the parameter space with particles that produced the best fits was preferentially explored. To obtain a point estimate of the posterior distribution on the model parameters, the particle with the smallest distance (SSR) at the final iteration was selected. The parameter values associated with the particle were used to produce the model fits shown in Fig. 4.3. Deviations of the fits from the experimental data were generally within the experimental error. Importantly, the model is capable of explaining the target phenotype, including the dynamics of TCR expression (in response to both a low- and a high-affinity pMHC), the dependence of TCR downregulation on TCR signalling when stimulating T cells with different doses of pMHC and adaptation of the cytokine response for all pMHC doses and affinities. The model furthermore explains the reduced response to high doses of a high-affinity pMHC compared to intermediate doses of pMHC (bell-shaped dose-response curve).

Two visible discrepancies exist between the model prediction and the time course

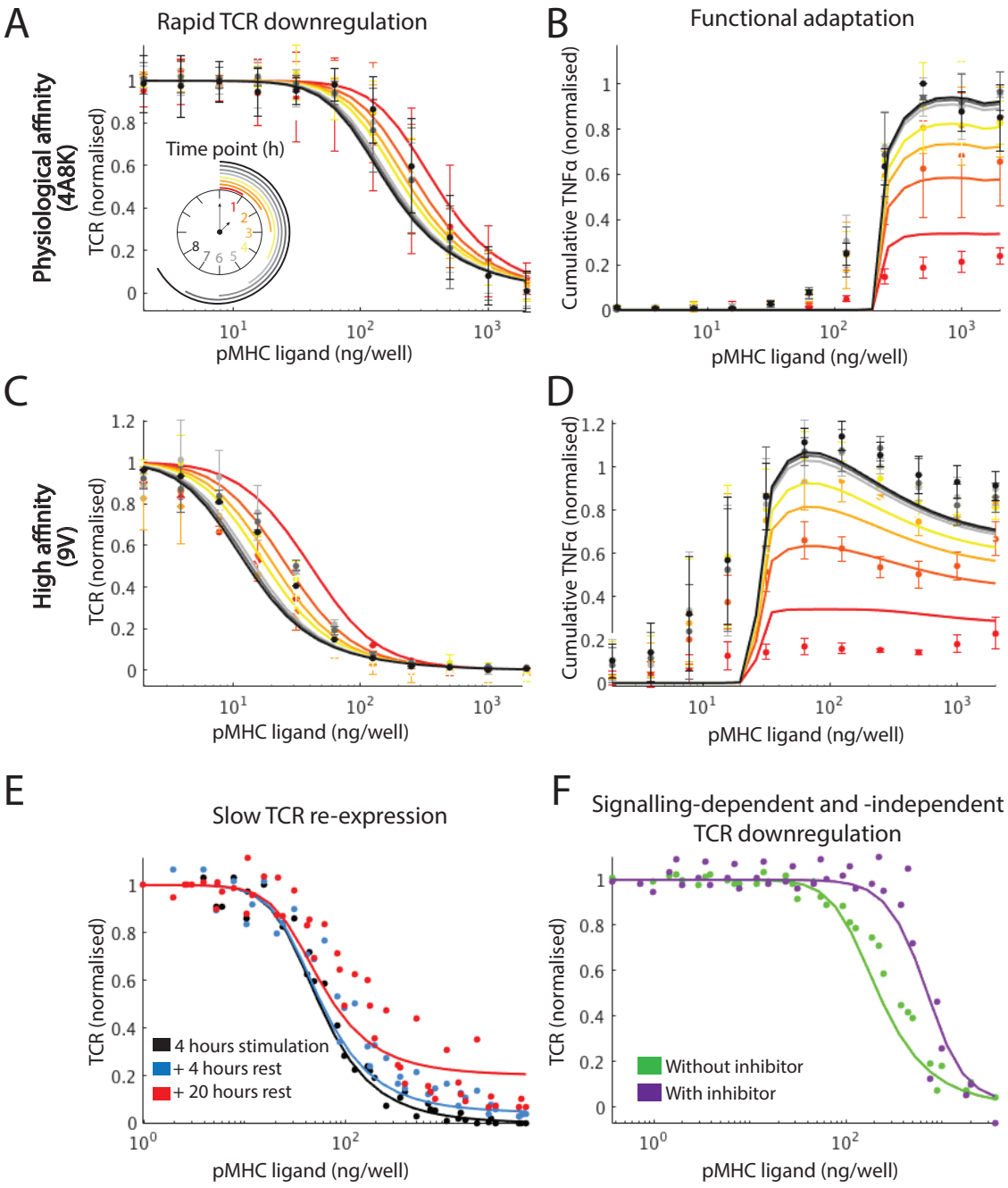


Figure 4.3: The phenotypic model is capable of explaining the full target phenotype. Fitted time course of **(A)** TCR expression and **(B)** TNFα secreted after 1–8 hours of stimulation with different doses of a low-affinity pMHC (4A8K) or **(C)**–**(D)** a high-affinity pMHC (9V). **(E)** Fit of TCR re-expression after 4 hours of stimulation and 4–20 hours of rest in the absence of pMHC ligand. **(F)** TCR downregulation after stimulation with different doses of pMHC in the presence (purple) or absence (green) of the Lck inhibitor A-770041. Data were normalised and averaged across independent repeats as described in Methods Section 2.7.1. Error bars on experimental data are the SD of 3–5 independent repeats and data fits are represented as solid lines.

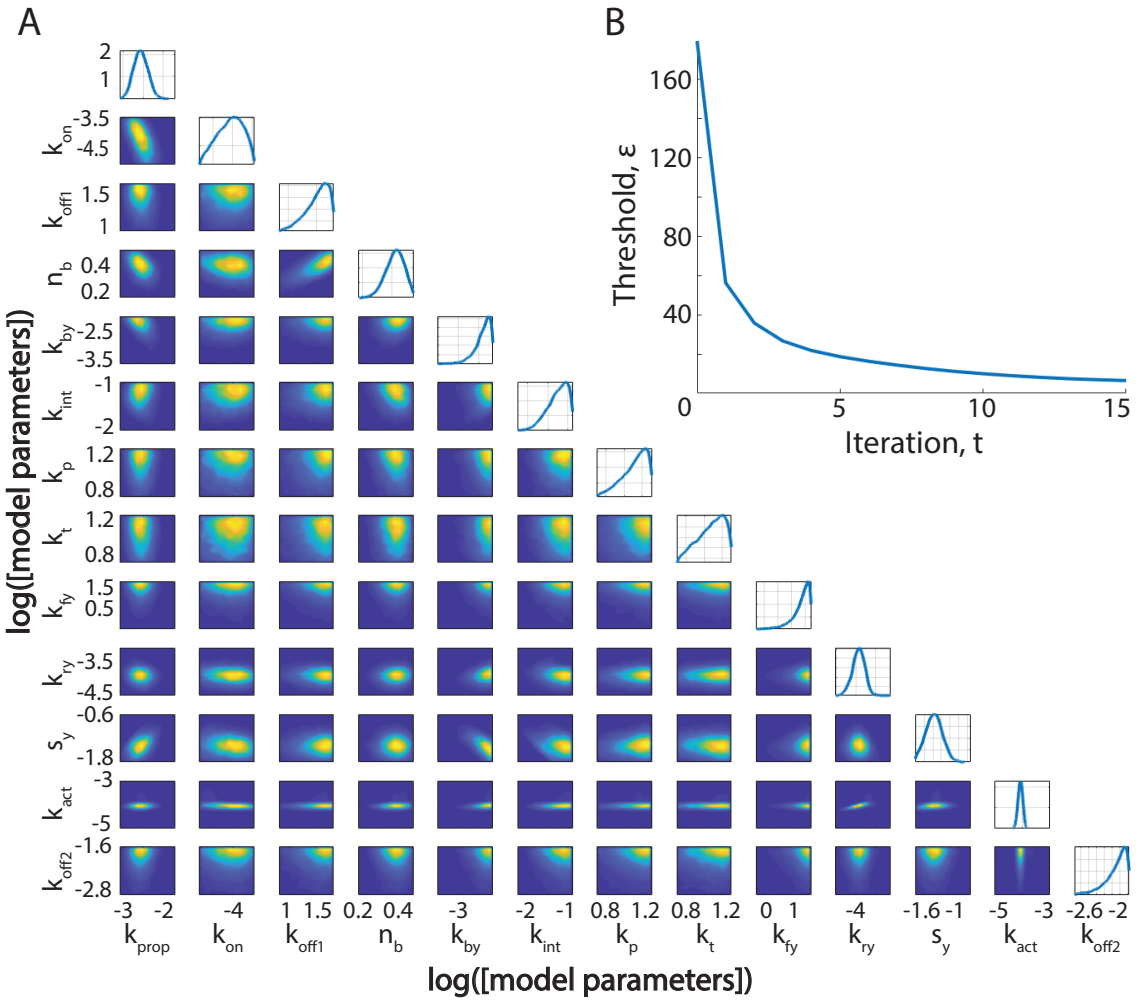


Figure 4.4: ABC-SMC illustrates correlations between model parameters. (A) Heat maps representing the distribution of 10,000 particles after 15 ABC-SMC iterations projected onto 2D parameter space on a log-scale. Distributions for individual parameters are shown on the diagonal. **(B)** The adaptive threshold, ϵ_t, after 1–15 iterations.

of TCR downregulation and TNFα secretion. First, the T cell response after 1 hour of stimulation deviates considerably from the experimental data (Fig. 4.3A–D). Small changes in TCR expression are still visible after 1–2 hours of stimulation and the model prediction for cytokine secreted after 1 hour of stimulation is significantly higher than the experimentally measured supernatant levels of TNFα at this time point. It is possible that downstream effects, such as the production of cytokine mRNA, are initiated with some time delay, which is not captured by our model [145, 246]. Secondly, the cytokine response to low doses of pMHC is consistently underestimated (Fig. 4.3B,D). The discrepancy likely arises because the model simulates the response by a single T cell, which is by

definition switch-like, while the experimental data described the response by a population of T cells. Population heterogeneity is expected in the activation threshold and other rate parameters [270] and it can explain why the model does not capture the slope of the population response accurately. Of note, the effect is particularly pronounced when simulating the stimulation of T cells with a high-affinity pMHC because, in experiments, a cytokine response is already elicited very low doses of the high-affinity pMHC. In the low dose regime, the number of pMHC ligands encountered by each cell likely contains a stochastic element, whereas the deterministic model predicts that the average pMHC dose will not be sufficient to trigger a cytokine response.

The model parameters could not all be determined independently. After 15 ABC-SMC iterations, the adaptive threshold, ϵ_t, had nearly plateaued indicating that additional iterations would only marginally improve the fit (Fig. 4.4B). An advantage of the ABC-SMC fitting algorithm is the intuitive visualisation of parameter correlations. Fig. 4.4A shows the particle population projected onto two-dimensional parameter space at the final iteration. Some parameters appeared well-defined (e.g. k_{act}), while others could not be determined independently. For example, k_{on} and k_{prop} correlated because both parameters have the ability to horizontally slide dose-response curves along the x-axis. An increase in one of these two parameters could thus be compensated for by a decrease in the other parameter.

4.2.2 Cooperative binding reconciles fast TCR downregulation and slow re-expression

The experimentally observed TCR downregulation dynamics cannot be explained by a simple binding model (Fig. 4.5). In a simple binding model, TCR downregulation is induced by engagement of the TCR by pMHC, and the rate of binding is directly proportional to the number of free TCRs and pMHCs. For the quasi-equilibrium in TCR levels to be reached within 1 hour of stimulation as determined experimentally, the TCR re-expression rate would have to be fast (on the order of minutes, Fig. 4.5A), so that the re-expression rate could balance the downregulation rate. However, the re-expression rate

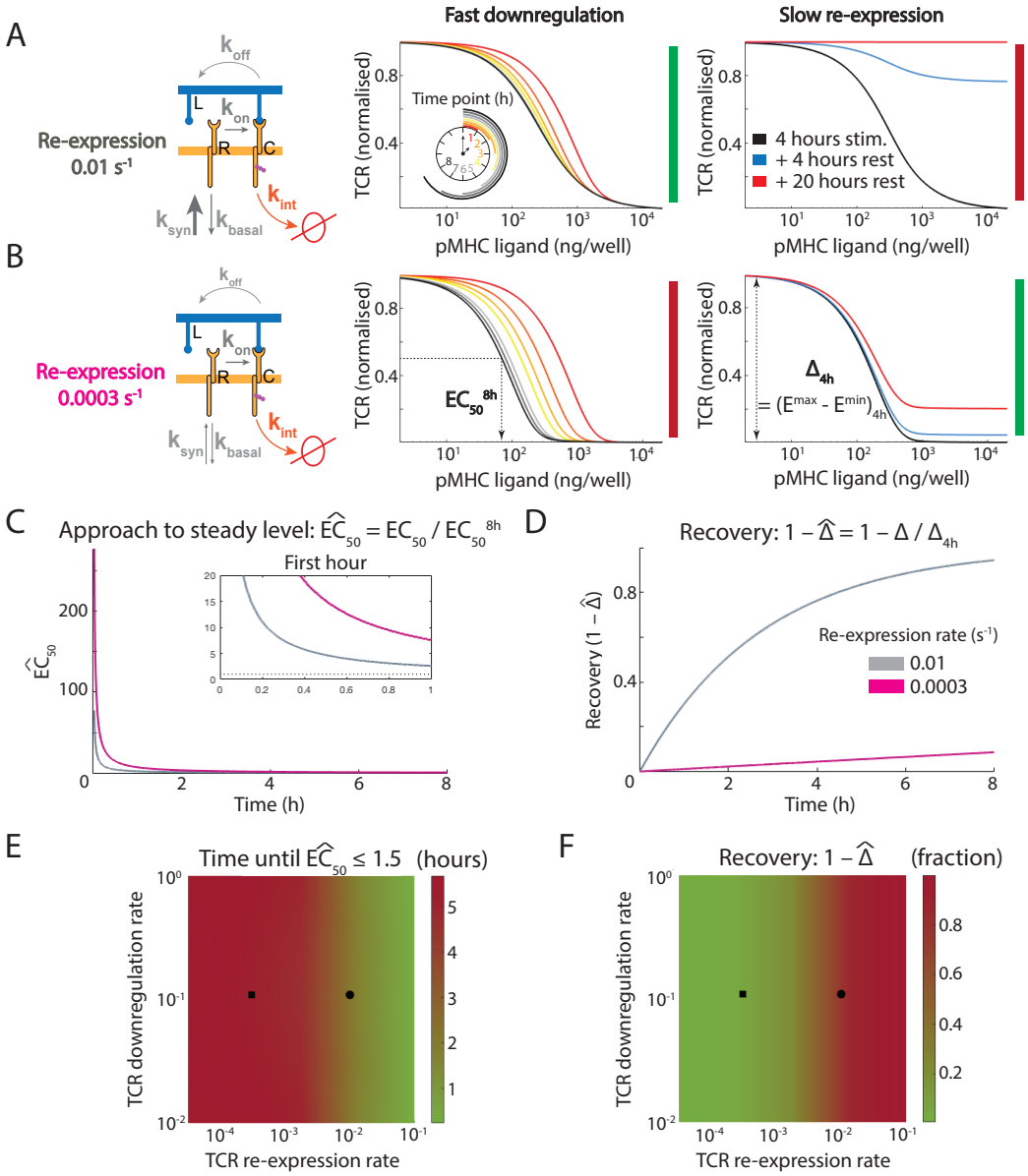


Figure 4.5: A simple binding model cannot simultaneously explain fast TCR downregulation and slow re-expression. (A) Fast re-expression of TCR can balance TCR downregulation and thus cause a rapid approach of ligand-induced TCR downregulation to a steady-level. Rapid TCR re-expression is, however, inconsistent with experimentally observed TCR re-expression kinetics. **(B)** Slow re-expression of TCR delays the approach of surface TCR to a steady-level. **(C)** The faster the TCR re-expression rate, the faster $\hat{EC}_{50}$ (EC_{50} relative to EC_{50} at 8 hours) approached 1. **(D)** TCR re-expression was quantified by normalising the difference (Δ) between the maximum and minimum plateau of the TCR dose-response curve to Δ_{4h} after 4 hours of stimulation. Intuitively, a fast re-expression rate results in a high degree of recovery ($1-\hat{\Delta}$). (E)-(F) 2D-parameter sweep showing mutually exclusive coupling of **(E)** TCR downregulation kinetics and **(F)** re-expression independent of the TCR downregulation rate over a wide range of parameter values. Black circle and square: Parameter combinations used for (A) and (B), respectively. Refer to Fig. B.2 for dose-response curves associated with 2D-parameter sweeps. Parameters as in Appendix Section B.1 except: $k_{on} = 1.6 \times 10^{-2} s^{-1} \mu m^2$, $k_{off} = 2.4 \times 10^{0} s^{-1}$.

of the TCR was experimentally determined to be slow (on the order of days). When the TCR re-expression rate was adjusted accordingly, the TCR downregulation dose-response curves only approached a steady level over several hours (Fig. 4.5B). A simple binding model thus seems to be able to explain either rapid TCR downregulation or slow TCR re-expression, but not both features at the same time.

We confirmed that rapid TCR downregulation to a steady level and slow TCR recovery are mutually exclusive in the simple binding model independent of the TCR downregulation rate by systematically varying the TCR downregulation rate (k_{int}) and the TCR recovery rate (k_{syn}) over 2–3 orders of magnitude. The agreement between the corresponding model predictions and the experimental data were analysed as described in Fig. 4.5C–D: $\hat{EC}_{50}$ denotes the fold-change in the EC_{50} of the dose-response curve at time t relative to the EC_{50} of the dose-response curve after 8 hours of stimulation. In agreement with the experimental data, $\hat{EC}_{50}$ should rapidly approach 1 as steady TCR expression levels were observed within 1–2 hours of stimulation. $\hat{\Delta}$ is the difference between the upper and lower plateau of the TCR dose-response curve at time t relative to Δ_{4h} after 4 hours of stimulation, and $1-\hat{\Delta}$ quantifies the degree of TCR recovery in the absence of pMHC ligand (0: no recovery; 1: full recovery). Rapid TCR downregulation to a steady level and slow TCR recovery could not be reconciled in the simple binding model over a wide range of TCR downregulation and re-expression rates (Fig. 4.5E–F). These findings are consistent with work by Utzny et al. [252], who tested different models in their ability to explain early (< 2 min) TCR downregulation kinetics.

Cooperative binding reconciles fast TCR downregulation to a steady level and slow TCR re-expression. Fig. 4.6 shows a direct comparison of ligand-induced TCR downregulation without and with cooperativity in binding between TCR and pMHC. Cooperative binding only affects the dynamics of TCR downregulation and not TCR re-expression in the absence of pMHC ligand, and the model feature therefore decouples the kinetics of the two processes. Fig. 4.6E–F shows that rapid TCR downregulation and slow TCR recovery were no longer mutually exclusive in a model that includes cooperative binding between pMHC ligand and the TCR. Cooperative binding between TCR and pMHC has been observed experimentally [148, 188], but the underlying mechanisms are currently

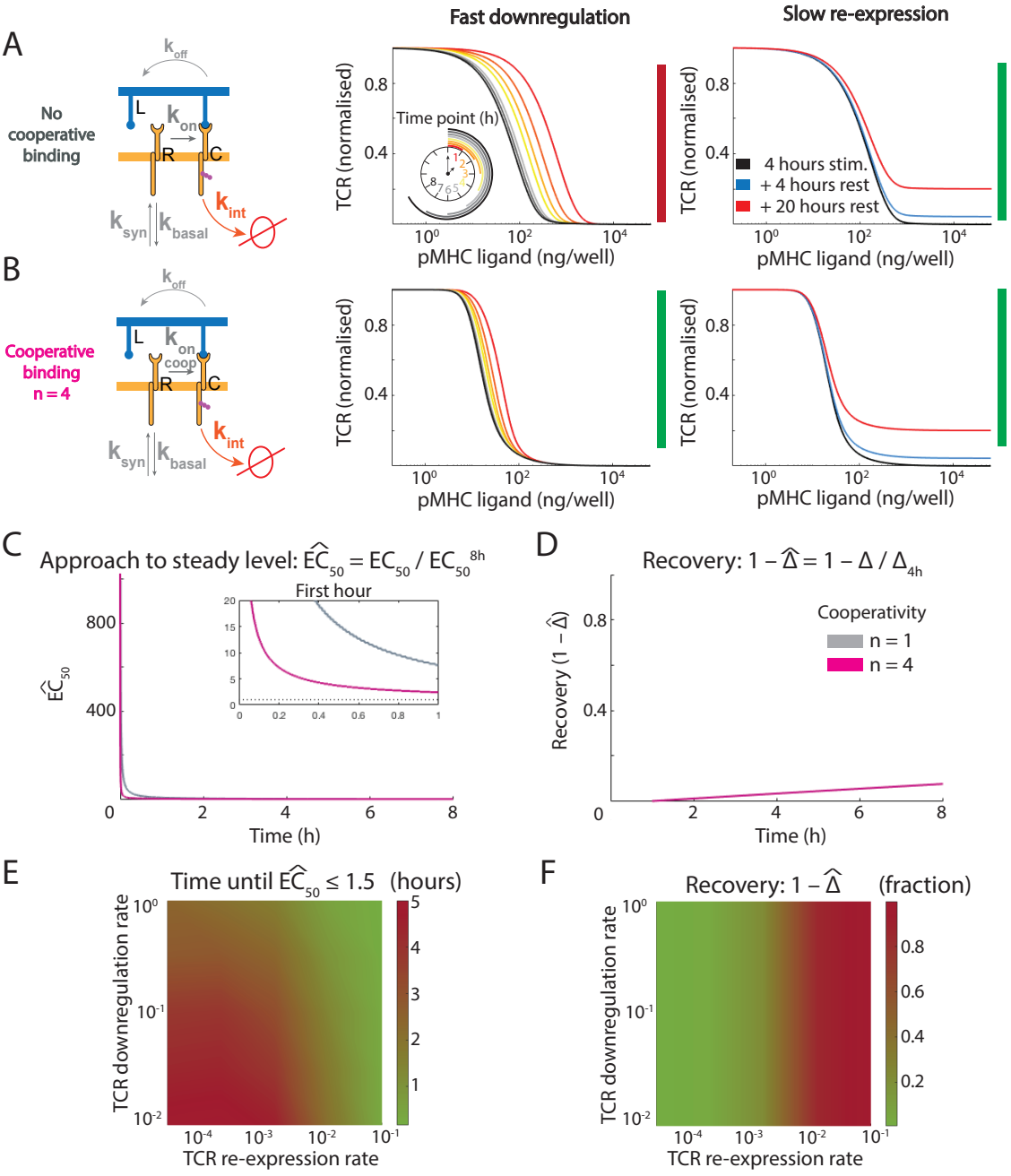


Figure 4.6: Cooperative binding reconciles fast TCR downregulation and slow re-expression. Comparison of ligand-induced TCR downregulation after 1–8 hours of stimulation and TCR re-expression in a model **(A)** without cooperative binding and **(B)** with cooperative binding (n = 4). Cooperative binding explains the fast approach of TCR surface expression to a steady level while TCR recovery remains slow. **(C)** The higher the degree of cooperativity, the faster $\widehat{EC}_{50}$ approaches 1. **(D)** TCR recovery in the absence of pMHC ligand remains slow independent of the degree of binding cooperativity. (E)-(F) 2D-parameter sweeps highlighting the decoupling of **(E)** fast TCR downregulation kinetics and **(F)** slow TCR re-expression. (C)-(F) were generated as in Fig. 4.5. Refer to Fig. B.3 for dose-response curves associated with 2D-parameter sweeps. Parameters as in Appendix Section B.1 except: $k_{on} = 1.6 \times 10^{-3} s^{-1} \mu m^2$, $k_{off} = 2.4 \times 10^{0} s^{-1}$, $k_{int} = 4.9 \times 10^{-1} s^{-1}$.

unclear.

The rate-limiting step for ligand-induced TCR downregulation becomes the frequency of TCR-pMHC binding events, and the approach of TCR expression to a steady-level can therefore not be accelerated arbitrarily by increasing the downregulation rate, k_{int}. The effective binding rate decreases with TCR downregulation because fewer TCRs are available and, as a result, TCR expression levels approach an apparent steady level both in the simple binding model and the cooperative binding model. The rate at which TCR expression approaches the steady level is dictated by the dependence of the effective binding rate on the amount of TCR already downregulated (Appendix Fig. B.1): In the simple binding model, the effective on-rate decreases proportionally to the amount of TCR downregulated because $k_{on}^{eff} = k_{on}LR$ according to mass action kinetics. In the cooperative binding model, the effective on-rate is nonlinearly dependent on the amount of TCR downregulated because $\hat{k_{on}^{eff}} = k_{on}(LR)^{n_b}$. Since ligation of the TCR is a prerequisite for TCR downregulation, it dominates the TCR downregulation kinetics and the cooperative binding rate more rapidly decreases for every TCR that is downregulated.

4.2.3 Signalling-dependent downregulation of non-engaged TCRs explains signalling requirements for TCR downregulation

Most mathematical models that include TCR downregulation allow for the downregulation of non-engaged TCRs if the TCR had previously bound pMHC and had become tagged for downregulation [37, 124, 252, 270]. These models cannot explain why several experimental studies found that a block in TCR signalling by inhibition of Lck did not prevent TCR downregulation [25, 210]. Contrary to previous studies, we thus modelled downregulation of and signalling by engaged TCRs as two independent mechanisms (Fig. 4.7A). In this model, the fraction of engaged TCR that is tagged for downregulation does not change when the phosphorylation of the TCR and, as a result, the occupancy of the signalling-competent TCR-pMHC states are altered.

A model with completely independent TCR downregulation and signalling is, however,

only consistent with a subset of experimental studies. Other studies showed that TCR signalling impacts the degree of TCR downregulation after stimulation with low doses of pMHC (Fig. 4.3F) [53, 165, 214] and that the downregulation of non-engaged TCRs in particular is regulated by TCR signalling [165, 214]. We therefore included in the model an additional signalling-dependent pathway that leads to the downregulation of non-engaged TCRs (Fig. 4.7B). The inhibition of TCR signalling then impacts TCR downregulation in a dose-dependent way: It completely prevents downregulation of the TCR when the dose of stimulating pMHC is low, but high doses of pMHC can overcome the signalling block and result in the same reduced level of TCR expression, consistent with experimental studies [165, 214].

4.2.4 Switch-like activation of downstream signalling explains functional adaptation

T cell adaptation can be explained if, as result of TCR downregulation, the amount of signalling TCR declines to a level that is insufficient to sustain downstream T cell signalling. The TCR downregulation module was coupled to the cytokine response as shown in Fig. 4.8A. The sum of signalling-competent TCRs ($C_p = C_{10} + C_{11}$) decreases in time as the TCR becomes downregulated (Fig. 4.8B, left column). It is furthermore assumed that the amount of C_p must exceed a threshold value (s_y) to activate the downstream intermediate Y (middle column). The rate at which the sum of signalling-competent receptors C_p activates the signalling intermediate Y is thus proportional to (see Appendix B.1 for complete system of ODEs)

$$(1 - Y)\ \frac{C_p^{n_y}}{C_p^{n_y} + s_y^{n_y}}$$

where (1-Y) ensures conservation of total (i.e. the sum of active and inactive) Y and the fraction enforces switch-like activation of Y by C_p. The cumulative cytokine response (right column) is directly dependent on signalling from Y, and reduced activity in Y eventually leads to a stop in the secretion of cytokine.

The degree of adaptation in cytokine secretion depends on the Hill number, n_y, associated with the activation threshold that determines whether C_p is sufficient to

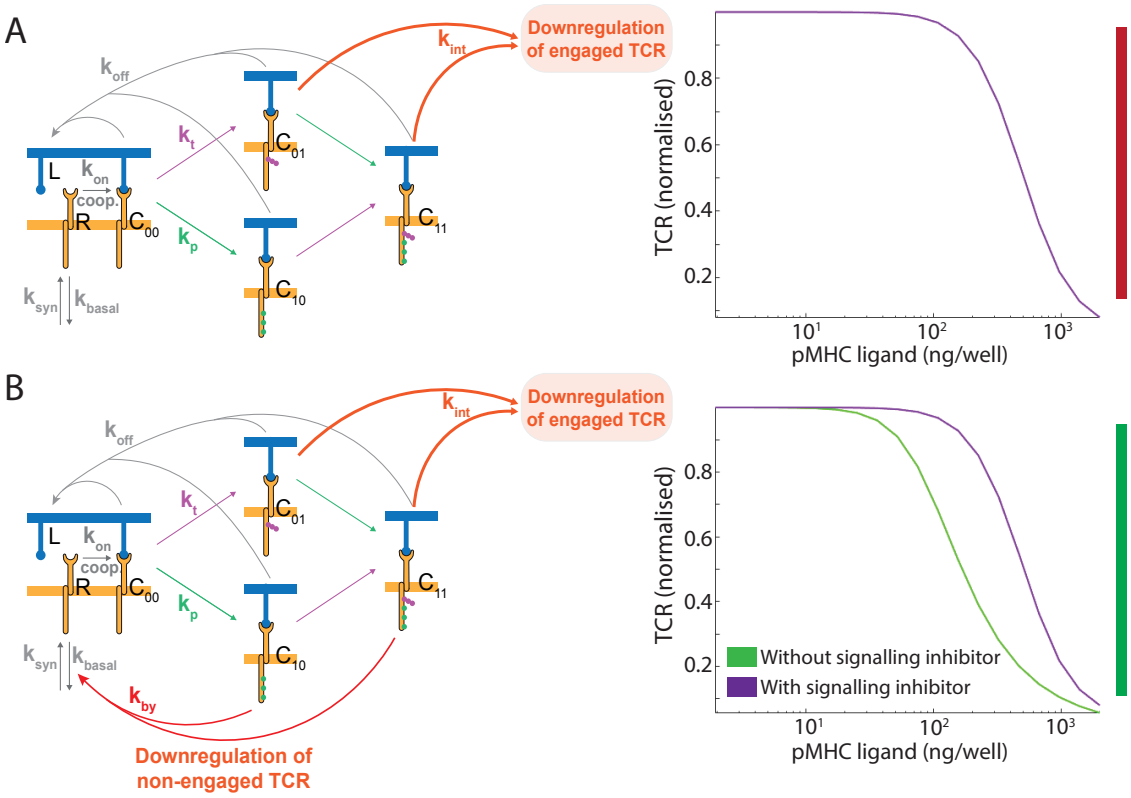


Figure 4.7: Signalling-dependent downregulation of non-engaged TCRs explains controversial findings about signalling requirements for TCR downregulation. (A) In some studies, inhibition of TCR signalling did not prevent TCR downregulation. Downregulation and signalling of ligated TCR were thus modelled as two independent pathways. The model is inconsistent with the experimental observation that TCR downregulation is altered at intermediate doses of pMHC when signalling is blocked by Src-family kinase inhibitors. **(B)** Other studies showed that non-engaged TCRs can become downregulated in a signalling-dependent manner. The model explains impaired TCR downregulation at intermediate but not at high pMHC doses in the presence of Src-family kinase inhibitors. Effect of Src-family kinase inhibitors was simulated by setting $k_p = 0\ s^{-1}$. Refer to Appendix Section B.1 for remaining parameter values.

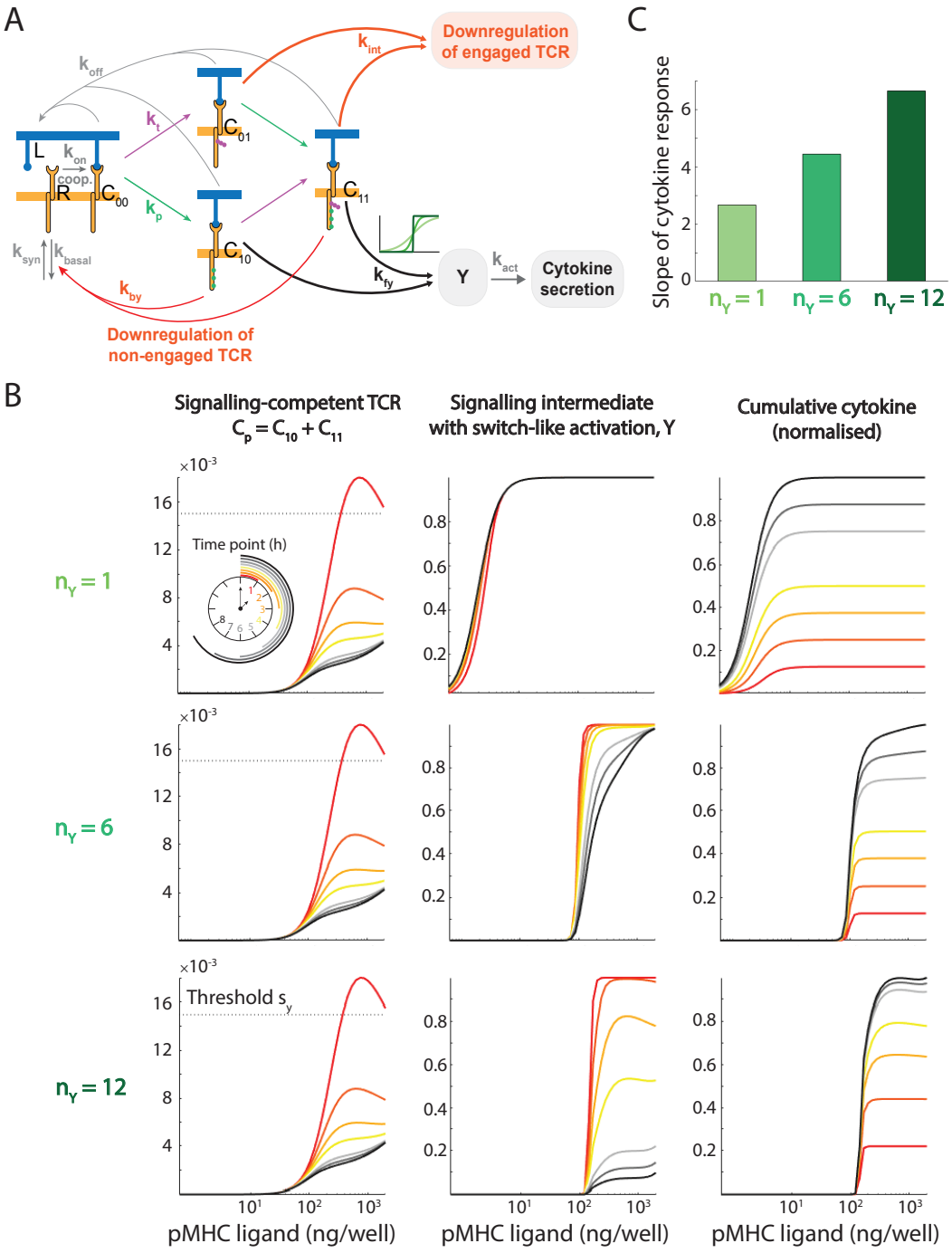


Figure 4.8: Switch-like activation of downstream signalling explains adaptation as a result of TCR downregulation. (A) Schematic of TCR downregulation module coupled to downstream T cell signalling. Activation of the signalling intermediate Y was assumed to be switch-like. **(B)** As surface TCR levels decrease, the amount of signalling-competent receptor (C_p, left column) decreases. C_p below a certain threshold (dotted line) is insufficient to sustain activation of the downstream intermediate Y (middle column). As a result, cytokine production (right column) stops if activation of Y is a nearly-perfect switch. **(C)** Increasing n_y increases the slope of the cytokine response. Parameters are as in Appendix Section B.1 except: $s_y = 1.5 \times 10^{-2}$.

activate Y. Fig. 4.8B illustrates that the adaptation phenotype is more pronounced the steeper the activation threshold (large n_y). An increase in n_y, however, also results in a steeper predicted cytokine dose-response curve (Fig. 4.8C). Of note, the phenotypic model simulates the response by a single T cell, while the experimental data in Fig. 4.3 summarises the cytokine response by a population of T cells. The discrepancy in the slope of the cytokine dose-response curve and the model simulation can be explained by cellular heterogeneity in the activation threshold, kinetic parameters and protein concentrations within the T cell population [270].

4.2.5 Temporal integration of short-lived TCR signals determines adaptation timescale

The signalling intermediate Y acts as a temporal integrator and reconciles the different time scales associated with TCR downregulation and adaptation (Fig. 4.9). TCR surface expression was found to reach a steady level within one hour of stimulation, whereas T cells stopped secreting TNFα only after ~4 hours (Fig. 4.3B,D). The fitted activation rate of Y ($k_{fy} = 1.37 \times 10^{1}$ s^{-1}) was 5 order of magnitude larger than the degradation rate ($k_{ry} = 1.32 \times 10^{-4}$ s^{-1}), so that short-lived TCR signals transiently accumulated in Y. Therefore, Y does not immediately stop signalling when C_p drops below the threshold s_y. Indeed, the lifetime of Y dictates the timescale of adaptation (Fig. 4.9B): The faster the rate at which active Y is deactivated, the sooner T cells adapt cytokine secretion. Temporal integration by Y bridges the rapid TCR downregulation dynamics with the slower and more prolonged cytokine secretion dynamics.

4.2.6 The model predicts reactivation of T cells adapted to a low-affinity pMHC by a high-affinity pMHC

In the previous chapter, we found that adaptation to a low-affinity pMHC can be overcome by transfer of adapted T cells to a high-affinity pMHC. The transfer of pre-stimulated T cells (5 hours) onto either the same stimulus (same dose, same affinity) or a different stimulus (same dose, different affinity) for an additional 5 hours was simulated (Fig. 4.10),

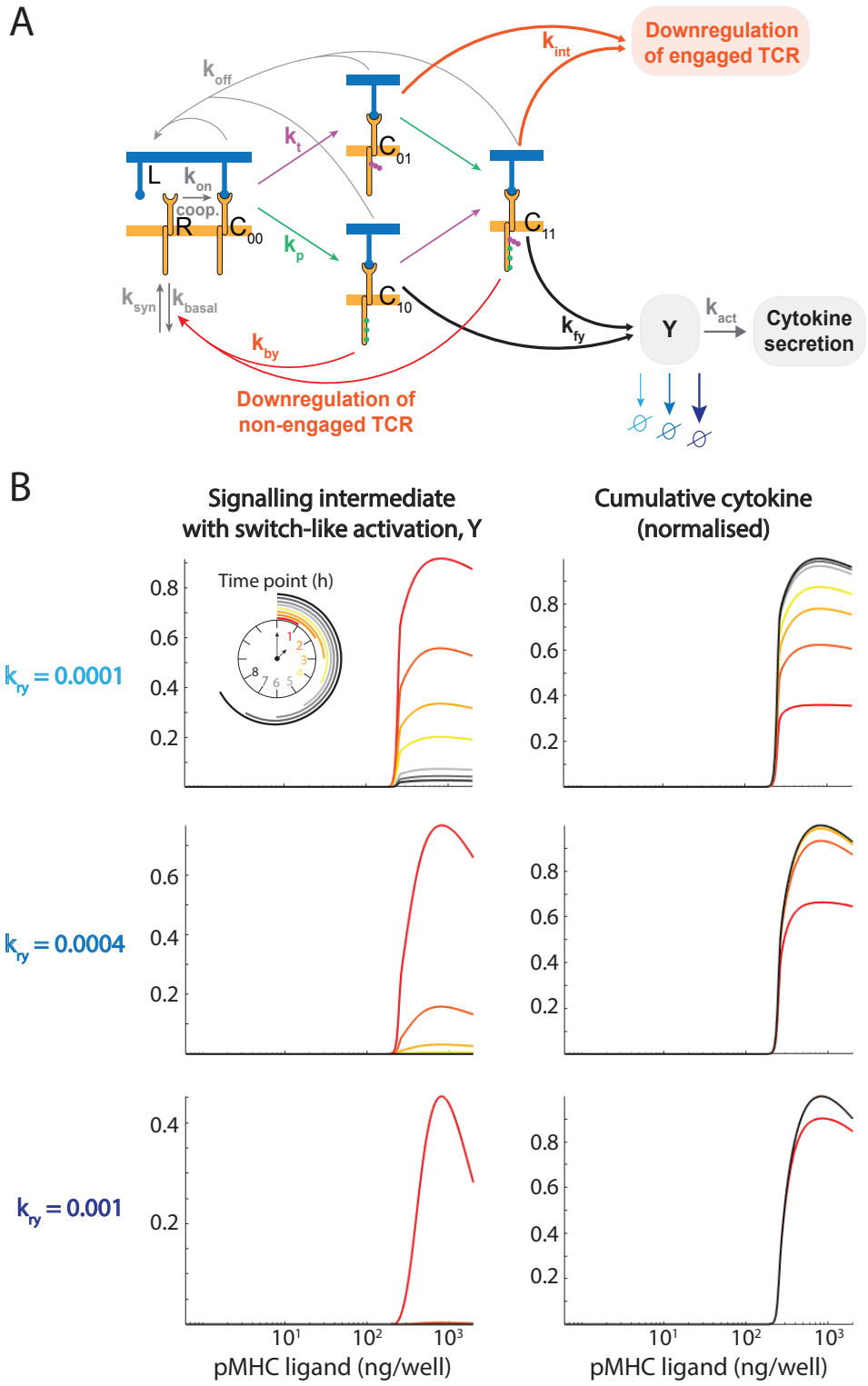


Figure 4.9: Temporal integration of short-lived TCR signals determines adaptation timescale. (A) Schematic of signalling intermediate Y with different degradation rates coupled to the TCR downregulation module. Darker shades of blue indicate faster degradation rates (less time integration) and are simulated in (B). **(B)** Slow degradation (low k_{ry}, light blue) of Y results in prolonged signalling, whereas faster degradation of Y (high k_{ry}, darker blue) decreases signal duration. The rate at which cytokine secretion (right column) stops, is therefore dictated by the lifetime of Y. Parameters are as in Appendix Section B.1.

analogous to the transfer experiment presented in Chapter 3 Section 3.2.5. Reduced TCR levels as well as accumulation of the slowly decaying signalling intermediate Y were taken into account in the initial conditions for the secondary simulation. The model predicted that adaptation to a high-affinity pMHC during primary stimulation rendered T cells unresponsive during secondary stimulation with a high- or a low-affinity pMHC (Fig. 4.10D). T cells pre-stimulated with and adapted to a low-affinity pMHC, however, could be reactivated by stimulation with a high-affinity pMHC during secondary stimulation. The model predictions are therefore consistent with the experimental data presented in the previous chapter (Fig. 3.14).

The phenotypic model successfully predicts the transfer experiment from Chapter 3 Section 3.2.5 because it explains adaptation of cytokine production at all doses and affinities of pMHC as a result of TCR downregulation. TCR downregulation is context-dependent: Both the dose and affinity of the stimulating pMHC determine by how much TCR expression is reduced when the T cell is presented with pMHC ligand. Similarly, downstream signalling ceases on the time scale at which Y is degraded in the absence of sufficient productive binding events between TCR and pMHC. As long as pMHC dose and affinity do not change, the model thus predicts that the T cell will adapt to the pMHC stimulus after prolonged stimulation at all pMHC doses and affinities. TCR expression levels were therefore sufficient to explain differential T cell responses in sequential ligand encounters.

4.3 Discussion

A phenotypic model was constructed to explain rapid ligand-induced TCR downregulation and slow TCR re-expression in the absence of ligand, the TCR signalling requirements for ligand-induced TCR downregulation and adaptation of the cytokine response. Cooperative binding, signalling-dependent downregulation of non-engaged TCRs and switch-like downstream activation of T cell signalling were the three key model features that sufficed to explain the target phenotype. The agreement of model predictions with experiments was confirmed by directly fitting the model to experimental data by ABC-

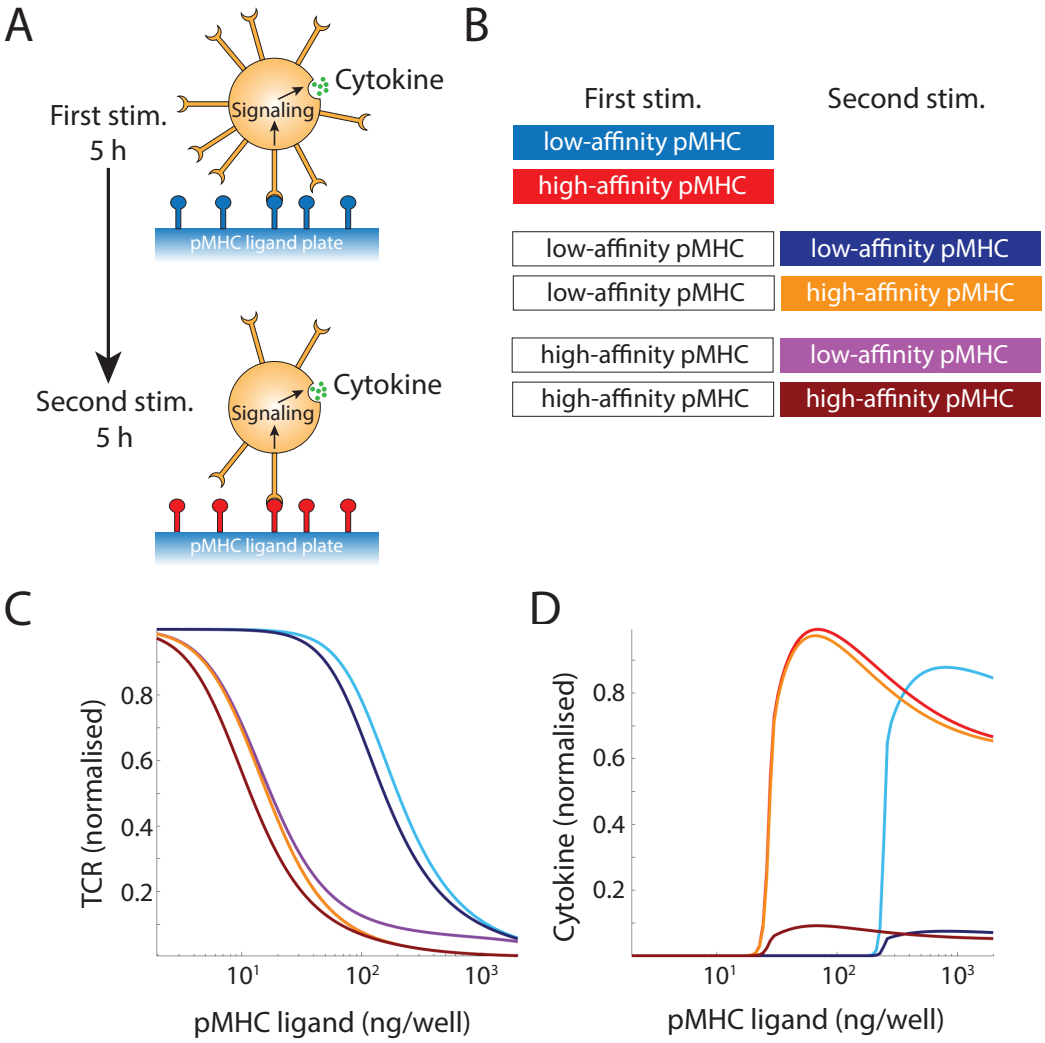


Figure 4.10: The phenotypic model predicts that T cells adapted to the low-affinity pMHC can be reactivated by stimulation with the high-affinity pMHC. (A) A primary 5 hour pre-stimulation period with either a low- or a high-affinity pMHC was simulated analogously to the experiment in Chapter 3 Section 3.2.5. TCR downregulation and the slowly decaying Y were adopted in the initial conditions for the secondary 5 hour stimulation at the same dose of either the same pMHC or a pMHC with higher/lower affinity. **(B)** The colour scheme is identical to the representation of experimental data in Fig. 3.14. The model prediction for **(C)** TCR levels and **(D)** cytokine secretion are consistent with experimental data in Fig. 3.14. T cells pre-stimulated with a high-affinity pMHC are predicted to be unresponsive to secondary stimulation with a low-affinity pMHC, while T cells pre-stimulated by a low-affinity pMHC can be reactivated by stimulation with a high-affinity pMHC.

SMC, and the model was also able to explain striking phenotypic features, such as the bell-shaped dose-response curve observed when stimulating T cells with high-affinity pMHC ligands. In addition, the model predicted that (1) the signalling intermediate Y acts as a temporal integrator downstream of short-lived TCR signals, and (2) T cells that have become unresponsive to a low-affinity pMHC can be reactivated by stimulation with a higher-affinity pMHC, consistent with the experimental data in Section 3.2.5 of the previous chapter. Experimental evidence for all model assumptions was presented in the Introductory Section 4.1 and is illustrated in Fig. 4.11.

4.3.1 Discussion of fit parameters

Despite the minimal structural complexity of the phenotypic model, not all parameters could be determined independently. The ABC-SMC output in Fig. 4.4 illustrates that correlations exist between some parameters, so that a range of parameter values can explain the experimental data depending on other model parameters. The fit parameters should therefore not be interpreted as fixed rates. Instead, the aim of this study was to investigate whether the overall mechanisms encoded by the model topology were capable of explaining the experimental data, and this was confirmed by fitting the model to the data.

The on- and off-rates of pMHC ligand binding to the 1G4Hi TCR were determined by SPR. Yet, both k_{on} and k_{off} were included in the list of parameters to be fitted by ABC-SMC because the binding kinetics in SPR experiments are likely to be different from the actual binding kinetics in a cellular context. First, the binding parameters that were determined experimentally by SPR describe the affinity between soluble 1G4Hi TCR and immobilised pMHC ligands. In the functional experiments, the 1G4Hi TCR is however anchored to the T cell membrane. A discrepancy between the 3D-affinity measured by SPR and the 2D-affinity *in situ* was expected, but the precise functional form of the factor that converts 2D into 3D binding parameters remains unknown [287]. Second, the TCR-pMHC bond is subjected to force when both the pMHC and TCR are anchored to different surfaces. Force can affect the binding interaction by increasing the rate of

unbinding (slip bonds) or by decreasing the rate of unbinding (catch bonds), and both of these have been reported for the interaction between pMHC and TCR [45, 132, 144]. Third, the CD8 co-receptor was not included in SPR experiments, but it is expressed on the primary T cells that were used for functional experiments. CD8 interacts with MHC to stabilise the interaction between the TCR and peptide and therefore affects the pMHC-TCR binding kinetics [278]. In sum, these effects nonlinearly convert the SPR measurements into appropriate *in situ* affinities by an unknown factor and the ligand on- and off-rates were therefore fitted [55, 56, 257, 287].

Multiple TCR-proximal signals such as CD3ζ phosphorylation and Ca^{2+} are short-lived [59, 204] and downstream signalling is digital, yet T cells achieve scaled responses through the temporal integration of discontinuous signals [35, 59, 154]. Consistent with this idea, temporal integration of TCR signals is predicted by the fitted lifetime parameters of Y. On a molecular level, several non-mutually exclusive mechanisms could account for temporal integration. First, hysteresis as a consequence of positive feedback (e.g. between SOS and Ras, Fig. 4.11B) constitutes a type of molecular memory as it prevents the immediate return to the basal signalling state once the stimulus is removed [41]. Second, molecular memory on the transcriptional level is mediated by extending the signalling lifetime of the transcription factors NFAT [146] and AP-1 [35, 204]. Finally, post-transcriptional modifications such as mRNA or protein stabilisation integrate signalling by augmenting the accumulation of gene products (Fig. 4.11D) [186]. Temporal integration of TCR signalling could increase specificity as signal duration encodes information about the dose and affinity of pMHC that is otherwise lost in digital downstream activation [154, 270].

4.3.2 Model improvements

Two discrepancies between the model prediction and the experimental data were pointed out. First, the model overestimates TNFα production after 1 hour of stimulation (Fig. 4.3B,D). This discrepancy could be a result of an initial lag time if cytokine secretion required chromatin remodelling, for example. A lag time on the order of roughly

90 minutes was reported in IFNγ secretion when T cells were stimulated with different pMHC variants, and the onset of cytokine production was independent of pMHC affinity [55]. We expect that including a delay between digital activation of Y and the production of cytokine Z in the model (e.g. $\frac{\partial Z}{\partial t} = \left(\frac{t}{t+t_{delay}}\right) k_{act} Y$) would improve the fit as it accounts for processes such as chromatin remodelling.

A second discrepancy between the model fit and the experimental data is the steepness of the cytokine dose-response curves. The model prediction increases more steeply as a function of pMHC dose than observed experimentally. The discrepancy arises because the model simulates the response by a single T cell, whereas the experimental data stems from a population of T cells. On a population level, heterogeneity in the activation threshold (and other rate parameters) likely exists [8, 293]. Simulating the single-cell response a large number of times with activation thresholds sampled from a distribution that takes into account population heterogeneity in the activation thresholds would reconcile the sharp single-cell responses with the shallower population response.

4.3.3 Alternative model architectures

Experimental support exists for all assumptions underlying the phenotypic model, but other model formulations or arrangements are conceivable. In particular, it appears in Fig. 4.1 that the addition of the Lck inhibitor results in a steeper TCR downregulation curve as a function of pMHC dose. A change in the steepness of the TCR dose-response curve could likely be achieved if, rather than binding, TCR downregulation itself was cooperative. In other words, TCR downregulation may require a minimum number of TCRs to be engaged for downregulation to proceed. Because the TCR dose-response is shallower in the absence of the Lck inhibitor, other hypotheses could be investigated regarding the signalling-dependent pathway of downregulation. It would be interesting to test (1) whether a minimum number of non-engaged TCRs is also required for downregulation to proceed via this pathways (i.e. downregulation of non-engaged TCRs is cooperative), and (2) whether assuming cooperativity in the rate of bystander downregulation is equivalent to placing the trigger for downregulation downstream of the switch. The

position of PKCθ, which plays an important role in downregulation of non-engaged TCRs [27, 49, 163, 251], relative to the switch is in our model unspecified, but it could be located downstream and it would be interesting to determine whether the models make differential predictions about the kinetics or the effect of signalling inhibitors that could invalidate one of these hypotheses.

4.3.4 Comparison to previously published models

On a molecular level, multiple mechanisms exist that can potentially reduce T cell signalling. The phenotypic model presented in this chapter tests the hypothesis that a decrease in TCR expression as a result of pMHC stimulation can reduce T cell responsiveness. The model fails to explain adaptation if the level of TCR that remains on the T cell surface is always sufficient to sustain downstream activation. In this case, additional motifs need to be invoked. To test other hypotheses, it would be interesting to replace the switch and TCR downregulation by other motifs that are capable of producing an adaptation phenotype. Promising candidate motifs are negative feedback or incoherent feed-forward loops (IFF) [3, 138, 228].

Negative feedback can lead to adaptation [3, 138, 228], but a simple negative feedback loop is not sufficient to explain the full target phenotype. We have previously shown, for example, that negative feedback alone cannot explain the bell-shaped dose-response curve [127]. Francois et al., however, implemented an atypical negative feedback that can reproduce the bell-shaped dose-response curve [64]. The model was motivated by the observation that the tyrosine phosphatase SHP-1 inhibits TCR-proximal signalling [8, 234] and it aimed to elucidate mechanisms that enable sensitive and specific antigen discrimination. In the model, a negative regulator is triggered by early KPR states and opposes progression through the KPR chain. Occupancy of the early KPR step that stimulates the negative regulator is itself reduced (negative feedback), but also increased as later KPR steps are reversed. The negative regulator is thus an atypical negative feedback loop with similarities to IFF. While the negative regulator is capable of explaining the bell-shaped dose-response curve, it remains to be determined whether

it is also consistent with the adaptation phenotype. It cannot, however, account for steep dose-response curves as it does not include sharp activation thresholds and it is inconsistent with the observation that low-affinity ligands can outperform high-affinity pMHC ligands at high doses (Fig. 3.14) [127]. Therefore, negative feedback or Francois et al.'s negative regulator are not *per se* sufficient to explain the full target phenotype.

Alternatively, it has been suggested that IFFs can lead to adaptation [3, 138, 228]. The KPL-IFF model that our group published previously (Section 3.2.3) aimed to explain the bell-shaped dose-response curve [127]. Based on modelling studies to identify motifs that achieve biochemical adaptation [3, 138, 228], the KPL-IFF model is likely also capable of reproducing the adaptation phenotype in a certain parameter regime. Whether it can explain a dynamically emerging bell-shaped dose-response curve and adaptation at the same time remains to be shown. Similar to the negative regulator model by Francois et al. [64], the KPL-IFF did not intend to reproduce steep dose-response curves and will therefore not be able to fully explain the target phenotype.

Previous studies, including the negative regulator and KPL-IFF models, have typically focused on understanding specific and distinct features of either the functional dose-response phenotype [8, 64, 127, 234] or TCR downregulation [12, 229, 252]. One novelty of the phenotypic model presented here is that it explicitly examines possible relations between these two cellular outcomes, and it is, to our knowledge, the first to consider the multiplicity of signalling pathways that can lead to TCR downregulation. A second novelty of the TCR downregulation model is that it reconciles a large number of experimental conditions and observables (time course, dose- and affinity-dependence of TCR downregulation as well as cytokine secretion and biochemical perturbation with the Lck inhibitor) in the same model. The molecular memory that is encoded in sustained TCR downregulation furthermore explains the sequential ligand encounter, consistent with the experimental data. It is unclear what molecular constituents in the negative regulator model or the KPL-IFF could act as a molecular memory, and it would be interesting to investigate whether an implementation of the negative regulator or the KPL-IFF model can be fitted to explain both adaptation and the sequential ligand encounter.

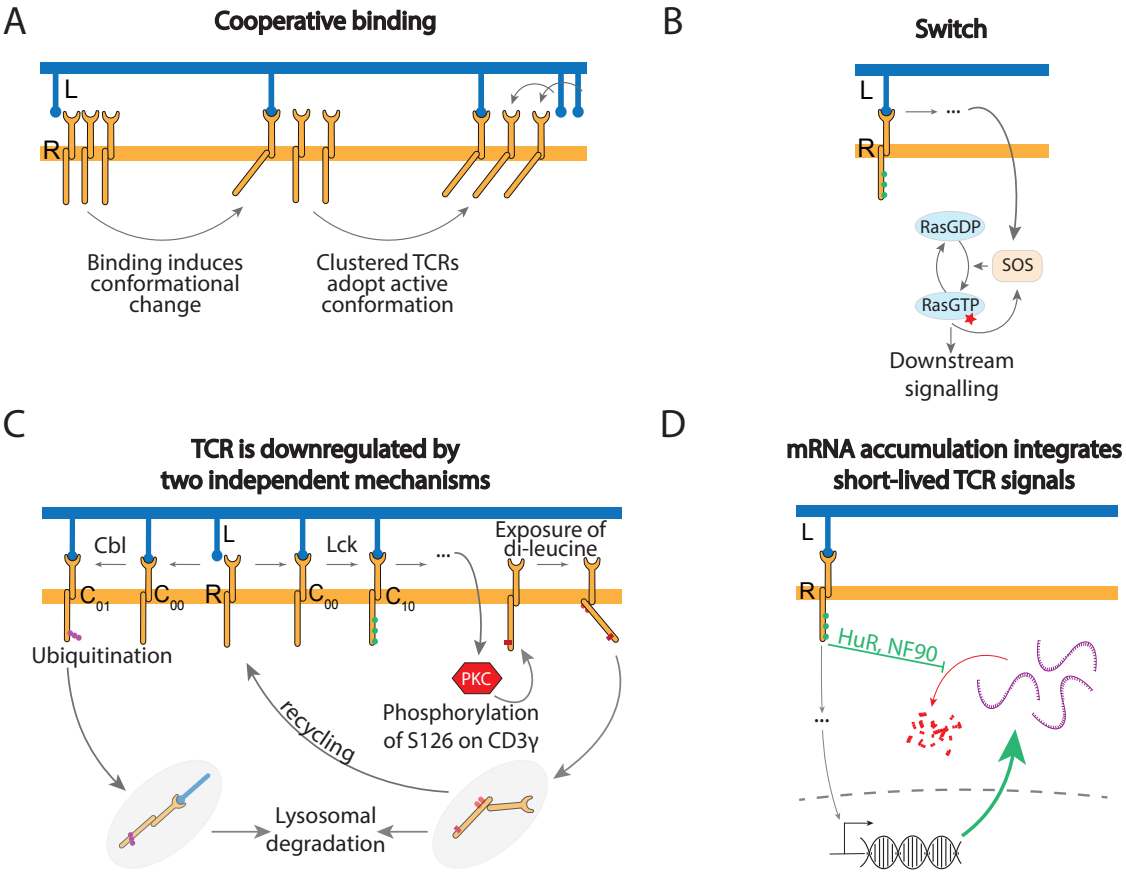


Figure 4.11: Examples of signalling modules for cooperative binding, switch-like T cell activation, TCR downregulation and temporal integration. (A) Clustering of TCRs could confer a ligand-induced conformational change in engaged TCRs to neighbouring TCRs and enhance their ability to bind ligands. **(B)** TCR signalling activates SOS, and SOS catalyses the conversion of inactive RasGDP into active RasGTP. The catalytic efficiency of SOS is enhanced when RasGTP binds to SOS, thus constituting a positive feedback loop that can lead to switch-like activation of RasGTP and downstream signalling. **(C)** TCRs can be downregulation by two independent mechanisms. Engaged TCRs are likely downregulated by ubiquitination through E3 ubiquitin ligases such as Cbl. Ubiquitinated TCRs are internalised and targeted to the lysosome for degradation. Non-engaged TCRs are downregulated by a signalling-dependent mechanism that involves activation of PKC, which in turn phosphorylates serine S126 on CD3γ. As a result, a di-leucine motif on CD3γ is exposed and initiates endosomal trafficking of TCRs that can lead to degradation or recycling of the TCR to the cell surface. **(D)** mRNA accumulation as a result of increased transcription and mRNA stabilisation constitutes a mechanism to integrate TCR signals.

CHAPTER 5

Different cytokines are secreted by CD8$^+$ T cells with a similar threshold but at a different rate

Polyfunctionality is defined as the ability of T cells to produce multiple effector molecules [21, 78] and it is has been linked to favourable outcomes in immune responses against infections [21] and cancer [50, 193, 194]. Given that effector molecules fulfil specific functions in immune responses, it is reasonable to assume that their quantities would be tightly regulated and indeed a number of studies have suggested that different effector molecules have different dependencies on the dose and affinity of pMHC. Key effector molecules secreted by CD8$^+$ T cells are TNFα, MIP-1β, IFNγ and IL-2. Here, CD8$^+$ primary human T cells were stimulated in systematic experiments with titrations of 8 pMHC variants that bind the 1G4Hi TCR with milli- to picomolar affinities. Surprisingly, only minimal cytokine-specific variations were identified in the overall dose-response phenotype and pMHC dose thresholds, whereas large variations characterised the absolute and relative amounts of each cytokine response in a donor-dependent manner. Our findings are consistent with a phenotypic model containing a single switch coupled to cytokine-specific temporal integrators.

5.1 Introduction

The magnitude and quality of cytokine secretion depend both on the dose and affinity of the stimulating pMHC (see Section 3.1.2). It is unclear whether these two parameters affect all cytokines equally. The simultaneous study of multiple cytokines secreted in response to pMHC stimulation has suggested that changes in the dose [83, 98, 201, 243, 253, 257] or affinity [57, 201, 243, 257] of pMHC can disproportionality affect certain cytokines and thus qualitatively change the T cell response.

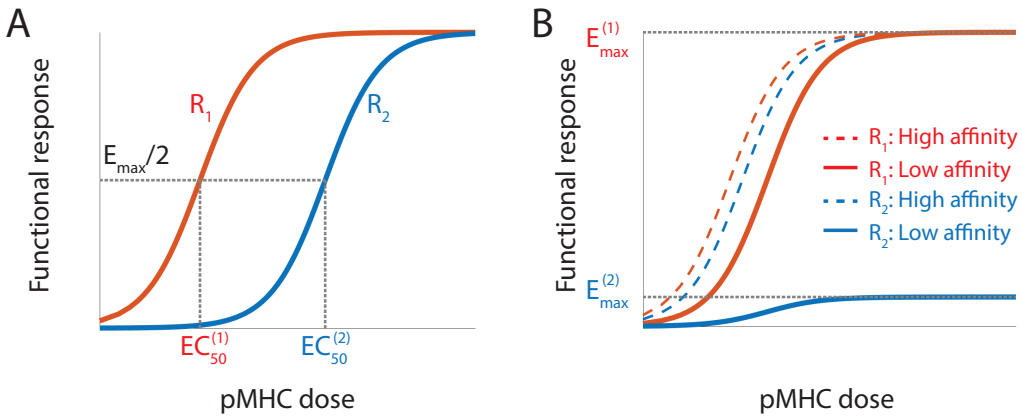


Figure 5.1: Use of EC_{50} and E_{max} to quantify how dose- and affinity-thresholds affect the quality of the T cell response. The quality of the T cell response can more formally be defined as the ratio of different cytokine readouts and it is affected by readout-specific dose- and affinity-thresholds. **(A)** Schematic example of two readouts R_1 and R_2 with different pMHC dose-thresholds (EC_{50}), defined as the dose eliciting a half-maximal response. Consequently, the quality of the response (R_1/R_2) differs at low and high doses of pMHC. **(B)** Schematic example of two readouts with different affinity thresholds. R_1 is only marginally affected by a change in pMHC affinity, whereas R_2 is nearly completely abolished. Consequently, the quality of the response at any given dose changes with the pMHC affinity.

5.1.1 Dose thresholds in CD8+ T cells

Fig. 5.1A illustrates schematically how differential sensitivities to pMHC dose can affect the quality of the T cell response in a dose-dependent manner. Multiple readouts of T cell activation, including cytotoxicity [83, 243, 253, 257], changes in the expression of surface markers such as CD69 [83], proliferation [83, 201] and secretion of cytokines [83,

98, 201, 243, 257], have been shown in $CD4^+$ and $CD8^+$ T cells to differ in their minimal dose requirements for activation. This chapter will focus on the secretion of the cytokines TNFα, MIP-1β, IFNγ and IL-2 by $CD8^+$ effector/T_{EM} cells. Two studies found that TNFα and MIP-1β were more sensitive to low doses of pMHC, whereas IFNγ and IL-2 required an up to a hundred-fold higher pMHC dose to be detected [243, 257]. In experiments with the $CD8^+$ ILA1 T cell clone recognising human telomerase reverse transcriptase, IFNγ was in one study found to be activated at a lower and in a second study at a higher concentrations of pMHC compared to IL-2 [243, 257], so that the exact hierarchy of cytokine dose thresholds in $CD8^+$ T cells is not clearly defined.

5.1.2 Affinity thresholds in $CD8^+$ T cells

Studies with pMHC mutants have shown that alterations in pMHC affinity can disproportionally affect some T cell responses (Fig. 5.1B). In $CD8^+$ T cells, polyfunctionality of the cytokine response to peptide-pulsed APCs correlated with pMHC affinity indicating that some cytokines required stimulation with a pMHC of higher affinity to be secreted than others [257]. The suggested hierarchy of affinity-thresholds mirrors the hierarchy of dose-thresholds discussed above: MIP-1β < TNFα < IFNγ < IL-2, with MIP-1β readily detectable in response to low-affinity pMHC stimuli and IL-2 secretion detected only after stimulation with higher-affinity pMHCs [243]. In $CD4^+$ T cells, mutation of the pMHC was shown to abrogate some responses completely, whereas others were affected to a lesser extent [57, 201]. These observations led researchers to hypothesise that the pMHC dose and affinity critically shape the quality of the T cell response.

5.1.3 Formalised analysis of dose- and affinity-thresholds

Experimental caveats have limited the quantitative analysis of dose- and affinity-thresholds associated with different cytokines. T cell stimulation experiments were often performed with pMHC-pulsed APCs, but the exact density and stability of pMHC are difficult to control on APCs [57, 83, 98, 243, 253, 257]. In addition, cytokine secreted by $CD8^+$ T cells was often measured by intracellular cytokine staining (IC) [243, 257], and although

IC is suitable to classify cells according to the cytokines they produce, it is not particularly quantitative. Finally, experiments were often conducted over long timescales, for example when proliferation was measured as a readout, but it is difficult to isolate TCR-mediated signals from other signals such as cytokine feedbacks at later times [57, 83, 98, 201, 243].

We therefore decided to use a reductionist experimental system in which pMHC doses can be directly controlled, short-term stimulation assays and ELISA to measure cytokines that were secreted into the supernatant. To formalise the search for signatures of dose- and affinity thresholds in our experiments, cytokine responses were evaluated for differences in their potency (EC_{50}) and amplitude (E_{max}). The quality of the T cell response will be defined as the ratio of cytokines secreted in response to a given pMHC dose or affinity. As illustrated schematically in Fig. 5.1A, differences in the EC_{50}s would indicate a dose-dependent change in the quality of the T cell response (R_1/R_2). Different affinity thresholds can be captured by considering how the quality of the response depends on pMHC affinity (Fig. 5.1B): The quality of the T cell response at a given dose or across all doses ($E^{(1)}_{max}/E^{(2)}_{max}$) will change if one of two readouts is disproportionately affected by pMHC affinity. Translation of hierarchical dose- and affinity-thresholds into quantitative differences in the EC_{50} and E_{max} will allow for a more precise articulation of a range of effects that pMHC dose and affinity could have on the quality of the T cell response.

5.1.4 Chapter overview

A large dataset was generated by stimulating T cells with titrations of pMHC ligands that bind the TCR with varying affinities for 8 hours and measuring the cytokines TNFα, MIP-1β, IFNγ and IL-2. As expected, both the potency and amplitude of each cytokine response were found to correlate with pMHC affinity (Section 5.2.1). The overall signalling phenotype consisted mostly of bell-shaped dose-response curves or saturating functions across the dataset, and was comparable for all cytokines within the same experimental repeat (Section 5.2.2). Surprisingly, only minimal variation could be detected in the EC_{50}s of the different cytokine responses (Section 5.2.3). Both the absolute E_{max} and E'_{max} relative to other cytokines in the same repeat were highly variable in our experiments

with no obvious hierarchy. Yet, the donor-specific hierarchy (Section 5.2.4) and quality (Section 5.2.5) of the response were conserved as the pMHC affinity decreased, indicating that the sensitivity of different readouts to changes in pMHC affinity were comparable. Our experimental findings are consistent with a model containing a single switch and cytokine-specific temporal integrators (Section 5.2.6). The systematic study of multiple effector functions in our minimal experimental system thus contrasts findings about differential pMHC dose- and affinity-requirements that dramatically changed the quality of the T cell response reported elsewhere [83, 98, 201, 243, 257].

5.2 Results

Our group has previously designed a panel of NY-ESO-$1_{157\text{-}165}$ pMHC ligands that bind the c58c61 1G4Hi TCR with varying affinities by introducing amino acid mutations on the peptide. The binding affinities between these mutants and the TCR were determined by Surface Plasmon Resonance (SPR) [126, 127, 131]. The most recent measurements of binding affinities for the 4A5A and 4A5P8K pMHC mutants are shown in Appendix Fig. C.1. An updated list of all NY-ESO-$1_{157\text{-}165}$ pMHC variants and their affinities to the 1G4Hi TCR is provided in Table 5.1. Binding affinities between the 1G4Hi and NY-ESO-$1_{157\text{-}165}$ pMHC mutants vary over nearly 20 million-fold from the physiological micro-/millimolar to the therapeutic picomolar regime. This is, to our knowledge, the largest pMHC affinity range covered within the same experimental system.

$CD8^+$ human T cells were stimulated with pMHC ligands from this panel at different doses to determine whether the signalling phenotypes for the 4 cytokines TNFα, MIP-1β, IFNγ and IL-2 were distinct in our minimal experimental system. 8 biotinylated pMHC mutants (Fig. 5.2A) were immobilised at different concentrations on a streptavidin-coated plate (Fig. 5.2B). T cells were added to the wells and cytokines were measured in the supernatant by ELISA after 8 hours of stimulation (Fig. 5.2C). Because the concentration of pMHC ligands varied between refolds, the amount of pMHC immobilised in each well was detected on a mock stimulation plate using a conformation-sensitive αHLA-A2 antibody and the pMHC dose estimation was corrected relative to an index pMHC as

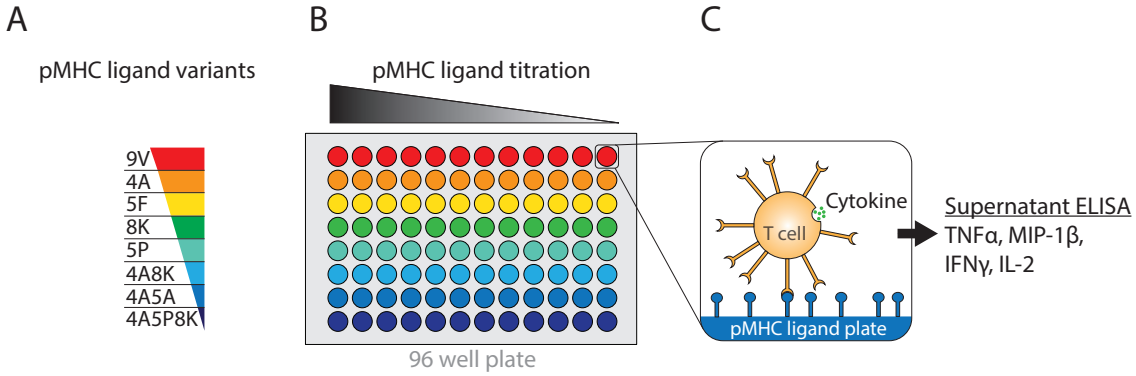


Figure 5.2: Schematic illustration of the experimental setup. A large dataset was generated by systematically stimulating T cells with a titration of different pMHC variants and measuring multiple readouts by ELISA. **(A)** Panel of pMHC variants used for stimulation of T cells. Colour coding for different pMHC variants is consistent throughout this chapter. **(B)** $CD8^+$ primary T cells expressing the 1G4Hi TCR were stimulated with a titration of different pMHC variants. **(C)** After 8 hours of stimulation, supernatants were harvested and the concentration of multiple cytokines was measured by ELISA. Differences in the immobilisation of pMHC variants were corrected for by including an immobilisation control (see Methods Section 2.6.2). This allowed us to directly compare different pMHC ligands.

Name	Sequence	Dissociation constant
9V	SLLMWITQV :	$K_D = 7.07 \times 10^{-5}$ µM
4A	SLLAWITQV :	$K_D = 1.09 \times 10^{-3}$ µM
5F	SLLMFITQV :	$K_D = 9.31 \times 10^{-2}$ µM
8K	SLLMWITKV :	$K_D = 2.03 \times 10^{-1}$ µM
5P	SLLMPITQV :	$K_D = 4.85 \times 10^{-1}$ µM
4A8K	SLLAWITKV :	$K_D = 1.78 \times 10^{0}$ µM
4A5A	SLLAAITQV :	$K_D = 9.67 \times 10^{1}$ µM
4A5P8K	SLLAPITKV :	$K_D = 1.40 \times 10^{3}$ µM

Table 5.1: Updated list of NY-ESO-$1_{157\text{-}165}$ pMHC variants that bind the 1G4Hi TCR with milli- to picomolar affinities. Amino acid substitutions relative to the 9V peptide are highlighted in red. The dissociation constants, K_D, range from picomolar therapeutic (9V) to micro-/millimolar physiological (4A8K, 4A5P8K) affinity. This panel allows for the, to our knowledge, largest variation of pMHC affinity within the same experimental system.

described in Methods Section 2.6.2. This experimental setup thus allowed us to directly compare the pMHC dose- and affinity-dependence of 4 cytokines.

Fig. 5.3 shows an overview of TNFα, MIP-1β, IFNγ and IL-2 secretion after stimulation of T cells derived from 9 donors. Missing datasets are the result of failed immobilisation controls for a particular pMHC or unavailability of the reagents for ELISA. This large datasets underlies all analyses in this chapter.

5.2.1 EC_{50} and E_{max} of the TNFα, MIP-1β, IFNγ and IL-2 response correlate with pMHC affinity

Numerous studies reported that the affinity of the pMHC ligand determines the pMHC dose at which a T cell response is triggered [10, 55, 86, 150] and the observation was confirmed in our experimental system. Irrespective of the cytokine, high-affinity pMHCs elicited a cytokine response at relatively low doses, whereas higher doses of low-affinity pMHCs were required to detect a cytokine response (Fig. 5.4A). To quantify the sensitivity of each cytokine response to pMHC dose, the EC_{50} for all dose-response curves in Fig. 5.3 were extracted by fitting an interpolating function to the experimental data and identifying the dose eliciting a half-maximal response as described in Methods Section 2.7.2. The two lowest-affinity pMHC ligands 4A5A and 4A5P8K were excluded from the analysis because the cytokine response to these ligands did not saturate even at the highest dose of pMHC (see Appendix Fig. C.2). The EC_{50} fold-changes relative to an index pMHC (5P) were then averaged across all donors (Fig. 5.4B). Comparison of absolute EC_{50}s across experimental repeats was not possible since the amount of plate-immobilised pMHC could vary between experimental repeats, for example as a result of variations in the concentration of correctly refolded pMHC. The relative EC_{50}s, however, could be averaged directly because differences in the immobilisation between pMHC ligands in the same experiment were corrected for (Methods Section 2.6.2). A significant correlation between the pMHC affinity, K_D, and the EC_{50} was found for all cytokine responses except IFNγ ($p = 0.1316$ by Spearman's non-parametric ranking).

The amplitude of the T cell response, E_{max}, was also previously found to correlate

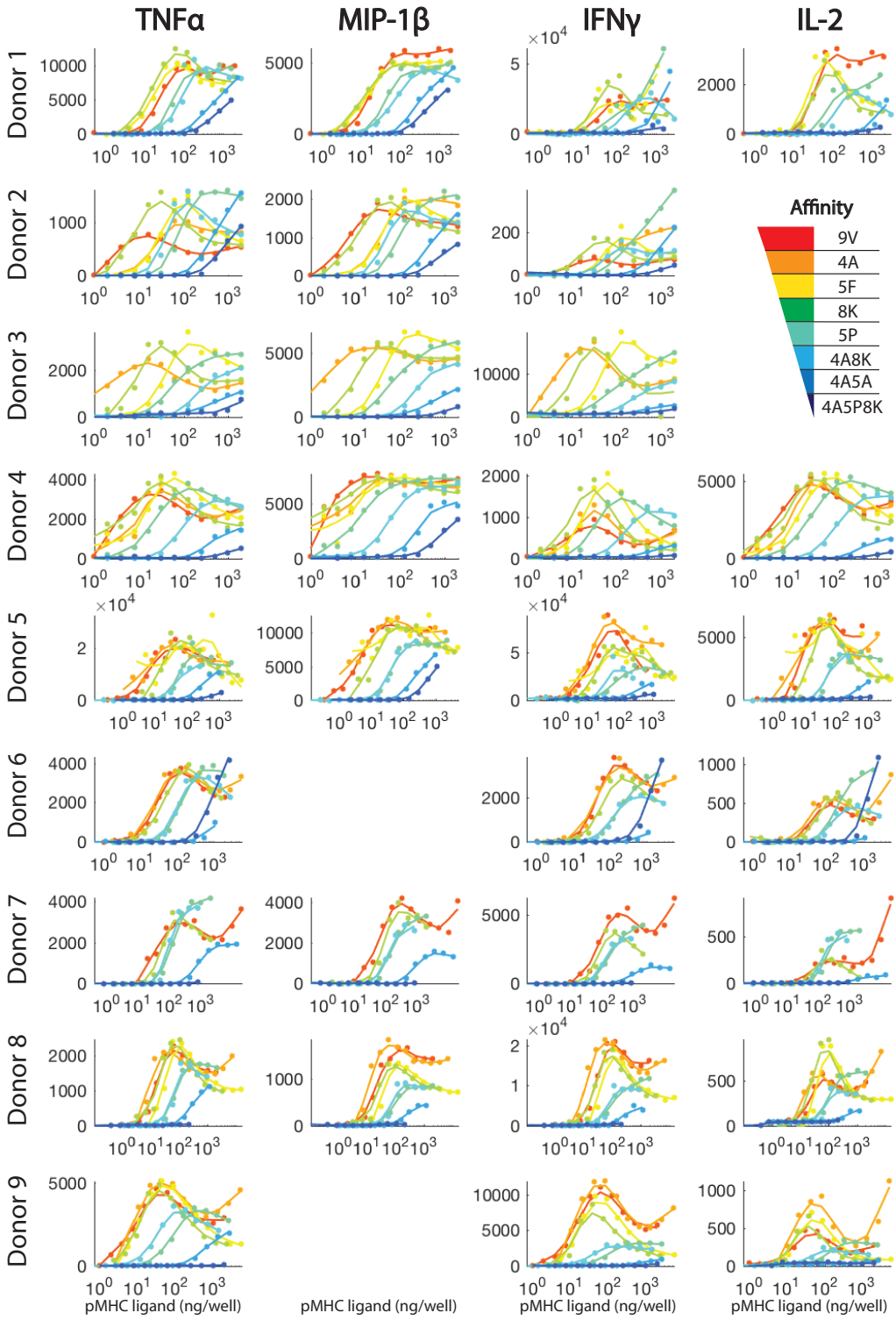


Figure 5.3: The TNFα, MIP-1β, IFNγ and IL-2 signalling phenotypes are similar across donors and pMHC variants. T cells derived from 9 different donors (rows) were stimulated with a titration of different pMHCs variants, and (from left to right) TNFα, MIP-1β, IFNγ and IL-2 were measured in the supernatant by ELISA after 8 hours of stimulation. A limited set of signalling phenotypes consisting of mainly bell-shaped and sigmoidal dose-response curves was observed across all donors. Within the same donor, the signalling phenotypes associated with different cytokines were similar. Symbols are experimental measurements and solid lines represent LOWESS smoothing curves. Units on y-axes are $\frac{\text{pg}}{\text{ml}}$.

with pMHC affinity [30, 55, 290]. The response to low-affinity pMHC mutants indeed appeared to saturate at lower cytokine levels in some but not all donors (compare Donors 1 and 9 in Fig. 5.3). Averaged across all donors, however, a significant negative correlation was found between the K_D and the E_{max} relative to E^{5P}_{max} for 3 of 4 cytokine responses (Fig. 5.4C). The E_{max} was normalised for each experiment to E^{5P}_{max} because the absolute amounts of cytokine produced varied up to 10-fold across experimental repeats, and the difference in scale could have distorted any affinity-dependent correlations. The E_{max} of the TNFα response did not correlate significantly with the K_D ($p = 0.0694$ by Spearman's non-parametric ranking). The mean of the relative E^{9V}_{max} and E^{4A}_{max} (the two highest-affinity pMHCs) was lower than the mean E^{5F}_{max} (intermediate affinity), but the apparent optimal affinity was not statistically significant (ordinary one-way ANOVA corrected for multiple comparisons by Tukey's test).

These findings are consistent with previous reports that support a correlation between the K_D and both the EC_{50} [10, 55, 86, 150] and E_{max} [30, 55, 290] of various T cell responses. In addition, we found saturating effects when the affinity was increased below approximately $K_D < 2.03\times10^{-1}\mu M$. These supraphysiological affinities did thus not result in further enhancement of the cytokine response. The observation is consistent with previous reports, but the cut-off affinity is slightly higher than the 1–5 μM that have been reported elsewhere [97, 243].

5.2.2 The overall TNFα, MIP-1β, IFNγ and IL-2 signalling phenotypes are similar

The dominant dose-response phenotypes found in our systematic study were bell-shaped and saturating functions. To directly compare whether the dose-response phenotypes associated with the cytokines TNFα, MIP-1β, IFNγ and IL-2 exhibited qualitative differences, the experimental data in Fig. 5.3 were normalised and all cytokine readouts were overlaid (Fig. 5.5). Sigmoidal and non-saturating signalling phenotypes were observed when T cells were stimulated with low-affinity pMHC ligands, whereas high-affinity pMHC ligands elicited bell-shaped dose-response curves, which is also called 'high-

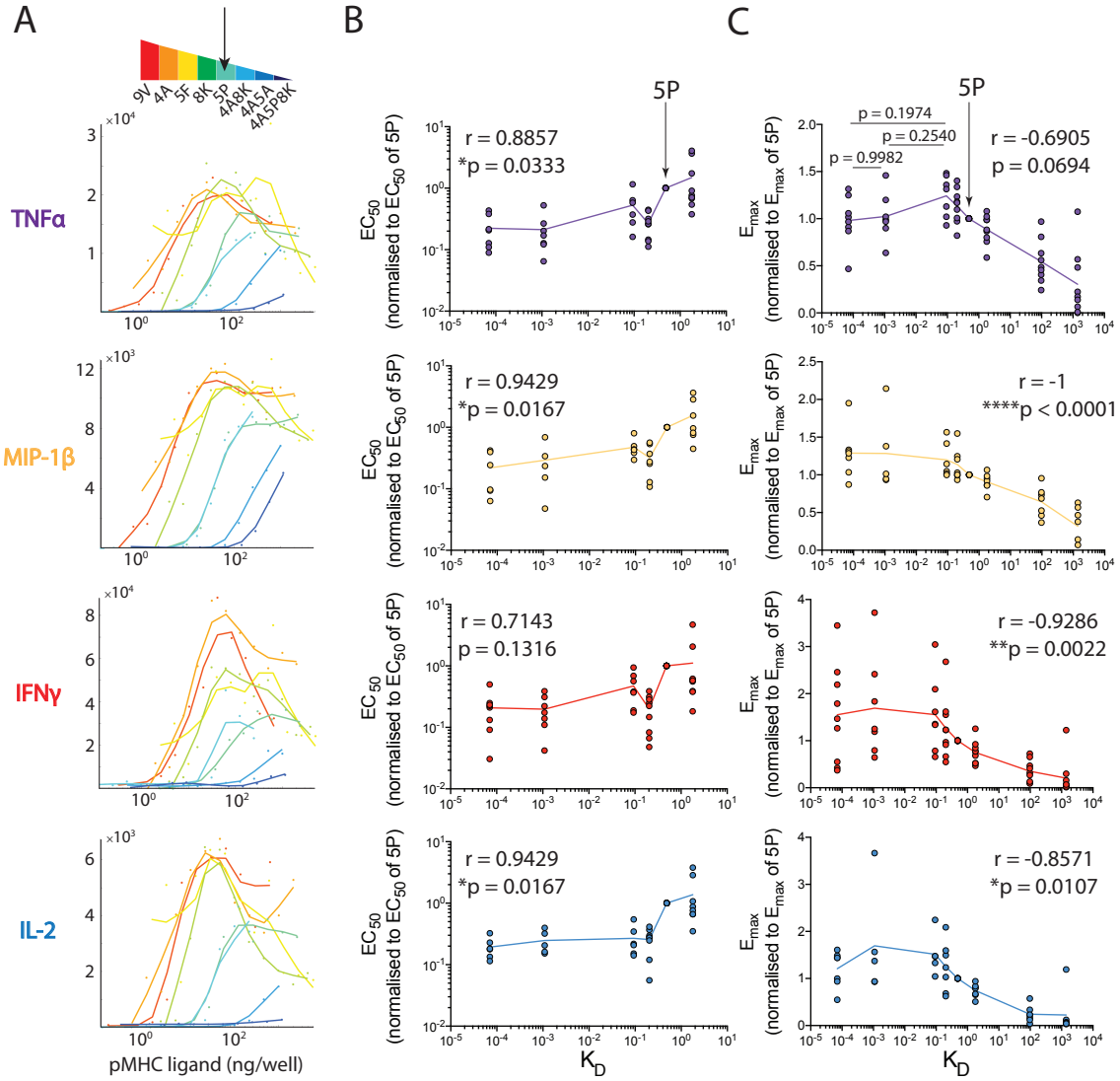


Figure 5.4: EC_{50} and E_{max} of the TNFα, MIP-1β, IFNγ and IL-2 response correlate with pMHC affinity. (A) Representative dataset of TNFα, MIP-1β, IFNγ and IL-2 in response to titrations of different pMHC mutants. Solid lines are LOWESS curves. **(B)** Fold-change in the EC_{50} relative to EC_{50}^{5P} as a function of the dissociation constant, K_D. The EC_{50} for the two lowest-affinity pMHCs could not be determined because the response did not saturate. See Appendix Fig. C.2 for dataset inclusion criteria. **(C)** Fold-change in the E_{max} relative to E_{max}^{5P} as a function of K_D. In (B) and (C), symbols are individual repeats and solid lines connect the mean normalised EC_{50} and E_{max}. The apparent optimal K_D for highest relative $E_{max}^{TNF\alpha}$ was not statistically significant (ordinary one-way ANOVA, corrected for multiple comparisons by Tukey's test). Statistical significance of correlations were evaluated by Spearman's non-parametric correlation coefficient (r) and p-values were determined for each cytokine separately.

dose suppression' and has been reported in other experimental systems and functional readouts [57, 127, 201, 238]. When stimulating T cells with the high-affinity pMHCs 9V or 4A, we frequently also observed a bell-shaped dose-response curve followed by an increase of the response at the highest pMHC doses (e.g. Donor 7). The overlay furthermore revealed slight differences in the shape of bell-shaped dose-response curves. Most notably, MIP-1β displayed a lower degree of high-dose suppression than the other cytokines. The overall shape of the dose-response curves, however, appeared similar for all cytokines given a particular pMHC and donor.

5.2.3 The dose thresholds for secretion of TNFα, MIP-1β, IFNγ and IL-2 are similar

Surprisingly, the overlay of normalised TNFα, MIP-1β, IFNγ and IL-2 responses in Fig. 5.5 indicated that the lowest doses of pMHC to trigger the secretion of each cytokine were roughly identical. It suggested that these cytokine readouts underlie similar dose thresholds, contrary to what has been reported previously in other experimental systems [83, 98, 201, 243, 253, 257]. Analysis of the EC_{50}s in each panel of Fig. 5.5 relative to the corresponding TNFα response revealed no significant difference between $EC_{50}^{TNF\alpha}$, $EC_{50}^{MIP\text{-}1\beta}$, $EC_{50}^{IFN\gamma}$ and $EC_{50}^{IL\text{-}2}$ in 3 out of 6 pMHCs (Fig. 5.6). Consistent across all pMHCs, $EC_{50}^{TNF\alpha}$ never deviated significantly from $EC_{50}^{MIP\text{-}1\beta}$, and $EC_{50}^{IFN\gamma}$ and $EC_{50}^{IL\text{-}2}$ were equally indistinguishable. Close inspection of the data in Fig. 5.6 indicated that $EC_{50}^{IFN\gamma}$ and $EC_{50}^{IL\text{-}2}$ tended to be slightly higher than $EC_{50}^{TNF\alpha}$ and $EC_{50}^{MIP\text{-}1\beta}$, but the difference was only statistically significant when stimulating T cells with the 9V, 4A (both supraphysiological) or 5P pMHC ligands.

The subtle hierarchy of EC_{50}s (TNFα/MIP-1β < IFNγ/IL-2) reported here is consistent with other studies [243, 257], but the differences between EC_{50}s were much smaller in our experimental system. In fact, most statistically significant discrepancies between cytokine-specific EC_{50}s were observed when T cells were stimulated with supraphysiological pMHC ligands. Overall, $EC_{50}^{TNF\alpha\ /\ MIP\text{-}1\beta}$ rarely deviated by more than two-fold from $EC_{50}^{IFN\gamma\ /\ IL\text{-}2}$ in our minimal experimental system (Fig. 5.6), whereas other studies

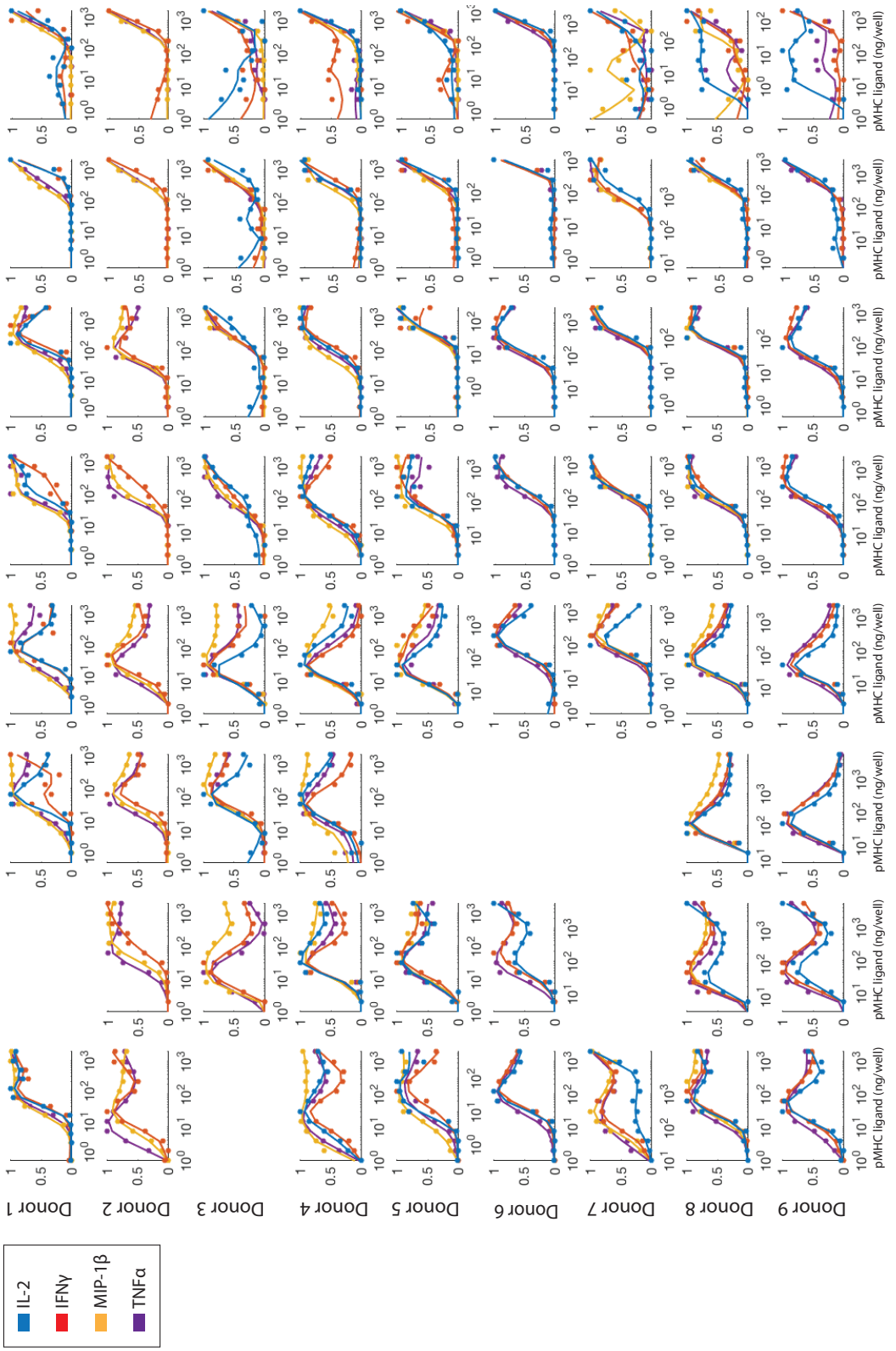


Figure 5.5: Overlay of the normalised TNFα, MIP-1β, IFNγ and IL-2 response highlights similar signalling phenotypes and activation thresholds.

report 100- and even 1000-fold variations [83, 243, 257]. Given that the overall signalling phenotypes and EC_{50}s associated with each cytokine response were similar, the quality of the T cell response defined as the ratio of cytokines produced did not change dramatically as a function of pMHC dose. These findings therefore contrast previous studies that found cytokine-specific dose thresholds.

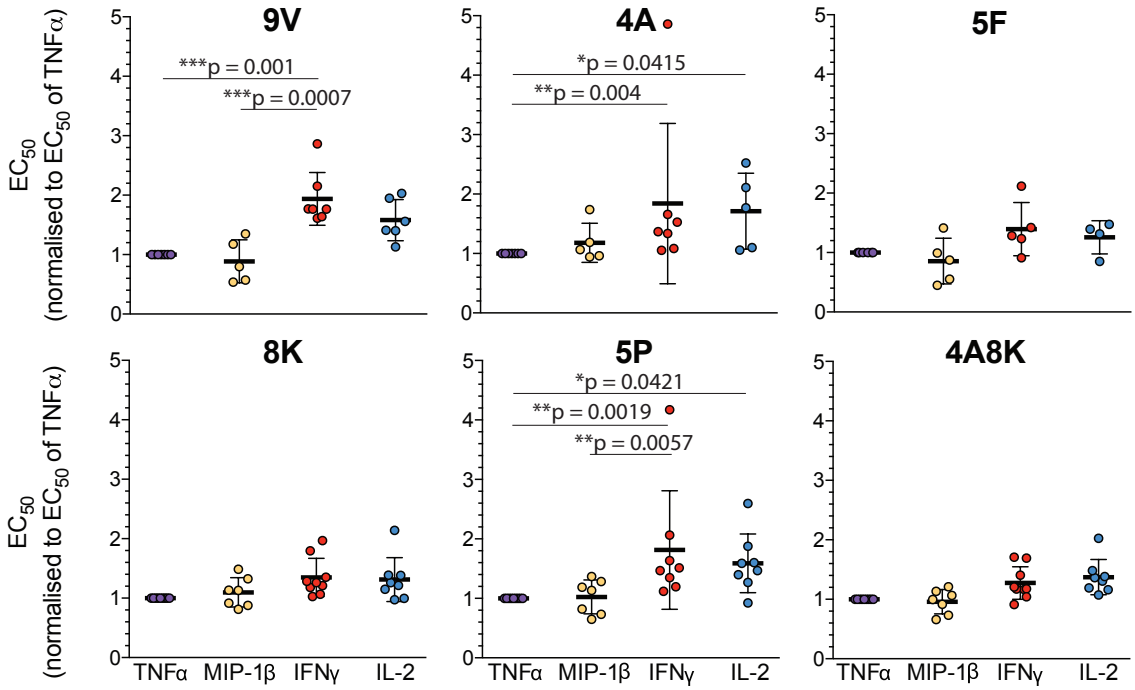


Figure 5.6: The EC_{50}s of the TNFα, MIP-1β, IFNγ and IL-2 responses are similar. EC_{50}s were extracted from experimental data as described in Methods Section 2.7.2 and normalised to the EC_{50} of the corresponding TNFα response. The two lowest-affinity pMHCs 4A5A and 4A5P8K were excluded from the analysis because the highest dose of pMHC did not saturate the cytokine response. Statistical significance was determined by ordinary two-way ANOVA and corrected for multiple comparisons by Tukey's test.

5.2.4 The absolute amounts and hierarchy of TNFα, MIP-1β, IFNγ and IL-2 secretion are heterogeneous and donor-specific

In contrast to the EC_{50}, the absolute maximal amount (E_{max}) of TNFα, MIP-1β, IFNγ and IL-2 varied appreciably both within and across experimental repeats. The overlay in Fig. 5.7 illustrates a high level of heterogeneity in the absolute amounts of cytokines

produced by T cells from different donors. Stimulation of T cells derived from Donor 1, for example, resulted in a maximal amount of ~20,000 $\frac{pg}{ml}$ of any cytokine produced, whereas T cells derived from Donor 2 only produced at most ~2,000 $\frac{pg}{ml}$ of any cytokine. Of note, the absolute amount of cytokine produced did not scale linearly with the TCR transduction level (Appendix Fig. C.3). Large variations in the absolute amount of cytokines were also found within the same donor: T cells from Donor 8, for instance, produced ~20,000 $\frac{pg}{ml}$ of IFNγ, and roughly 10-fold less of all other cytokines. Similar donor-dependent discrepancies have been observed in other studies [195, 243].

Despite the high level of heterogeneity in the absolute amounts of cytokine produced, a dominant hierarchy of cytokines secreted could be identified by ranking the E_{max} of the TNFα, MIP-1β, IFNγ and IL-2 responses (Fig. 5.8). On average, IFNγ was produced the most and IL-2 the least ($p < 0.0001$ by Friedman's non-parametric ranking and Dunn's multiple comparisons test). However, the E_{max} hierarchy was also donor-dependent (compare grey dashed lines in Fig. 5.9). The statistically most likely ranking was only found in 2 donors, as in particular the ranking of $E_{max}^{TNF\alpha}$ relative to $E_{max}^{MIP\text{-}1\beta}$ was variable (Donors 1, 5 and 8 in Fig. 5.9). Interestingly, T cells are known to lose the ability to produce both TNFα and IL-2 secretion and gain the ability to produce IFNγ as they progress through several differentiation stages [98, 118, 143, 174, 226], possibly because IFNγ transcription requires epigenetic modifications and multiple rounds of proliferation [174, 264]. The dominant hierarchy observed here is thus indicative of memory or terminally-differentiated T cell populations and donor-dependent variations in the absolute amount and hierarchy of cytokines produced could be explained by age differences between the T cell populations used for experiments.

5.2.5 The quality of the T cell response is similar for a wide range of pMHC doses and affinities

Previous studies had found that the quality of the T cell response, defined as the ratio of different cytokines produced, is a function of the pMHC dose and affinity [98, 257]. The striking similarity of the overall signalling phenotypes and EC_{50}s associated with TNFα,

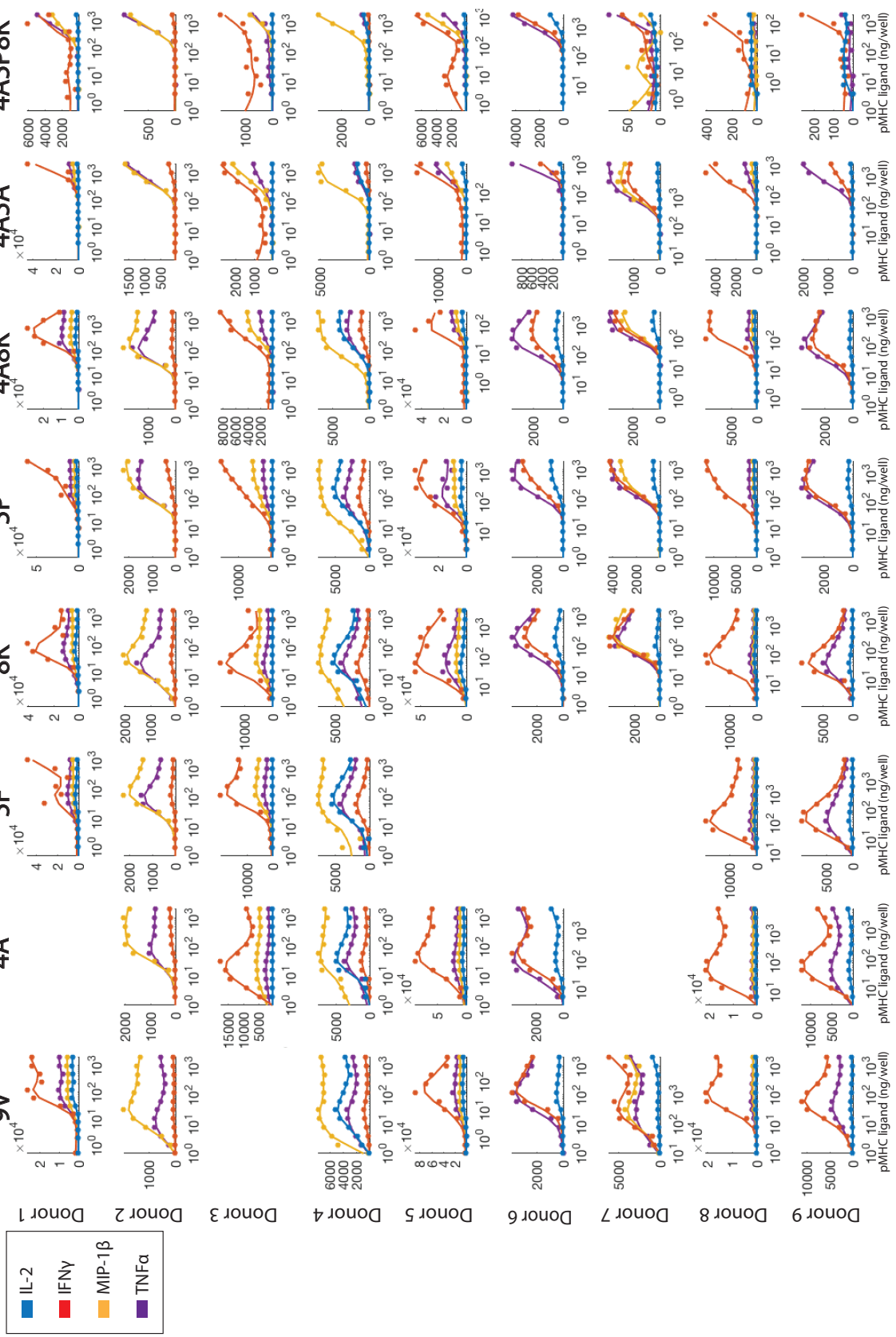


Figure 5.7: Overlay of the TNFα, MIP-1β, IFNγ and IL-2 response (absolute amounts) highlights donor-specific differences in the amount and hierarchy of cytokines produced.

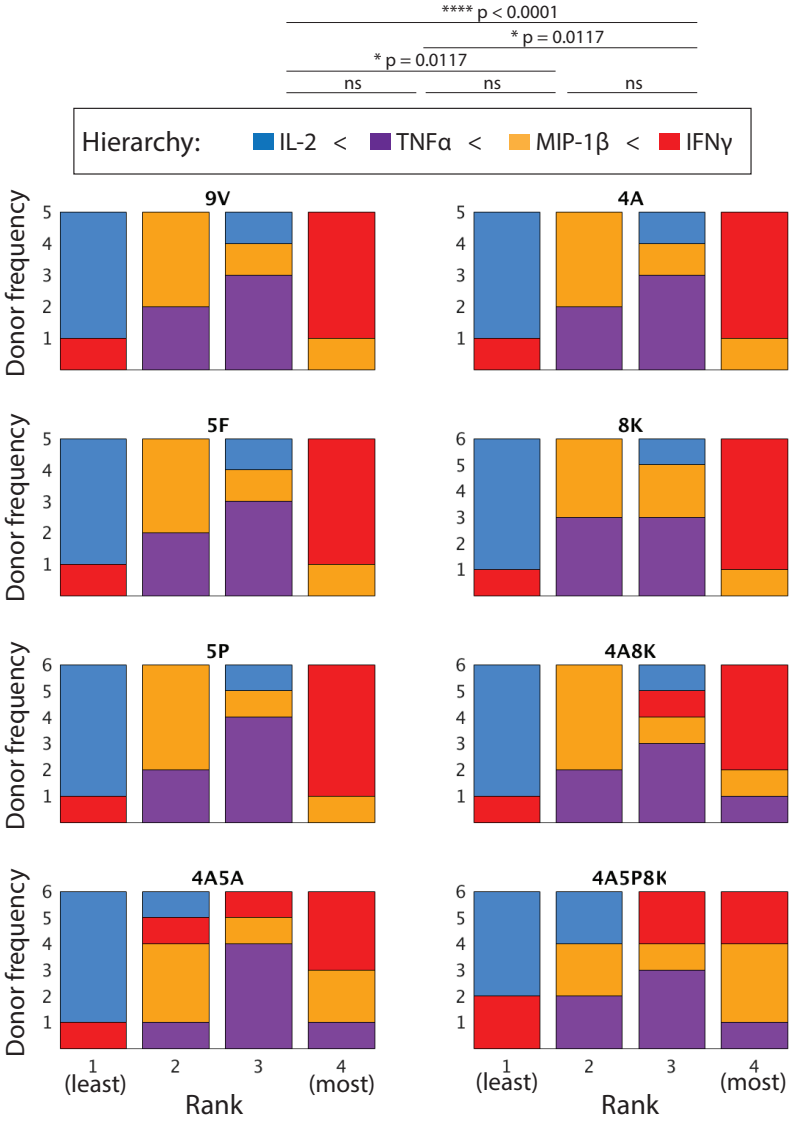


Figure 5.8: E_{max} ranking of the TNFα, MIP-1β, IFNγ and IL-2 response suggests a dominant IL-2^{low}IFNγ^{high} secretion profile. The E_{max} of TNFα, MIP-1β, IFNγ and IL-2 were ranked in increasing order for each panel in Fig. 5.7 and results are summarised here across all donors. The different cytokines are encoded by colour, the rank is shown on the x-axis and the frequency of donors with a particular ranking on the y-axis. In most donors, IL-2 was ranked lowest and IFNγ highest. The dominant hierarchy and statistical significance were determined by repeated measures Friedman non-parametric ranking and p-values were corrected by Dunn's multiple comparisons test. Only repeats with measurements for all 4 cytokines were included for ranking and statistical analyses.

MIP-1β, IFNγ and IL-2 responses that was established in Sections 5.2.2–5.2.3 suggested a relatively constant scaling of cytokines secreted by T cells from the same donor in response to a given pMHC at all doses. In other words, the quality of the response was expected to not change dramatically as a function of pMHC dose. To simplify the analysis, we therefore collapsed the dose-dimension by only comparing the maximal response, $E_{max}^{(i)}$, associated with each cytokine response, i, and relative changes in the $E_{max}^{(i)}$ as a function of pMHC affinity.

The same E_{max} hierarchy was conserved across a wide range of pMHC affinities. Fig. 5.9 overlays the ranking of the maximal TNFα, MIP-1β, IFNγ and IL-2 responses in response to different pMHC mutants. While the donor-specific hierarchy across all pMHCs (grey dashed line) is different between donors, the response only rarely deviated from the dominant hierarchy within the same donor, independent of pMHC affinity. Deviations from the donor-specific hierarchy typically occurred when T cells were stimulated with the lowest-affinity pMHC mutants (4A5A and 4A5P8K) that provoked a generally weak cytokine response with lower signal-to-noise ratios (Fig. 5.7). In most donors, the E_{max} hierarchy was thus robust over a wide range of pMHC affinities (nearly 5 orders of magnitude).

The quality of the response could still change if secretion of some cytokines were more dramatically affected by changes in pMHC affinity than others [83]. To detect subtle changes in the quality of the T cell response, we thus also considered the absolute amount of each cytokine produced relative to a reference cytokine (here IFNγ), $E_{max}^{(i)\prime} = E_{max}^{(i)} / E_{max}^{IFN\gamma}$, and evaluated whether $E_{max}^{(i)\prime}$ had differential sensitivities to changes in pMHC affinity. Because the ratio of cytokines produced varied between donors, $E_{max}^{(i)\prime}$ were furthermore normalised to the 9V condition, so that we could isolate and average the effect of the pMHC affinity on relative changes in the ratio of different cytokines produced. Intermediate steps before averaging are included in Appendix Fig. C.4–C.5. On average, $E_{max}^{(i)\prime}$ remained constant over the whole range of pMHC affinities (Fig. 5.10, unpaired t-test, corrected for multiple comparisons by Holm-Sidak). Close inspection of the data in Fig. 5.10 suggested that the relative amount of TNFα and MIP-1β compared to IFNγ and IL-2 increased when T cells were stimulated with low-affinity

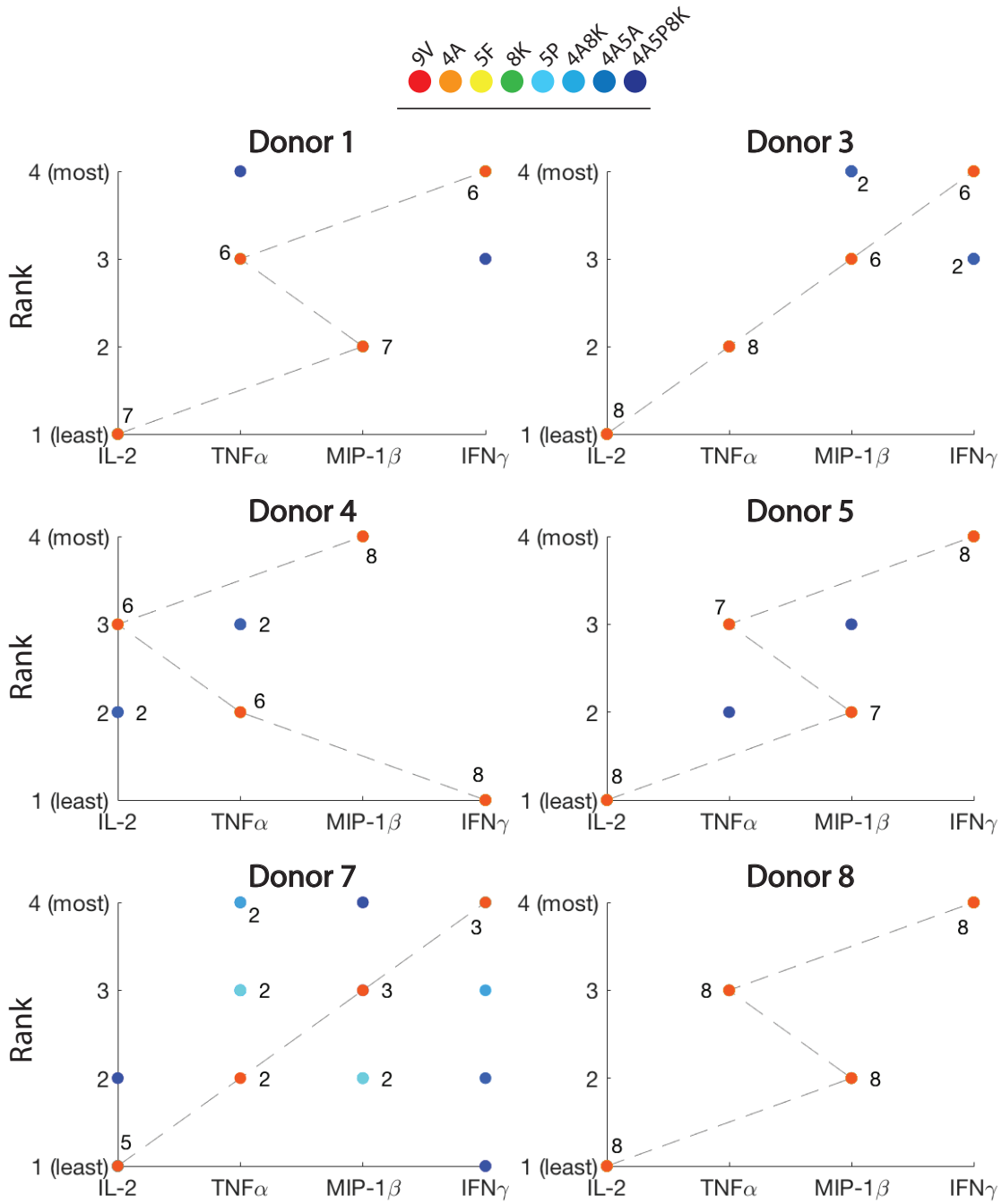


Figure 5.9: Hierarchies are variable between donors, but consistent over a large range of pMHC affinity within each donor. The statistically most likely hierarchy, IL-2 < TNFα < MIP-1β < IFNγ, is shown on the x-axis. It was identical to the dominant cytokine hierarchy across pMHCs in Donors 3 and 7 and similar to hierarchies in Donors 1, 5 and 8 (compare grey dashed lines). The ranking of the 4 cytokine responses was overlaid for different pMHC mutants. Within each donor, the hierarchy is similar for different pMHCs (number next to symbols indicates number of overlaid rankings). Only repeats with measurements for all 4 cytokines were included for ranking and statistical analyses.

pMHC ligands. In addition to the subtle differences in $EC_{50}^{IFN\gamma/IL2}$ and $EC_{50}^{TNF\alpha/MIP\text{-}1\beta}$ reported in Section 5.2.3, secretion of IFNγ and IL-2 thus appeared to be also more similarly affected by changes in pMHC affinity than TNFα and MIP-1β.

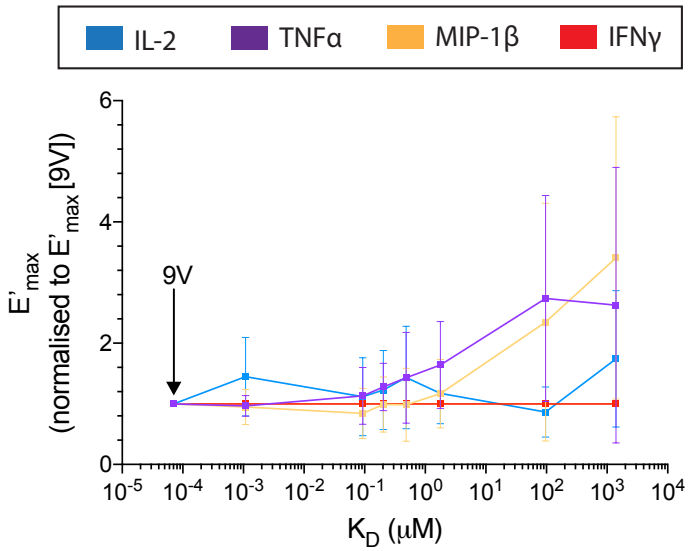


Figure 5.10: The quality of the cytokine response is similar over a wide range of affinities. The y-axis is defined as $E_{max}^{(i)\prime} = E_{max}^{(i)}/E_{max}^{IFN\gamma}$, with i indexing the different cytokine responses. $E_{max}^{(i)\prime}$ varies between donors (see Fig. 5.7), and it was therefore normalised to the $E_{max}^{(i)}$ after stimulation with 9V within each experimental repeat for averaging. A trend in the mean $\langle E_{max}^{(i)\prime} \rangle$ suggested that the overall cytokine response changed qualitatively as the ratio of TNFα and MIP-1β to IFNγ changed when T cells were stimulated with low-affinity pMHC ligands. But the differences in $E_{max}^{(i)\prime}$ were not statistically significant at any pMHC affinity (unpaired t-test and correction for multiple comparisons by the Holm-Sidak method). Solid lines connect mean $E_{max}^{(i)\prime}$ and errorbars are the SD. Refer to Appendix Fig. C.4– C.5 for absolute amounts and $E_{max}^{(i)\prime}$ by donor (not averaged).

5.2.6 A single-switch model with differential temporal integration is consistent with the experimental data

It is unclear on a molecular level where the regulation of TNFα, MIP-1β, IFNγ and IL-2 diverges. Using the phenotypic model presented in Chapter 4, we identified phenotypic parameters that could explain the experimental findings reported here. The model was thus far fitted to a time course of TNFα secretion (Section 4.2.1) and it is generally consistent with a positive correlation between the EC_{50} and the K_D of the pMHC and

a negative correlation between E_{max} and K_D after 8 hours of stimulation (Fig. 5.11A). Additional features we aimed to explain were the slight differences in $EC_{50}^{TNF\alpha/MIP\text{-}1\beta}$ and $EC_{50}^{IFN\gamma/IL\text{-}2}$, and a less dramatic, affinity-dependent decrease in the E_{max} of the TNFα and MIP-1β responses to low-affinity pMHCs compared to the IFNγ and IL-2 responses.

Previous studies that observed large differences in cytokine-specific EC_{50}s concluded that the threshold level of TCR signalling, s_y, that must be exceeded to trigger a response is specific to each cytokine (Fig. 5.11B) [243, 257]. Given that the variations in the EC_{50}s and slopes associated with the TNFα, MIP-1β, IFNγ and IL-2 responses were small in our minimal experimental system (Fig. 5.5), we explored alternative model hypotheses that were based on a shared switch. Each cytokine could, for example, be regulated by separate temporal integrators that are either activated at a slower or degraded at a faster rate (Fig. 5.11C). Modifying the corresponding phenotypic rates k_{fy} and k_{ry}, respectively, has the capacity to decrease the E_{max} (Fig. 5.11D) and increase the EC_{50} (Fig. 5.11E) of the cytokine response. In addition, increased activity of Y also leads to increased sensitivity of E'_{max} on the pMHC affinity (Fig. 5.11F). Slight variations in the timescales of signal integration that differentially affect TNFα, MIP-1β, IFNγ and IL-2 are therefore consistent with the experimental data presented here (compare (F) in Fig. 5.11 to Fig. 5.6 and Fig. 5.10).

Signal processing leading to production of TNFα, MIP-1β, IFNγ and IL-2 could be heterogeneous in more than one parameter and the phenotypic parameters we identified above do not have unique effects on the cytokine response. We note that the amplitude of cytokine secretion can be scaled independently of the EC_{50} by adjusting the cytokine production rate, k_{act} (data not shown), possibly explaining the highly donor-specific variation in the amount and ratios, but not the EC_{50}s of cytokines secreted. Importantly, the preliminary model in Fig. 5.11 highlights that the secretion of 4 key cytokines in this minimal experimental system does not require the assumption of multiple activation thresholds.

5.3 Discussion

In summary, a large dataset was generated to investigate whether cytokine responses have different sensitivities to pMHC dose and affinity that affect the quality (ratio of cytokines produced) of the T cell response in a ligand-dependent manner. Detailed analysis of TNFα, MIP-1β, IFNγ and IL-2 secretion showed that each cytokine response depends similarly on pMHC dose and affinity in our minimal experimental system. While both the EC_{50} and E_{max} of individual cytokines changed as the affinity of the stimulating pMHC was altered (Section 5.2.1), the dose-response phenotype was identical between different cytokines (Section 5.2.2). The fold-difference between EC_{50}s of cytokine responses to the same stimulus varied by a factor of two at most, suggesting that similar activation thresholds underlie the regulation of these cytokines (Section 5.2.3). Large variation between readouts was observed in the absolute and relative E_{max} (Section 5.2.4), but within each donor, the ratio of cytokines produced remained nearly constant over the whole range of pMHC affinities (Section 5.2.5). Most variability in the quality of the response was thus observed between donors and we found limited evidence for T cell-intrinsic cytokine-specific susceptibilities to pMHC dose and affinity. Finally, we showed using the phenotypic model from the previous chapter that a single-switch model with cytokine-specific temporal integrators is consistent with the experimental data, and did not require the assumption that cytokine readouts are activated in a hierarchical manner as a result of varying activation thresholds (Section 5.2.6).

5.3.1 Comparison to previous studies

Previous studies have found large differences in the dose thresholds that must be met to trigger various functional readouts, and a number of factors could account for the discrepancy to the findings in this study. First, different cytokine detection methods could influence the results. Early studies used indicator cells to estimate relative cytokine levels [201], other studies, similar to ours, detected cytokines in the supernatant by ELISA [83, 243, 253] and a third method frequently employed was intracellular staining of cytokines followed by flow cytometry [83, 98, 257]. Each method has advantages and

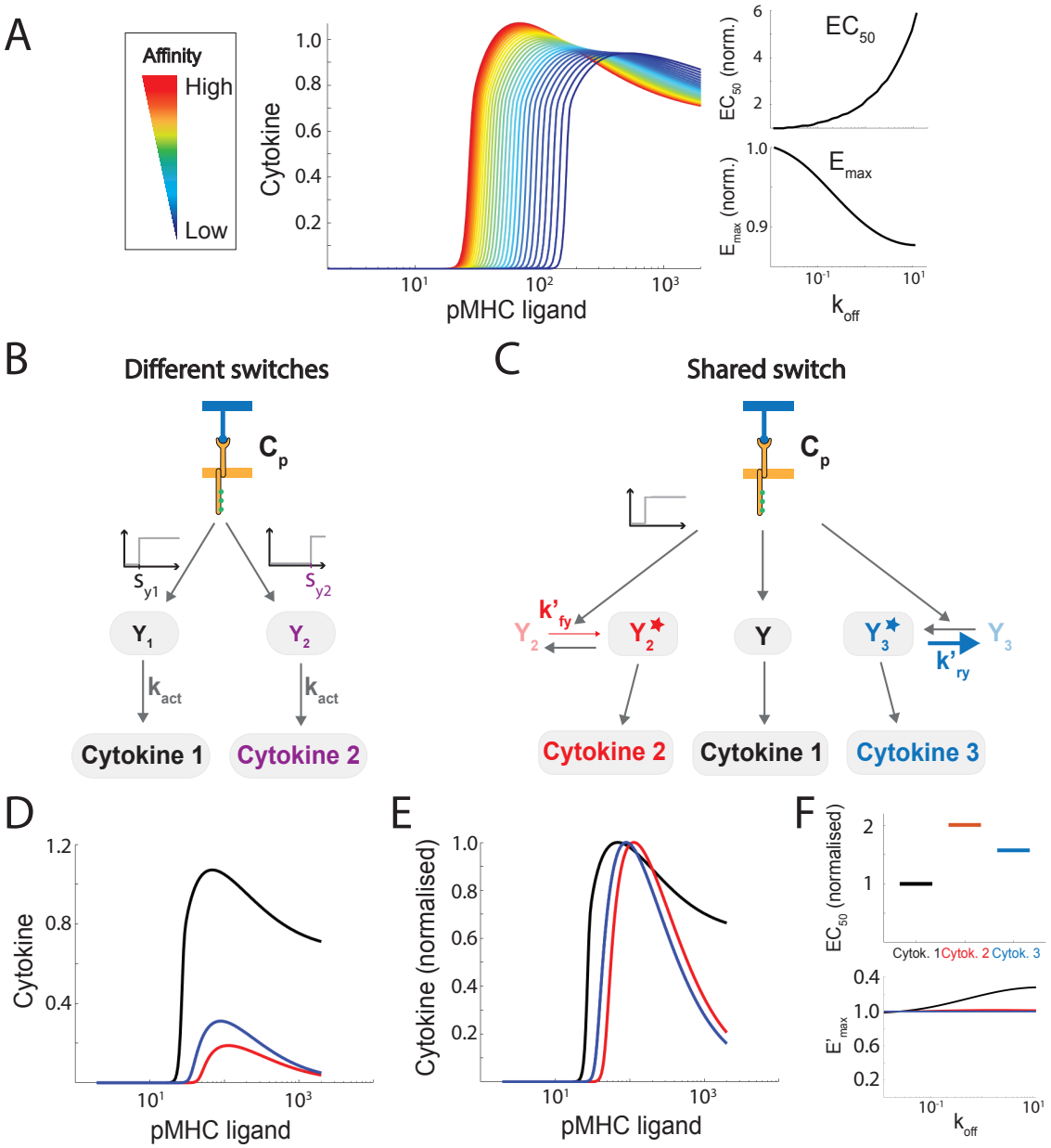


Figure 5.11: A single-switch model is consistent with the experimental data. (A) The phenotypic model presented in the previous chapter is consistent with the observed dependence of EC_{50} and E_{max} on pMHC affinity. **(B)** Cytokine-specific differences in the EC_{50} can be explained with signalling cascades activated by separate molecular switches [257], corresponding to s_y in our phenotypic model. **(C)** The slightly higher EC_{50}s for IFNγ and IL-2 that we report here are also consistent with a single-switch model and cytokine-specific temporal integrators (decreased activation rate, k_{fy}, in red or increased degradation rate, k_{ry}, in blue). **(D)** Cytokine as a function of pMHC dose for the 3 cytokines in (C). **(E)** Normalised cytokine as a function of pMHC dose for the 3 cytokines in (C). Cytokine 1 (black) was simulated with fit parameters from Chapter 4, whereas Y_2 (red cytokine) is activated at a slower rate ($k'_{fy} = 1.3 \times 10^{-4} s^{-1}$), and Y_3 (blue cytokine) is degraded at a faster rate ($k'_{ry} = 1.4 \times 10^{-1} s^{-1}$). **(F)** Both modifications in k_{fy} and k_{ry} lead to small differences in the EC_{50} of the respective cytokine response (top, compare Fig. 5.6), and change the sensitivity of $E'^{(i)}_{max} = E^{(i)}_{max}/E^{3}_{max}$ to pMHC affinity (bottom, compare Fig. 5.10).

disadvantages: ELISA assays is a relatively precise method to measure the concentration of cytokines, but it does not reveal information about the single-cell response. Intracellular cytokine staining, on the contrary, provides information about single-cell responses, but it is not a quantitative method and possibly sensitive to gating strategies and the quality of fluorophore-conjugated antibodies. Direct evidence that these detection methods can yield qualitatively different results can be seen in a study by Tan et al. [243], where measurements of cytokines in the supernatant by ELISA revealed no apparent difference in the EC_{50} of TNFα, MIP-1β, IFNγ and IL-2, but parallel measurements of the EC_{50}s of the percentage of T cells expressing each cytokine as determined by intracellular cytokine staining varied up to 100-fold (Figure 2 in [243]).

Second, not all studies measured cytokines (and other readouts) on the same timescale as we did here. Between studies, time scales range from 5 hours [83, 98, 243, 253, 257] over 24 hours [98, 201, 243] to $>$ 48 hours [57, 83, 201], or a mix of timescales [83, 98, 201, 243]. It is difficult to conclusively attribute differences in EC_{50}s to differential sensitivities of readouts to TCR signalling when they occur on separate timescales. Cytokine and other feedbacks are likely to play a role on long timescales, and it is known, for example, that feedback through the IL-2 pathway selectively amplifies IFNγ secretion [78, 107, 156, 246]. In addition, some readouts can eventually be consumed (cytokines) or downregulated (surface markers), and measuring functional readouts in different phases of their activation complicates the interpretation of the data. Finally, most studies utilised APCs to stimulate T cells, but the stability of peptide loading over long time scales cannot be guaranteed [147, 247]. Measuring activation markers and their EC_{50}s at different time points and comparing them directly could therefore be potentially misleading, as the pMHC dose presented to T cells may have changed throughout the experiment.

Third, all studies discussed here were conducted with antigen presenting cells (APCs) for stimulation [83, 98, 201, 243, 253, 257], whereas we used plate-immobilised pMHC. The stimulation strategies could lead to discrepancies between reported cytokine hierarchies because APCs provide co-stimulatory signals and grant mobility of pMHC and other ligands. Co-stimulation has been shown by some authors to differentially affect cytokine

readouts. IL-2, for example, has been shown to be more strongly affected by co-stimulation through CD28 than IL-3 [201] or IFNγ [98] in CD4$^+$ T cells. Interestingly, Racioppi et al. [201] found a 100-fold difference in the EC_{50}s of IL-2 and IL-3 when stimulating T cells with live APCs, but no difference when APCs were fixed. Fixation can have denaturing effects on several components at the APC interface, including a decrease in the motility of membrane-anchored molecules. Similarly, the motility of pMHC ligands on our plate is likely different to pMHC ligands anchored to a cellular membrane, but it is worth noting that the stimulation plates that we use in our assays (Pierce™ Streptavidin-coated High Capacity 96-well-plates, Thermo Fisher Scientific) are coated with a polymer membrane that probably allows for a certain degree of flexibility [46]. Nonetheless, it is unclear how co-stimulation and ligand-mobility could achieve differences in the EC_{50} rather than just amplify individual responses, but it would be interesting to test this hypothesis by adding co-stimulatory molecules or perform the experiments on lipid bilayers to allow pMHC ligands to move. Altogether, these differences between experimental systems used in our study and studies that reported large differences in the activation thresholds of cytokine readouts provide several potential explanations for the observed discrepancies.

5.3.2 Support for cytokine-specific temporal integration

Transient TCR signals are integrated in time at various levels in T cell signalling (Section 4.3.1). A ligand-induced increase in the rate of gene transcription into mRNA or a decrease in the degradation of mRNA could integrate TCR-mediated signalling by mRNA accumulation. TNFα, MIP-1β, IFNγ and IL-2 mRNA have indeed recently been shown to be regulated differently. High levels of pre-formed TNFα mRNA allow for immediate translation and rapid TNFα protein production [174, 208]. IL-2 mRNA, on the contrary, is unstable in the resting state, and the production of IL-2 protein in response to pMHC stimulation relies on *de novo* transcription [174, 187, 208, 291]. MIP-1β and IFNγ are both produced from pre-formed mRNA as well as *de novo* transcription. The enhancement of ligand-induced transcription is, however, stronger for MIP-1β than IFNγ. In addition, ligand-induced stabilisation of IFNγ mRNA is delayed and generally

less efficient than stabilisation of MIP-1β mRNA [186]. A phenotypic model, in which these cytokine-specific ligand-induced rates of transcription and mRNA stabilisation are absorbed into the activation and degradation rates of the temporal integrator Y, k_{fy} and k_{ry}, is congruent with the phenotypic model in Fig. 5.11 and could thus explain the experimental data.

5.3.3 Concluding remarks

Several hypotheses exist about the functional benefit of subjecting T cell functions to different activation thresholds. A modelling study suggested that hierarchical thresholds are exceeded at different times after stimulation of T cells with pMHC and that the delay of some responses confers differential specificity to individual responses [270]. However, the hierarchical order of function-specific activation thresholds does not necessarily correlate with their destructive potential as, for example, killing of target cells by granzymes and perforin seems to be associated with the lowest activation threshold [253, 270]. Alternatively, hierarchical activation thresholds were thought to direct the polarisation of $CD4^+$ T cells into one of the functionally specialised helper subsets by favouring secretion of counterregulatory cytokines depending on the dose- and affinity of the pMHC [83, 98, 259, 275]. Activation thresholds may indeed be more hierarchical in $CD4^+$ T cells than in the $CD8^+$ T cells studied here, but it is unclear how pMHC dose and affinity alone contain sufficient information about the type of threat to trigger an appropriate response. Van Panhuys et al. [259] argue that the dose of pathogenic peptides presented to $CD4^+$ T cells may be higher in the case of intravesiculars pathogens that have entered the APC (T_H1 polarisation) compared to large extracellular pathogens such as helminths (T_H2 polarisation), of which smaller amounts of secreted products are taken up from the environment and presented on the APC. The precise contribution of co-stimulation and cytokines to the polarisation of $CD4^+$ T cells is, however, unclear and could furthermore be different for $CD8^+$ T cells.

The threshold hierarchies documented previously in $CD4^+$ and $CD8^+$ T cells were not always consistent across experimental systems [98, 243, 257] and T cell clones [83].

These discrepancies are difficult to reconcile with an inherently hierarchical response. Instead, the data presented in this chapter raise the possibility that hierarchical T cell responses are less hardwired and more context-dependent. Based on the finding that in this minimal experimental system the dose- and affinity-thresholds for activation of 4 key cytokines were similar, we propose a model in which the all-or-none decision whether to react to a pMHC is made once (single-switch model), setting a homogeneous intrinsic dose- and affinity-threshold. It is known that the antigen dose and affinity are not the only cues about the nature of the pathogenic threat that are carried by APCs [1, 196], and the timed summation of multiple cues likely shapes the overall and long-term quality of the T response.

CHAPTER 6

General discussion

Cytokine production by T cells is an important effector function that can initiate and regulate immunity. However, excessive cytokine release can have detrimental consequences for the organism [248]. Here we found that $CD8^+$ T cells are capable of limiting their early (1–8 hours) cytokine response to pMHC stimulation in a minimal experimental system by a mechanism that is independent of other cell types or signalling through co-inhibitory receptors such as PD-1 (Chapter 3). Receptor downregulation has been described as a mechanism of adaptation in other receptor-ligand systems [65, 70, 135, 137, 155], and similarly T cell adaptation was here paralleled by rapid and long-lasting downregulation of the TCR. A phenotypic model informed by known features of TCR downregulation and T cell signalling showed that TCR downregulation is sufficient to explain the experimental phenotype (Chapter 4). Importantly, adapted T cells could be reinvigorated by stimulation with a higher-affinity pMHC, implying that they have not become intrinsically inactive and unable to confer protection. Unexpectedly, we found that the signalling phenotypes, including early adaptation kinetics and activation thresholds, associated with the four key cytokines TNFα, MIP-1β, IFNγ and IL-2 were comparable despite the specialised roles these cytokines fulfil (Chapter 5). Overall, these reductionist experiments and modelling show a relatively uniform early activation phenotype that is limited in time and similarly reflected in multiple effector molecules.

6.1 Mechanistic evidence that TCR downregulation can induce adaptation

The combined approach of systematic experiments and minimal modelling has shown that TCR downregulation is sufficient to explain the adaptation phenotype, but a causal link between TCR downregulation and adaption was not established experimentally. A key remaining question is therefore if adaptation can be prevented or delayed when the TCR is not downregulated. The multiplicity of mechanisms that lead to TCR downregulation and their entanglement with signalling pathways that lead to T cell activation make an isolated examination of these processes challenging. In an attempt to elucidate the effect of TCR downregulation on signalling, several studies interfered with endocytosis of the TCR [11, 273] or degradation mediated by the E3 ubiquitin ligases Cbl-b [100, 170], c-Cbl [169–171] and GRAIL [177]. It is likely, however, that perturbation of endocytosis and E3 ubiquitin ligases affected a large number of signalling molecules and not specifically the TCR [68, 88, 273]. The identification and perturbation of a suitable target to conclusively determine whether TCR downregulation causes adaptation was beyond the scope of this work as it is currently limited by our incomplete understanding of all molecular mechanisms underlying TCR downregulation.

The hypothesis that TCR downregulation induces adaptation is consistent with studies tracing adaptation to a TCR-proximal signalling block [31, 74, 244]. Teague et al. [244], for example, generated a transgenic mouse model with dual-receptor $CD8^+$ T cells that recognised both a constitutively-expressed self-antigen and a viral antigen. Intriguingly, they find that dual-receptor T cells tolerised to self-antigen responded normally to the viral antigen through the second TCR [244]. In other transgenic mouse models, studies of biochemical changes in tolerised T cells found decreased ZAP-70 [31] and Lck activity as well as reduced CD3ζ-chain tyrosine phosphorylation [74]. The change in TCR surface expression was often subtle [74, 244], and the precise molecular mechanism that induced adaptation in these mouse models remained unspecified. But the phenotypic model presented here highlights that overt TCR downregulation is not required for functional

adaptation, so that these studies can be consistent with TCR downregulation as the mechanism underlying adaptation.

6.2 Functional significance of TCR downregulation in peripheral tolerance

One remaining question concerns the relevance of TCR downregulation and the cellular adaptation phenotype that we identified in our minimal experimental system in the more complex *in vivo* setting. It has been hypothesised that TCR downregulation could mediate extra-thymic peripheral tolerance to constitutively expressed antigens, and the analysis of *in vivo* tolerised T cells was indeed found to correlate with decreased TCR levels in several transgenic mouse models [60, 74, 218, 241]. Interestingly, the tolerant T cell state was reversible and the recovery of effector functions was associated with re-expression of the TCR [60, 218, 241]. It was observed when T cells were removed from the body and cultured *in vitro* for 4 days [218], but also when the expression level of the cognate antigen changed *in vivo* [60, 241]. Tafuri et al. [241], for example, showed that maternal T cells became temporarily unresponsive to paternal MHC-antigens during pregnancy, but responsiveness was restored after delivery. Peripheral tolerance was therefore context-dependent and T cells were not rendered intrinsically inert, consistent with our findings. The observation that *in vivo* adaptation and recovery correlated with TCR expression levels furthermore suggests a role for tuning of TCR expression in adaptation *in vivo*.

But the importance of TCR downregulation in T cell adaptation remains controversial. Not all *in vivo* studies with transgenic mice observed overt TCR downregulation and did therefore not identify a clear correlation between unresponsive T cells and TCR downregulation [81, 205, 225]. Our phenotypic model offers the explanation that the extent of TCR downregulation depends on the pMHC dose and affinity, and even minute changes in TCR expression can lead to complete adaptation. A second possible reason for the discrepancy is that multiple layers of protective mechanisms co-exist *in vivo* to prevent excessive and possibly fatal immune responses. These include deletion by

AICD [125, 205], inhibition of the T cell response through co-modulatory receptors such as PD-1 [87] and regulation through CD5 [54, 81, 205, 233]. We could exclude AICD and co-inhibition in our minimal experimental system, but it is possible that these mechanisms masked the effect of TCR downregulation *in vivo*.

6.3 Relevance for CAR immunotherapies

A better mechanistic understanding of TCR downregulation could be of benefit for CAR (Chimeric Antigen Receptor) immunotherapies. Han et al. [77] recently found that T cells expressing HLA-DR-specific CARs which weakly recognised epitopes on autologous MHC molecules exhibited reduced CAR expression. These T cells were functionally desensitised and less likely to commit fratricide, but they were still capable of specifically killing target cells with higher HLA-DR expression levels in transfer experiments. The authors speculated whether the same cellular mechanisms mediate CAR and TCR downregulation. In support of this hypothesis, an identical adaptation phenotype observed here for the 1G4Hi TCR was also observed in CAR-transduced T cells (unpublished data by Philipp Kruger). CAR-transduced T cells may thus employ a similar tuning mechanism to adapt CAR levels to previous antigen encounters, and a better understanding of the regulatory mechanisms of TCR downregulation could aid the design of CAR T cells.

6.4 The single-switch model of T cell activation

T cells are thought to tailor their cytokine response to the kind of pathogenic threat by polarisation of T cells into specialised subsets. The uniform early activation phenotype that was found here for TNFα, MIP-1β, IFNγ and IL-2 secretion in response to a large range of pMHC doses and affinities in the minimal experimental system contrasts the assertion that ligands with different affinities to the TCR can qualitatively change the T cell response. Previous studies observed cytokine-specific dose- and affinity-thresholds in other experimental systems and argued that the dose and affinity of pMHC could instruct the polarisation of T cells into subsets [83, 98, 275]. Data from our minimal

experimental system challenge this idea: Our study of the early T cell response has revealed surprisingly similar signalling phenotypes for secretion of the four key cytokines TNFα, MIP-1β, IFNγ and IL-2. Contrary to previous reports, we found no evidence that different TCR signalling thresholds must be met to trigger secretion of each cytokine. The kinetics, including the adaptation phenotype, were also roughly identical for all cytokines at early times with the exception that IFNγ was produced in a second surge at later time points, likely as a result of cytokine feedbacks [78, 107, 156, 246]. Large differences were only observed in the absolute amount and hierarchy of TNFα, MIP-1β, IFNγ and IL-2 secreted, but this was dependent on the state of the cell rather than differential susceptibilities to TCR signalling as most variation occurred across human donors. Overall, the kinetics and activation thresholds in response to pMHC alone were therefore strikingly similar and suggest an early and transient default activation mode that is reflected in all cytokines.

How can we reconcile the conclusion that different cytokines have the same phenotype with the versatility and specificity of the T cell response required for effective pathogen clearance? We propose a single-switch model in which an all-or-none decision whether to react to a pMHC is made equally for all cytokines, thus setting a homogeneous intrinsic dose- and affinity-threshold. Polarisation and fine-tuning of the cytokine response may then rely on additional cues provided by APCs and the microenvironment [1, 196]. It seems unlikely that pMHC dose and affinity alone encode information about the type of threat (intracellular pathogen, parasite, extracellular pathogen etc.) to be the only determinants that shape the cytokine response. In fact, because T cells presented only with pMHC ligands of a given dose and affinity were found to adapt their cytokine response to the pMHC stimulus, this effectively 'normalised' the response and may allow T cells to be quantitatively controlled by other cues (e.g. co-modulatory ligands and cytokines). Such a model is consistent with the finding that adapted T cells were not inert and could be rescued by stimulation with a higher-affinity pMHC, co-stimulation through CD28 or 4-1BB (data not shown, unpublished data by Philipp Kruger and John Nguyen) and presumably cytokine feedbacks (late surge in IFNγ secretion). In an inflammatory setting, the T cell response therefore appears as a compromise between preventing tissue

damage and protection against exogenous threats by conditioning the T cell response calibrated by TCR downregulation on complementary signals and the summation of multiple cues likely shapes the overall and long-term quality of the T cell response.

6.5 Future directions

The experimental data in Chapter 3 demonstrate clearly that $CD8^+$ transduced and antigen-experienced primary human T cells adapt their cytokine response to persistent stimulation with plate-bound recombinant pMHC. The minimal experimental setup we used allowed us to interrogate the T cell response to pMHC only in isolation, but in a physiological setting, T cells experience additional stimuli, for example through co-stimulatory receptors. It has been suggested previously that co-stimulation lowers the T cell activation threshold, and it is ongoing work in our laboratory to explore the hypothesis that co-stimulatory ligands immobilised on the pMHC stimulation plate can reverse the adaptation phenotype. It would furthermore be interesting to determine whether other T cell subsets also adapt to persistent pMHC stimulation. One possibility would be to electroporate naïve $CD8^+$ primary human T cells with the 1G4Hi TCR and to subject them to the same stimulation conditions as the antigen-experienced T cells used here. Finally, it would be of interest to test whether $CD4^+$ primary human T cells (naïve or antigen-experienced) downregulate the TCR and adapt their cytokine response to pMHC, which consists of different subset-specific cytokines, with the same kinetics as $CD8^+$ primary human T cells.

Besides addressing the discrepancies between experimental data and the phenotypic model fit that were outlined in Chapter 4, it would be informative to explore alternative model architectures that could explain the experimental phenotype. Network motifs that can result in adaptation, for example, have been discussed in Chapter 4. These could be coupled to the TCR downregulation module and compared in their ability to explain the experimental phenotype. Ideally, these competing models would be used to produce predictions that we can then test in the laboratory.

Chapter 5 showed that different cytokines and chemokines secreted by antigen-

experienced $CD8^+$ primary human T cells in response to pMHC had similar sensitivities to pMHC dose and affinity. This finding contrasts previous reports that suggested differences of several orders of magnitude in potency when comparing the dose-response curves associated with different cytokines. Most of these studies were conducted using peptide-pulsed APCs to stimulate T cells, and it would be interesting to investigate whether our results are reproducible when T cells are stimulated with APCs. Finally, variation between experiments in the T cell differentiation state (naïve rather than antigen-experienced) or co-receptor subset ($CD4^+$) could account for some discrepancy, and it would be the goal of future experiments to determine whether a difference in the type of T cells used for experiments and/or the experimental setup can explain diverging conclusions about cytokine-specific activation thresholds.

APPENDIX A

Supplementary information to Chapter 3

A.1 Supplementary figures

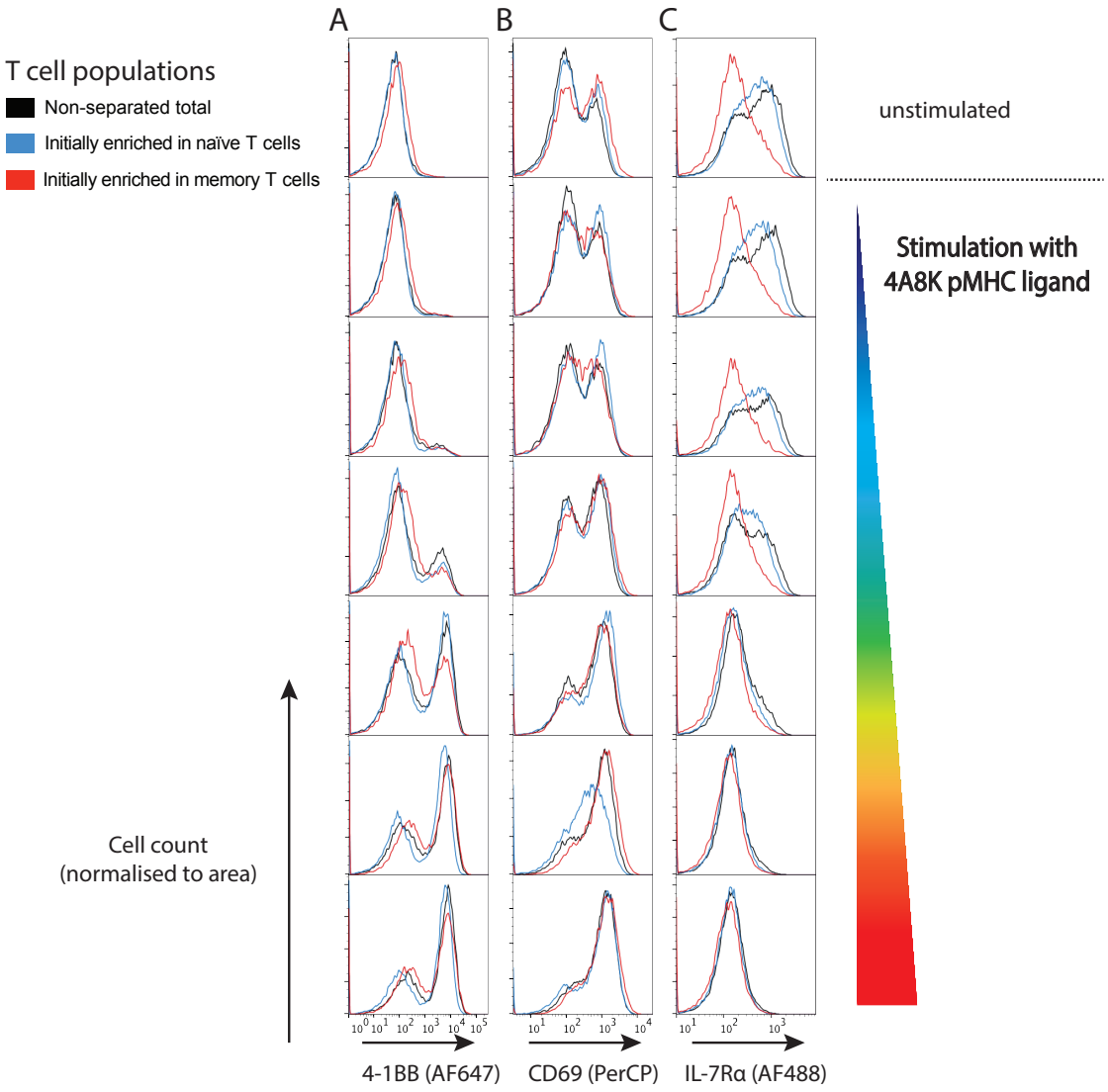


Figure A.1: Overlay of single-cell activation marker expression in populations derived from bulk, naïve-enriched or memory-enriched T cells confirms similar activation thresholds. (A) 4-1BB is not expressed on unstimulated T cells but is increased independently of the starting population as T cells are stimulated with 4A8K pMHC for 8 hours. **(B)** CD69 is expressed on a large fraction of unstimulated T cells and increases further upon stimulation in a way that is comparable between the bulk and enriched populations. **(C)** While few cells derived from the memory-enriched T cell population express IL-7Rα, its downregulation is induced at the same doses between all subsets. Shown are only the six highest doses of pMHC ligand in Fig. 3.7 as no activation was detected at lower doses. Differences in the gMFI seem to be within experimental error.

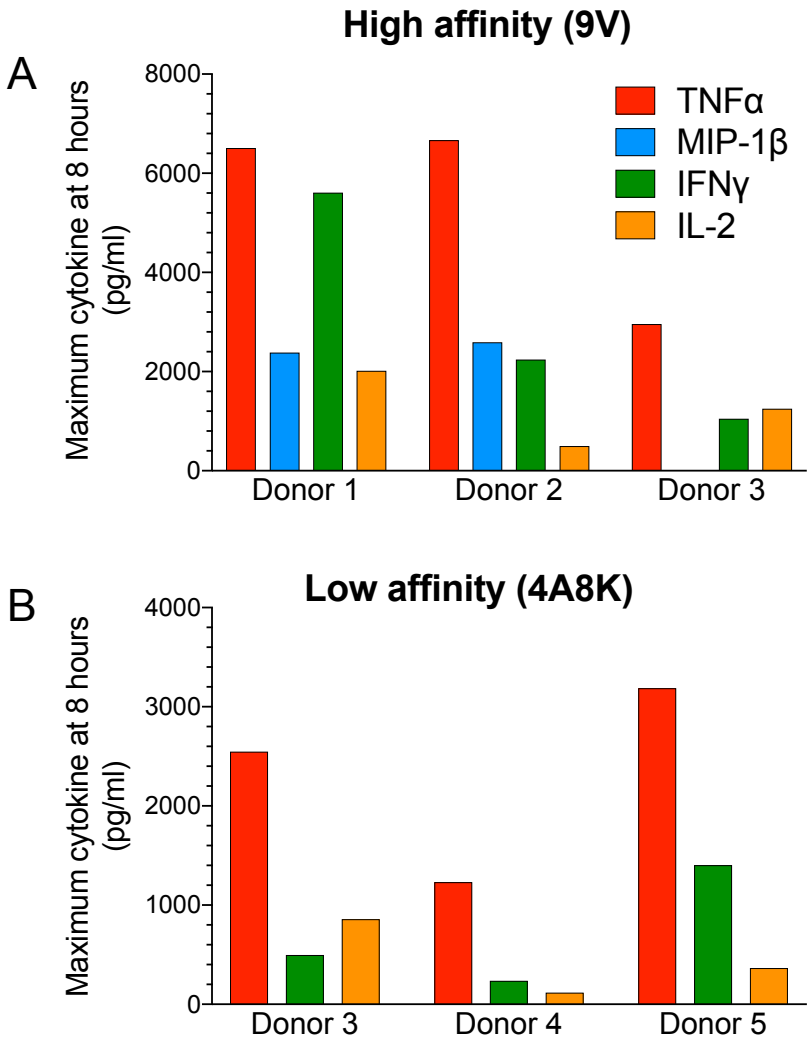


Figure A.2: The absolute amount and hierarchy of cytokines produced varies between donors. Maximum amount of TNFα, MIP-1β, IFNγ and IL-2 produced after 8 hours of stimulation with a **(A)** high-affinity pMHC (9V, $K_D = 7.07 \times 10^{-5}\mu M$) or **(B)** low-affinity pMHC (4A8K, $K_D = 1.78 \times 10^{0}\mu M$). The absolute amounts of each cytokine produced varied between donors. TNFα was consistently produced in the largest amounts. But while T cells from Donors 1 and 2 in (A) produced similar amounts of TNFα, T cells from Donor 2 produced less than half the amount of IFNγ. In addition, T cells from Donor 1 and 2 consistently produced more IFNγ than IL-2, but this was not the case for T cell from Donor 3. Therefore, the amount of different cytokines produced by each donor did not scale linearly between experimental repeats.

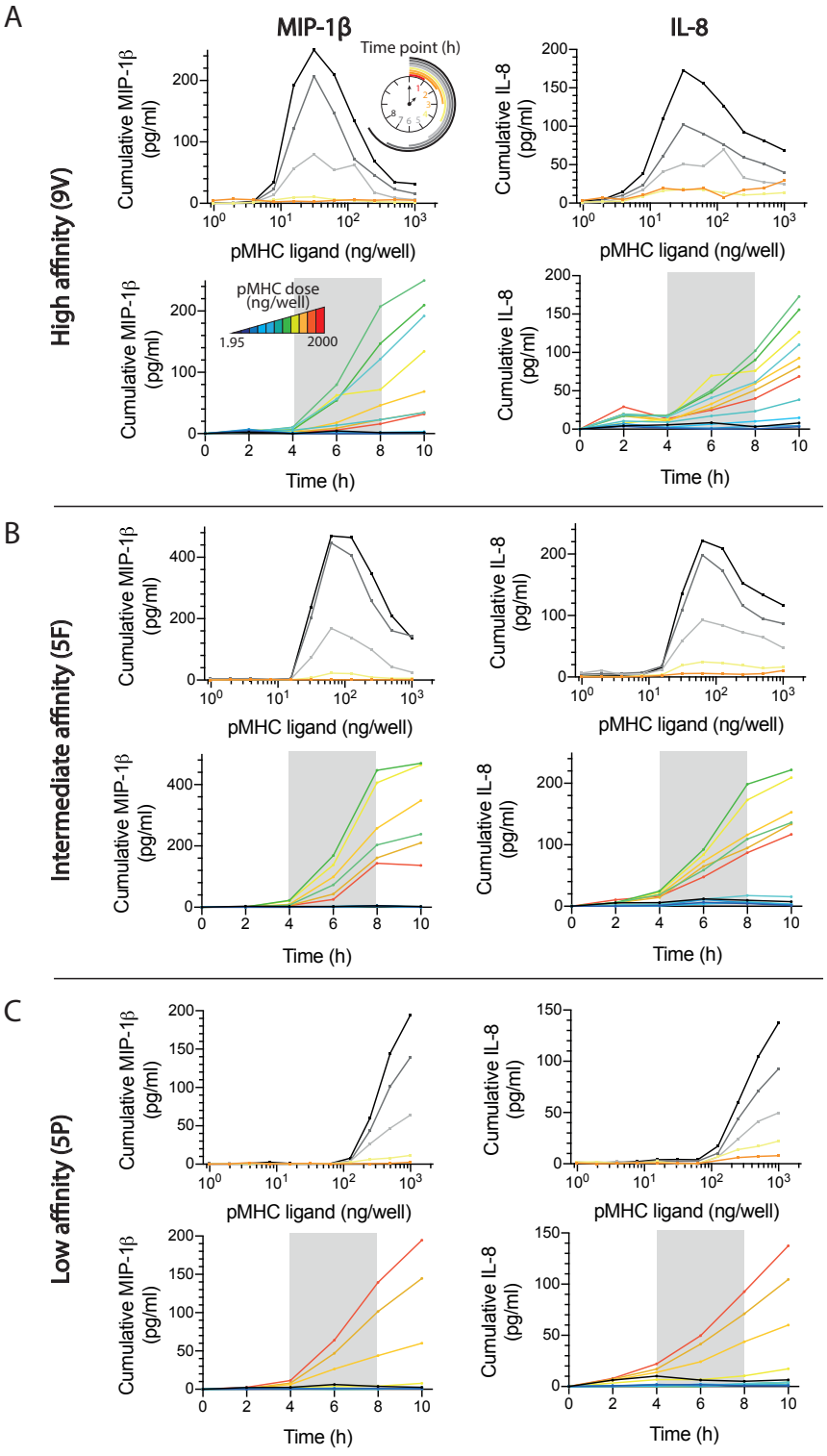


Figure A.3: The timescale of adaptation is delayed in Jurkat cells. Jurkat T cells expressing the 1G4Hi TCR were stimulated with the **(A)** 9V, **(B)** 5F and **(C)** 5P pMHC variants, respectively. MIP-1β and IL-8 were measured in the supernatant by ELISA after 2–10 hours of stimulation as a proxy for T cell activation because this Jurkat cell line does not produce TNFα, IFNγ or IL-2. The rate of cytokine secretion indeed appeared constant within the timeframe considered in previous experiments (4–8 hours, highlighted in gray), but Jurkat cells were found to adapt their MIP-1β and IL-8 response to the pMHC stimulus after ≥ 8–10 hours of stimulation.

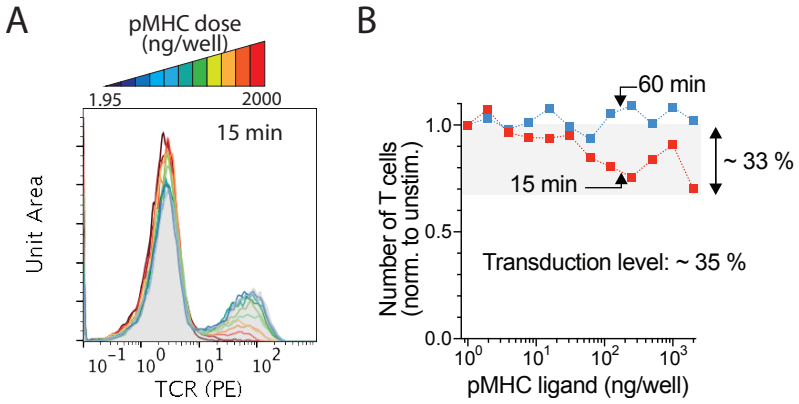


Figure A.4: TCR downregulation could not be determined reliably at early time points. Primary $CD8^+$ T cells were stimulated with the 9V pMHC for 15–60 minutes. TCR expression was detected by staining with fluorescently-labelled PE-pMHC tetramers. **(A)** Histogram of TCR expression on T cells stimulated for 15 minutes with different doses of pMHC shows signatures of digital signalling. As the dose of pMHC was increased, the frequency of TCR expressing T cells decreased rather than the TCR expression level per T cell. **(B)** At 15 minutes after stimulation, there was also a dose-dependent decrease in the number of T cells retrieved from the stimulation plate. The decrease in the frequency of $1G4Hi^+$ T cells in (A) thus coincided with a decrease in the number of T cell retrieved from the stimulation plate that was at the highest dose of pMHC similar to the transduction level, likely because T cells adhered to the stimulation plate. The same bias was not observed after 60 minutes of stimulation with pMHC.

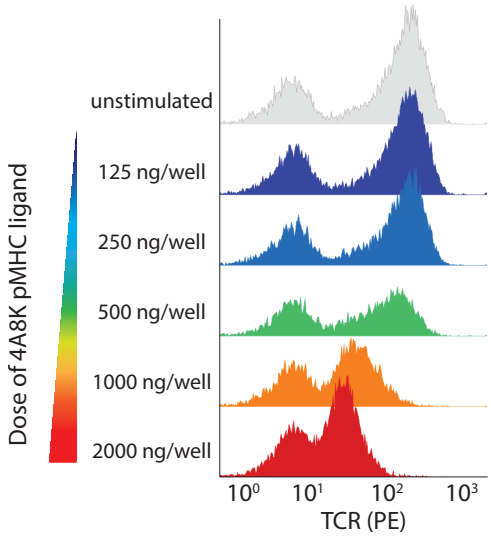


Figure A.5: pMHC tetramers staining of the 1G4Hi on CD4$^+$ primary human T cells. CD4$^+$ primary human T cells transduced with the 1G4Hi TCR were stimulated with a titration of the 4A8K pMHC ligand for 8 hours. An analogue dose-dependent decrease in TCR expression could be observed with sufficient resolution suggesting that CD8 expression is not required to detect the 1G4Hi TCR by pMHC tetramer staining.

APPENDIX B

Supplementary information to Chapter 4

B.1 ODEs

The models presented schematically in Chapter 4 were translated into coupled systems of Ordinary Differential Equations (ODEs). Interactions between model species were described by mass action kinetics unless stated otherwise. Bound pMHC ligand was assumed to return to the pool of free pMHC when TCR becomes downregulated, so that the total amount of pMHC ligand was conserved. Similarly, the signalling intermediate Y was assumed to be conserved according to $Y_T = Y_{free} + Y$ and normalised so that $Y_{free} = 1 - Y$. Models were evaluated using the inbuilt MATLAB (MathWorks, Inc.) ODE solver *ode15s*.

B.1.1 Complete model

$$\frac{\partial L}{\partial t} = -k_{on}(LR)^{n_b} + (k_{off} + k_{basal})C_{total} + k_{int}C_t$$

$$\frac{\partial R}{\partial t} = -k_{on}(LR)^{n_b} + k_{off}C_{total} + k_{syn} - k_{basal}R - k_{by}RC_p$$

$$\frac{\partial C_{00}}{\partial t} = k_{on}(LR)^{n_b} - (k_{off} + k_{basal} + k_p + k_t)C_{00}$$

$$\frac{\partial C_{01}}{\partial t} = k_t C_{00} - (k_{off} + k_{basal} + k_p + k_{int})C_{01}$$

$$\frac{\partial C_{10}}{\partial t} = k_p C_{00} - (k_{off} + k_{basal} + k_t)C_{10}$$

$$\frac{\partial C_{11}}{\partial t} = k_p C_{01} + k_t C_{10} - (k_{off} + k_{basal} + k_{int})C_{11}$$

$$\frac{\partial Y}{\partial t} = k_{fy}(1 - Y)\frac{C_p^{n_y}}{C_p^{n_y} + s_y^{n_y}} - k_{ry}Y$$

$$\frac{\partial Z}{\partial t} = k_{act}Y$$

where Z is the cumulative cytokine response, $C_{total} = C_{00} + C_{01} + C_{10} + C_{11}$, $C_p = C_{10} + C_{11}$ and $C_t = C_{01} + C_{11}$. A near-perfect switch with $n_y = 12$ was enforced for the model fit by ABC-SMC.

Parameters: k_{prop} = 1.6 × 10^{-3} $ng^{-1}\mu m^{-2}$, k_{syn} = 3.1178 × 10^{-4} $s^{-1}\mu m^{-2}$, k_{basal} = 3.1178 × 10^{-6} s^{-1}, k_{on} = 1.6149 × 10^{-4} $s^{-1}\mu m^2$, k_{off1} = 2.38063 × 10^{1} s^{-1}, k_{koff2} = 1.17 × 10^{-2} s^{-1}, n_b = 2.5326, k_{by} = 6.2 × 10^{-3} $s^{-1}\mu m^2$, k_{int} = 4.99 × 10^{-2} s^{-1},

$k_p = 1.72763 \times 10^1\ s^{-1}$, $k_t = 1.00939 \times 10^1\ s^{-1}$, $k_{fy} = 1.36701 \times 10^1\ s^{-1}$, $k_{ry} = 1.4164 \times 10^{-4}\ s^{-1}$, $s_y = 4.46 \times 10^{-2}\ \mu m^{-2}$, $k_{act} = 9.4785 \times 10^{-5}\ s^{-1}$.

B.1.2 Simple binding and cooperative binding models

The system of ODEs was identical for the simple binding and the cooperative binding models with the only difference that $n_b = 1$ for the simple binding model to describe simple mass action kinetics.

$$\frac{\partial L}{\partial t} = -k_{on}(LR)^{n_b} + (k_{off} + k_{basal} + k_{int})C$$
$$\frac{\partial R}{\partial t} = -k_{on}(LR)^{n_b} + k_{off}C + k_{syn} - k_{basal}R$$
$$\frac{\partial C}{\partial t} = k_{on}(LR)^{n_b} - (k_{off} + k_{basal} + k_{int})C$$

B.2 MATLAB implementation of ABC-SMC

```
%% May 23, 2018
%  ABC-SMC code for fitting the TCR downregulation model
%  Nicola Trendel

clear variables
close all
%%%%%%%%%%%%%%%%%%%%%%%%%%%%%%%%%%%%%%%%%%%%%%%%%%%%%%%%%%%%%%%%%%%%%%%%%%%%
%%%%%%%%%%%%%%%%%%%%%%%%%%%%%%%%%%%%%%%%%%%%%%%%%%%%%%%%%%%%%%%%%%%%%%%%%%%%

%% Load experimental data
load 20180619Data_Norm2

% x are the doses
x = data.x;

% y are TCR (4A8K), TNFa (4A8K), TCR (9V), TNFa (9V), TCR (inhibitor) as
% one large column vector
y_TCR1 = data.r1(:);
y_cyto1 = data.c1(:);
y_TCR2 = data.r2(:);
y_cyto2 = data.c2(:);
y_inhib = data.r3(:);
y = [y_TCR1; y_cyto1;y_TCR2; y_cyto2; y_inhib];

%% SMC parameters
T = 15;                 % Number of populations (iterations)
N = 10000;              % Size of each population (number of particles)

perturbationWidth = 1.2;    % Multiplies covariance matrix
perc = 50;                  % Percentile of particles to accept

%% Define model and parameters
model = 'bystander05';          % Name of function that contains the model
parameter_names = {'kprop','kon','koff1','nb','kby','kint','kp','kt', ...
                   'kfy','kry','sy','kact','koff2'};
n_params = length(parameter_names); % Number of parameters
fh = str2func(model);

% Initial parameter guess (log scale)
p0 = [-2.3979, -4.1467, 1.3165, 2.7742, -2.8297, -1.5702, 1.0030, 1.0000,...
        0.6990, -3.8239, -1.1135, -4.0000, -0.6835];

% Boundaries of parameter space (+/- 0.5 log of initial guess)
lb = zeros(n_params,1);
ub = zeros(n_params,1);
lb = p0-0.5;
ub = p0+0.5;
lb = lb'.*ones(n_params,N); lb = lb(:); % [N*n_params x 1] column vector
ub = ub'.*ones(n_params,N); ub = ub(:); % [N*n_params x 1] column vector
%%%%%%%%%%%%%%%%%%%%%%%%%%%%%%%%%%%%%%%%%%%%%%%%%%%%%%%%%%%%%%%%%%%%%%%%%%%%
%%%%%%%%%%%%%%%%%%%%%%%%%%%%%%%%%%%%%%%%%%%%%%%%%%%%%%%%%%%%%%%%%%%%%%%%%%%%

%% ABC-SMC
% Initialise arrays to save data
particles = zeros(N*n_params,T+1);
d = zeros(N,T+1);                           % Distance y_data <-> sim
w = zeros(N,T+1);                           % Particle weights
e = zeros(T,1);                             % Adaptive thresholds
sampled = zeros(T,1);                       % Count sampled to compute rejection rate
sigmas_Kt = zeros(n_params,n_params,T+1);   % Covariance matrix for Kt
particlesSORTED = zeros(n_params,N);

% Generating the first population of particles
t = 0;
particles(:,t+1) = initialise_particles(N,n_params,lb,ub);

% Evaluate first population of particles
sim = fh(particles(:,t+1),x,n_params,N);
w(:,t+1) = 1/ sum(ones(N,1));               % Uniform weighting initially
d(:,t+1) = dist_fn(y,sim)';
e(t+1) = prctile(d(:,t+1),perc);

particlesSORTED(:) = particles(:,t+1);
sigmas_t = cov(particlesSORTED');
sigmas_Kt(:,:,t+1) = perturbationWidth*sigmas_t;

% Start SMC
t = 1
idxEVALUATE = 1:N;
idxUPDATE = 1:N*n_params;
sample_count = 0;
while t <= T
    iN = length(idxEVALUATE);
    sample_count = sample_count + iN;

    % Sample to get N new particles from the previous population
    wcumsum = cumsum(w(:,t)).*ones(N,iN);           % Cumulative sum of weights (iN identical columns)
    rand01 = rand(1,iN);                            % Pick iN random numbers
```

```
    [idxROW, idxCOL] = find((wcumsum-rand01)>=0);   % Find particles associated with random number
    idxFIRST = [1; (find(diff(idxCOL))+1)];
    idxPARAMS = ((idxROW(idxFIRST)'.*ones(n_params,iN))-1)*n_params + (1:n_params)';
    idxPARAMS = idxPARAMS(:);

    params = particles(idxPARAMS,t);               % Parameter vector for iN particles

    % Perturb particles
    paramsp = perturb_particles(params,sigmas_Kt(:,:,t),lb,ub,iN,n_params)';
    particles(idxUPDATE,t+1) = paramsp;

    % Evaluate model at perturbed particle
    sim = fh(paramsp,x,n_params,iN);

    % Calculate distance function
    d_temp(idxEVALUATE) = dist_fn(y,sim);

    idxACCEPT = find(d_temp < e(t));
    idxREJECT = find(d_temp >= e(t));

    if numel(idxREJECT) == 0    % Save results and move on to next population
        d(:,t+1) = d_temp';
        w(:,t+1) = part_weight(particles(:,t),sigmas_Kt(:,:,t),particles(:,t+1),n_params,N,w(:,t));

        sampled(t) = sample_count;
        e(t+1) = prctile(d(:,t+1),perc);
        particlesSORTED(:) = particles(:,t+1);
        sigmas_t = cov(particlesSORTED');
        sigmas_Kt(:,:,t+1) = perturbationWidth*sigmas_t;

        save(strcat(['SMCPOP',num2str(t)]))

        t = t+1
        idxEVALUATE = 1:N;
        idxUPDATE = 1:(N*n_params);
        sample_count = 0;
    else                        % Re-evaluate only the particles that do not meet the adaptive threshold
        idxEVALUATE = idxREJECT;
        idxUPDATE = n_params*(idxEVALUATE-1)+ (1:n_params)';
        idxUPDATE = idxUPDATE(:);
    end
end
save lastSMC

%% Visualisation
parameter_namesp = {'k_{prop}','k_{on}','k_{off1}','n_b','k_{by}','k_{int}','k_p','k_t', ...
                        'k_{fy}','k_{ry}','s_y','k_{act}','k_{off2}'};

visualise(T, N, n_params, e, particles, parameter_namesp)
```

```
function [params] = initialise_particles(N,n_params,lb,ub)

    % Uniform prior
    range = ub - lb;
    params = lb + range .* rand(N*n_params,1);

end
```

```
function [OUTPUT] = bystander05(paramsp,x,n_params,iN)

    OUTPUT = zeros(374,iN); % Size of y

    % These parameters are fixed
    R0 = 100;
    ksyn = 3.1178e-04;
    kbasal = ksyn/R0;
    ny = 12;
    op=odeset('RelTol',1e-5,'AbsTol',1e-5);

    parfor iPart = 1:iN
        % Initialise structures
        RT1 = zeros(11,8);
        RT2 = zeros(11,8);
        RTl = zeros(11,2);
        CT1 = zeros(11,8);
        CT2 = zeros(11,8);

        % Retrieve parameter values for this particle
        kprop = 10^paramsp((iPart-1)*n_params+1);
        kon = 10^paramsp((iPart-1)*n_params+2);
        koff1 = 10^paramsp((iPart-1)*n_params+3);
        nb = paramsp((iPart-1)*n_params+4); % Exponent is searched on a linear scale
        kby = 10^paramsp((iPart-1)*n_params+5);
        kint = 10^paramsp((iPart-1)*n_params+6);
        kp = 10^paramsp((iPart-1)*n_params+7);
        kt = 10^paramsp((iPart-1)*n_params+8);
        kfy = 10^paramsp((iPart-1)*n_params+9);
        kry = 10^paramsp((iPart-1)*n_params+10);
        sy = 10^paramsp((iPart-1)*n_params+11);
        kact = 10^paramsp((iPart-1)*n_params+12);
        koff2 = 10^paramsp((iPart-1)*n_params+13);

        % Compute y_sim for particle
        %Generate timecourse low affinity
        for i = 1:length(x)
            koff = koff1;
            X0 = [kprop.*x(i),R0,0,0,0,0,0,0];
            [Tout, Yout] = ode23s(@(t,y) bystander05_odes(t,y,kon,koff,nb,...
                ksyn,kbasal,kby,kint,kp,kt,kfy,kry,ny,sy,kact), ...
                [0:(60*60):(60*60*8)], X0,op);
            RT1(i,:) = sum(Yout(2:end,2:6),2)'./R0;
            CT1(i,:) = Yout(2:end,8)';
        end

        %Generate timecourse high affinity
        for i = 1:length(x)
            koff = koff2;
            X0 = [kprop.*x(i),R0,0,0,0,0,0,0];
            [Tout, Yout] = ode23s(@(t,y) bystander05_odes(t,y,kon,koff,nb,...
                ksyn,kbasal,kby,kint,kp,kt,kfy,kry,ny,sy,kact), ...
                [0:(60*60):(60*60*8)], X0,op);
            RT2(i,:) = sum(Yout(2:end,2:6),2)'./R0;
            CT2(i,:) = Yout(2:end,8)';
        end

        %Generate Lck inhibitor
        for i = 1:length(x)
            koff = koff1
           X0 = [kprop.*x(i),R0,0,0,0,0,0,0];
           [Tout, Yout] = ode23s(@(t,y) bystander05_odes(t,y,kon,koff,nb,...
               ksyn,kbasal,kby,kint,kp,kt,kfy,kry,ny,sy,kact), ...
               [0:(60*60*4):(60*60*4)] , X0,op);
           RTl(i,1) = sum(Yout(end,2:6),2)./R0';
           [Tout, Yout] = ode23s(@(t,y) bystander05_odes(t,y,kon,koff,nb,...
               ksyn,kbasal,kby,kint,0,kt,kfy,kry,ny,sy,kact),...
               [0:(60*60*4):(60*60*4)] , X0,op);
           RTl(i,2) = sum(Yout(end,2:6),2)./R0';
        end

        y_sim = [RT1(:) ; CT1(:) ; RT2(:) ; CT2(:) ; RTl(:) ];
        OUTPUT(:,iPart) = y_sim;
    end
end
```

```
function yp = bystander05_odes(t,y,kon,koff,nb,ksyn,kbasal,kby,kint,kp,kt,kfy,kry,ny,sy,kact)

%Model of TCR downregulation and cytokine production

%Chemical states
%1 - L
%2 - R
%3 - C00 (bound)
%4 - C10 (tagged)
%5 - C01 (phosphorylated)
%6 - C11 (tagged + phosphorylated)
%7 - Y (switch)
%8 - Z (cytokine)

%1 - L
yp(1,1) = - kon*(y(1)*y(2))^nb + (koff+kbasal)*(y(3)+y(4)+y(5)+y(6)) + kint*(y(4) + y(6));

%2 - R
yp(2,1) = ksyn - kbasal*y(2) - kby*y(2)*(y(5) + y(6)) - kon*(y(1)*y(2))^nb + koff*(y(3)+y(4)+y(5)+y(6));

%3 - C00
yp(3,1) = kon*(y(1)*y(2))^nb - (koff + kp + kt)*y(3) - kbasal*y(3);

%4 - C10
yp(4,1) = kt*y(3) - (koff + kp + kint)*y(4) - kbasal*y(4);

%5 - C01
yp(5,1) = kp*y(3) - (koff + kt)*y(5) - kbasal*y(5);

%6 - C11
yp(6,1) = kp*y(4) + kt*y(5) - (koff + kint)*y(6) - kbasal*y(6);

%7 - Y
yp(7,1) = kfy * ((y(5) + y(6))^ny)/(sy^ny + (y(5) + y(6))^ny) * (1 - y(7)) - kry*y(7);

%8 - Z
yp(8,1) = kact.*y(7);
```

```
function d = dist_fn(y,sim)

    d = sum((y - sim).^2);

end
```

```
function wt_next = part_weight(params,sigmas_Kt,paramsp,n_params,N,wt)

    paramsOLD = zeros(n_params,N);
    paramsOLD(:) = params;
    paramsOLD = paramsOLD';         % N x n_params matrix

    wK = zeros(N);
    %% For each particle, calculate the pdf seen from all of the other particles
    parfor iPart = 1:N
        paramsNEW = paramsp((iPart-1)*n_params+1:iPart*n_params)';
        Kt = mvnpdf(paramsOLD,paramsNEW,sigmas_Kt); % Nx1 column vector

        % Multiply by weight of respective particles in old population
        wK(iPart,:) = wt .* Kt;
    end

    %% Sum over all old particles and normalise
    wt_next = [1./sum(wK,2)];
    wt_next = wt_next/sum(wt_next);
end
```

```
function paramsp = perturb_particles(params,sigmas_Kt,lb,ub,iN,n_params)
    k = 0;

    % To use mvnrnd, particles and boundaries need to be in [iN x n_params] array
    particlesSORTED = zeros(n_params,iN);
    particlesSORTED(:) = params;
    particlesSORTED = particlesSORTED';

    lbSORTED = zeros(n_params,iN);
    ubSORTED = zeros(n_params,iN);
    lbSORTED(:) = lb(1:n_params*iN);
    ubSORTED(:) = ub(1:n_params*iN);
    lbSORTED = lbSORTED';
    ubSORTED = ubSORTED';

    paramspSORTED = zeros(iN,n_params);

    % Perturb particles
    perturbPART = [1:iN]';
    perturbPARAMS = [1:n_params]';
    while k == 0
        paramsp_test = mvnrnd(particlesSORTED(perturbPART,perturbPARAMS), ...
            sigmas_Kt(perturbPARAMS,perturbPARAMS));
        paramspSORTED(perturbPART,perturbPARAMS) = paramsp_test;

        % Check boundaries
        [idxLBpart, idxLBparam] = find(paramspSORTED < lbSORTED);
        [idxUBpart, idxUBparam] = find(paramspSORTED > ubSORTED);

        dimLBpart = size(idxLBpart);
        dimUBpart = size(idxUBpart);
        dimLBparam = size(idxLBparam);
        dimUBparam = size(idxUBparam);

        if numel(idxLBparam) == 0 && numel(idxUBparam) == 0
            % all within boundaries
            paramspSORTED = paramspSORTED';
            paramsp = paramspSORTED(:);
            k = 1;
        elseif numel(idxLBparam) ~= 0 || numel(idxUBparam) ~= 0
            % else: perturb selected particles and params out of bounds
            if dimLBpart(2) > 1
                idxLBpart = idxLBpart';
            end
            if dimLBparam(2) > 1
                idxLBparam = idxLBparam';
            end
            if dimUBpart(2) > 1
                idxUBpart = idxUBpart';
            end
            if dimUBparam(2) > 1
                idxUBparam = idxUBparam';
            end
            perturbPART = unique([idxLBpart; idxUBpart]);
            perturbPARAMS = unique([idxLBparam; idxUBparam]);
        end
    end
end
```

B.3 Supplementary figures

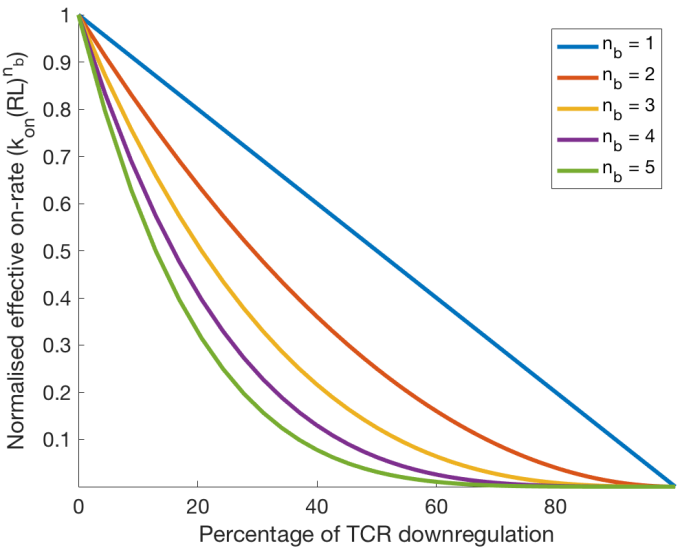


Figure B.1: The sensitivity of the effective on-rate to TCR downregulation increases with the degree of cooperativity.

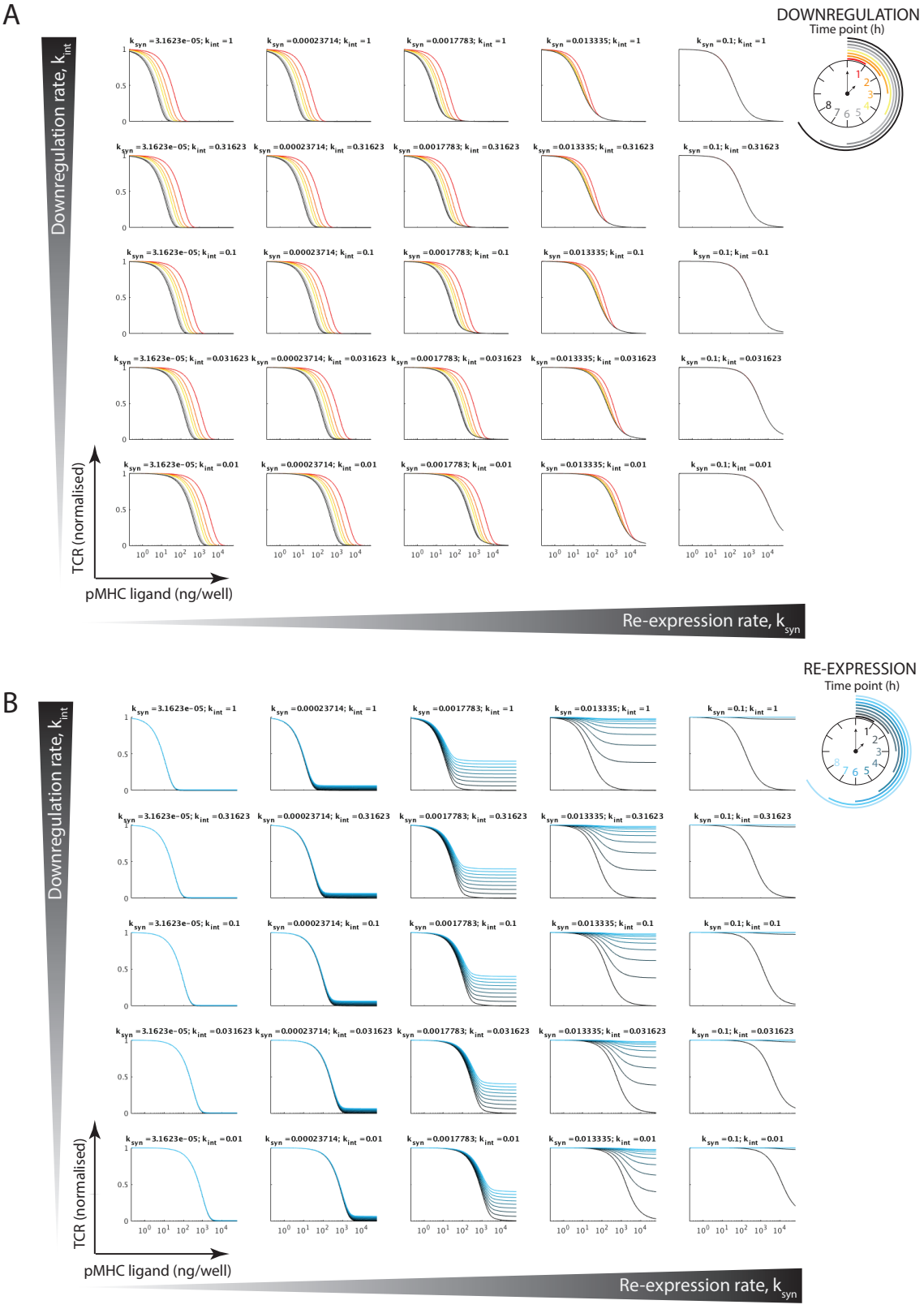


Figure B.2: Systematic variation of TCR re-expression and downregulation rates in the simple binding model. (A) TCR downregulation time course. **(B)** TCR recovery time course.

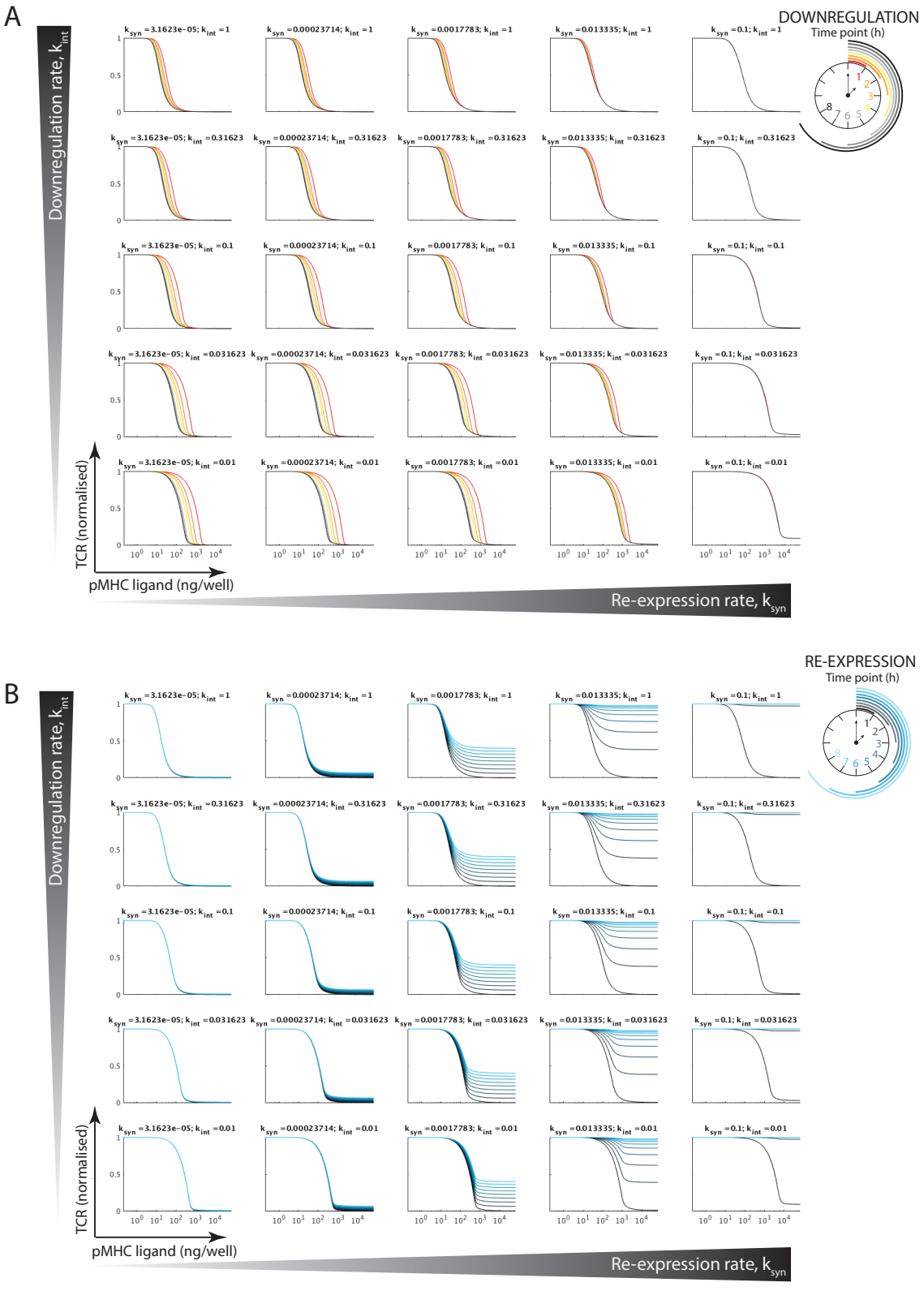
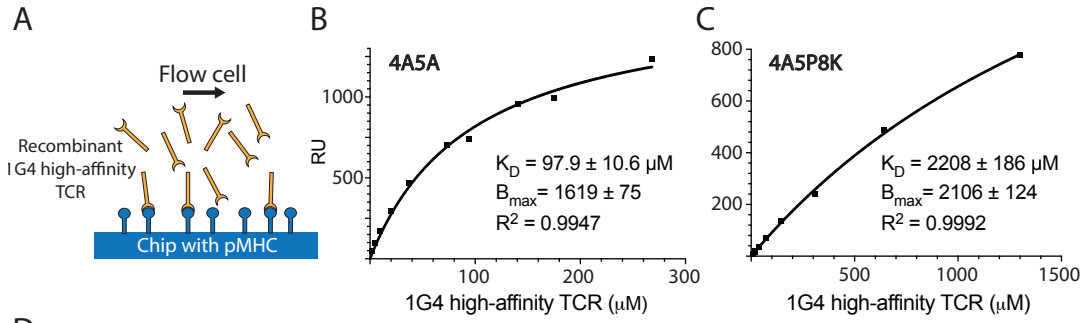


Figure B.3: Systematic variation of TCR re-expression and downregulation rates in the cooperative binding model. (A) TCR downregulation time course. **(B)** TCR recovery time course.

APPENDIX C

Supplementary information to Chapter 5

C.1 Supplementary figures



D

	4A5A			4A5P8K			
	Repeat 1	Repeat 2	Repeat 3	Repeat 1	Repeat 2	Repeat 3	Repeat 4
K_D (µM)	100.1 ± 11.2	97.9 ± 10.6	103.3 ± 11.6	1048 ± 83	793 ± 53.5	1607 ± 288	2208 ± 186
B_{max}	1707 ± 83	1619 ± 75	1372 ± 68	833.7 ± 49.6	437 ± 25.5	1253 ± 185	2106 ± 124
R^2	0.9944	0.9947	0.9944	0.9996	0.9995	0.9990	0.9992

Figure C.1: Overview of SPR measurements to determine binding parameters between the 4A5A and 4A5P8K low-affinity pMHC variants and the 1G4Hi TCR. (A) Schematic of Surface Plasmon Resonance (SPR) experiment to determine binding affinities between pMHC mutants immobilised on a chip and soluble 1G4Hi TCR. **(B)** Binding of the 1G4Hi TCR to immobilised 4A5A pMHC as a function of the concentration of TCR (representative dataset). **(C)** Binding of the 1G4Hi TCR to immobilised 4A5P8K pMHC as a function of the concentration of TCR (representative dataset). Dissociation constants, K_D, and maximal binding, B_{max}, were determined by fitting a simple binding model (solid lines) to the experimental data as described in Methods Section 2.3. **(D)** Overview of fit parameters for the 4A5A and 4A5P8K pMHC mutants from 3 and 4 independent repeats, respectively. The dissociation constants, K_D, for these low-affinity mutants were $K_D \approx 100$ µM and $K_D \approx 2$ mM, respectively. The estimate for the affinity of the triple mutant is however associated with a high degree of uncertainty as even the highest concentration of soluble TCR in these assays was significantly lower than the apparent millimolar K_D and did therefore not saturate binding (C). Repeats highlighted in red are shown in (B) and (C). These experiments were performed by Mikhail Kutuzov.

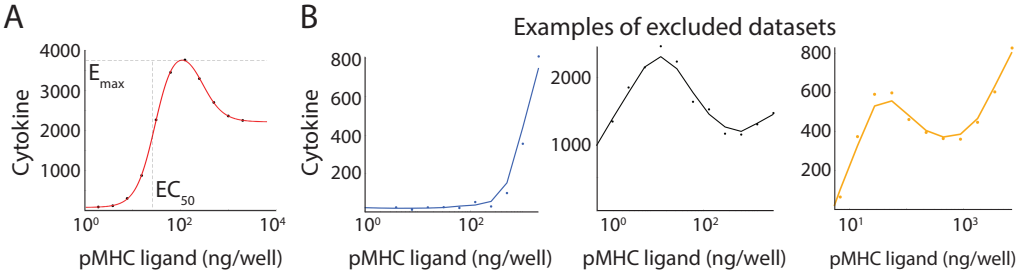


Figure C.2: Determination of EC_{50} from an interpolating function (A) An interpolating function (difference of two sigmoidal curves, solid line) with 10,000 datapoints evenly spaced on a log-axis was fitted to experimental data in Fig. 5.3 to empirically determine the EC_{50} defined as the pMHC dose producing a half-maximal response. **(B)** Examples of excluded datasets (solid lines are LOWESS fits). The EC_{50} could not be reliably determined if the cytokine response did not saturate at high doses (left) or T cells secreted more than $\frac{1}{2}E_{max}$ of cytokine already at the lowest dose of pMHC (middle). Phenotypes other than sigmoids and bell-shapes could not be fitted with the interpolating function (right).

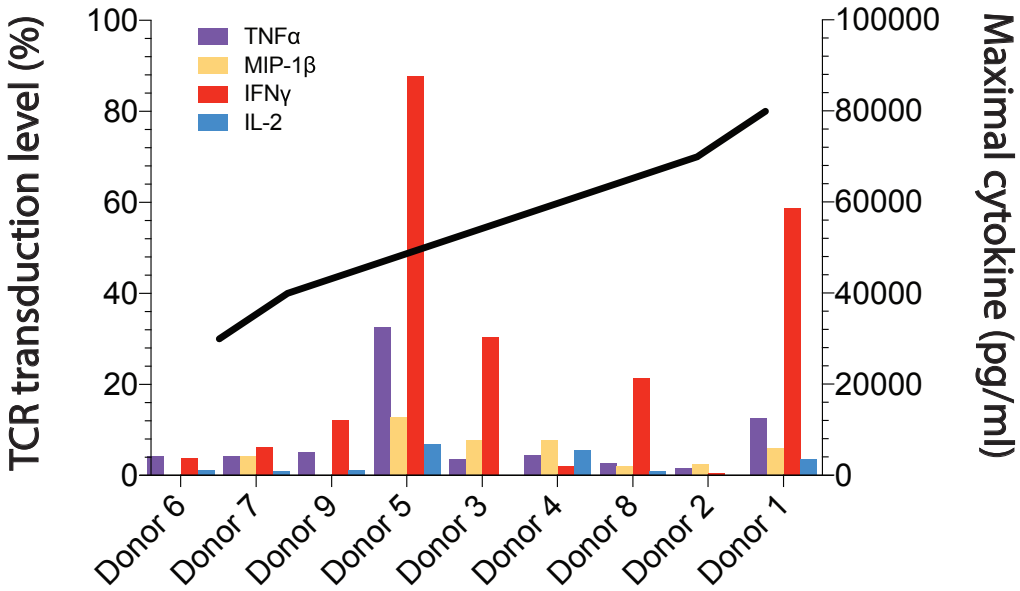


Figure C.3: Cytokine secretion does not scale linearly with the TCR transduction level. Donors on the x-axis were arranged in increasing order of the TCR transduction level (solid line). Bars are the overall maximal amount of TNFα (purple), MIP-1β (yellow), IFNγ (red) and IL-2 (blue) in the respective experimental repeat.

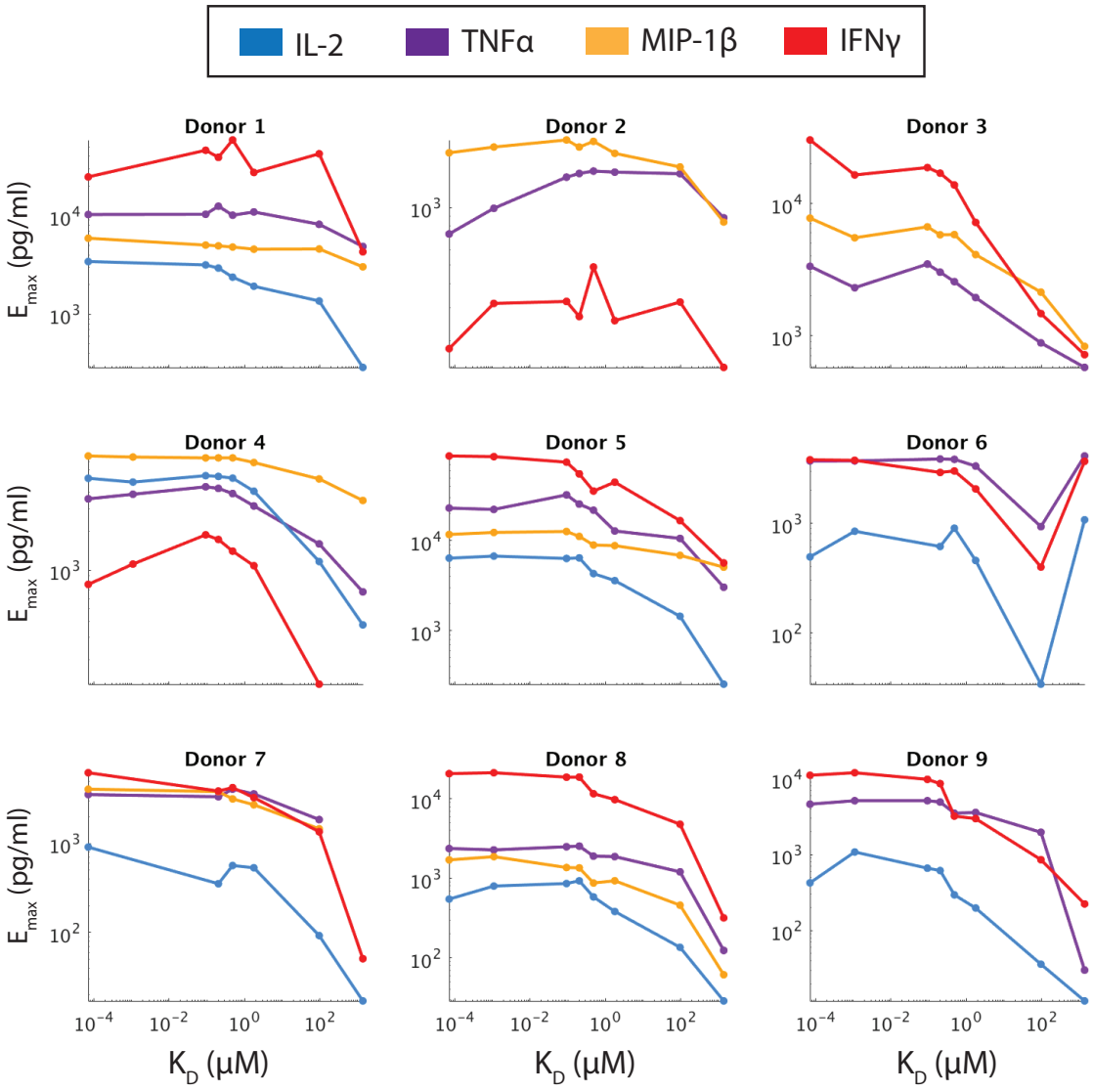


Figure C.4: The E_{max} of different cytokine responses changes similarly with pMHC affinity. The maximum absolute amount of each cytokine produced is shown on the y-axis and the pMHC affinity, K_D, on the x-axis. The trend by which the E_{max} of each cytokine changes with pMHC affinity appears comparable.

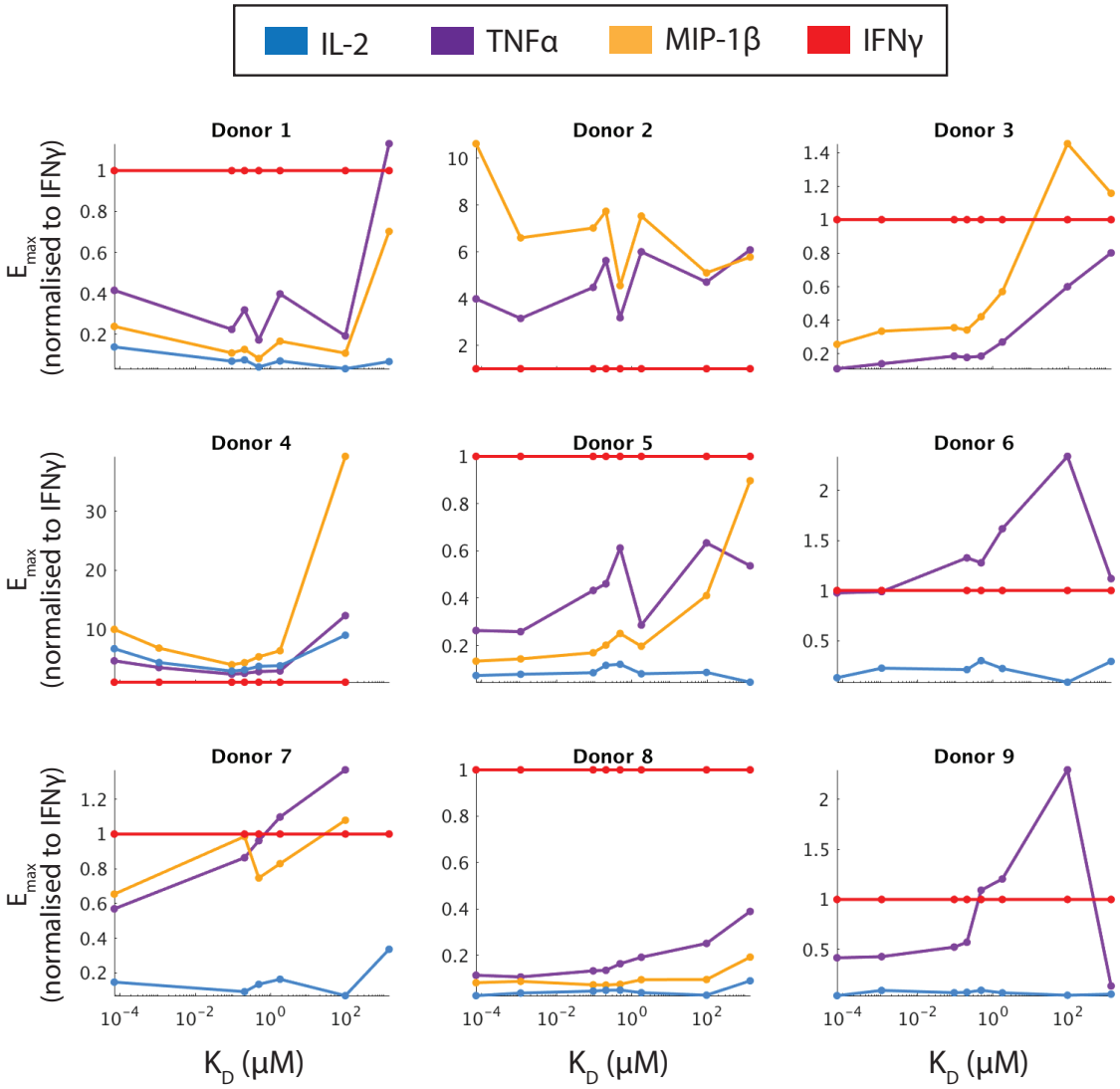


Figure C.5: Relative changes in $E^{(i)\prime}_{max}$ between cytokine readouts as a function of pMHC affinity for all donors. The absolute amount of each cytokine produced was normalised to $E^{IFN\gamma}_{max}$ within the same experimental repeat. The normalised E'_{max} is shown on the y-axis as a function of the pMHC affinity, K_D, on the x-axis. For some donors, the relative amounts of different cytokines produced did not change much (e.g. Donor 2), while a clear trend was observed for other donors (e.g. Donor 3). Trends were however not consistent between donors.

Bibliography

[1] V. Abadie, O. Bonduelle, D. Duffy, C. Parizot, B. Verrier, and B. Combadière, *Original Encounter with Antigen Determines Antigen-Presenting Cell Imprinting of the Quality of the Immune Response in Mice*, PLoS ONE, 4 (2009).

[2] O. Acuto, V. Di Bartolo, and F. Michel, *Tailoring T-cell receptor signals by proximal negative feedback mechanisms*, Nature Reviews Immunology, 8 (2008), pp. 699–712.

[3] M. Adler, P. Szekely, A. Mayo, and U. Alon, *Optimal Regulatory Circuit Topologies for Fold-Change Detection*, Cell Systems, 4 (2017), pp. 171–181.

[4] B. B. Aggarwal, *Signalling pathways of the TNF superfamily: A double-edged sword*, Nature Reviews Immunology, 3 (2003), pp. 745–756.

[5] A. Alcover, B. Alarcón, and V. Di Bartolo, *Cell Biology of T Cell Receptor Expression and Regulation*, Annual Review of Immunology, 36 (2018).

[6] M. Aleksic, O. Dushek, H. Zhang, E. Shenderov, J.-L. Chen, V. Cerundolo, D. Coombs, and P. A. van der Merwe, *Dependence of T Cell Antigen Recognition on T Cell Receptor-Peptide MHC Confinement Time*, Immunity, 32 (2010), pp. 163–174.

[7] K. A. Allison, E. Sajti, J. G. Collier, D. Gosselin, T. D. Troutman, E. L. Stone, S. M. Hedrick, and C. K. Glass, *Affinity and dose of TCR engagement yield proportional enhancer and gene activity in CD4$^+$ T cells*, eLife, 5 (2016), pp. 1–28.

[8] G. Altan-Bonnet and R. N. Germain, *Modeling T cell antigen discrimination based on feedback control of digital ERK responses*, PLoS Biology, 3 (2005), pp. 1925–1938.

[9] P. S. Andersen, C. Geisler, S. Buus, R. A. Mariuzza, and K. Karjalainen, *Role of the T Cell Receptor Ligand Affinity in T Cell Activation by Bacterial Superantigens*, Journal of Biological Chemistry, 276 (2001), pp. 33452–33457.

[10] P. S. Andersen, C. Menné, R. A. Mariuzza, C. Geisler, and K. Karjalainen, *A Response Calculus for Immobilized T Cell Receptor Ligands*, Journal of Biological Chemistry, 276 (2001), pp. 49125–49132.

[11] P. Andre, J. Boretto, A.-O. Hueber, A. Regnier-Vigouroux, J.-P. Gorvel, P. Ferrier, and P. Chavrier, *A Dominant-Negative Mutant of the Rab5 GTPase Enhances T Cell Signaling by Interfering with TCR Down-Modulation in Transgenic Mice*, The Journal of Immunology, 159 (1997), pp. 5253–5263.

[12] M. F. Bachmann, M. Salzmann, A. Oxenius, and P. S. Ohashi, *Formation of TCR dimers/trimers as a crucial step for T cell activation*, European Journal of Immunology, 28 (1998), pp. 2571–2579.

[13] L. Balagopalan, N. P. Coussens, E. Sherman, L. E. Samelson, and C. L. Sommers, *The LAT Story: A Tale of Cooperativity, Coordination, and Choreography*, Cold Spring Harbor Perspectives in Biology, 2 (2010), pp. 1–22.

[14] S. D. Blackburn, H. Shin, W. N. Haining, T. Zou, C. J. Workman, A. Polley, M. R. Betts, G. J. Freeman, D. A. A. Vignali, and E. J. Wherry, *Coregulation of CD8$^+$ T cell exhaustion by multiple inhibitory receptors during chronic viral infection*, Nature Immunology, 10 (2009), pp. 29–37.

[15] T. J. Boggon and M. J. Eck, *Structure and regulation of Src family kinases*, Oncogene, 23 (2004), pp. 7918–7927.

[16] C. M. Bonefeld, M. Haks, B. Nielsen, M. von Essen, L. Boding, A. K. Hansen, J. M. Larsen, N. Odum, P. Krimpenfort, A. Kruisbeek, J. P. Christensen, A. R. Thomsen, and C. Geisler, *TCR Down-Regulation Controls Virus-Specific CD8$^+$ T cell Responses*, Journal of Immunology, 181 (2008), pp. 7786–99.

[17] C. M. Bonefeld, A. B. Rasmussen, J. P. H. Lauritsen, M. von Essen, N. Ødum, P. S. Andersen, and C. Geisler, *TCR Comodulation of Nonengaged TCR Takes Place by a Protein Kinase C and CD3γ Di-Leucine-Based Motif-Dependent Mechanism*, The Journal of Immunology, 171 (2003), pp. 3003–3009.

[18] M. Boothby and K. Lee, *A 'Tsc, Tsc' keeps the kids quie(scen)t and holds down ROS*, Nature Immunology, 12 (2011), pp. 811–812.

[19] J. M. Boulter, M. Glick, P. T. Todorov, E. Baston, M. Sami, P. Rizkallah, and B. K. Jakobsen, *Stable, soluble T-cell receptor molecules for crystallization and therapeutics*, Protein Engineering Design and Selection, 16 (2003), pp. 707–711.

[20] J. M. Boulter and B. K. Jakobsen, *Stable, soluble, high-affinity, engineered T cell receptors: Novel antibody-like proteins for specific targeting of peptide antigens*, Clinical and Experimental Immunology, 142 (2005), pp. 454–460.

[21] A. Boyd, J. R. Almeida, P. a. Darrah, D. Sauce, R. a. Seder, V. Appay, G. Gorochov, and M. Larsen, *Pathogen-Specific T Cell Polyfunctionality Is a Correlate of T Cell Efficacy and Immune Protection*, PLoS One, 10 (2015).

[22] A. Braiman, M. Barda-Saad, C. L. Sommers, and L. E. Samelson, *Recruitment and activation of PLCγ1 in T cells: A new insight into old domains*, EMBO Journal, 25 (2006), pp. 774–784.

[23] M. Brameshuber, F. Kellner, B. K. Rossboth, H. Ta, K. Alge, E. Sevcsik, J. Göhring, M. Axmann, F. Baumgart, N. R. Gascoigne, S. J. Davis, H. Stockinger, G. J. Schütz, and J. B. Huppa, *Monomeric TCRs drive T cell antigen recognition article*, Nature Immunology, 19 (2018), pp. 487–496.

[24] R. S. Bystry, V. Aluvihare, K. A. Welch, M. Kallikourdis, and A. G. Betz, *B cells and professional APCs recruit regulatory T cells via CCL4*, Nature Immunology, 2 (2001), pp. 1126–1132.

[25] Z. Cai, H. Kishimoto, A. Brunmark, M. R. Jackson, P. A. Peterson, and J. Sprent, *Requirements for Peptide-Induced T Cell Receptor Downregulation on Naive CD8$^+$ T Cells*, Journal of Experimental Medicine, 185 (1997), pp. 641–51.

[26] D. J. Campbell, *Control of Regulatory T Cell Migration, Function, and Homeostasis*, Journal of Immunology, 195 (2015), pp. 2507–2513.

[27] D. A. Cantrell, A. A. Davies, and M. J. Crumpton, *Activators of protein kinase C down-regulate and phosphorylate the T3/T-cell antigen receptor complex of human T lymphocytes*, Proceedings of the National Academy of Sciences of the United States of America, 82 (1985), pp. 8158–8162.

[28] J. Casas, J. Brzostek, V. I. Zarnitsyna, J.-s. Hong, Q. Wei, J. A. H. Hoerter, G. Fu, J. Ampudia, R. Zamoyska, C. Zhu, and N. R. J. Gascoigne, *Ligand-engaged TCR is triggered by Lck not associated with CD8 coreceptor*, Nature Communications, 5 (2014).

[29] L. Chen and D. B. Flies, *Molecular mechanisms of T cell co-stimulation and co-inhibition*, Nature Reviews Immunology, 13 (2013), pp. 227–242.

[30] A. S. Chervin, J. D. Stone, P. D. Holler, A. Bai, J. Chen, H. N. Eisen, and D. M. Kranz, *The impact of TCR-binding properties and antigen presentation format on T cell responsiveness*, Journal of Immunology, 183 (2009), pp. 1166–78.

[31] L. Chiodetti, S. Choi, D. L. Barber, and R. H. Schwartz, *Adaptive Tolerance and Clonal Anergy Are Distinct Biochemical States*, The Journal of Immunology, 176 (2006), pp. 2279–2291.

[32] S. Choi and R. H. Schwartz, *Molecular mechanisms for adaptive tolerance and other T cell anergy models*, Seminars in Immunology, 19 (2007), pp. 140–152.

[33] K. Choudhuri, J. Llodrá, E. W. Roth, J. Tsai, S. Gordo, K. W. Wucherpfennig, L. C. Kam, D. L. Stokes, and M. L. Dustin, *Polarized release of T-cell-receptor-enriched microvesicles at the immunological synapse*, Nature, 507 (2014), pp. 118–123.

[34] N. Cieri, B. Camisa, F. Cocchiarella, M. Forcato, G. Oliveira, E. Provasi, A. Bondanza, C. Bordignon, J. Peccatori, F. Ciceri, M. T. Lupo-Stanghellini, F. Mavilio, A. Mondino, S. Bicciato, A. Recchia, and C. Bonini, *IL-7 and IL-15 instruct the generation of human memory stem T cells from naive precursors*, Blood, 121 (2013), pp. 573–585.

[35] C. E. Clark, M. Hasan, and P. Bousso, *A role for the immediate early gene product c-fos in imprinting T cells with short-term memory for signal summation*, PLoS ONE, 6 (2011), pp. 1–8.

[36] D. Colquhoun, *Binding, gating, affinity and efficacy: The interpretation of structure-activity relationships for agonists and of the effects of mutating receptors*, British Journal of Pharmacology, 125 (1998), pp. 924–947.

[37] D. Coombs, A. M. Kalergis, S. G. Nathenson, C. Wofsy, and B. Goldstein, *Activated TCRs remain marked for internalization after dissociation from pMHC*, Nature Immunology, 3 (2002), pp. 926–931.

[38] P. S. Costello, M. Gallagher, and D. A. Cantrell, *Sustained and dynamic inositol lipid metabolism inside and outside the immunological synapse*, Nature immunology, 3 (2002), pp. 1082–1089.

[39] A. Csikász-Nagy and O. S. Soyer, *Adaptive dynamics with a single two-state protein*, Journal of the Royal Society Interface, 5 (2008).

[40] J. M. Curtsinger and M. F. Mescher, *Inflammatory cytokines as a third signal for T cell activation*, Current Opinion in Immunology, 22 (2010), pp. 333–340.

[41] J. Das, M. Ho, J. Zikherman, C. Govern, M. Yang, A. Weiss, A. K. Chakraborty, and J. P. Roose, *Digital Signaling and Hysteresis Characterize Ras Activation in Lymphoid Cells*, Cell, 136 (2009), pp. 337–351.

[42] V. Das, B. Nal, A. Dujeancourt, M. I. Thoulouze, T. Galli, P. Roux, A. Dautry-Varsat, and A. Alcover, *Activation-induced polarized recycling targets T cell antigen receptors to the immunological synapse: Involvement of SNARE complexes*, Immunity, 20 (2004), pp. 577–588.

[43] W. Dawicki and T. H. Watts, *Expression and function of 4-1BB during CD4 versus CD8 T cell responses in vivo*, European Journal of Immunology, 34 (2004), pp. 743–751.

[44] N. Demotte, V. Stroobant, P. J. Courtoy, P. Van Der Smissen, D. Colau, I. F. Luescher, C. Hivroz, J. Nicaise, J. L. Squifflet, M. Mourad, D. Godelaine, T. Boon, and P. van der Bruggen, *Restoring the Association of the T Cell Receptor with CD8 Reverses Anergy in Human Tumor-Infiltrating Lymphocytes*, Immunity, 28 (2008), pp. 414–424.

[45] D. Depoil and M. L. Dustin, *Force and affinity in ligand discrimination by the TCR*, Trends in Immunology, 35 (2014), pp. 597–603.

[46] S. Desai, M. Rickerd, and I. Horneij, *Coated Surfaces With High Capacity For Capturing Target Molecules*, 2003.

[47] J. Dietrich, X. Hou, A.-M. K. Wegener, and C. Geisler, *CD3γ contains a phoshoserine-dependent di-leucine motif involved in down-regulation of the T cell receptor*, EMBO Journal, 13 (1994), pp. 2156–2166.

[48] J. Dietrich, J. Kastrup, B. L. Nielsen, N. Ødum, and C. Geisler, *Regulation and Function of the CD3γ DxxxLL Motif: A Binding Site for Adaptor Protein-1 and Adaptor Protein-2 in Vitro*, Journal of Cell Biology, 138 (1997), pp. 271–281.

[49] J. Dietrich, C. Menne, J. P. H. Lauritsen, M. von Essen, A. B. Rasmussen, N. Odum, and C. Geisler, *Ligand-Induced TCR Down-Regulation Is Not Dependent on Constitutive TCR Cycling*, The Journal of Immunology, 168 (2002), pp. 5434–5440.

[50] Z.-C. Ding, L. Huang, B. R. Blazar, H. Yagita, A. L. Mellor, D. H. Munn, W. Dc, and G. Zhou, *Polyfunctional CD4⁺ T cells are essential for eradicating advanced B-cell lymphoma after chemotherapy*, Blood, 120 (2012), pp. 2229–2239.

[51] J. Dinic, A. Riehl, J. Adler, and I. Parmryd, *The T cell receptor resides in ordered plasma membrane nanodomains that aggregate upon patching of the receptor*, Scientific Reports, 5 (2015).

[52] S. Dong, B. Corre, E. Foulon, E. Dufour, A. Veillette, O. Acuto, and F. Michel, *T cell receptor for antigen induces linker for activation of T cell-dependent activation of a negative signaling complex involving Dok-2, SHIP-1, and Grb-2*, The Journal of Experimental Medicine, 203 (2006), pp. 2509–2518.

[53] U. D'Oro, M. S. Vacchio, A. M. Weissman, and J. D. Ashwell, *Activation of the Lck tyrosine kinase targets cell surface T cell antigen receptors for lysosomal degradation*, Immunity, 7 (1997), pp. 619–628.

[54] G. Dorothee, I. Vergnon, F. El Hage, B. L. M. Chansac, V. Ferrand, Y. Lecluse, P. Opolon, S. Chouaib, G. Bismuth, and F. Mami-Chouaib, *In Situ Sensory Adaptation of Tumor-Infiltrating T Lymphocytes to Peptide-MHC Levels Elicits Strong Antitumor Reactivity*, The Journal of Immunology, 174 (2005), pp. 6888–6897.

[55] O. Dushek, M. Aleksic, R. J. Wheeler, H. Zhang, S.-P. Cordoba, Y.-C. Peng, J.-L. Chen, V. Cerundolo, T. Dong, D. Coombs, and P. A. van der Merwe, *Antigen Potency and Maximal Efficacy Reveal a Mechanism of Efficient T Cell Activation*, Science Signaling, 4 (2011).

[56] O. Dushek and P. A. van der Merwe, *An induced rebinding model of antigen discrimination*, Trends in Immunology, 35 (2014), pp. 153–158.

[57] B. D. Evavold and P. M. Allen, *Separation of IL-4 production from Th cell proliferation by an altered T cell receptor ligand*, Science, 252 (1991), pp. 1308–1310.

[58] J. Eyquem, J. Mansilla-Soto, T. Giavridis, S. J. C. van der Stegen, M. Hamieh, K. M. Cunanan, A. Odak, M. Gönen, and M. Sadelain, *Targeting a CAR to the TRAC locus with CRISPR/Cas9 enhances tumour rejection*, Nature, 543 (2017), pp. 113–117.

[59] M. Faroudi, R. Zaru, P. Paulet, S. Muller, and S. Valitutti, *Cutting Edge: T Lymphocyte Activation by Repeated Immunological Synapse Formation and Intermittent Signaling*, The Journal of Immunology, 171 (2003), pp. 1128–1132.

[60] I. Ferber, G. Schonrich, J. Schenkel, A. L. Mellor, G. J. Hammerling, and B. Arnold, *Levels of Peripheral T Cell Tolerance Induced by Different Doses of Tolerogen*, Science, 263 (1994), pp. 674–676.

[61] E. Fernández-Arenas, E. Calleja, N. Martínez-Martín, S. I. Gharbi, R. Navajas, N. García-Medel, P. Penela, A. Alcamí, F. Mayor, J. P. Albar, and B. Alarcon, *β-arrestin-1 mediates the TCR-triggered re-routing of distal receptors to*

the immunological synapse by a PKC-mediated mechanism, EMBO Journal, 33 (2014), pp. 559–577.

[62] F. Finetti, C. Cassioli, and C. T. Baldari, *Transcellular communication at the immunological synapse: A vesicular traffic-mediated mutual exchange*, F1000Research, 6 (2017), p. 1880.

[63] D. K. Finlay, E. Rosenzweig, L. V. Sinclair, C. Feijoo-Carnero, J. L. Hukelmann, J. Rolf, A. A. Panteleyev, K. Okkenhaug, and D. A. Cantrell, *PDK1 regulation of mTOR and hypoxia-inducible factor 1 integrate metabolism and migration of $CD8^+$ T cells*, The Journal of Experimental Medicine, 209 (2012), pp. 2441–2453.

[64] P. François, G. Voisinne, E. D. Siggia, G. Altan-Bonnet, and M. Vergassola, *Phenotypic model for early T-cell activation displaying sensitivity, specificity, and antagonism*, Proceedings of the National Academy of Sciences of the United States of America, 110 (2013).

[65] S. J. Frank and S. Y. Fuchs, *Modulation of growth hormone receptor abundance and function: Roles for the ubiquitin-proteasome system*, Biochimica et Biophysica Acta, 1782 (2008), pp. 785–794.

[66] K. C. Garcia, M. Degano, R. L. Stanfield, A. Brunmark, M. R. Jackson, P. A. Peterson, L. Teyton, and I. A. Wilson, *An $\alpha\beta$ T Cell Receptor Structure at 2.5 Å and Its Orientation in the TCR-MHC Complex*, Science, 274 (1996), pp. 209–219.

[67] E. Genot and D. A. Cantrell, *Ras regulation and function in lymphocytes*, Current Opinion in Immunology, 12 (2000), pp. 289–294.

[68] T. S. Gomez, M. J. Hamann, S. McCarney, D. N. Savoy, C. M. Lubking, M. P. Heldebrant, C. M. Labno, D. J. McKean, M. A. McNiven, J. K. Burkhardt, and D. D. Billadeau, *Dynamin 2 regulates T cell activation by controlling actin polymerization at the immunological synapse*, Nature Immunology, 6 (2005), pp. 261–270.

[69] P. A. González, L. J. Carreño, D. Coombs, J. E. Mora, E. Palmieri, B. Goldstein, S. G. Nathenson, and A. M. Kalergis, *T cell receptor binding kinetics required for T cell activation depend on the density of cognate ligand on the antigen-presenting cell*, Proceedings of the National Academy of Sciences of the United States of America, 102 (2005), pp. 4824–4829.

[70] M. R. Goodier, C. Lusa, S. Sherratt, A. Rodriguez-Galan, R. Behrens, and E. M. Riley, *Sustained immune complex-mediated reduction in CD16 expression after vaccination regulates NK cell function*, Frontiers in Immunology, 7 (2016).

[71] D. R. Green, N. Droin, and M. Pinkoski, *Activation-induced cell death in T cells*, Immunological Reviews, 193 (2003), pp. 70–81.

[72] Z. Grossman and W. E. Paul, *Adaptive Cellular Interactions in the Immune System: The Tunable Activation Threshold and the Significance of Subthreshold Responses*, Proceedings of the National Academy of Sciences of the United States of America, 89 (1992), pp. 10365–10369.

[73] P. M. Gubser, G. R. Bantug, L. Razik, M. Fischer, S. Dimeloe, G. Hoenger, B. Durovic, A. Jauch, and C. Hess, *Rapid effector function of memory CD8$^+$ T cells requires an immediate-early glycolytic switch*, Nature Immunology, 14 (2013), pp. 1064–1072.

[74] S. Guillaume, L. Tuosto, C. Tanchot, V. Di Bartolo, O. Acuto, and B. Rocha, *Proximal changes in signal transduction that modify CD8$^+$ T cell responsiveness in vivo*, European Journal of Immunology, 33 (2003), pp. 2551–2556.

[75] J. Gunawardena, *Models in biology: 'Accurate descriptions of our pathetic thinking'*, BMC Biology, 12 (2014), p. 29.

[76] S. Halle, K. A. Keyser, F. R. Stahl, A. Busche, A. Marquardt, X. Zheng, M. Galla, V. Heissmeyer, K. Heller, J. Boelter, K. Wagner, Y. Bischoff, R. Martens, A. Braun, K. Werth, A. Uvarovskii, H. Kempf, M. Meyer-Hermann, R. Arens, M. Kremer, G. Sutter, M. Messerle, and R. Förster, *In Vivo Killing Capacity of Cytotoxic T Cells Is Limited and Involves Dynamic Interactions and T Cell Cooperativity*, Immunity, (2016), pp. 233–245.

[77] C. Han, S.-J. Sim, S.-H. Kim, R. Singh, S. Hwang, Y. I. Kim, S. H. Park, K. H. Kim, D. G. Lee, H. S. Oh, S. Lee, Y. H. Kim, B. K. Choi, and B. S. Kwon, *Desensitized chimeric antigen receptor T cells selectively recognize target cells with enhanced antigen expression*, Nature Communications, 9 (2018), p. 468.

[78] Q. Han, N. Bagheri, E. M. Bradshaw, D. a. Hafler, D. a. Lauffenburger, and J. C. Love, *Polyfunctional responses by human T cells result from sequential release of cytokines*, Proceedings of the National Academy of Sciences of the United States of America, 109 (2012), pp. 1607–1612.

[79] S. Han, A. Asoyan, H. Rabenstein, N. Nakano, and R. Obst, *Role of antigen persistence and dose for CD4$^+$ T-cell exhaustion and recovery*, Proceedings of the National Academy of Sciences of the United States of America, 107 (2010), pp. 20453–20458.

[80] T. B. Hansen, T. I. Jensen, B. H. Clausen, J. B. Bramsen, B. Finsen, C. K. Damgaard, and J. Kjems, *Natural RNA circles function as efficient microRNA sponges*, Nature, 495 (2013), pp. 384–388.

[81] D. Hawiger, R. F. Masilamani, E. Bettelli, V. K. Kuchroo, and M. C. Nussenzweig, *Immunological unresponsiveness characterized by increased expression of CD5 on peripheral T cells induced by dendritic cells in vivo*, Immunity, 20 (2004), pp. 695–705.

[82] M. Hebeisen, L. Baitsch, D. Presotto, P. Baumgaertner, P. Romero, O. Michielin, D. E. Speiser, and N. Rufer, *SHP-1 phosphatase activity counteracts increased T cell receptor affinity*, The Journal of Clinical Investigation, 123 (2013), pp. 1044–1056.

[83] B. Hemmer, I. Stefanova, M. Vergelli, R. N. Germain, and R. Martin, *Relationships among TCR ligand potency, thresholds for effector function elicitation, and the quality of early signaling events in human T cells*, Journal of Immunology, 160 (1998), pp. 5807–5814.

[84] K. A. Hogquist and S. C. Jameson, *The self-obsession of T cells: How TCR signaling thresholds affect fate 'decisions' and effector function*, Nature Immunology, 15 (2014), pp. 815–823.

[85] A. D. Holdorf, J. M. Green, S. D. Levin, M. F. Denny, D. B. Straus, V. Link, P. S. Changelian, P. M. Allen, and A. S. Shaw, *Proline Residues in CD28 and the Src Homology (SH)3 Domain of Lck Are Required for T Cell Costimulation*, The Journal of Experimental Medicine, 190 (1999), pp. 375–84.

[86] P. D. Holler and D. M. Kranz, *Quantitative analysis of the contribution of TCR/pepMHC affinity and CD8 to T cell activation*, Immunity, 18 (2003), pp. 255–264.

[87] T. Honda, J. G. Egen, T. Lämmermann, W. Kastenmüller, P. Torabi-Parizi, and R. N. Germain, *Tuning of Antigen Sensitivity by T Cell Receptor-Dependent Negative Feedback Controls T Cell Effector Function in Inflamed Tissues*, Immunity, 40 (2014), pp. 235–47.

[88] H. Hu and S. C. Sun, *Ubiquitin signaling in immune responses*, Cell Research, 26 (2016), pp. 457–483.

[89] J. Huang, M. Brameshuber, X. Zeng, J. Xie, Q.-j. Li, Y.-h. Chien, S. Valitutti, and M. M. Davis, *A Single peptide-major histocompatibility complex ligand triggers digital cytokine secretion in CD4$^+$ T Cells*, Immunity, 39 (2013), pp. 846–857.

[90] E. Hui, J. Zhu, J. Cheung, X. Su, M. Taylor, J. Kim, I. Mellman, and R. D. Vale, *The T cell costimulatory receptor CD28 is a primary target of PD-1 mediated inhibition*, Science, 4 (2016), pp. 1–14.

[91] S. Hulpke and R. Tampé, *The MHC I loading complex: A multitasking machinery in adaptive immunity*, Trends in Biochemical Sciences, 38 (2013), pp. 412–420.

[92] J. B. Huppa, M. Gleimer, C. Sumen, and M. M. Davis, *Continuous T cell receptor signaling required for synapse maintenance and full effector potential*, Nature Immunology, 4 (2003), pp. 749–55.

[93] M. Huse, B. F. Lillemeier, M. S. Kuhns, D. S. Chen, and M. M. Davis, *T cells use two directionally distinct pathways for cytokine secretion*, Nature Immunology, 7 (2006), pp. 247–255.

[94] M. Huse, E. J. Quann, and M. M. Davis, *Shouts, whispers and the kiss of death: Directional secretion in T cells*, Nature Immunology, 9 (2008), pp. 1105–1111.

[95] G. Iezzi, K. Karjalainen, and A. Lanzavecchia, *The duration of antigenic stimulation determines the fate of naive and effector T cells*, Immunity, 8 (1998), pp. 89–95.

[96] K. Inoki, Y. Li, T. Zhu, J. Wu, and K. L. Guan, *TSC2 is phosphorylated and inhibited by Akt and suppresses mTOR signalling*, Nature Cell Biology, 4 (2002), pp. 648–657.

[97] M. Irving, V. Zoete, M. Hebeisen, D. Schmid, P. Baumgartner, P. Guillaume, P. Romero, D. Speiser, I. Luescher, N. Rufer, and O. Michielin, *Interplay between T Cell Receptor Binding Kinetics and the Level of Cognate Peptide Presented by Major Histocompatibility Complexes Governs CD8$^+$ T Cell Responsiveness*, Journal of Biological Chemistry, 287 (2012), pp. 23068–23078.

[98] Y. Itoh and R. N. Germain, *Single Cell Analysis Reveals Regulated Hierarchical T Cell Antigen Receptor Signaling Thresholds and Intraclonal Heterogeneity for Individual Cytokine Responses of CD4$^+$ T Cells*, The Journal of Experimental Medicine, 186 (1997), pp. 757–766.

[99] M. Iwashima, B. a. Irving, N. S. van Oers, a. C. Chan, and A. Weiss, *Sequential Interactions of the TCR with Two Distinct Cytoplasmic Tyrosine Kinases*, Science, 263 (1994), pp. 1136–1139.

[100] M.-S. Jeon, A. Atfield, K. Venuprasad, C. Krawczyk, R. Sarao, C. Elly, C. Yang, S. Arya, K. Bachmaier, L. Su, D. Bouchard, R. Jones, M. Gronski, P. Ohashi, T. Wada, D. Bloom, C. Fathman, Y.-C. Liu, and J. M. Penninger, *Essential Role of the E3 Ubiquitin Ligase Cbl-b in T Cell Anergy Induction*, Immunity, 21 (2004), pp. 167–177.

[101] R. G. Jones and C. B. Thompson, *Revving the Engine: Signal Transduction Fuels T Cell Activation*, Immunity, 27 (2007), pp. 173–178.

[102] Y. Jung, I. Riven, S. W. Feigelson, E. Kartvelishvily, K. Tohya, M. Miyasaka, R. Alon, and G. Haran, *Three-dimensional localization of T-cell receptors in relation to microvilli using a combination of superresolution microscopies*, Proceedings of the National Academy of Sciences of the United States of America, 113 (2016), pp. 5916–5924.

[103] S. M. Kaech, J. T. Tan, E. J. Wherry, B. T. Konieczny, C. D. Surh, and R. Ahmed, *Selective expression of the interleukin 7 receptor identifies effector CD8 T cells that give rise to long-lived memory cells*, Nature Immunology, 4 (2003), pp. 1191–1198.

[104] Y. Kaizuka, A. D. Douglass, R. Varma, M. L. Dustin, and R. D. Vale, *Mechanisms for segregating T cell receptor and adhesion molecules during immunological synapse formation in Jurkat T cells*, Proceedings of the National Academy of Sciences of the United States of America, 104 (2007), pp. 20296–20301.

[105] A. M. Kalergis, N. Boucheron, M.-A. Doucey, E. Palmieri, E. C. Goyarts, Z. Vegh, I. F. Luescher, and S. G. Nathenson, *Efficient T cell activation requires an optimal dwell-time of interaction between the TCR and the pMHC complex*, Nature Immunology, 2 (2001), pp. 229–234.

[106] K. Karwacz, C. Bricogne, D. MacDonald, F. Arce, C. L. Bennett, M. Collins, and D. Escors, *PD-L1 co-stimulation contributes to ligand-induced T cell receptor down-modulation on CD8$^+$ T cells*, EMBO Molecular Medicine, 3 (2011), pp. 581–592.

[107] T. Kasahara, J. J. Hooks, S. F. Dougherty, and J. J. Oppenheim, *Interleukin 2-mediated immune interferon (IFNγ) production by human T cells and T cell subsets*, Journal of Immunology, 130 (1983), pp. 1784–1789.

[108] K. Katagiri, M. Hattori, N. Minato, and T. Kinashi, *Rap1 Functions as a Key Regulator of T-Cell and Antigen-Presenting Cell Interactions and Modulates T-Cell Responses*, Molecular and Cellular Biology, 22 (2002), pp. 1001–1015.

[109] K. Katagiri, A. Maeda, M. Shimonaka, and T. Kinashi, *RAPL, a Rap1-binding molecule that mediates Rap1-induced adhesion through spatial regulation of LFA-1*, Nature Immunology, 4 (2003), pp. 741–748.

[110] G. J. Kersh, E. N. Kersh, D. H. Fremont, and P. M. Allen, *High- and Low-Potency Ligands with Similar Affinities for the TCR: The Importance of Kinetics in TCR Signaling*, Immunity, 9 (1998), pp. 817–826.

[111] P. W. Kim, Z.-Y. J. Sun, S. C. Blacklow, G. Wagner, and M. J. Eck, *A Zinc Clasp Structure Tethers Lck to T Cell Coreceptors CD4 and CD8*, Science, 301 (2003), pp. 1725–1728.

[112] K. Kimachi, K. Sugie, and H. M. Grey, *Effector T cells have a lower ligand affinity threshold for activation than naive T cells*, International Immunology, 15 (2003), pp. 885–892.

[113] L. M. Kingeter, S. Paul, S. K. Maynard, N. G. Cartwright, and B. C. Schaefer, *Cutting Edge: TCR Ligation Triggers Digital Activation of NF-κB*, Journal of Immunology, 185 (2010), pp. 4520–4524.

[114] C. A. Klebanoff, C. D. Scott, A. J. Leonardi, T. N. Yamamoto, A. C. Cruz, C. Ouyang, M. Ramaswamy, R. Roychoudhuri, Y. Ji, R. L. Eil, M. Sukumar, J. G. Crompton, D. C. Palmer, Z. A. Borman, D. Clever, S. K. Thomas, S. Patel, Z. Yu, P. Muranski, H. Liu, E. Wang, F. M. Marincola, A. Gros, L. Gattinoni, S. A. Rosenberg, R. M. Siegel, and N. P. Restifo, *Memory T cell-driven differentiation of naive cells impairs adoptive immunotherapy*, Journal of Clinical Investigation, 126 (2016), pp. 318–334.

[115] L. Klein, B. Kyewski, P. M. Allen, and K. A. Hogquist, *Positive and negative selection of the T cell repertoire: What thymocytes see (and don't see)*, Nature Reviews Immunology, 14 (2014), pp. 377–391.

[116] S. Koch, A. Larbi, E. Derhovanessian, D. Özcelik, E. Naumova, and G. Pawelec, *Multiparameter flow cytometric analysis of CD4 and CD8 T cell subsets in young and old people*, Immunity & Ageing, 5 (2008).

[117] M. S. Krangel, *Endocytosis and recycling of the T3-T cell receptor complex: The Role of T3 Phosphorylation*, Journal of Experimental Medicine, 165 (1987), pp. 1141–1159.

[118] N. N. Kristensen, A. N. Madsen, A. R. Thomsen, and J. P. Christensen, *Cytokine production by virus-specific $CD8^+$ T cells varies with activation state and localization, but not with TCR avidity*, The Journal of General Virology, 85 (2004), pp. 1703–1712.

[119] S. Kumari, S. Curado, V. Mayya, and M. L. Dustin, *T cell antigen receptor activation and actin cytoskeleton remodeling*, Biochimica et Biophysica Acta, 1838 (2014), pp. 546–556.

[120] A. Kupfer, T. R. Mosmann, and H. Kupfer, *Polarized expression of cytokines in cell conjugates of helper T cells and splenic B cells*, Proceedings of the National Academy of Sciences of the United States of America, 88 (1991), pp. 775–779.

[121] B. Laugel, D. K. Cole, M. Clement, L. Wooldridge, D. A. Price, and A. K. Sewell, *The multiple roles of the CD8 coreceptor in T cell biology: Opportunities for the selective modulation of self-reactive cytotoxic T cells*, Journal of Leukocyte Biology, 90 (2011), pp. 1089–1099.

[122] J. P. Lauritsen, M. D. Christensen, J. Dietrich, J. Kastrup, N. Odum, and C. Geisler, *Two distinct pathways exist for down-regulation of the TCR*, Journal of Immunology, 161 (1998), pp. 260–267.

[123] A. Le Floc'H and M. Huse, *Molecular mechanisms and functional implications of polarized actin remodeling at the T cell immunological synapse*, Cellular and Molecular Life Sciences, 72 (2015), pp. 537–556.

[124] K.-H. Lee, A. R. Dinner, C. Tu, G. Campi, S. Raychaudhuri, R. Varma, T. N. Sims, W. R. Burack, H. Wu, J. Wang, O. Kanagawa, M. Markiewicz, P. M. Allen, M. L. Dustin, A. K. Chakraborty, and A. S. Shaw, *The Immunological Synapse Balances T Cell Receptor Signaling and Degradation*, Science, 302 (2003), pp. 1218–1223.

[125] J. R. Lees, B. Charbonneau, A. K. Swanson, R. Jensen, J. F. Zhang, R. Matusik, and T. L. Ratliff, *Deletion is neither sufficient nor necessary for the induction of peripheral tolerance in mature CD8+T cells*, Immunology, 117 (2006), pp. 248–261.

[126] M. Lever, *Phenotypic models of T cell activation*, doctoral thesis, University of Oxford, 2015.

[127] M. Lever, H.-S. Lim, P. Kruger, J. Nguyen, N. Trendel, E. Abu-Shah, P. K. Maini, P. A. van der Merwe, and O. Dushek, *Architecture of a minimal signaling pathway explains the T-cell response to a 1 million-fold variation in antigen affinity and dose*, Proceedings of the National Academy of Sciences of the United States of America, 113 (2016).

[128] Y. Li and R. J. Kurlander, *Comparison of anti-CD3 and anti-CD28-coated beads with soluble anti-CD3 for expanding human T cells: Differing impact on CD8 T cell phenotype and responsiveness to restimulation.*, Journal of Translational Medicine, 8 (2010).

[129] Y. Li, R. Moysey, P. E. Molloy, A.-L. Vuidepot, T. Mahon, E. Baston, S. Dunn, N. Liddy, J. Jacob, B. K. Jakobsen, and J. M. Boulter, *Directed evolution of human T-cell receptors with picomolar affinities by phage display*, Nature Biotechnology, 23 (2005), pp. 349–354.

[130] N. Liddy, G. Bossi, K. J. Adams, A. Lissina, T. M. Mahon, N. J. Hassan, J. Gavaret, F. C. Bianchi, N. J. Pumphrey, K. Ladell, E. Gostick, A. K. Sewell, N. M. Lissin, N. E. Harwood, P. E. Molloy, Y. Li, B. J. Cameron, M. Sami, E. E. Baston, P. T. Todorov, S. J. Paston, R. E. Dennis, J. V. Harper, S. M. Dunn, R. Ashfield, A. Johnson, Y. McGrath, G. Plesa, C. H. June, M. Kalos, D. A. Price, A. Vuidepot, D. D. Williams, D. H. Sutton, and B. K. Jakobsen, *Monoclonal TCR-redirected tumor cell killing*, Nature Medicine, 18 (2012), pp. 980–987.

[131] H.-S. Lim, *Ligand Binding and Signalling by the T Cell Antigen Receptor and CD28*, Doctoral Thesis, University of Oxford, 2014.

[132] B. Liu, W. Chen, B. D. Evavold, and C. Zhu, *Accumulation of Dynamic Catch Bonds between TCR and Agonist Peptide-MHC Triggers T cell Signaling*, Cell, 157 (2014), pp. 357–68.

[133] H. Liu, M. Rhodes, D. L. Wiest, and D. A. Vignali, *On the dynamics of TCR:CD3 complex cell surface expression and downmodulation*, Immunity, 13 (2000), pp. 665–675.

[134] W. L. Lo, N. H. Shah, N. Ahsan, V. Horkova, O. Stepanek, A. R. Salomon, J. Kuriyan, and A. Weiss, *Lck promotes Zap70-dependent LAT phosphorylation by bridging Zap70 to LAT*, Nature Immunology, 19 (2018), pp. 733–741.

[135] M. J. Lohse, *Molecular mechanisms of membrane receptor desensitization*, Biochimica et Biophysica Acta, 1179 (1993), pp. 171–188.

[136] F. Luton, M. Buferne, J. Davoust, A. M. Schmitt-Verhulst, and C. Boyer, *Evidence for protein tyrosine kinase involvement in ligand-induced TCR/CD3 internalization and surface redistribution*, The Journal of Immunology, 153 (1994), pp. 63–72.

[137] E. Lyashenko, M. Niepel, P. Dixit, S. K. Lim, P. Sorger, and D. Vitkup, *Receptor-Based Mechanism of Relative Sensing in Mammalian Signaling Networks*, BioRxiv, (2017).

[138] W. Ma, A. Trusina, H. El-Samad, W. a. Lim, and C. Tang, *Defining network topologies that can achieve biochemical adaptation*, Cell, 138 (2009), pp. 760–73.

[139] F. Macian, *NFAT proteins: Key regulators of T-cell development and function*, Nature Reviews Immunology, 5 (2005), pp. 472–484.

[140] F. Macian, C. Lopez-Rodriguez, and A. Rao, *Partners in transcription: NFAT and AP-1*, Oncogene, 20 (2001), pp. 2476–2489.

[141] C. R. Mackay, *Homing of naive, memory and effector lymphocytes*, Current Opinion in Immunology, 5 (1993), pp. 423–427.

[142] C. R. Mackay, *Dual personality of memory T cells*, Nature, 401 (1999), pp. 659–660.

[143] Y. D. Mahnke, T. M. Brodie, F. Sallusto, M. Roederer, and E. Lugli, *The who's who of T-cell differentiation: Human memory T-cell subsets*, European Journal of Immunology, 43 (2013), pp. 2797–2809.

[144] B. Malissen and P. Bongrand, *Early T Cell Activation: Integrating Biochemical, Structural, and Biophysical Cues*, Annual Review of Immunology, 33 (2015), pp. 539–561.

[145] S. Mangan, A. Zaslaver, and U. Alon, *The coherent feedforward loop serves as a sign-sensitive delay element in transcription networks*, Journal of Molecular Biology, 334 (2003), pp. 197–204.

[146] F. Marangoni, T. T. Murooka, T. Manzo, E. Y. Kim, E. Carrizosa, N. M. Elpek, and T. R. Mempel, *The Transcription Factor NFAT Exhibits Signal Memory during Serial T Cell Interactions with Antigen-Presenting Cells*, Immunity, 38 (2013), pp. 237–249.

[147] S. Martin and M. J. Bevan, *Transient alteration of T cell fine specificity by a strong primary stimulus correlates with T cell receptor down-regulation*, European Journal of Immunology, 28 (1998), pp. 2991–3002.

[148] N. Martin-Blanco, R. Blanco, C. Alda-Catalinas, E. R. Bovolenta, C. L. Oeste, E. Palmer, W. W. Schamel, G. Lythe, C. Molina-Paris, M. Castro, and B. Alarcon, *A window of opportunity for allostery in the T Cell Receptor*, Nature Communications, 9 (2018), pp. 1–15.

[149] N. Martínez-Martín, E. Fernández-Arenas, S. Cemerski, P. Delgado, M. Turner, J. Heuser, D. J. Irvine, B. Huang, X. R. Bustelo, A. Shaw, and B. Alarcón, *T Cell Receptor Internalization from the Immunological Synapse Is Mediated by TC21 and RhoG GTPase-Dependent Phagocytosis*, Immunity, 35 (2011), pp. 208–222.

[150] K. Matsui, J. J. Boniface, P. Steffner, P. A. Reay, and M. M. Davis, *Kinetics of T-cell receptor binding to peptide/I-E^k complexes: Correlation of the dissociation rate with*

T-cell responsiveness, Proceedings of the National Academy of Sciences of the United States of America, 91 (1994), pp. 12862–12866.

[151] R. Matsumoto, D. Wang, M. Blonska, H. Li, M. Kobayashi, B. Pappu, Y. Chen, D. Wang, and X. Lin, *Phosphorylation of CARMA1 Plays a Critical Role in T Cell Receptor-Mediated NF-κB Activation*, Immunity, 23 (2005), pp. 575–585.

[152] P. Matzinger, *The Danger Model: A Renewed Sense of Self*, Science, 296 (2002).

[153] M. V. Maus, J. A. Fraietta, B. L. Levine, M. Kalos, Y. Zhao, and C. H. June, *Adoptive Immunotherapy for Cancer or Viruses*, Annual Review of Immunology, 32 (2014), pp. 189–225.

[154] V. Mayya and M. L. Dustin, *What Scales the T Cell Response?*, Trends in Immunology, 37 (2016), pp. 513–522.

[155] C. A. McArdle, J. Franklin, L. Green, and J. N. Hislop, *Signalling, cycling and desensitisation of gonadotrophin-releasing hormone receptors*, Journal of Endocrinology, 173 (2002), pp. 1–11.

[156] J. F. McDyer, Z. Li, S. John, X. Yu, C. Y. Wu, and J. A. Ragheb, *IL-2 Receptor Blockade Inhibits Late, But Not Early, IFN-γ and CD40 Ligand Expression in Human T Cells: Disruption of Both IL-12-Dependent and -Independent Pathways of IFN-γ Production*, Journal of Immunology, 169 (2002), pp. 2736–2746.

[157] T. W. McKeithan, *Kinetic proofreading in T-cell receptor signal transduction*, Proceedings of the National Academy of Sciences of the United States of America, 92 (1995), pp. 5042–5046.

[158] R. Medzhitov and C. Janeway Jr, *Innate immune recognition: mechanisms and pathways*, Immunological Reviews, 173 (2000), pp. 89–97.

[159] R. Medzhitov and C. Janeway Jr., *Innate Immunity*, The New England Journal of Medicine, 343 (2000), pp. 338–344.

[160] T. R. Mempel, S. E. Henrickson, and U. H. Von Andrian, *T-cell priming by dendritic cells in lymph nodes occurs in three distinct phases*, Nature, 427 (2004), pp. 154–9.

[161] C. Menné, T. M. Sørensen, V. Siersma, M. Von Essen, N. Ødum, and C. Geisler, *Endo- and exocytic rate constants for spontaneous and protein kinase C-activated T cell receptor cycling*, European Journal of Immunology, 32 (2002), pp. 616–626.

[162] C. A. Michie, A. McLean, C. Alcock, and P. C. L. Beverley, *Lifespan of human lymphocyte subsets defined by CD45 isoforms*, Nature, 360 (1992), pp. 264–265.

[163] Y. Minami, L. E. Samelson, and R. D. Klausner, *Internalization and cycling of the T cell antigen receptor: Role of protein kinase C*, The Journal of Biological Chemistry, 262 (1987), pp. 13342–13347.

[164] Y. Minami, A. M. Weissman, L. E. Samelson, and R. D. Klausner, *Building a multichain receptor: Synthesis, degradation, and assembly of the T-cell antigen receptor*, Proceedings of the National Academy of Sciences of the United States of America, 84 (1987), pp. 2688–2692.

[165] A. Monjas, A. Alcover, and B. Alarcón, *Engaged and bystander T cell receptors are down-modulated by different endocytotic pathways*, Journal of Biological Chemistry, 279 (2004), pp. 55376–55384.

[166] A. Mor, M. L. Dustin, and M. R. Philips, *Small GTPases and LFA-1 reciprocally modulate adhesion and signaling*, Immunological Reviews, 218 (2007), pp. 114–125.

[167] H. Mukhopadhyay, B. De Wet, L. Clemens, P. K. Maini, J. Allard, P. A. Van Der Merwe, and O. Dushek, *Multisite Phosphorylation Modulates the T Cell Receptor ζ-Chain Potency but not the Switchlike Response*, Biophysical Journal, 110 (2016), pp. 1896–1906.

[168] K. Murphy and C. Weaver, *Janeway's Immunobiology*, Garland Science, 9th ed., 2016.

[169] M. A. Murphy, R. G. Schnall, D. J. Venter, L. Barnett, I. Bertoncello, C. B. Thien, W. Y. Langdon, and D. D. Bowtell, *Tissue hyperplasia and enhanced T-cell signalling via ZAP-70 in c-Cbl-deficient mice*, Molecular and Cellular Biology, 18 (1998), pp. 4872–4882.

[170] M. Naramura, I. K. Jang, H. Kole, F. Huang, D. Haines, and H. Gu, *C-Cbl and Cbl-b regulate T cell responsiveness by promoting ligand-induced TCR down-modulation*, Nature Immunology, 3 (2002), pp. 1192–1199.

[171] M. Naramura, H. K. Kole, R. J. Hu, and H. Gu, *Altered thymic positive selection and intracellular signals in Cbl-deficient mice*, Proceedings of the National Academy of Sciences of the United States of America, 95 (1998), pp. 15547–15552.

[172] M. N. Navarro, C. Feijoo-Carnero, A. G. Arandilla, M. Trost, and D. A. Cantrell, *Protein kinase D2 is a digital amplifier of T cell receptor-stimulated diacylglycerol signaling in naïve CD8$^+$ T cells*, Science Signaling, 7 (2014).

[173] T. Newman, *Biology is simple*, Physical Biology, 12 (2015).

[174] B. P. Nicolet, A. Guislain, and M. C. Wolkers, *Combined Single-Cell Measurement of Cytokine mRNA and Protein Identifies T Cells with Persistent Effector Function*, The Journal of Immunology, 198 (2017), pp. 962–970.

[175] F. Niedergang, A. Dautry-Varsat, and A. Alcover, *Peptide antigen or superantigen-induced down-regulation of TCRs involves both stimulated and unstimulated receptors*, Journal of Immunology, 159 (1997), pp. 1703–10.

[176] K. Nika, C. Soldani, M. Salek, W. Paster, A. Gray, R. Etzensperger, L. Fugger, P. Polzella, V. Cerundolo, O. Dushek, T. Höfer, A. Viola, and O. Acuto, *Constitutively active Lck kinase in T cells drives antigen receptor signal transduction*, Immunity, 32 (2010), pp. 766–777.

[177] R. I. Nurieva, S. Zheng, W. Jin, Y. Chung, Y. Zhang, G. J. Martinez, J. M. Reynolds, S. L. Wang, X. Lin, S. C. Sun, G. Lozano, and C. Dong, *The E3 ubiquitin ligase GRAIL regulates T cell tolerance and regulatory T cell function by mediating T cell receptor-CD3 degradation*, Immunity, 32 (2010), pp. 670–680.

[178] J. Oates, N. J. Hassan, and B. K. Jakobsen, *ImmTACs for targeted cancer therapy: Why, what, how, and which*, Molecular Immunology, 67 (2015), pp. 67–74.

[179] H. Okamura, C. Garcia-Rodriguez, H. Martinson, J. Qin, D. M. Virshup, and A. Rao, *A Conserved Docking Motif for CK1 Binding Controls the Nuclear Localization of NFAT1*, Molecular and Cellular Biology, 24 (2004), pp. 4184–4195.

[180] A. Onnis, F. Finetti, and C. T. Baldari, *Vesicular trafficking to the immune synapse: How to assemble receptor-tailored pathways from a basic building set*, Frontiers in Immunology, 7 (2016), pp. 1–9.

[181] C. S. Palmer, T. Hussain, G. Duette, T. J. Weller, M. Ostrowski, I. Sada-Ovalle, and S. M. Crowe, *Regulators of Glucose Metabolism in $CD4^+$ and $CD8^+$ T Cells*, International Reviews of Immunology, 35 (2016), pp. 477–488.

[182] K. C. Pang, M. E. Dinger, T. R. Mercer, L. Malquori, S. M. Grimmond, W. Chen, and J. S. Mattick, *Genome-Wide Identification of Long Noncoding RNAs in $CD8^+$ T Cells*, The Journal of Immunology, 182 (2009), pp. 7738–7748.

[183] W. Paster, A. M. Bruger, K. Katsch, C. Grégoire, R. Roncagalli, G. Fu, N. R. J. Gascoigne, K. Nika, A. Cohnen, S. M. Feller, P. C. Simister, K. C. Molder,

S.-P. Cordoba, O. Dushek, and B. Malissen, *A THEMIS:SHP1 complex promotes T-cell survival*, The EMBO Journal, 34 (2015), pp. 393–409.

[184] N. Patsoukis, J. Brown, V. Petkova, F. Liu, L. Li, and V. A. Boussiotis, *Selective Effects of PD-1 on Akt and Ras Pathways Regulate Molecular Components of the Cell Cycle and Inhibit T Cell Proliferation*, Science Signaling, 5 (2012), pp. 1–15.

[185] S. Paul and B. C. Schaefer, *A new look at T cell receptor signaling to nuclear factor-κB*, Trends in Immunology, 34 (2013), pp. 269–281.

[186] T. L. Payne, J. Blackinton, A. Frisbee, J. Pickeral, S. Sawant, N. A. Vandergrift, S. A. Freel, G. Ferrari, J. D. Keene, and G. D. Tomaras, *Transcriptional and Posttranscriptional Regulation of Cytokine Gene Expression in HIV-1 Antigen-Specific $CD8^+$ T Cells That Mediate Virus Inhibition*, Journal of Virology, 88 (2014), pp. 9514–9528.

[187] Y. Pei, P. Zhu, Y. Dang, J. Wu, X. Yang, B. Wan, J. O. Liu, Q. Yi, and L. Yu, *Nuclear Export of NF90 to Stabilize IL-2 mRNA Is Mediated by AKT-Dependent Phosphorylation at Ser647 in Response to CD28 Costimulation*, The Journal of Immunology, 180 (2008), pp. 222–229.

[188] R. M. Pielak, G. P. O'Donoghue, J. J. Lin, K. N. Alfieri, N. C. Fay, S. T. Low-Nam, and J. T. Groves, *Early T cell receptor signals globally modulate ligand:receptor affinities during antigen discrimination*, Proceedings of the National Academy of Sciences of the United States of America, (2017).

[189] D. R. Plas, R. Johnson, J. T. Pingel, R. J. Matthews, M. Dalton, G. Roy, A. C. Chan, and M. L. Thomas, *Direct Regulation of ZAP-70 by SHP-1 in T Cell Antigen Receptor Signaling*, Science, 272 (1996), pp. 1173–1176.

[190] D. L. Porter, B. L. Levine, N. Bunin, E. A. Stadtmauer, S. M. Luger, S. Goldstein, A. Loren, J. Phillips, S. Nasta, A. Perl, S. Schuster, D. Tsai, A. Sohal, E. Veloso, S. Emerson, and C. H. June, *A phase 1 trial of donor lymphocyte infusions expanded and activated ex vivo via CD3/CD28 costimulation*, Blood, 107 (2006), pp. 1325–1331.

[191] T. Pradeu, S. Jaeger, and E. Vivier, *The speed of change: Towards a discontinuity theory of immunity?*, Nature Reviews Immunology, 13 (2013), pp. 764–769.

[192] D. Presotto, E. Erdes, M. N. Duong, M. Allard, P.-O. Regamey, M. Quadroni, M.-A. Doucey, N. Rufer, and M. Hebeisen, *Fine-Tuning of Optimal TCR Signaling*

in Tumor-Redirected CD8 T Cells by Distinct TCR Affinity-Mediated Mechanisms, Frontiers in Immunology, 8 (2017).

[193] A. Prévost-Blondel, M. Neuenhahn, M. Rawiel, and H. Pircher, *Differential requirement of perforin and IFN-γ in CD8 T cell-mediated immune responses against B16.F10 melanoma cells expressing a viral antigen*, European Journal of Immunology, 30 (2000), pp. 2507–15.

[194] A. Prévost-Blondel, E. Roth, F. M. Rosenthal, and H. Pircher, *Crucial Role of TNF-α in CD8 T Cell-Mediated Elimination of 3LL-A9 Lewis Lung Carcinoma Cells In Vivo*, Journal of Immunology, 164 (2000), pp. 3645–3651.

[195] D. A. Price, A. K. Sewell, T. Dong, R. Tan, P. J. Goulder, S. L. Rowland-Jones, and R. E. Phillips, *Antigen-specific release of β-chemokines by anti-HIV-1 cytotoxic T lymphocytes*, Current Biology, 8 (1998), pp. 355–358.

[196] B. Pulendran, *Modulating vaccine responses with dendritic cells and toll-like receptors*, Immunological Reviews, 199 (2004), pp. 227–250.

[197] M. A. Purbhoo, H. Liu, S. Oddos, D. M. Owen, M. A. Neil, S. V. Pageon, P. M. French, C. E. Rudd, and D. M. Davis, *Dynamics of subsynaptic vesicles and surface microclusters at the immunological synapse*, Science Signaling, 3 (2010).

[198] E. J. Quann, E. Merino, T. Furuta, and M. Huse, *Localized diacylglycerol drives the polarization of the microtubule-organizing center in T cells*, Nature Immunology, 10 (2009), pp. 627–635.

[199] M. Raab, Y. C. Cai, S. C. Bunnell, S. D. Heyeck, L. J. Berg, and C. E. Rudd, *$p56^{Lck}$ and $p59^{Fyn}$ regulate CD28 binding to phosphatidylinositol 3-kinase, growth factor receptor-bound protein GRB-2, and T cell-specific protein-tyrosine kinase ITK: Implications for T-cell costimulation*, Proceedings of the National Academy of Sciences of the United States of America, 92 (1995), pp. 8891–8895.

[200] M. Raab, H. Wang, Y. Lu, X. Smith, Z. Wu, K. Strebhardt, J. E. Ladbury, and C. E. Rudd, *T Cell Receptor "Inside-Out" Pathway via Signaling Module SKAP1-RapL Regulates T Cell Motility and Interactions in Lymph Nodes*, Immunity, 32 (2010), pp. 541–556.

[201] L. Racioppi, F. Ronchese, L. a. Matis, and R. N. Germain, *Peptide-Major Histocompatibility Complex Class II Complexes with Mixed Agonist/Antagonist Properties Provide Evidence for Ligand-related Differences in T Cell Receptor-dependent Intracellular Signaling*, The Journal of Experimental Medicine, 177 (1993), pp. 1047–60.

[202] A. P. Rapoport, E. A. Stadtmauer, G. K. Binder-Scholl, O. Goloubeva, D. T. Vogl, S. F. Lacey, A. Z. Badros, A. Garfall, B. Weiss, J. Finklestein, I. Kulikovskaya, S. K. Sinha, S. Kronsberg, M. Gupta, S. Bond, L. Melchiori, J. E. Brewer, A. D. Bennett, A. B. Gerry, N. J. Pumphrey, D. Williams, H. K. Tayton- Martin, L. Ribeiro, T. Holdich, S. Yanovich, N. Hardy, J. Yared, N. Kerr, S. Philip, S. Westphal, D. L. Siegel, B. L. Levine, B. K. Jakobsen, M. Kalos, and C. H. June, *NY-ESO-1-specific TCR-engineered T cells mediate sustained antigen-specific antitumor effects in myeloma*, Nature Medicine, 21 (2015), pp. 914–921.

[203] A. M. Rasmussen, G. Borelli, H. J. Hoel, K. Lislerud, G. Gaudernack, G. Kvalheim, and T. Aarvak, *Ex vivo expansion protocol for human tumor specific T cells for adoptive T cell therapy*, Journal of Immunological Methods, 355 (2010), pp. 52–60.

[204] C. Rosette, G. Werlen, M. A. Daniels, P. O. Holman, S. M. Alam, P. J. Travers, N. R. Gascoigne, E. Palmer, and S. C. Jameson, *The Impact of Duration versus Extent of TCR Occupancy on T Cell Activation: A Revision of the Kinetic Proofreading Model*, Immunity, 15 (2001), pp. 59–70.

[205] K. R. Ryan, D. McCue, and S. M. Anderton, *Fas-mediated death and sensory adaptation limit the pathogenic potential of autoreactive T cells after strong antigenic stimulation*, Journal of Leukocyte Biology, 78 (2005), pp. 43–50.

[206] S. Sakaguchi, N. Sakaguchi, M. Asano, M. Itoh, and M. Toda, *Immunologic Self-Tolerance Maintained by Activated T Cells Expressing IL-2 Receptor α-Chains (CD25): Breakdown of a Single Mechanism of Self-Tolerance Causes Various Autoimmune Diseases*, The Journal of Immunology, 155 (1995), pp. 1151–1164.

[207] M. Salek, S. McGowan, D. C. Trudgian, O. Dushek, B. de Wet, G. Efstathiou, and O. Acuto, *Quantitative Phosphoproteome Analysis Unveils LAT as a Modulator of CD3ζ and ZAP-70 Tyrosine Phosphorylation*, PloS ONE, 8 (2013), pp. 1–9.

[208] F. Salerno, N. A. Paolini, R. Stark, M. von Lindern, and M. C. Wolkers, *Distinct PKC-mediated posttranscriptional events set cytokine production kinetics in CD8$^+$ T cells*, Proceedings of the National Academy of Sciences of the United States of America, 114 (2017).

[209] F. Salerno and M. C. Wolkers, *T-cells require post-transcriptional regulation for accurate immune responses*, Biochemical Society Transactions, 43 (2015), pp. 1201–1207.

[210] M. Salio, S. Valitutti, and A. Lanzavecchia, *Agonist-induced T cell receptor down-regulation: Molecular requirements and dissociation from T cell activation*, European Journal of Immunology, 27 (1997), pp. 1769–1773.

[211] F. Sallusto, D. Lenig, R. Förster, M. Lipp, and A. Lanzavecchia, *Two subsets of memory T lymphocytes with distinct homing potentials and effector functions*, Nature, 401 (1999), pp. 708–712.

[212] R. J. Salmond, J. Emery, K. Okkenhaug, and R. Zamoyska, *MAPK, Phosphatidylinositol 3-Kinase, and Mammalian Target of Rapamycin Pathways Converge at the Level of Ribosomal Protein S6 Phosphorylation to Control Metabolic Signaling in CD8 T Cells*, The Journal of Immunology, 183 (2009), pp. 7388–7397.

[213] M. Sami, P. J. Rizkallah, S. Dunn, P. Molloy, R. Moysey, A. Vuidepot, E. Baston, P. Todorov, Y. Li, F. Gao, J. M. Boulter, and B. K. Jakobsen, *Crystal structures of high affinity human T-cell receptors bound to peptide major histocompatibility complex reveal native diagonal binding geometry*, Protein Engineering, Design & Selection, 20 (2007), pp. 397–403.

[214] E. San Jose, A. Borroto, F. Niedergang, A. Alcover, and B. Alarcón, *Triggering the TCR complex causes the downregulation of nonengaged receptors by a signal transduction-dependent mechanism*, Immunity, 12 (2000), pp. 161–170.

[215] R. Sandberg, J. R. Neilson, A. Sarma, P. A. Sharp, and C. B. Burge, *Proliferating Cells Express mRNAs with Shortened 3' Untranslated Regions and Fewer MicroRNA Target Sites*, Science, 320 (2008), pp. 1643–1648.

[216] A. Schietinger and P. D. Greenberg, *Tolerance and exhaustion: Defining mechanisms of T cell dysfunction*, Trends in Immunology, 35 (2014), pp. 51–60.

[217] J. R. Schoenborn, Y. X. Tan, C. Zhang, K. M. Shokat, and A. Weiss, *Feedback circuits monitor and adjust Basal Lck-dependent events in T cell receptor signaling*, Science Signaling, 4 (2011).

[218] G. Schönrich, U. Kalinke, F. Momburg, M. Malissen, A. M. Schmitt-Verhulst, B. Malissen, G. J. Hämmerling, and B. Arnold, *Down-Regulation of T Cell Receptors on Self-Reactive T Cells as a Novel Mechanism for Extrathymic Tolerance Induction*, Cell, 65 (1991), pp. 293–304.

[219] K. Schroder, P. J. Hertzog, T. Ravasi, and D. A. Hume, *Interferon-γ: An overview of signals, mechanisms and functions*, Journal of Leukocyte Biology, 75 (2004), pp. 163–189.

[220] R. H. Schwartz, *T Cell Anergy*, Annual Review of Immunology, 21 (2003), pp. 305–334.

[221] A. K. Sewell, *Why must T cells be cross-reactive?*, Nature Reviews Immunology, 12 (2012), pp. 669–677.

[222] E. Shaulian and M. Karin, *AP-1 as a regulator of cell life and death*, Nature Cell Biology, 4 (2002).

[223] J. Shim, H. Lim, J. R. Yates, and M. Karin, *Nuclear Export of NF90 Is Required for Interleukin-2 mRNA Stabilization*, Molecular Cell, 10 (2002), pp. 1331–1334.

[224] A. Sica, L. Dorman, V. Viggiano, M. Cippitelli, P. Ghosh, N. Rice, and H. A. Young, *Interaction of NF-κB and NFAT with the Interferon-γ promoter*, The Journal of Biological Chemistry, 272 (1997), pp. 30412–30420.

[225] N. J. Singh and R. H. Schwartz, *The Strength of Persistent Antigenic Stimulation Modulates Adaptive Tolerance in Peripheral CD4$^+$ T Cells*, The Journal of Experimental Medicine, 198 (2003), pp. 1107–1117.

[226] M. K. Slifka and J. L. Whitton, *Activated and Memory CD8+ T Cells Can Be Distinguished by Their Cytokine Profiles and Phenotypic Markers*, The Journal of Immunology, 164 (2000), pp. 208–216.

[227] L. Sompayrac, *How The Immune System Works*, WILEY Blackwell, Chichester, 5 ed., 2016.

[228] E. D. Sontag, *Incoherent feedforward motifs as immune change detectors*, BioRxiv, (2015), pp. 1–11.

[229] J. Sousa and J. Carneiro, *A mathematical analysis of TCR serial triggering and down-regulation*, European Journal of Immunology, 30 (2000), pp. 3219–3227.

[230] R. Spolski, P. Li, and W. J. Leonard, *Biology and regulation of IL-2: From molecular mechanisms to human therapy*, Nature Reviews Immunology, (2018).

[231] K. Srpan, A. Ambrose, A. Karampatzakis, M. Saeed, A. N. Cartwright, K. Guldevall, G. Dos Santos Cruz De Matos, B. Önfelt, and D. M. Davis, *Shedding of CD16 disassembles the NK cell immune synapse and boosts serial engagement of target cells*, Journal of Cell Biology, (2018), pp. 1–17.

[232] R. F. Stachlewitz, M. a. Hart, B. Bettencourt, T. Kebede, A. Schwartz, S. E. Ratnofsky, D. J. Calderwood, W. O. Waegell, and G. C. Hirst, *A-770041, a Novel and Selective Small-Molecule Inhibitor of Lck, Prevents Heart Allograft Rejection*, The Journal of Pharmacology and Experimental Therapeutics, 315 (2005), pp. 36–41.

[233] P. Stamou, J. de Jersey, D. Carmignac, C. Mamalaki, D. Kioussis, and B. Stockinger, *Chronic Exposure to Low Levels of Antigen in the Periphery Causes Reversible Functional Impairment Correlating with Changes in CD5 Levels in Monoclonal CD8 T Cells*, The Journal of Immunology, 171 (2003), pp. 1278–1284.

[234] I. Štefanová, B. Hemmer, M. Vergelli, R. Martin, W. E. Biddison, and R. N. Germain, *TCR ligand discrimination is enforced by competing ERK positive and SHP-1 negative feedback pathways*, Nature Immunology, 4 (2003), pp. 248–254.

[235] J. C. Stinchcombe, E. Majorovits, G. Bossi, S. Fuller, and G. M. Griffiths, *Centrosome polarization delivers secretory granules to the immunological synapse*, Nature, 443 (2006), pp. 462–465.

[236] J. D. Stone, A. S. Chervin, and D. M. Kranz, *T-cell receptor binding affinities and kinetics: Impact on T-cell activity and specificity*, Immunology, 126 (2009), pp. 165–176.

[237] D. B. Straus and A. Weiss, *The CD3 Chains of the T-Cell Antigen Receptor Associate with the Zap-70 Tyrosine Kinase and Are Tyrosine-Phosphorylated after Receptor Stimulation*, Journal of Experimental Medicine, 178 (1993), pp. 1523–1530.

[238] G. Suzuku, Y. Kawase, S. Koyasu, I. Yahara, Y. Kobayashi, and R. H. Schwartz, *Antigen-induced suppression of the proliferative response of T cell clones*, The Journal of Immunology, 140 (1988), pp. 1359–1365.

[239] Y. Sykulev, R. J. Cohen, and H. N. Eisen, *The law of mass action governs antigen-stimulated cytolytic activity of CD8$^+$ cytotoxic T lymphocytes*, Proceedings of the National Academy of Sciences of the United States of America, 92 (1995), pp. 11990–11992.

[240] A. L. Szymczak and D. A. A. Vignali, *Plasticity and Rigidity in Adaptor Protein-2-Mediated Internalization of the TCR:CD3 Complex*, The Journal of Immunology, 174 (2005), pp. 4153–4160.

[241] A. Tafuri, J. Alferink, P. Moller, G. J. Hammerling, and B. Arnold, *T cell awareness of paternal alloantigens during pregnancy*, Science, 270 (1995), pp. 630–633.

[242] H. Tan, K. Yang, Y. Li, T. I. Shaw, Y. Wang, D. B. Blanco, X. Wang, J. H. Cho, H. Wang, S. Rankin, C. Guy, J. Peng, and H. Chi, *Integrative Proteomics and Phosphoproteomics Profiling Reveals Dynamic Signaling Networks and Bioenergetics Pathways Underlying T Cell Activation*, Immunity, 46 (2017), pp. 488–503.

[243] M. P. Tan, A. B. Gerry, J. E. Brewer, L. Melchiori, J. S. Bridgeman, A. D. Bennett, N. J. Pumphrey, B. K. Jakobsen, D. A. Price, K. Ladell, and A. K. Sewell, *T cell receptor binding affinity governs the functional profile of cancer-specific CD8$^+$ T cells.*, Clinical and Experimental Immunology, 180 (2014), pp. 255–70.

[244] R. M. Teague, P. D. Greenberg, C. Fowler, M. Z. Huang, X. Tan, J. Morimoto, M. L. L. Dossett, E. S. Huseby, and C. Öhlén, *Peripheral CD8$^+$ T Cell Tolerance to Self-Proteins Is Regulated Proximally at the T Cell Receptor*, Immunity, 28 (2008), pp. 662–674.

[245] T. J. Thauland and D. C. Parker, *Diversity in immunological synapse structure*, Immunology, 131 (2010), pp. 466–472.

[246] K. Thurley, L. F. Wu, and S. J. Altschuler, *Modeling Cell-to-Cell Communication Networks Using Response-Time Distributions*, Cell Systems, (2018), pp. 1–13.

[247] S. Tian, R. Maile, E. J. Collins, and J. A. Frelinger, *CD8$^+$ T Cell Activation Is Governed by TCR-Peptide/MHC Affinity, Not Dissociation Rate*, The Journal of Immunology, 179 (2007), pp. 2952–2960.

[248] J. R. Tisoncik, M. J. Korth, C. P. Simmons, J. Farrar, T. R. Martin, and M. G. Katze, *Into the Eye of the Cytokine Storm*, Microbiology and Molecular Biology Reviews, 76 (2012), pp. 16–32.

[249] K. Tkach and G. Altan-Bonnet, *T cell responses to antigen: Hasty proposals resolved through long engagements*, Current Opinion in Immunology, 25 (2013), pp. 120–125.

[250] T. Toni, D. Welch, N. Strelkowa, A. Ipsen, and M. P. H. Stumpf, *Approximate Bayesian computation scheme for parameter inference and model selection in dynamical systems*, Journal of the Royal Society Interface, 6 (2009), pp. 187–202.

[251] P. S. Torres, A. Alcover, D. A. Zapata, J. Arnaud, A. Pacheco, J. M. Martin-Fernandez, E. M. Villasevil, O. Sanal, and J. R. Regueiro, *TCR Dynamics in Human Mature T Lymphocytes Lacking CD3γ*, The Journal of Immunology, 170 (2003), pp. 5947–5955.

[252] C. Utzny, D. Coombs, S. Müller, and S. Valitutti, *Analysis of Peptide/MHC-Induced TCR Downregulation: Deciphering the Triggering Kinetics*, Cell Biochemistry and Biophysics, 46 (2006), pp. 101–11.

[253] B. S. Valitutti, S. Miiuer, M. Dessing, and A. Lanzavecchia, *Different Responses Are Elicited in Cytotoxic T Lymphocytes by Different Levels of T Cell Receptor Occupancy*, Journal of Experimental Medicine, 183 (1996), pp. 1917–1921.

[254] S. Valitutti and A. Lanzavecchia, *Serial triggering of TCRs: A basis for the sensitivity and specificity of antigen recognition*, Immunology Today, 18 (1997), pp. 299–304.

[255] S. Valitutti, S. Muller, M. Cella, E. Padovan, and A. Lanzavecchia, *Serial triggering of many T-cell receptors by a few peptide-MHC complexes*, 1995.

[256] S. Valitutti, S. Müller, M. Dessing, and A. Lanzavecchia, *Signal extinction and T cell repolarization in T helper cell-antigen-presenting cell conjugates*, European Journal of Immunology, 26 (1996), pp. 2012–2016.

[257] H. A. van den Berg, K. Ladell, K. Miners, B. Laugel, S. Llewellyn-Lacey, M. Clement, D. K. Cole, E. Gostick, L. Wooldridge, A. K. Sewell, J. S. Bridgeman, and D. A. Price, *Cellular-level versus receptor-level response threshold hierarchies in T-cell activation*, Frontiers in Immunology, 4 (2013), p. 250.

[258] P. A. Van Der Merwe and O. Dushek, *Mechanisms for T cell receptor triggering*, Nature Reviews Immunology, 11 (2011), pp. 47–55.

[259] N. van Panhuys, F. Klauschen, and R. Germain, *T-Cell-Receptor-Dependent Signal Intensity Dominantly Controls CD4+ T Cell Polarization In Vivo*, Immunity, 41 (2014), pp. 63–74.

[260] R. Varma, G. Campi, T. Yokosuka, T. Saito, and M. L. Dustin, *T Cell Receptor-Proximal Signals Are Sustained in Peripheral Microclusters and Terminated in the Central Supramolecular Activation Cluster*, Immunity, 25 (2006), pp. 117–127.

[261] H. Veiga-Fernandes, U. Walter, C. Bourgeois, A. McLean, and B. Rocha, *Response of naïve and memory CD8$^+$ T cells to antigen stimulation in vivo*, Nature Immunology, 1 (2000), pp. 47–53.

[262] M. Vig, C. Peinelt, A. Beck, D. L. Koomoa, D. Rabah, M. Koblan-Huberson, S. Kraft, H. Turner, A. Fleig, R. Penner, and J.-P. Kinet, *CRACM1 Is a Plasma Membrane Protein Essential for Store-Operated Ca^{2+} Entry*, Science, 312 (2006), pp. 1220–1224.

[263] A. Viola and A. Lanzavecchia, *T cell activation determined by T cell receptor number and tunable thresholds*, Science, 273 (1996), pp. 104–106.

[264] J. P. B. Viola and A. Rao, *Molecular Regulation of Cytokine Gene Expression During the Immune Response*, Journal of Clinical Immunology, 19 (1999), pp. 98–108.

[265] M. von Essen, C. M. Bonefeld, V. Siersma, A. B. Rasmussen, J. P. H. Lauritsen, B. L. Nielsen, and C. Geisler, *Constitutive and Ligand-Induced TCR Degradation*, The Journal of Immunology, 173 (2004), pp. 384–393.

[266] M. von Essen, M. W. Nielsen, C. M. Bonefeld, L. Boding, J. M. Larsen, M. Leitges, G. Baier, N. Odum, and C. Geisler, *Protein Kinase C (PKC)α and PKCθ Are the Major PKC Isotypes Involved in TCR Down-Regulation*, The Journal of Immunology, 176 (2006), pp. 7502–7510.

[267] D. Wang, R. Matsumoto, Y. You, T. Che, X.-Y. Lin, S. L. Gaffen, and X. Lin, *CD3/CD28 Costimulation-Induced NF-κB Activation Is Mediated by Recruitment of Protein Kinase C-θ, Bcl10, and IκB Kinase β to the Immunological Synapse through CARMA1*, Molecular and Cellular Biology, 24 (2004), pp. 164–171.

[268] D. Wang, Y. You, S. M. Case, L. M. McAllister-Lucas, L. Wang, P. S. DiStefano, G. Nuñez, J. Bertin, and X. Lin, *A requirement for CARMA1 in TCR-induced NF-κB activation*, Nature Immunology, 3 (2002), pp. 830–835.

[269] J. G. Wang, M. Collinge, V. Ramgolam, O. Ayalon, X. C. Fan, R. Pardi, and J. R. Bender, *LFA-1-Dependent HuR Nuclear Export and Cytokine mRNA Stabilization in T Cell Activation*, The Journal of Immunology, 176 (2006), pp. 2105–2113.

[270] J. Wedagedera and N. Burroughs, *T-Cell Activation: A Queuing Theory Analysis at Low Agonist Density*, Biophysical Journal, 91 (2006), pp. 1604–1618.

[271] A. M. Weissman, M. Baniyash, D. Hou, L. E. Samelson, W. H. Burgess, and R. D. Klausner, *Molecular Cloning of the Zeta Chain of the T Cell Antigen Receptor*, Science, 239 (1988), pp. 1018–1021.

[272] E. J. Wherry and M. Kurachi, *Molecular and cellular insights into T cell exhaustion*, Nature Reviews Immunology, 15 (2015), pp. 486–499.

[273] T. Willinger, M. Staron, S. M. Ferguson, P. De Camilli, and R. A. Flavell, *Dynamin 2-dependent endocytosis sustains T-cell receptor signaling and drives metabolic reprogramming in T lymphocytes*, Proceedings of the National Academy of Sciences of the United States of America, 112 (2015), pp. 4423–4428.

[274] D. B. Wilson, D. H. Wilson, K. Schroder, C. Pinilla, S. Blondelle, R. A. Houghten, and K. C. Garcia, *Specificity and degeneracy of T cells*, Molecular Immunology, 40 (2004), pp. 1047–1055.

[275] A. Windhagen, C. Scholz, A. Sette, and D. A. Hager, *Modulation of Cytokine Patterns of Human Autoreactive T Cell Clones by a Single Amino Acid Substitution of Their Peptide Ligand*, Immunity, 2 (1995), pp. 373–380.

[276] L. Wooldridge, J. Ekeruche-Makinde, H. A. Van Den Berg, A. Skowera, J. J. Miles, M. P. Tan, G. Dolton, M. Clement, S. Llewellyn-Lacey, D. A. Price, M. Peakman, and A. K. Sewell, *A single autoimmune T cell receptor recognizes more than a million different peptides*, Journal of Biological Chemistry, 287 (2012), pp. 1168–1177.

[277] L. Wooldridge, B. Laugel, J. Ekeruche, M. Clement, H. A. van den Berg, D. A. Price, and A. K. Sewell, *CD8 Controls T Cell Cross-Reactivity*, The Journal of Immunology, 185 (2010), pp. 4625–4632.

[278] L. Wooldridge, H. A. Van Den Berg, M. Glick, E. Gostick, B. Laugel, S. L. Hutchinson, A. Milicic, J. M. Brenchley, D. C. Douek, D. A. Price, and A. K. Sewell, *Interaction between the CD8 coreceptor and major histocompatibility complex class I stabilizes T cell receptor-antigen complexes at the cell surface*, Journal of Biological Chemistry, 280 (2005), pp. 27491–27501.

[279] J. Xie, J. B. Huppa, E. W. Newell, J. Huang, P. J. R. Ebert, Q.-J. Li, and M. M. Davis, *Photocrosslinkable pMHC monomers stain T cells specifically and cause ligand-bound TCRs to be 'preferentially' transported to the cSMAC*, Nature Immunology, 13 (2012), pp. 674–680.

[280] D. Yablonski, T. Kadlecek, and A. Weiss, *Identification of a Phospholipase C-γ1 (PLC-γ1) SH3 Domain-Binding Site in SLP-76 Required for T-Cell Receptor-Mediated Activation of PLC-γ1 and NFAT*, Molecular and Cellular Biology, 21 (2001), pp. 4208–4218.

[281] H. Yamaguchi and W. A. Hendrickson, *Structural basis for activation of human lymphocyte kinase Lck upon tyrosine phosphorylation*, Nature, 384 (1996), pp. 484–489.

[282] Q. Yan, T. Barros, P. R. Visperas, S. Deindl, T. A. Kadlecek, A. Weiss, and J. Kuriyan, *Structural Basis for Activation of ZAP-70 by Phosphorylation of the SH2-Kinase Linker*, Molecular and Cellular Biology, 33 (2013), pp. 2188–2201.

[283] J. Yi, X. S. Wu, T. Crites, and J. A. Hammer, *Actin retrograde flow and actomyosin II arc contraction drive receptor cluster dynamics at the immunological synapse in Jurkat T cells*, Molecular Biology of the Cell, 23 (2012), pp. 834–852.

[284] T. Yokosuka, K. Sakata-Sogawa, W. Kobayashi, M. Hiroshima, A. Hashimoto-Tane, M. Tokunaga, M. L. Dustin, and T. Saito, *Newly generated T cell receptor microclusters initiate and sustain T cell activation by recruitment of Zap70 and SLP-76*, Nature Immunology, 6 (2005), pp. 1253–1262.

[285] T. Yokosuka, M. Takamatsu, W. Kobayashi-Imanishi, A. Hashimoto-Tane, M. Azuma, and T. Saito, *Programmed cell death 1 forms negative costimulatory microclusters that directly inhibit T cell receptor signaling by recruiting phosphatase SHP2*, The Journal of Experimental Medicine, 209 (2012), pp. 1201–1217.

[286] E. D. Zanders, J. R. Lamb, M. Feldmann, N. Green, and P. C. Beverley, *Tolerance of T-cell clones is associated with membrane antigen changes*, Nature, 303 (1983), pp. 625–627.

[287] V. Zarnitsyna and C. Zhu, *T cell triggering: Insights from 2D kinetics analysis of molecular interactions*, Physical Biology, 9 (2012).

[288] R. Zeng, J. L. Cannon, R. T. Abraham, M. Way, D. D. Billadeau, J. Bubeck-Wardenberg, and J. K. Burkhardt, *SLP-76 Coordinates Nck-Dependent Wiskott-Aldrich Syndrome Protein Recruitment with Vav-1/Cdc42-Dependent Wiskott-Aldrich Syndrome Protein Activation at the T Cell-APC Contact Site*, The Journal of Immunology, 171 (2003), pp. 1360–1368.

[289] Y. Zhao, A. D. Bennett, Z. Zheng, Q. J. Wang, P. F. Robbins, L. Y. L. Yu, Y. Li, P. E. Molloy, S. M. Dunn, B. K. Jakobsen, S. a. Rosenberg, and R. a. Morgan, *High-affinity TCRs generated by phage display provide CD4$^+$ T cells with the ability to recognize and kill tumor cell lines*, Journal of Immunology, 179 (2007), pp. 5845–54.

[290] S. Zhong, K. Malecek, L. A. Johnson, Z. Yu, E. Vega-Saenz de Miera, F. Darvishian, K. McGary, K. Huang, J. Boyer, E. Corse, Y. Shao, S. A. Rosenberg, N. P. Restifo, I. Osman, and M. Krogsgaard, *T-cell receptor affinity and avidity defines antitumor response and autoimmunity in T-cell immunotherapy*, Proceedings of the National Academy of Sciences of the United States of America, 110 (2013), pp. 6973–6978.

[291] P. Zhu, W. Jiang, L. Cao, W. Yu, Y. Pei, X. Yang, B. Wan, J. O. Liu, Q. Yi, and L. Yu, *IL-2 mRNA Stabilization upon PMA Stimulation Is Dependent on NF90-Ser^{647} Phosphorylation by Protein Kinase C βI*, The Journal of Immunology, 185 (2010), pp. 5140–5149.

[292] Y. Zhu, S. Yao, and L. Chen, *Cell Surface Signaling Molecules in the Control of Immune Responses: A Tide Model*, Immunity, 34 (2011), pp. 466–478.

[293] J. Zikherman and B. Au-Yeung, *The role of T cell receptor signaling thresholds in guiding T cell fate decisions*, Current Opinion in Immunology, 33 (2015), pp. 43–48.